

GEOLOGICA ULTRAIECTINA

Medelingen van de
Faculteit Aardwetenschappen der
Rijksuniversiteit te Utrecht

No. 90

SUBDUCTION OF CONTINENTAL MATERIAL IN THE
BANDA ARC, EASTERN INDONESIA

Sr-Nd-Pb isotope and trace-element evidence from
volcanics and sediments

P.Z. Vroon

GEOLOGICA ULTRAIECTINA

Medelingen van de
Faculteit Aardwetenschappen der
Rijksuniversiteit te Utrecht

No. 90

SUBDUCTION OF CONTINENTAL MATERIAL IN THE BANDA ARC, EASTERN INDONESIA

Sr-Nd-Pb isotope and trace-element evidence from
volcanics and sediments

24 - 016

CIP-GEGEVENS KONINKLIJKE BIBLIOTHEEK, DEN HAAG

Vroon, Pieter Zeger

Subduction of continental material in the Banda Arc,
Eastern Indonesia : Sr-Nd-Pb isotope and trace-element
evidence from volcanics and sediments / Pieter Zeger
Vroon - [Utrecht : Faculteit Aardwetenschappen der
Rijksuniversiteit Utrecht]. - (Geologica Ultraiectina,
ISSN 0072-1026 ; no. 90)

Proefschrift Rijksuniversiteit Utrecht. - Met lit. opg. -
Met samenvatting in het Nederlands.

ISBN 90-71577-44-9

Trefw.: geomorfologie ; Oost-Indonesië.

SUBDUCTION OF CONTINENTAL MATERIAL IN THE
BANDA ARC, EASTERN INDONESIA

Sr-Nd-Pb isotope and trace-element evidence from
volcanics and sediments

SUBDUCTIE VAN CONTINENTAAL MATERIAAL IN DE
BANDA BOOG, OOST INDONESIË

Bewijs met behulp van Sr-Nd-Pb isotopen en sporenelementen
van vulkanieten en sedimenten

(MET EEN SAMENVATTING IN HET NEDERLANDS)

PROEFSCHRIFT

TER VERKRIJGING VAN DE GRAAD VAN DOCTOR
AAN DE RIJKSUNIVERSITEIT TE UTRECHT
OP GEZAG VAN DE RECTOR MAGNIFICUS, PROF. DR. J.A. VAN GINKEL,
INGEVOLGE HET BESLUIT VAN HET COLLEGE VAN DEKANEN
IN HET OPENBAAR TE VERDEDIGEN OP MAANDAG
16 NOVEMBER 1992 DES NAMIDDAGS OM 16.15 UUR

DOOR

PIETER ZEGER VROON

GEBOREN OP 26 MEI 1963 TE CULEMBORG

PROMOTOR: PROF. DR. R.D. SCHUILING

CO-PROMOTOR: DR. M.J. VAN BERGEN

Dit proefschrift werd mede mogelijk gemaakt met financiële steun van het Greshoff Rumphius Fonds

Aan Marietta
Aan mijn ouders

CONTENTS

Voorwoord	v
Summary	vii
Samenvatting	ix
Chapter 1. General introduction	
1.1. Sediment subduction	1
1.2. Why the Banda Arc?	3
1.3. Scope and organisation of this study	3
Chapter 2. Geological, volcanological and tectonic framework of the Banda Sea area	
2.1. Geology and tectonics of East Indonesia	5
2.2. The volcanic Banda Arc	7
2.3. Volcanological remarks, sample distribution and rock-types	8
Chapter 3. Sr, Nd and Pb isotope systematics of the Banda Arc, combined subduction and assimilation of continental material	
3.1. Abstract	13
3.2. Introduction	14
3.3. Results	15
3.3.1. Rock types and SiO ₂ -K ₂ O relationships	15
3.3.2. Sr and Nd isotopic compositions	17
3.3.3. Pb isotopic compositions	23
3.4. Discussion	24
3.4.1 Introduction	24

3.4.2. Evidence for local effects of assimilation	25
3.4.3. Geological arguments against large-scale effects of assimilation	31
3.4.4. Acidic melts derived from subducted continental material?	31
3.4.5. Source-mixing models assuming an I-MORB mantle wedge	33
3.4.5.1. I-MORB + bulk SCM	33
3.4.5.2. I-MORB + fluid/melt derived from SCM	35
3.4.6. Source mixing models assuming an OIB-type mantle wedge	37
3.4.7. Models invoking mantle wedge magma mixing (MWMM)	39
3.5. Conclusions	41

Chapter 4. Trace-element constraints on the role of subducted continental material in the Banda Arc

4.1. Abstract	43
4.2. Introduction	44
4.3. Results	46
4.3.1. Major elements	46
4.3.2. Trace elements	47
4.3.2.1. Large ion lithophile elements	48
4.3.2.2. Rare earth elements and Yttrium	48
4.3.2.3. High field strength elements	50
4.3.2.4. Scandium, Chromium and Cobalt	50
4.3.3. Correspondance with trace-element signatures of local sediments	52
4.4. Discussion	52
4.4.1. Introduction	52
4.4.2. REE mixing-melting models	55
4.4.2.1. Assumptions for the mixing step	56
4.4.2.2. Assumptions for the melting step	56
4.4.2.3. Evaluation of mixing-melting models	58
4.4.3. Evidence for SCM from incompatible trace-element ratios: comparison with local sediments, MORB, OIB and other island-arcs	59
4.4.4. Comparison with isotope evidence	64
4.4.5. Additional role of fluids	65
4.4.6. Two-stage source contamination?	68
4.5. Conclusions	70

Chapter 5. Sr, Nd and Pb isotopic and trace-element signatures of the East Indonesian Sediments: provenance and geodynamical implications

5.1. Abstract	73
5.2. Introduction	74
5.3. Tectonic framework and lithofacies of the Banda Sea area	75
5.3.1. General	75
5.3.2. The back-arc basin	75
5.3.3. The volcanic Banda Arc	77
5.3.4. The fore-arc basins	77
5.3.5. The structural highs and collision complex	77
5.3.6. The subduction trenches	78
5.3.7. The North Australian and New Guinea continental slope and shelf	78
5.3.8. Outline of the North Australia-West New Guinea geology	79
5.3.9. Previous geochemical work	79
5.4. Sample selection and analytical techniques	80
5.5. Results	80
5.5.1. General geochemical characteristics of sediment types	81
5.5.2. Trace-element variations in East Indonesian Sediments	83
5.5.2.1. LILE	83
5.5.2.2. REE	85
5.5.2.3. HFSE (Nb, Ta, Zr, Hf)	85
5.5.2.4. Transitional elements (Sc, Co, Cr)	86
5.5.3. Isotopes	88
5.5.3.1. General ranges and correlations	88
5.5.3.2. Comparison with Indian-, Pacific- and Atlantic-Ocean sediments	88
5.5.3.3. The $^{147}\text{Sm}/^{144}\text{Nd}$ ratios and Nd model ages	89
5.6. Discussion	91
5.6.1. Introduction	91
5.6.2. The provenance of East Indonesian sediments	91
5.6.3. Some implications for continental fragments in East Indonesia	96
5.6.4. Geochemical comparison between the East Indonesian sediments and Average Upper Continental Crust	97
5.6.5. Implications for the recycling of continental material in the Banda Arc	100
5.7. Conclusions	101

Chapter 6. Implications for island-arc magmatism, the nature of the subducted continental material and EMII OIB sources

6.1. Introduction	103
6.2. Implications for island-arc magmatism	103
6.3. The nature of SCM: subducted continental crust or continent-derived sediments?	104
6.4. Is EMII OIB source generated by sediment subduction?	108
References	113
Appendices	129
Curriculum Vitae	205

Chapter 3 has been submitted to *Journal of Geophysical Research* under the title 'Sr-Nd-Pb systematics of the Banda Arc, Indonesia: combined subduction and assimilation of continental material'. Co-authors: M.J. van Bergen, W.M. White and J.C. Varekamp.

VOORWOORD

Dit proefschrift kwam tot stand met hulp en medewerking van veel mensen. Allereerst wil ik mijn co-promotor, Manfred van Bergen, bedanken. Zijn enthousiasme voor alles wat met vulkanen te maken heeft en zijn precieze werkwijze ("beter geen getal dan een slecht getal") hebben mij sterk gestimuleerd. Onze vele discussies over de Banda Boog en analyse-technieken hebben een grote invloed gehad op het eindresultaat van mijn onderzoek. Mijn promotor, professor R.D. Schuiling, wil ik graag bedanken voor het doorlezen van de manuscripten en zijn waardevolle suggesties.

De basis voor dit onderzoek is gelegd tijdens de Snellius II expeditie in 1984-1985, onder de gezamenlijke leiding van de Stichting Onderzoek der Zee (SOZ) en het Indonesische Instituut voor wetenschap (LIPI). De organisatoren van Thema 1 "Geologie van de Banda Zee", Prof. Dr. H.E van Hinte en Dr. H. Hartono hebben dit onderzoek in eerste instantie mogelijk gemaakt. De monsters voor deze studie zijn verzameld gedurende een succesvol gezamenlijk veldwerk door René Poorter, Manfred van Bergen, Joop Varekamp, Achmed Wirakusumah, Rizal Erfan, Kardi Suharyono, Terry Sriwana en Connie van Bergen. Hen en de bemanning van het Indonesische onderzoekschip 'Jalanidh' wil ik bedanken voor de prettige samenwerking in het veld. De samenwerking met de Vulkanologische Dienst te Bandung (VSI) is essentieel geweest, zowel tijdens het veldwerk als gedurende het verdere verloop van dit onderzoek. De sedimenten zijn verzameld en bewerkt door de vakgroep marine geologie van de Vrije Universiteit te Amsterdam. Gerard Klaver wil ik bedanken voor de introductie in de chemie van de sedimenten.

Aangezien de data van dit proefschrift verkregen zijn door middel van vele verschillende analyse technieken hebben veel mensen tot de resultaten van dit proefschrift bijgedragen: de mensen van de slijpkamer, Bob Stokvis en Jan Drenth voor de monstervoorbereiding, Theo van Zessen, Vian Govers en Joep Huijsmans voor het XRF werk, Thea Meertens en Chiel Eussen voor het INAA werk, Peter Wilkens voor de CaCO_3 bepalingen en Else Henneke en Jurian Hoogewerff voor organisch koolstof. Het grootste gedeelte van het isotopenwerk werd uitgevoerd aan het SIGO, nu onderdeel van de Vrije Universiteit te Amsterdam. Lodewijk IJst, Koos van Belle, Piet Remkers, Richard Smeets, Ehrard Hebeda, Pauline Smedley, Frans Benavente, Bert Voorhorst, Paul Andriessen en Jan Wijbrans wil ik bedanken voor hun hulp en bijdragen. Prof. Dr. W.M. White, verbonden aan de Cornell Universiteit, Ithaca (VS), wil ik bedanken voor de mogelijkheid om Pb-isotopen te analyseren op de massa-spectrometer, en zeldzame aarden op de ICP-MS. Mike Cheatham's hulp was onmisbaar bij deze analyses.

Marlina Elburg heeft zeer veel werk verzet met het opwerken van Sr-isotoop preparaten en de interpretaties van Serua, terwijl Timo Fliervoet en Patrick Speck in hun doctoraal scripties de data van respectievelijk Nila en Banda gemodelleerd hebben. Appendix 3 werd kritisch bekeken door Dr. M.F. Thirlwall en Simon Vriend. De Audio-Visuele Dienst van het Instituut voor Aardwetenschappen (Utrecht), met name Jaco van Bergen-Henegouwen, wil ik bedanken voor het vele tekenwerk.

Zowel op het SIGO als in Utrecht heb ik een goede tijd gehad. Hiervoor wil ik bedanken: Kay Beets, José van Duin, Jan Schijf, Peter Valbracht, Marjan van der Wiel, 'de Egyptenaar', Hans Eggenkamp, Guiseppa Frapporti, Geert-Jan de Haas, Else Henneke, Timo Nijland, Bertil van Os en het Chalet Universitaire. Jurian Hoogewerff wil ik hartelijk bedanken voor het delen van de computer en de vele discussies over vulkanisme en software. Karen Harpp, Karl Wirth, Gene Yogodzinsky en Jay Romenick bedank ik voor de leuke periode aan de Cornell Universiteit.

Mijn ouders dank ik voor hun onvoorwaardelijke steun die ik altijd ondervonden heb. Marietta, jouw praktische en morele bijdrage is onmisbaar geweest!!

SUMMARY

This thesis presents the results of a geochemical study of the Banda Arc (East Indonesia) where magma genesis is influenced by subducted source components that are controlled by an active arc-continent collision. The main objective of this study is to investigate the role of subducted continental material on the magma genesis using isotopic and chemical compositions of samples from volcanoes and sediments distributed along the whole stretch of the arc.

Sr-Nd-Pb isotope ratios and major and trace-element contents were determined for a total of 152 rocks from seven volcanic islands, 127 surface sediments from seven locations and five sediment samples from the DSDP Site 262 hole in the Timor Trough. The composition of these sediments is considered to represent that of a subducted component with continental affinity which is currently involved in magma genesis.

This data set is used to (1) assess the importance of subducted continental material as opposed to material assimilated from the arc crust; (2) quantify the contribution of subducted continental material to magma sources; (3) discuss the mode of transfer from the slab to magma sources in the overlying mantle wedge, and (4) determine the role of sediment provenance in generating isotopic heterogeneities within the arc.

Large variations in the isotopic composition were found between the volcanoes. These variations are matched by similar variations in the sediments along the arc. This parallelism is most evident for Pb isotopes and is considered as strong evidence for the involvement of subducted continental material in magma genesis. Conventional bulk mixing models indicate that the contribution of subducted continental material increases along the arc from <1% in the NE to 5-10% in the SW. Important within-suite Sr-Nd isotopic ranges were also found for individual volcanoes. Assimilation is thought to be significant in one volcano and probably occurs to some extent on most islands. However, it cannot explain the conspicuous 'continental' signatures of the more mafic Banda Arc volcanics.

Trace-element compositions of the volcanics show upper continental crust signatures. Many ratios of incompatible elements (e.g. LILE/HFSE and LILE/REE) and rare-earth patterns display an increasing correspondence with those of the sediments in the same direction. REE mixing-melting models were applied using a typical MORB source mantle and a representative sediment as end members. The results are consistent with the isotopic mixing models in terms of quantities and with the NE-SW along-arc changes. These models indicate that the bulk addition of subducted continental material to mantle sources is an important characteristic of the Banda Arc which can explain many of its

trace-element signatures. Addition in the form of large-degree melts rather than mechanical mixing is considered to be the most plausible bulk-addition mechanism, particularly in the SW Banda Arc.

Nevertheless, some trace-element ratios (e.g. Ba/Nb, Th/Nb, Th/Zr) cannot be explained by bulk mixing and must be due to a process of selective mobilization, probably by fluids escaping from the slab. It is suggested that bulk transfer of subducted continental material dominates and is most conspicuous in the SW whereas fluid transfer is more evident in the NE.

Despite the evidence for the involvement of subducted continental material, the Banda Arc volcanics are characterized by higher $^{208}\text{Pb}/^{204}\text{Pb}$ at a given $^{206}\text{Pb}/^{204}\text{Pb}$ compared to the sediments. This difference becomes more pronounced from NE to SW along the arc. High $^{208}\text{Pb}/^{204}\text{Pb}$ is a typical characteristic of the Indian ocean MORB and OIB (so-called Dupal anomaly), and the high $^{208}\text{Pb}/^{204}\text{Pb}$ component in the volcanics could thus be derived from a mantle contribution. Because of the high Pb concentration in continental material compared to the Pb concentration in any solid mantle type, it is suggested that small-degree partial melts from a mantle source are involved.

The terrigenous fraction in the sediments is thought to be responsible for the overall 'continental' character of the arc. From the combined isotopic and trace-element ratios in this fraction two provenance areas can be distinguished: in the NE part of the arc the sediments originate from Phanerozoic New Guinea and in the SW they originate mainly from Proterozoic Australia. A further subdivision can be made on the basis of Th/Sc, $^{147}\text{Sm}/^{144}\text{Nd}$, Pb and Nd isotopes into: North New Guinea+Seram, South New Guinea, Timor and Australia. In trace-element ratios and REE patterns the sediments are generally similar to published estimates for average Upper Continental Crust and Post Archean Australian Shale. No systematic difference was found between the compositions of sediments from shelf, wedge and back arc.

The results for the Banda Arc highlight the importance of the subducted component in controlling inter- and intra-arc variations in chemical and isotopic signatures. Therefore, data from local sediments are indispensable for models of arc magma genesis in individual cases. The potential variability of subducted sediments also has important implications for the origin and scale of mantle heterogeneities.

SAMENVATTING

In dit proefschrift worden de resultaten gepresenteerd van een geochemische studie naar de invloed van gesubduceerd continentaal materiaal op de magmagenese in de Banda Boog (Oost-Indonesië). Het onderzochte materiaal bestaat zowel uit monsters van vulkanieten als sedimenten, verspreid langs de gehele lengte van de Banda Boog.

Sr-, Nd-, Pb-isotopen samenstelling en concentraties van hoofd- en sporenelementen zijn bepaald voor 152 vulkanieten van zeven vulkanische eilanden, 127 recente sedimenten van zeven lokaties en vijf monsters van de DSDP-Site 262 boring in de Timor Trog. De samenstelling van deze sedimenten wordt verondersteld gelijk te zijn aan die van het gesubduceerd continentaal materiaal.

Met behulp van deze dataset wordt: (1) de rol van assimilatie versus gesubduceerd continentaal materiaal geëvalueerd; (2) de hoeveelheid gesubduceerd materiaal die betrokken is bij de generatie van magma bepaald; (3) geanalyseerd via welk mechanisme het gesubduceerde materiaal van de slab naar de mantelwig getransporteerd wordt; (4) onderzocht of de mantel heterogeniteiten in de boog verklaard kunnen worden door de herkomst van het sediment.

Tussen de vulkanen onderling bestaan grote verschillen in Sr-, Nd-, en Pb-isotopen samenstelling. Deze variaties komen overeen met vergelijkbare variaties van de sedimenten langs de boog; een overeenkomst die een sterk bewijs vormt voor de subductie van continentaal materiaal in de Banda Boog. Conventionele bulk-mixing modellen geven aan dat de hoeveelheid van gesubduceerd continentaal materiaal toeneemt langs de Banda Boog van minder dan 1% in het noordoosten tot 5-10% in het zuidwesten.

Ook binnen één vulkaan komen significante variaties in Sr- en Nd-isotopen samenstelling voor. Assimilatie is een belangrijk proces voor één vulkaan en komt waarschijnlijk in enige mate voor op de meeste eilanden. Assimilatie kan echter niet de 'continentale' signaturen van de meer mafische gesteenten van de Banda Boog verklaren.

De sporenelement samenstelling van de vulkanieten komt overeen met die van de gemiddelde boven-continentale korst. Veel ratio's van incompatibele sporenelementen (b.v. LILE/HFSE en LILE/REE) en patronen van zeldzame aarden vertonen een toenemende gelijkenis met die van sedimenten van noordoost naar zuidwest. REE mixing-smelt modellen werden toegepast met een MORB mantel en een representatief sediment als eindleden. De resultaten zijn consistent met de isotopen-bulk-mixing modellen wat betreft de toenemende hoeveelheden continentaal materiaal langs de Banda Boog van noordoost naar zuidwest. De modellen tonen aan dat bulk toevoeging van

gesubduceerd continentaal materiaal aan de mantel in belangrijke mate de sporenelement signatuur van de vulkanieten bepaalt. Toevoeging van smelten afkomstig van continentaal materiaal aan de MORB mantelwig, in plaats van mechanische mixing is waarschijnlijker, vooral in het zuidwesten van de boog.

Sommige sporenelement ratio's (b.v. Ba/Nb, Th/Nb, Th/Zr) kunnen echter niet verklaard worden met bulk toevoeging. Selectieve mobilisatie door fluids afkomstig van de gesubduceerde slab is waarschijnlijker. Smelten van gesubduceerd continentaal materiaal is belangrijk in het zuidwesten, in het noordoosten daarentegen domineert de rol van fluid transport.

Ondanks het bewijs voor de rol van gesubduceerd continentaal materiaal worden de Banda Boog vulkanieten gekarakteriseerd door hoger $^{208}\text{Pb}/^{204}\text{Pb}$ voor een gegeven $^{206}\text{Pb}/^{204}\text{Pb}$ in vergelijking met de sedimenten. Van het noordoosten naar het zuidwesten langs de boog wordt dit verschil groter. Hoog $^{208}\text{Pb}/^{204}\text{Pb}$ is een typische kenmerk van de Indische Oceaan MORB en OIB (de zogenoemde Dupal anomalie), en de hoge $^{208}\text{Pb}/^{204}\text{Pb}$ component kan dus van deze mantel types afkomstig zijn. De Pb concentratie in het continentale materiaal, die hoog is in vergelijking met elk type mantel materiaal, suggereert dat er een kleine hoeveelheid van partiële smelt van een Dupal mantel component betrokken is.

De terrigene fractie van de sedimenten is verantwoordelijk voor het continentale karakter van de Boog. Twee herkomst gebieden voor de terrigene fractie kunnen met behulp van de Pb-, Nd-isotopen en sporenelement ratio's worden onderscheiden. In het noordoosten van de boog zijn de sedimenten afkomstig van Phanerozoïsch Nieuw Guinea en in het zuidwesten van Proterozoïsch Australië. Op basis van Th/Sc, $^{147}\text{Sm}/^{144}\text{Nd}$, Pb en Nd isotopen kan een verdere indeling gemaakt worden in vier gebieden van sediment herkomst: Noord Nieuw-Guinea en Seram, Zuid Nieuw-Guinea, Timor, en Australië. De sedimenten zijn over het algemeen in sporenelement ratio's en zeldzame-aarden patronen gelijk aan gepubliceerde gemiddelden van de boven-continentale korst. Er is geen systematisch verschil tussen sedimenten van de shelf, accretie-prisma of back-arc.

De resultaten van deze geochemische studie van de Banda Boog benadrukken het belang van de gesubduceerde component in het bepalen van zowel inter- als intra-boog variaties in chemie en isotopen samenstelling. Daarom zijn gegevens van lokale sedimenten onmisbaar voor modellen van eiland-boog magmagenese voor elke boog. De variaties in de potentieel gesubduceerde sedimenten hebben ook belangrijke gevolgen voor het ontstaan en de schaal van mantel heterogeniteiten.

CHAPTER 1

GENERAL INTRODUCTION

1.1. SEDIMENT SUBDUCTION

Recycling of continental material into the mantle has played a central role in the debates concerning crust and mantle evolution in earth sciences. It is of importance for the evolution of the continental crust (e.g. McLennan, 1988), the petrogenesis of island-arcs (e.g. Gill, 1981; Arculus and Powell, 1986) and the genesis of the sources of ocean island basalts (e.g. Zindler and Hart, 1986; Weaver, 1991).

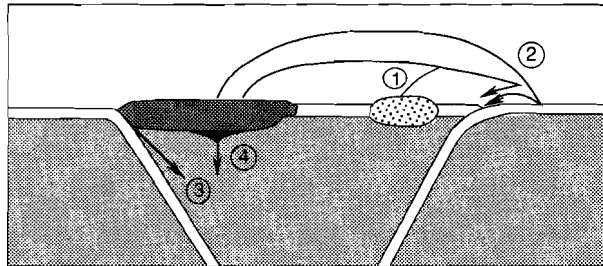


Fig. 1.1. Schematic diagram illustrating the various possibilities to recycle continental material into the mantle: (1) subduction of sediments; (2) subduction of altered oceanic crust; (3) tectonic erosion of continental crust; (4) assimilation of continental crust by the mantle at the base of the crust. After McLennan (1988).

Figure 1.1 illustrates four potential ways to recycle continental material into the mantle (McLennan, 1988): (1) subduction of sediment or continental crust, (2) subduction of oceanic crust enriched in continent-derived elements by interaction with sea water, (3) tectonic erosion of continental crust in subduction zones and (4) direct incorporation of lower continental crust by the mantle. Of these processes, subduction is probably the most important mechanism by which continental material is returned to the mantle (McLennan, 1988).

The hypothesis of sediment involvement in island-arc magma genesis was first put forward by Coats (1962) as an alternative to the generally held view at that time that andesites are generated by the assimilation of continental material. Armstrong (1968) invoked sediment subduction to explain the evolution of the continental crust: in his model the volume of continental crust had been almost constant since the early Archean. Consequently,

continental material must have been recycled back into the mantle to balance the amount of newly formed crust since then. The first geochemical evidence for sediment subduction was presented by Tatsumoto and Knight (1969) and Armstrong (1971); this evidence was based on similarities between the Pb isotopes of arc volcanics and sediments. This idea initiated a vigorous debate on whether sediment subduction was in fact physically possible. An important counter-argument was that sediment in the mantle was too buoyant to be subducted (e.g. Moorbath, 1978).

However, an increasing number of geochemical arguments strongly favoured the case for sediment subduction. First of all, the correspondence between the Pb isotope signatures of arc volcanics and sediments appeared to hold for both inter- and intra-arc variations (e.g. Armstrong, 1971; White and Dupre, 1986). Supporting evidence was obtained from Nd isotopes (e.g. Cohen and O'Nions, 1982), Hf isotopes (e.g. White and Patchett, 1984) and trace elements (e.g. Kay, 1980). The discovery of ^{10}Be in subduction zone rocks (Brown et al., 1981; 1982; Tera et al., 1986) is the latest and perhaps most persuasive evidence for sediment involvement in arc volcanism. Physical objections were weakened by seismic evidence that sediments can be transported into the mantle once they become trapped in grabens at the surface of subducting oceanic crust (e.g. Hilde, 1983; Uyeda, 1983).

Despite the current consensus that sediments are subducted a number of important questions are still being debated. Major topics are the precise quantification of budgets and the details of processes operating during the subduction. In particular, more information is required concerning the way in which magma sources are generated as a result of mixing between slab-derived material (solid, melt or fluid) and the overlying mantle wedge.

It is difficult to draw generalized conclusions from arc studies because there are considerable geochemical differences between arcs, as well as variations within individual arcs (Gill, 1981). These apparently reflect the complex sources and processes involved:

- (1) In most cases the composition of subducted source components is insufficiently known, mainly due to the lack of data on local sediments.
- (2) The effect of assimilation is difficult to determine; it may be pronounced in continental arcs (e.g. Hildreth and Moorbath, 1988), but may also be significant in island arcs (e.g. Davidson, 1986).
- (3) There is no consensus concerning the kind of mantle wedge that underlies most arcs: is it either similar to the source of Normal-Mid Oceanic Ridge Basalts (N-MORB), or to the source of Ocean Island Basalts (OIB).
- (4) Subduction-related tectonic factors (e.g. age and dip of the slab) can influence magma chemistry (e.g. Defant et al., 1991; Carr et al., 1990).

The above factors are investigated in this study by means of accurate geochemical analyses of a single volcanic arc, for which both the output (volcanic rocks) and the

potentially dominant input (sediments) have been determined.

1.2. WHY THE BANDA ARC?

The geological setting of the Banda Arc provides a unique opportunity for studying the subduction of continental material, for the following reasons:

(1) Large quantities of continent-derived sediments and continental crust lie in front of the trenches. These are derived from the old Australian craton; therefore they should have very radiogenic Sr and Pb isotopic and unradiogenic Nd isotopic compositions. The extreme composition of the subducted component in the Banda Arc should make it possible to detect even the smallest amount of sediment that has been added to the source of the Banda Arc magmas.

(2) The Banda Arc volcanoes stand upon oceanic crust. Therefore, assimilation of continental crust or sediments is unlikely to play a major role in determining the compositions of erupted magmas.

(3) Previous geochemical studies of the Banda Arc (Whitford et al., 1977; Magaritz et al., 1978; Whitford and Jezek, 1979; Whitford et al., 1981; Morris and Hart, 1980; Morris, 1984) have already drawn attention to the conspicuous 'continental' signatures of the volcanics. These signatures were attributed to source contamination through subduction but reservations were made as to the relative importance of assimilation of the arc crust.

1.3. SCOPE AND ORGANIZATION OF THIS STUDY

The main objectives of the research described in this thesis are: (1) to assess the importance of subducted continental material as opposed to assimilated material from the arc crust; (2) to quantify the contribution of subducted continental material to magma sources; (3) to discuss the mode of transfer from the slab to magma sources in the overlying mantle wedge, and (4) to determine the role of sediment provenance in generating isotopic heterogeneities within the arc.

In order to achieve these objectives, 152 volcanic rocks and 132 sediments obtained during the Snellius II Expedition (1984-1985) to the Banda Arc region have been analyzed for major and trace elements and Sr, Nd and Pb isotopes. The results are presented and discussed as follows:

Chapter 2 summarizes relevant aspects of the geology and geophysics of the Banda Arc region. Chapter 3 presents the Sr, Nd and Pb isotope systematics of the volcanics.

Compelling evidence for the subduction of continental material is presented on the basis of the along-arc isotopic similarities of volcanics and sediments on the Australian shelf. It is further demonstrated that assimilation occurs, but that it is an unlikely cause of the along-arc variations.

Chapter 4 presents the trace-element results for the volcanics. Mixing-melting models are used to show that the contribution of the subducted continental component increases along the arc from NE to SW, in agreement with the isotopic results of Chapter 3. Bulk transfer of continental material to the mantle wedge is considered to be the dominant mechanism, although in the NE fluids derived from continental material also play a role.

Chapter 5 presents the Sr-Nd-Pb isotope and trace-element data for the sediments from the Banda Arc region, and discusses their provenance. The sediments are also used to estimate the composition of the North Australian Upper Continental Crust. Chapter 6 evaluates the results in terms of implications for island-arc magma genesis and for the generation of mantle heterogeneities caused by the subduction of continental material.

CHAPTER 2

GEOLOGICAL, VOLCANOLOGICAL AND TECTONIC FRAMEWORK OF THE BANDA SEA AREA

2.1. GEOLOGY AND TECTONICS OF EAST INDONESIA

The Banda Arc, at the eastern end of the Sunda-Banda Arc system, is situated at the SE border of the South-East-Asian plate in a region where there is complex interaction between the northward moving Indo-Australian plate and the westward moving Pacific plate (Hamilton, 1979). Forming a morphological curve over nearly 180 degrees, the arc encloses the oceanic Banda Sea, but is surrounded to the South, East and North by continental lithosphere which is approaching the region (Fig. 2.1). Due to the converging movements of these passive (micro-)continental margins, the arc is undergoing the effects of collisions in various stages of development. These are most pronounced in the Timor area where collision between the Australian continent and the arc started some 3 Ma ago (Audley-Charles et al., 1979; Abbott and Chamalaun, 1981).

The Timor, Aru and Seram troughs (Fig. 2.1), with relatively shallow water depths (< 3000 m) surround the arc, and are underlain by continental crust, whereas the fore-arc basins are essentially oceanic (Bowin et al., 1980) and reach depths > 3000 m (Savu Basin) and even > 7000 m (Weber Deep). The Australian continental crust, subducted along the Timor Trough, is up to 40 km thick (Jacobson et al., 1978) and thins towards New Guinea. This presumably Precambrian-aged crust (Powell and Mills, 1978) is covered by sequences of Phanerozoic sediments reaching thicknesses in excess of 10 km in several of the shelf basins (Hamilton, 1979; Veevers, 1984; Butcher, 1989).

There are conflicting views on the geometry of the subducting lithosphere, but recent seismological interpretations suggest the existence of two distinct plates subducting beneath the Banda Sea area (Cardwell and Isacks, 1978; McCaffrey, 1989) instead of one tightly curved continuous structure (Hamilton, 1979). The Indo-Australian plate is subducting at a velocity of 7-8 cm/yr in a NNE direction (Minster and Jordan, 1978). The distribution of earthquake hypocentres suggests that the slab dips gently down to 200 km, then steepens to 60-70 degrees until it flattens again at the deepest level of observed seismicity. The slab can be traced to a depth of more than 600 km and is steeper in the Eastern Sunda Arc than in the bend of the Banda Arc. Absence of shallow earthquake foci (70-380 km) marks the volcanically extinct sector north of Timor (McCaffrey, 1989), compatible with a major

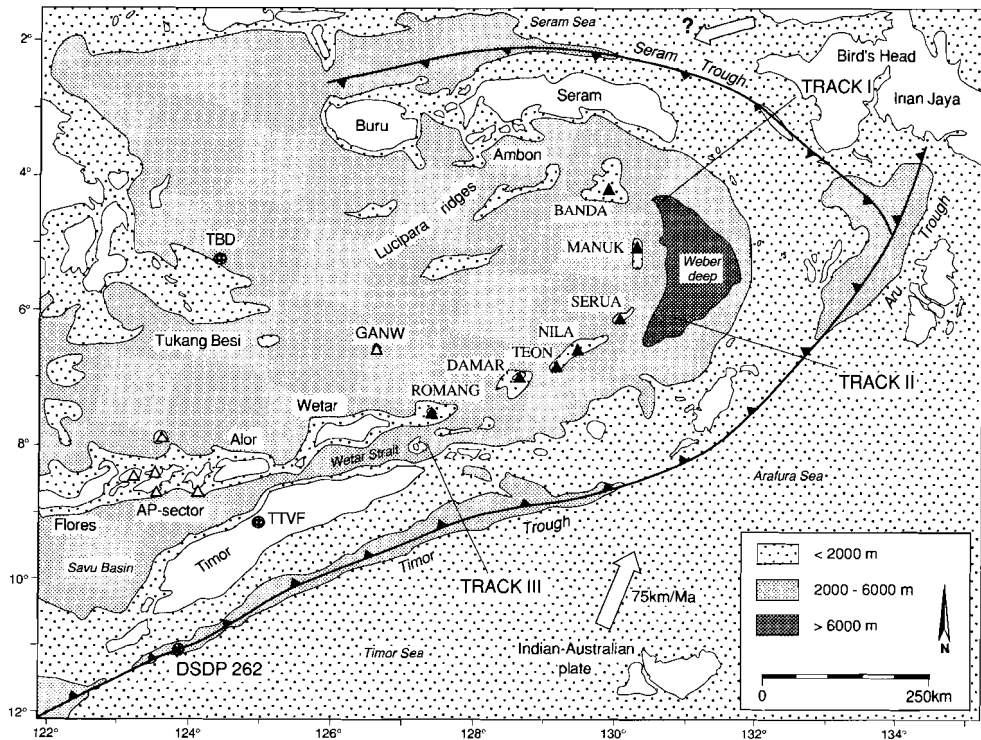


Fig. 2.1. Map of the Banda Sea region showing the volcanic islands studied (solid black triangles) and active volcanoes (unlabelled open triangles). Romang, Wetar and Alor form an inactive segment between the Banda and Sunda Arcs. Sediment box- and piston cores are from the Snellius II Expedition Tracks I, II and III (Jongsma et al., 1989; Situmorang, 1992). GANW: Gunung Api North of Wetar; TTVF: location of sample TTVF, a 6-7 Ma basaltic-andesitic pillow lava from the Manamas Formation in Oecusse, Timor (Wensink; pers. comm., with age date based on Abbott and Chamalaun, 1981); TBD: Tukang Besi Diabase (Silver et al., 1985; Morris et al, 1984, Schwartz et al., 1984). AP-sector: Adonara-Pantor sector of the East Sunda Arc. Subduction directions and velocities are from Minster and Jordan (1978) and DeSmet (1989).

disturbance of the subduction pattern due to the collision of the arc with the passive continental margin of Australia. A slab with a southward vector of movement is entering the Seram Trough (Fig. 2.1) and dips with an angle of about 35 degrees to the SW to a depth of 300 km (McCaffrey, 1989; Ritsema et al., 1989). Because of a large strike-slip component and the complex interplay of microcontinents accommodating the relative motions of the Eurasian and Pacific plates (cf. Hartono, 1990; Nishimura and Suparka, 1990), it is difficult to make a reliable estimate of the convergence rate along this boundary.

The outer arc consists of non-volcanic islands including Timor, Tanimbar, Seram and Buru (Fig. 2.1). According to Hamilton (1979), they represent a Tertiary melange system

with a wide variety of crystalline and sedimentary rock types. Considerable recent uplifts (De Smet et al., 1989) are consistent with the supposition (Hamilton, 1979) that the leading portions of the subducted Australian continent have reached the inner border of these islands (cf. Fig. 2.1).

The volcanic arc is built on oceanic crust, that is considered to form much of the Banda Sea floor (Bowin et al., 1980). Although Hamilton (1979) proposed that back-arc spreading and a Neogene age could be responsible for its oceanic origin, most authors (e.g. Bowin et al., 1980; Lee and McCabe, 1986) currently believe that it is relatively old (dating back to Cretaceous) and probably represents a trapped piece of Indian-Ocean crust.

NE-SW trending ridges present in the central part of the Banda Sea contain clastic sedimentary and metamorphic rocks, two of which were dated at 11 and 22 Ma (Silver et al., 1985). Dredging of the ridges also revealed andesites with an age of 6-7 Ma (Silver et al., 1985). The ridges have been interpreted as continental fragments transported into the area from the northern part of New Guinea along major transform faults (Silver et al., 1985). Major westward movements along such faults could also have introduced pieces of Pacific oceanic crust into the northern regions of the Banda Sea area (cf. Katili, 1978).

Nearly flat sediments cover the oceanic crust (Bowin et al., 1980). The seismic data of Bowin et al. (1980) suggest that the sediment thickness is approximately 1.7 km (Hartono, 1990). The topography of the Banda Sea is irregular, however, and thicknesses are likely to vary considerably (cf. Bowin et al., 1980, their Fig. 28).

2.2. THE VOLCANIC BANDA ARC

The volcanic inner arc consists of three parts: a southern inactive sector forming the connection with the Sunda Arc, a central active sector, and an inactive sector at the northern end. The southern sector (including Alor, Wetar and Romang) originated as an intra-oceanic arc (Hamilton, 1979). A maximum age of 12 Ma was found for intrusives of Wetar, while magmatism ceased some 3 Ma ago (Abbott and Chamalaun, 1981). However, a 400 ka old high-Mg basalt was dredged off the north coast of Wetar (Schwartz et al., 1984; Silver et al., 1985). Back-arc thrusts found north of this sector (Alor-Romang) and behind Flores may reflect the incipient reversal of the subduction polarity (Silver et al., 1983).

Six volcanic islands form the active arc. Manuk, Serua, Nila and Teon emerge from a narrow ridge rising steeply between the Weber Deep and the Banda Sea floor (Fig. 2.1). The Banda archipelago is situated on a triangular platform, separated from the Manuk-Teon ridge by water depths > 4000 m. Damar is separated from Teon and Romang by channels deeper than 3000 m.

The northern inactive sector including Ambon is underlain by a continental-crystalline basement as shown by abundant polymetamorphic xenoliths present within the volcanics (e.g. Van Bergen et al., 1989). Volcanism on land probably also ceased some 3 Ma ago (Abbott and Chamalaun, 1981; Priem et al., 1978), but an andesite as young as 750 ka was dredged from one of the ridges adjacent to Ambon (Silver et al., 1985).

Gunung Api north of Wetar has been described by Verbeek (1908) and Kuenen (1935). It is a small volcano, 282 m high, rising steeply from the ocean floor 5000 m beneath sea level. The last reported eruption was in 1699. The volcano is composed of lavas which are similar in major-, trace- and isotopic-composition as those of the South Banda Arc volcanics (Schwartz et al., 1984; Morris et al., 1984). The depth to the Benioff zone is 400 km and its connection to the current subduction zone is not clear (e.g. Silver et al., 1985).

2.3. VOLCANOLOGICAL REMARKS, SAMPLE DISTRIBUTION AND ROCK-TYPES

Details of the individual volcanoes and references are given in Table 2.1. Sample locations are given in Appendix 1.1 and brief petrographic descriptions in Appendix 2.1. Previous descriptions of the Banda Arc volcanics have been given in Jezek and Hutchison (1978), Hutchison and Jezek (1978) and Van Bergen et al. (1989).

The rocks from the active volcanoes can be subdivided into three groups, based on potassium contents (cf. Van Bergen et al., 1989; Fig. 3.1): (1) the low-K Banda Archipelago, (2) the medium-K Manuk-Serua group and (3) the high-K Nila-Teon-Damar group (using the classification of Gill, 1981). Andesites are the most abundant rock types, followed by basaltic andesites, whereas basalts are scarce. Acidic lavas occur only in the Banda Archipelago.

The *Banda Archipelago* consists of ten islands. The three main islands were sampled: Banda Api, Banda Neira and Banda Besar (or Lonthor). The geology of these islands has been described by Verbeek (1900). Rock compositions show the widest range in SiO₂ (51-70%) of all Banda Arc volcanoes. There is a small compositional gap between 56 and 58 % SiO₂.

Banda Api is the currently active strato-volcano and has a nearly perfect cone. Banda Api has formed within a caldera (Verbeek, 1900) and had many eruptions in historic times (Simkin et al., 1981), the latest being in May 1988. One sample (Banda 4) is from a lava flow from this eruption. Samples BA4-7 are from the summit area, all others, with label BA, are from coastal exposures around the volcano. The lavas from Banda Api are almost exclusively dacitic in composition.

Table 2.1. Characteristics of volcanoes from the Banda Arc

Code	Island	Active volcano	Depth Benioff zone (km)	Shortest distance to trench (km)	SiO ₂ range	K _{57.5}	Hydrous phases
BA	Banda	Banda Api	130	220	59-67	0.57	-
BN	Neira	-	130	220	51-66	0.64	-
BB	Besar	-	130	220	51-70	0.59	-
MA	Manuk	-	110	300	55-58	1.14	-
SE	Serua	Legatala	115	260	56-60	1.15	-
NI	Nila	Laworkawra	125	220(260)	52-63	2.12	amph
TE	Teon	Serawerna	130	220(240)	53-61	1.89	amph
DA	Damar	Wurlali	155	200(220)	53-60	2.43	amph, bi
RO	Romang	-	-	180(220)	57-72	1.70	amph

Depths to the Benioff zone are from Hutchinson (1982). A recent interpretation of seismic data (McCaffrey, 1989) indicates a different depth to the Benioff zone for the Banda Archipelago (BA, BN, BB): ≈ 90 km. The numbers in parenthesis are the distances measured along the convergence vector of the Indian-Australian plate (Minster and Jordan, 1978). No values can be given for the northern part due to unknown subduction geometry (see introduction). The SiO₂ range and K_{57.5} are based on Hutchison and Jezek (1978) and data from Chapter 4. K_{57.5} is wt% K₂O at SiO₂=57.5% (see also Fig. 3.1) based on linear correlations for every volcano. Hydrous phases: amph=amphibole and bi=biotite.

Verbeek (1900) interpreted the curved island of Banda Besar as a remnant of a caldera rim. Samples from Banda Besar are basalts (BB21A3, BB28), basaltic andesitic lava flows, hyaloclastics and pumice deposits (BL5-8).

Banda Neira is an elongated island, smaller than Banda Api and Banda Besar. Verbeek interpreted some of the hills (e.g. Papenberg) as remnants of old crater rims. Our samples are from coastal exposures. Sample BN9A is from Pulau Krakah, an islet between Banda Api and Banda Neira.

Manuk is a small, uninhabited strato-volcano. It has been described by Verbeek (1908) and is reported to be in a fumarolic stage (Simkin et al., 1981). However, we found a young block lava flow (less than 100 yr old?) at the summit. The crater of Manuk is open towards the sea in SE direction. The samples were obtained from coastal exposures (MA1-2) and from summit flows (MA3-5, of which MA3A-C are from the presumably young flow). The lavas from Manuk display relatively little compositional variation: $\text{SiO}_2=54-58\%$.

Serua has been described by Verbeek (1908) and Kuenen (1935). The main island is composed of an old eruption centre in the east, a young active volcano in the centre of the island (Gunung Legatala), and another old eruption centre in the west. Gunung Legatala's most recent eruption was in September 1921 (Simkin et al., 1981). Its summit is composed of a dome-like structure from which samples SE16-17 were taken. Pyroclastic rocks occur on the northern coast (e.g. pumice sample SE14). Samples SE26-28 are from two islets off the NW coast of Serua, the larger of which is named Kekeh-Besar. The Serua volcanics show a small range of composition (55-60% SiO_2), which is remarkable since the samples include the young cone, the older centres and the islets. There is a minor gap between 57 and 59% SiO_2 .

Nila, Teon and Damar have been described by Verbeek (1908) and Molengraaff (1916). Nila is a complex volcanic island with a caldera structure. The currently active part is on the southern slope of a cone (Laworkawra) which was developed on the caldera rim. This area has been highly altered by hydrothermal activity. Only phreatic eruptions have been reported. The latest event was on 4 May 1968 (Simkin et al., 1981). Samples NI15 and 16 are from the cone, all other samples are from the caldera rim, mainly from coastal exposures.

Teon is small island with a nearly round outline. The active centre is on the northern slopes of the mountain (Serawerna). The most recent eruption was in June 1904. Pyroclastic flows were found on the north-west coast (Verbeek, 1908). Sample TE5 is from this ash-flow deposit, presumably from the 1659-1693 eruptions, as suggested by ^{14}C datings on charcoal (Varekamp, pers. comm., 1992). Samples TE11, 12 and 13 are from the active area. All other samples are from coastal exposures in the NW (TE1-5, 15) and SW (TE14).

The island of Damar consists of an older volcanic complex in the western part and the active volcano (Gunung Wurali) on the eastern peninsula. Its latest eruption was in June 1892. The crater area is characterized by dome-like structures and has two craters (Molengraaff, 1916). Sample DA9A is from a dome-like structure on the summit. Samples DA5 and 8 are from the older volcanic complex, the others (DA1-4,6-7) from the south flank of Wurali volcano.

Nila, Teon and Damar are characterized by high-K compositions, except for the most mafic lavas which fall in the medium-K field. Andesites are the most common rock types,

followed by basaltic andesites. Only at Nila ($\text{SiO}_2=51-63\%$) were basaltic rocks found as mafic inclusions in andesites. Teon has SiO_2 between 53 and 62%. The small range found for Damar ($\text{SiO}_2=52-60\%$) may be the result of the limited number of fresh samples available for study.

The Romang Archipelago is composed of nine islands, of which *Romang* is the largest. They are briefly described by Verbeek (1908). This island group forms the eastern part of the southern inactive segment. Only hot-spring activity is still present. According to Verbeek (1908) the main island Romang consists largely of andesitic breccias and pyroclastic rocks (lapilli). Reef limestone occurs up to 535 m. All our samples are from western coastal exposures. The lavas are medium- to high-K, similar to those of the adjacent active volcanoes, and have a bimodal distribution of andesites ($\text{SiO}_2=57-60\%$) and rhyodacites ($\text{SiO}_2=71-72\%$).

Petrographical remarks

All of the lavas are highly porphyritic with plagioclase as a dominant phenocryst. Clinopyroxene, orthopyroxene and Fe-Ti oxide are the principle mafic phases. Olivine may occur in relatively SiO_2 -poor rocks and is sometimes replaced by orthopyroxene in samples with $\text{SiO}_2 > 55\%$. Hydrous minerals characterize lavas of Nila, Teon (amphibole) and Damar (amphibole+biotite). Their presence seems to be independent of SiO_2 content. Pseudomorphic aggregates of Fe-Ti oxide and clinopyroxene after amphibole were occasionally found as well. Amphibole also occurs in the rhyodacites of Romang.

Disequilibrium is an important petrographic characteristic of many of the Banda Arc volcanics. Colour banding and the presence of magmatic inclusions indicate this on a macroscopic scale. Basaltic or basalt-andesitic inclusions were found in andesitic host rocks at Nila, Teon and Damar. One type shows quench textures (small crystals and glass-rich groundmass; NI5B, NI15II, NI18A1, TE1B2, TE2B1, DA4), while another type has a cumulate-like texture (abundant large crystals and little or no glass; NI6, NI10AII-III). Microscopic disequilibrium (textures, mineral chemistry) is widespread: e.g. complex zoning patterns in clinopyroxenes, sieve textures in plagioclases, coexistence of different phenocryst populations in individual samples, the presence of quartz in the groundmass and of olivines with $\text{Fo} > 80\%$ in Serua samples.

Minor amounts of small xenoliths were occasionally found in thin sections of samples from each volcano. They mostly contain plag-cpx-opx and sometimes quartz. Metasedimentary carbonate-quartz xenoliths with diopside and hedenbergite as reaction products were found on Nila (e.g. lava NI10).

CHAPTER 3

SR-ND-PB ISOTOPE SYSTEMATICS OF THE BANDA ARC, INDONESIA: COMBINED SUBDUCTION AND ASSIMILATION OF CONTINENTAL MATERIAL

3.1. ABSTRACT

We present Sr, Nd and Pb isotope results and SiO₂, Rb, Sr, Sm, Nd, U, Th and Pb data for six active volcanoes and one extinct volcanic island distributed over the whole length of the Banda Arc. Rock types range from low-K tholeiitic in the NE to high-K calc-alkaline in the SW. The volcanoes in the NE have 'normal' arc signatures ($^{87}\text{Sr}/^{86}\text{Sr}=0.7045\text{-}0.7055$; $^{143}\text{Nd}/^{144}\text{Nd}=0.51273\text{-}0.51291$; $^{206}\text{Pb}/^{204}\text{Pb}=18.66\text{-}18.75$), whereas those in the SW have extreme values: $^{87}\text{Sr}/^{86}\text{Sr}=0.7065\text{-}0.7083$, $^{143}\text{Nd}/^{144}\text{Nd}=0.51252\text{-}0.51267$, $^{206}\text{Pb}/^{204}\text{Pb}=19.28\text{-}19.43$. Serua, situated in the central part, is the most anomalous volcano with regard to its Sr and Nd isotopic composition: $^{87}\text{Sr}/^{86}\text{Sr}=0.7075\text{-}0.7095$, $^{143}\text{Nd}/^{144}\text{Nd}=0.51240\text{-}0.51260$, but not with regard to Pb isotopes: $^{206}\text{Pb}/^{204}\text{Pb}=19.02\text{-}19.08$. The inactive island of Romang in the SW overlaps the Serua trends. The volcanoes display variable within-suite ranges in $^{87}\text{Sr}/^{86}\text{Sr}$ and $^{143}\text{Nd}/^{144}\text{Nd}$. Large ranges (e.g. at Nila) are consistent with assimilation (10-20%) of carbonate-bearing sediments from the arc crust. Despite the evidence for assimilation, it cannot explain all of the Sr-Nd isotopic trends found, and Banda Arc magmas must have already obtained a 'continental' signature at depth before they reached the arc crust.

Within-suite trends of Pb-isotopes are virtually absent. We found an extreme range in the volcanics along the arc which coincide with a similar trend in sediments in front of the arc, and consider this as strong evidence for the contribution of subducted continent-derived material (SCM) to magma sources. Bulk addition of 0.1-2% of local sediment in the NE Banda Arc, and of 1-3% in the SW Banda Arc, to an Indian-ocean MORB (I-MORB) source can explain the isotopic trends; both Serua and Romang require > 5% sediment. The Pb isotopes (e.g. $^{207}\text{Pb}/^{204}\text{Pb}$ - $^{208}\text{Pb}/^{204}\text{Pb}$) also suggest changes in the mantle end member from I-MORB to OIB-type. The latter becomes more conspicuous towards the SW, and has the high $^{208}\text{Pb}/^{204}\text{Pb}$ characteristic of Indian Ocean (Dupal) OIBs.

We suggest that mixing of magmas in the mantle wedge and/or in the arc crust was an important mechanism by which mantle and subducted end members were incorporated in the final products.

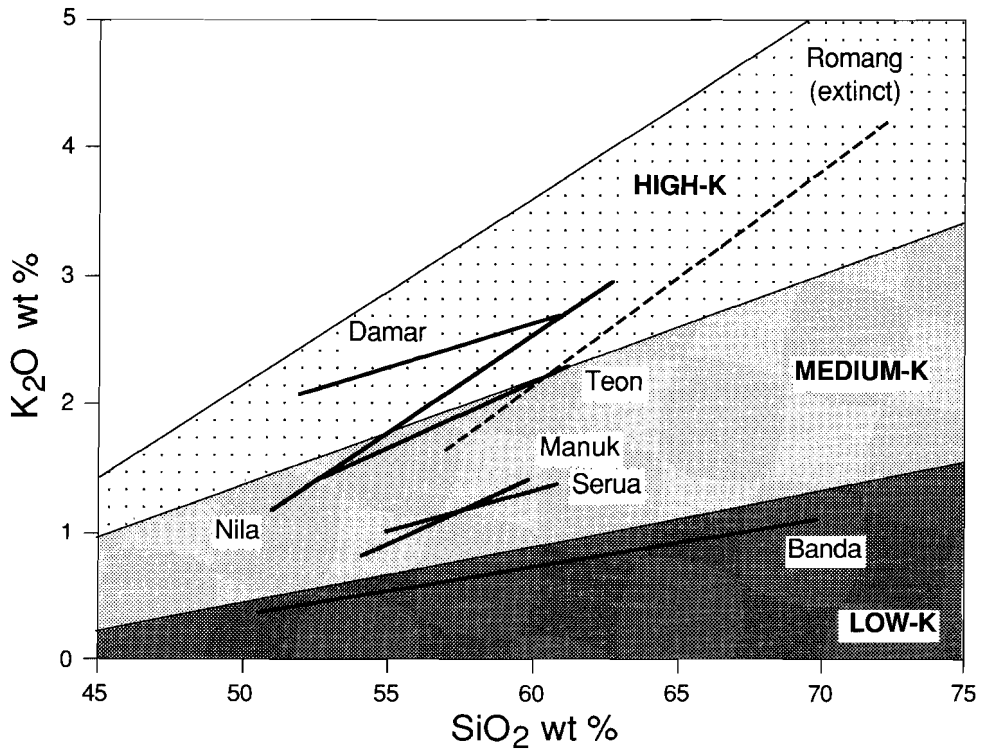


Fig. 3.1. SiO_2 - K_2O diagram (Gill, 1981) showing linear regression lines for individual volcanic centres of the Banda Arc. Note the large variation in K_2O at a given SiO_2 , the steep trends of Nila and Romang, and the limited within-suite ranges of Manuk and Serua.

3.2. INTRODUCTION

Since the pioneering isotopic studies of Whitford and co-workers (Whitford et al., 1977; Magaritz et al., 1978; Whitford and Jezek., 1979; Whitford et al., 1981) the Banda Arc has been widely cited as an example of an intra-oceanic island arc where terrigenous sediments are a conspicuous subducted source component. However, a reservation was made concerning the role of high-level assimilation processes within the arc crust, and subsequent work (Morris, 1984) has emphasized the potential importance of this.

The arc provides an unique setting for studying the contributions of subducted continental material because: (1) It is situated on oceanic crust which precludes major contamination with continental crustal lithosphere. (2) Large quantities of Precambrian continental material (reworked into sediments and in the form of Australian crustal

lithosphere) are available in front of the trench. (3) There are marked geochemical variations along the arc that allow us to test inferred sources and processes.

In this chapter, we discuss new Sr, Nd, Pb isotopic data and selected trace-element results for volcanoes along the full length of the arc, our aim being to assess the relative importance of subducted and assimilated material. We present evidence for along-arc changes in the nature and contributions of mantle sources and of the subducted components, using the isotopic signatures of sediments on the adjacent Australian shelf. Finally, we discuss mixing mechanisms by which subducted material became incorporated in the arc magmas.

3.3. RESULTS

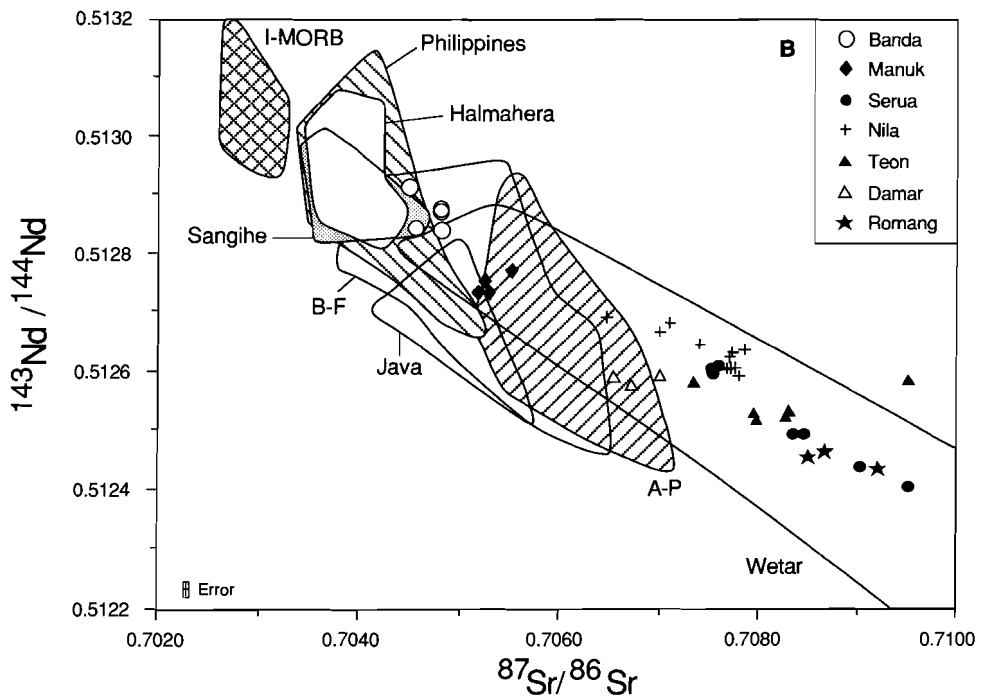
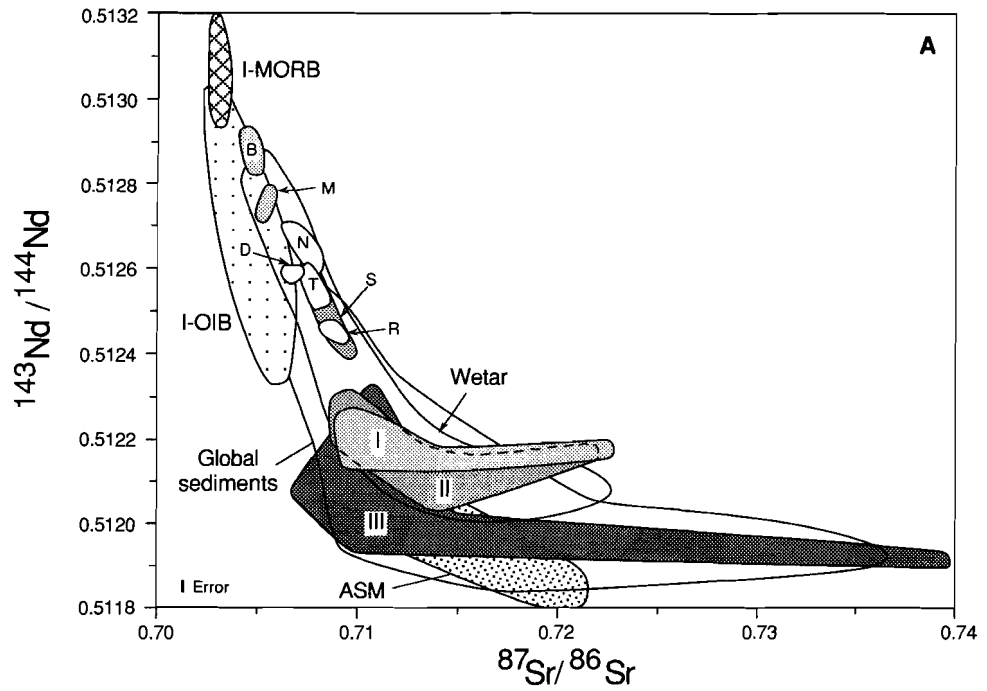
3.3.1. Rock-types and SiO₂-K₂O relationships

The rocks from the active Banda Arc volcanoes can be subdivided into three groups, based on potassium contents (cf. Van Bergen et al., 1989; Fig. 3.1): (1) the low-K Banda Archipelago, (2) the medium-K Manuk-Serua group and (3) the high-K Nila-Teon-Damar group (using the classification of Gill, 1981). Andesites are the most abundant rock types, followed by basaltic andesites, whereas true basalts are scarce. Acidic lavas occur only in the Banda archipelago.

(1) The *Banda Archipelago* show the widest range in SiO₂ (51-70%). A small gap exists between 56 and 58% SiO₂. Lavas from the currently active cone are almost exclusively dacitic.

(2) *Manuk and Serua* display slight variations in SiO₂ (54-58 and 55-60% SiO₂ respectively). The small range for Serua is remarkable since samples include the young cone, older parts of the main island as well as from some islets off the NW coast. There is a minor gap between 57 and 59% SiO₂.

(3) *Nila, Teon and Damar* are characterized by high-K compositions, except for the most mafic lavas which fall in the medium-K field. Andesites are the most common rock types, followed by basaltic andesites. Only at Nila (SiO₂=51-63%) were basaltic rocks found as mafic inclusions in andesites. Teon has SiO₂ between 53 and 62%. The small range found for Damar (SiO₂=52-60%) may be the result of the limited number of fresh samples available for study. We also analyzed volcanic rocks from Timor in the outer arc and the inactive island of Romang. The Timor sample (TTVF) is a 6-7 Ma old low-K tholeiitic pillow lava with SiO₂=53.3% (not shown in Fig. 3.1). The lavas from Romang are medium- to high-K, similar to those of the adjacent active volcanoes, and have a bimodal distribution of andesites (SiO₂=57-60%) and rhyodacites (SiO₂=71-72%).



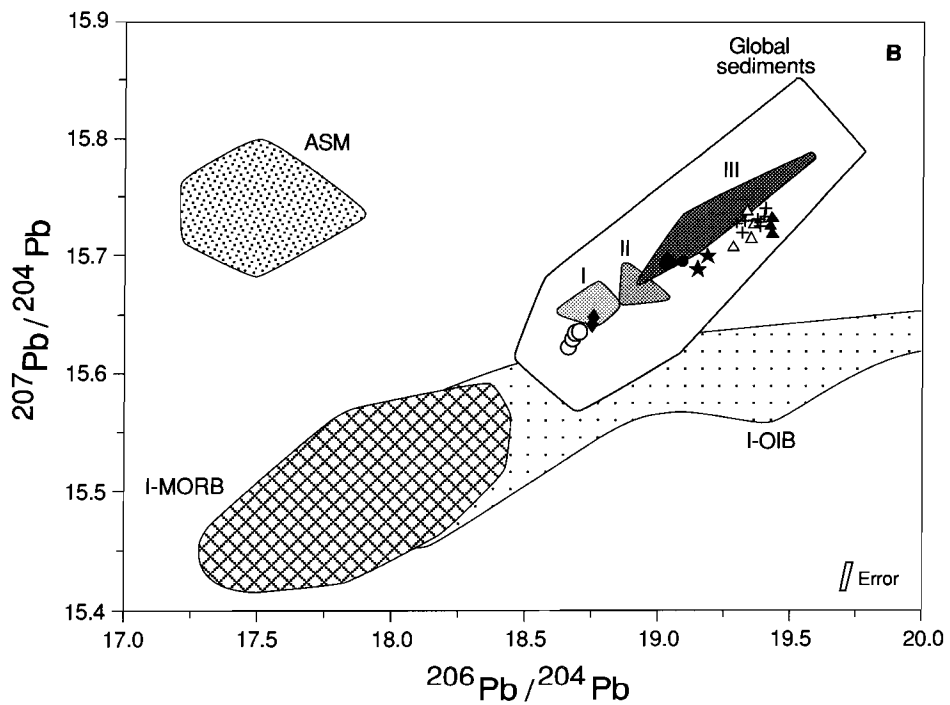
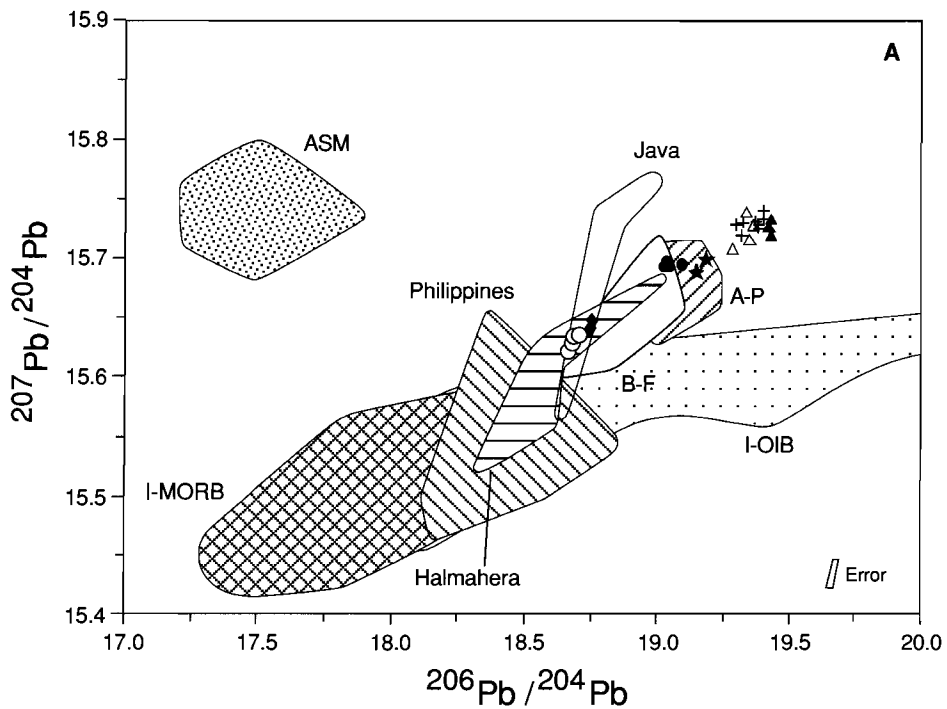
As was noted by Whitford and Jezek (1979), there is a systematic increase in potassium from Ambon-Banda in the NE to Damar in the SW. $K_{57.5}$ (% K_2O at 57.5% SiO_2) increases about fourfold along the arc from Ambon to Romang. The Nila and Romang lavas display steep SiO_2 - K_2O trends compared to the other volcanoes (Fig. 3.1), and are probably the result of magma mixing.

3.3.2. Sr and Nd isotopic compositions

Sr and Nd isotopic results are listed in Appendix 6 and are shown in Fig. 3.2. The Banda Arc volcanics display an extremely wide range in $^{87}Sr/^{86}Sr$ (0.7045-0.7095) and in $^{143}Nd/^{144}Nd$ (0.51291-0.51240). The $^{87}Sr/^{86}Sr$ ratios found are unusually high, and $^{143}Nd/^{144}Nd$ ratios low for 'normal' intra-oceanic island arcs (e.g. the Marianas, Lin et al., 1990), or even compared to arcs built on continental crust (e.g. parts of the Andes, Hildreth and Moorbath, 1988; Hickey et al., 1986). The Banda Arc shares these general characteristics with other arcs that provide evidence for subducted terrigenous sediments (e.g. Antilles, White and Dupre, 1986; Eolian Islands, Ellam et al., 1988; 1989).

(1) The *Banda Archipelago* display a small range in $^{87}Sr/^{86}Sr$ (0.70450-0.70485) and $^{143}Nd/^{144}Nd$ (0.51283-0.51291). Lavas from the active cone (Banda Api) have $^{87}Sr/^{86}Sr$ between 0.70475-0.70485 and a $^{143}Nd/^{144}Nd$ ratio of 0.51287. Slightly lower $^{87}Sr/^{86}Sr$ values (0.70450-0.70481) were found on two adjacent islands (Banda Neira and Lonthor), with variable $^{143}Nd/^{144}Nd$ (0.51283-0.51291).

Fig. 3.2a (overview) and 3.2b (detail). Sr and Nd isotopic ratios of the Banda Arc. Open circles: Banda Archipelago (B); diamonds: Manuk (M); solid circles: Serua (S); plusses: Nila (N); solid triangles: Teon (T); open triangles: Damar (D); stars: Romang (R). For comparison: I-MORB, global sediments, local sediments (Track I, II and III, see Fig. 2.1), Australian Subcontinental Mantle (ASM), the Philippines, the Sangihe Arc, Halmahera Arc and the Java, Bali-Flores (B-F), Adonara-Pantar (A-P) and Wetar sectors of the Sunda-Banda Arc. Errors based on 2 sd. Data sources: I-MORB: Hamelin and Allegre (1985), Hamelin et al. (1986), Price et al. (1986), Michard et al. (1986), Ito et al. (1987), Dosso et al. (1988), anomalous samples not plotted; I-OIB: literature compilation by W.M. White; ASM: McCulloch et al. (1983), Fraser et al. (1986) and Nelson et al. (1986); Global sediment: Goldstein and O'Nions (1981), White et al. (1985), Von Drach et al. (1986), Ben Othman et al. (1989), Chen et al. (1990), McLennan et al. (1990). Local sediments: box- and piston cores from the wedge and shelf (see Chapter 5; Fig. 2.1 for locations of Track I, II and III). Philippines: Knittel et al. (1988), Defant et al. (1991); Sangihe: Tatsumi et al. (1991); Halmahera: Morris et al. (1983); Java: Whitford et al. (1975), Whitford et al. (1981), White and Pachett (1984); Bali-Flores: Varne and Foden (1987), Wheller et al. (1987); Stolz et al. (1990); A-P: Stolz et al. (1988), Stolz et al. (1990), Vroon et al. (1990a); Wetar: McCulloch et al. (1982).



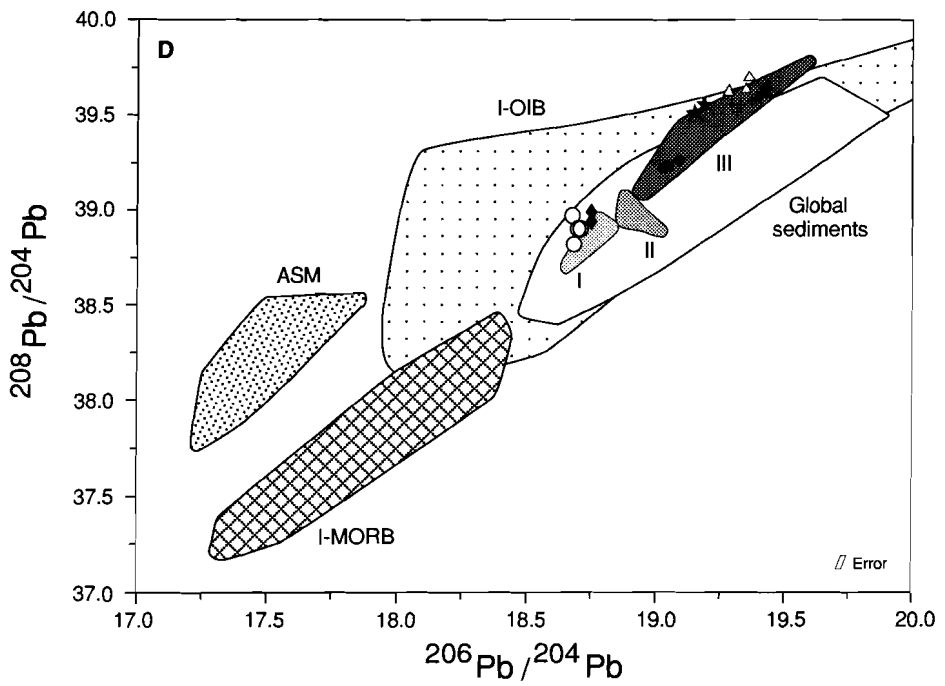
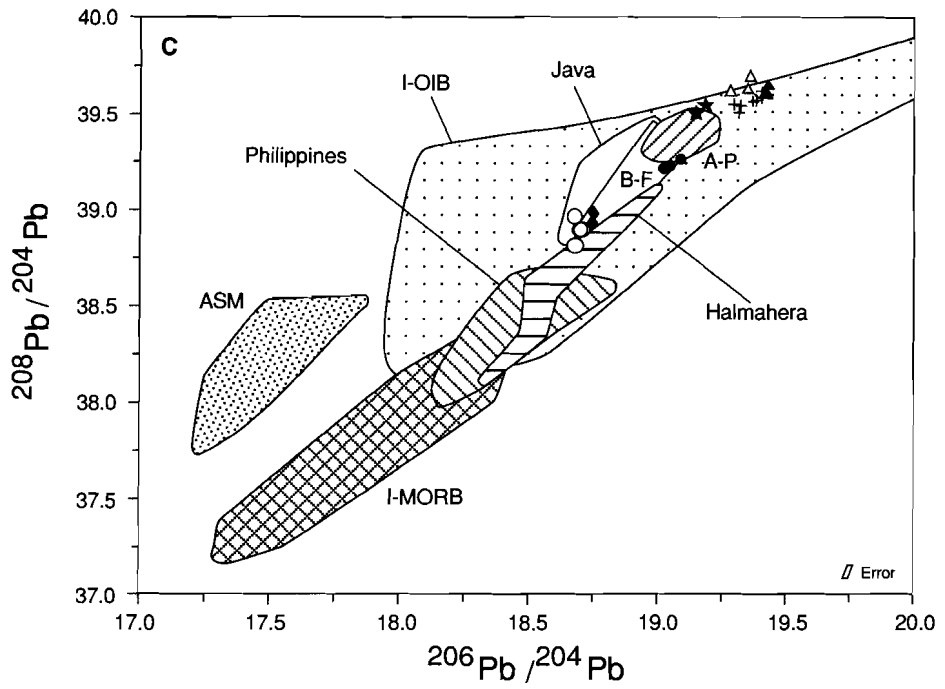
(2) Although *Manuk and Serua* have similar major- and trace-element compositions, there are large isotopic differences between these centres. The lavas from *Manuk* display a very small range in $^{87}\text{Sr}/^{86}\text{Sr}$ (0.70519-0.70552) and $^{143}\text{Nd}/^{144}\text{Nd}$ (0.51273-0.51277). *Serua* shows an extremely large variation and, together with *Romang*, the most 'continental' values (e.g. radiogenic $^{87}\text{Sr}/^{86}\text{Sr}$, $^{206}\text{Pb}/^{204}\text{Pb}$ and unradiogenic $^{143}\text{Nd}/^{144}\text{Nd}$) of the whole arc. There are three isotopically distinct groups: (i) Lavas from the two islets off the northeast coast and a pumice sample from one locality on the main island give $^{87}\text{Sr}/^{86}\text{Sr}$ values of 0.70755-0.70779 and $^{143}\text{Nd}/^{144}\text{Nd}$ of 0.51259-0.51260. (ii) Two samples from the currently active cone have $^{87}\text{Sr}/^{86}\text{Sr}$ of 0.70835 and 0.70841 and $^{143}\text{Nd}/^{144}\text{Nd}$ of 0.51249. (iii) Samples from the NW part the main island have $^{87}\text{Sr}/^{86}\text{Sr}$ between 0.70895-0.70952 and $^{143}\text{Nd}/^{144}\text{Nd}$ between 0.51240-0.51244. A similar grouping is visible in the $^{87}\text{Sr}/^{86}\text{Sr}$ data of Whitford and Jezek (1979). The wide isotopic range of *Serua* is remarkable given the limited spread in most major and incompatible trace-element concentrations.

(3) *Nila, Teon and Damar*. Within this group *Nila* shows the widest range: $^{87}\text{Sr}/^{86}\text{Sr}=0.70646-0.70784$ and $^{143}\text{Nd}/^{144}\text{Nd}=0.51259-0.51269$. The least radiogenic Sr and most radiogenic Nd values were found in the basaltic-andesitic and basaltic inclusions. The andesitic host lavas have significantly higher $^{87}\text{Sr}/^{86}\text{Sr}$ ratios (e.g. NI18AI+II; mafic inclusion: 0.70646, host: 0.70700, see Fig. 3.6b). Nd isotopes show similar differences. Macroscopically visible colour streaks in these hosts are indicative of incomplete magma mixing, which may imply that these samples contain end-member components that are still higher in $^{87}\text{Sr}/^{86}\text{Sr}$ and lower in $^{143}\text{Nd}/^{144}\text{Nd}$. The Sr-Nd isotope trend of the *Nila* samples tends to plot at higher $^{143}\text{Nd}/^{144}\text{Nd}$ values for given $^{87}\text{Sr}/^{86}\text{Sr}$ values compared to the other islands in the southern and central Banda Arc. On average *Teon* exhibits somewhat more 'continental' values than *Nila*; these roughly overlap with groups i and ii of *Serua* ($^{87}\text{Sr}/^{86}\text{Sr}=0.70734-0.70830$ and $^{143}\text{Nd}/^{144}\text{Nd}=0.51252-0.51259$).

In contrast to the *Nila* results, one mafic inclusion analyzed (TE1B2) is identical to the andesitic host (TE1C). A second mafic inclusion (TE2B1) has an anomalously high $^{87}\text{Sr}/^{86}\text{Sr}$ ratio of 0.70951 but a slightly higher $^{143}\text{Nd}/^{144}\text{Nd}$ (0.51258, values of the host TE1C are 0.70797 and 0.51252). Because of its fresh appearance in thin section, and because there was little change in the result after strong leaching with hot 6N HCl, the values are not

Fig. 3.3a. $^{206}\text{Pb}/^{204}\text{Pb}$ - $^{207}\text{Pb}/^{204}\text{Pb}$ diagram: Banda Arc volcanoes compared to I-MORB, OIB, ASM, other arcs (Philippines and Halmahera) and sectors of the Sunda Arc (Java, B-F, A-P). Symbols and abbreviations as in Fig. 3.2b.

Fig. 3.3b. $^{206}\text{Pb}/^{204}\text{Pb}$ - $^{207}\text{Pb}/^{204}\text{Pb}$ diagram: Banda Arc volcanics compared to I-MORB, OIB, ASM, global- and local sediments (Tracks I, II and III, see Fig. 2.1). Symbols and abbreviations as in Fig. 3.2b.



considered to be the result of any alteration. In the absence of a satisfactory explanation we shall omit this sample in further discussions. The lavas from Damar have fairly constant Sr- and Nd-isotopic ratios: $^{87}\text{Sr}/^{86}\text{Sr}=0.70654\text{-}0.70702$ and $^{143}\text{Nd}/^{144}\text{Nd}=0.51257\text{-}0.51259$. One basaltic-andesitic inclusion analyzed (DA4) is identical to the lavas.

No isotopic data have been previously reported for the inactive island of Romang. Both the basaltic andesites and the rhyodacites have high $^{87}\text{Sr}/^{86}\text{Sr}$ (0.70852-0.70926) and low $^{143}\text{Nd}/^{144}\text{Nd}$ ratios (0.51243-0.51245). Whitford et al. (1977) reported a similar Sr-isotope ratio of 0.70908 for one lava from Maupura in the vicinity of Romang.

The extremely 'continental' signatures for the arc as a whole are broadly consistent with the previous results of Whitford and Jezek (1979); Whitford et al. (1977, 1981). Only Banda and Manuk in the NE have $^{87}\text{Sr}/^{86}\text{Sr}$ and $^{143}\text{Nd}/^{144}\text{Nd}$ values close to those of 'normal' island arcs (e.g. the low Ce/Yb group of Hawkesworth et al., 1991). The considerable within-suite ranges often found for the other volcanoes are indicative of different styles of evolution processes and will be discussed below.

Compared to the other arcs in the Indonesian region, the Banda Arc tends to plot at higher $^{87}\text{Sr}/^{86}\text{Sr}$ for a given $^{143}\text{Nd}/^{144}\text{Nd}$ (Fig. 3.2a). The Banda Archipelago partly overlap with the Sangihe Arc (Tatsumi et al., 1991) of North Sulawesi and are similar in $^{143}\text{Nd}/^{144}\text{Nd}$ but somewhat more radiogenic in $^{87}\text{Sr}/^{86}\text{Sr}$ than the Halmahera Arc (Morris et al., 1983) situated north of the Banda Arc. The SW volcanoes of the Banda Arc partly overlap with the easternmost sector of the active Sunda Arc. (Stolz et al., 1988, 1990; Vroon et al., 1990a).

The entire trend of the Banda Arc is encompassed by Wetar Island, within the extinct transition between the arcs (McCulloch et al., 1982). Sr-isotope data reported for other extinct volcanic islands of this segment, e.g. Alor (0.7077) and Autauro (0.7066-0.7082) (Whitford et al., 1977) overlap with those of the Southern Banda Arc volcanoes. The 0.4 Ma high-Mg basalt dredged from a sea-mount north of Wetar is comparable in $^{87}\text{Sr}/^{86}\text{Sr}$ (0.7074)

Fig. 3.3c. $^{206}\text{Pb}/^{204}\text{Pb}$ - $^{208}\text{Pb}/^{204}\text{Pb}$ diagram: Banda Arc volcanoes compared to I-MORB, OIB, ASM, other arcs (Philippines and Halmahera) and sectors of the Sunda Arc (Java, B-F, A-P). Symbols and abbreviations as in Fig. 3.2b.

Fig. 3.3d. $^{206}\text{Pb}/^{204}\text{Pb}$ - $^{207}\text{Pb}/^{204}\text{Pb}$ diagram: Banda Arc volcanics compared with I-MORB, OIB, ASM, global- and local sediments (Tracks I, II and III, see Fig. 2.1). Errors are based on 2 sd on 18 runs of NBS981. Symbols and abbreviations as in Fig. 3.2b. References: I-MORB: Sun (1980), Dupre and Allegre (1983), Hamelin and Allegre (1985), Hamelin et al. (1986), Michard et al. (1986), Price et al. (1986), Ito et al. (1987), Dosso et al. (1988), anomalous samples omitted; I-OIB: literature compilation by W.M. White. ASM: Frasnier et al. (1986) and Nelson et al. (1986); Global sediment: Church (1976), Meijer (1976), Sun (1980), Barreiro (1983), White et al. (1985), Woodhead and Fraser (1985), Ben Othman et al. (1989); Philippines: Mukasa et al. (1987); Halmahera: Morris et al. (1983); Java: Whitford (1975b); Bali-Flores (B-F): Varne and Foden (1987), Wheller et al. (1987), Stolz et al. (1990); A-P: Stolz et al. (1988); Stolz et al. (1990); Vroon et al. (1990).

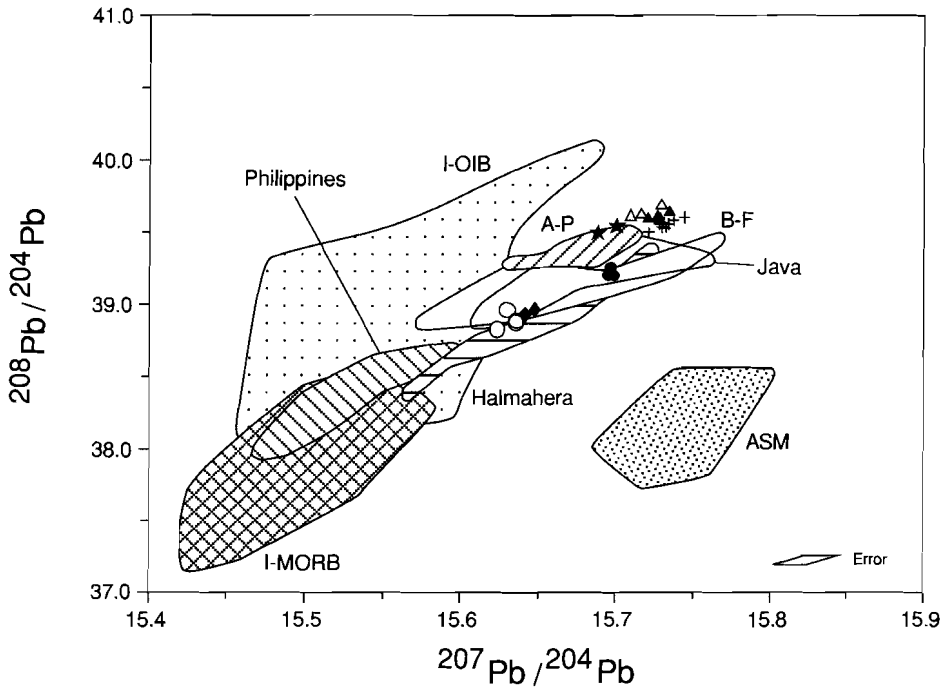


Fig. 3.4. $^{207}\text{Pb}/^{204}\text{Pb}$ - $^{208}\text{Pb}/^{204}\text{Pb}$ diagram for Banda Arc lavas, I-MORB, ASM, OIB and SE Asian arcs. Note that the AP segment and Southern Banda Arc islands (Nila-Teon-Damar-Romang) do not point towards the I-MORB field, in contrast to Halmahera and the Philippines. Symbols and abbreviations as in Fig. 3.2b. References as in Fig. 3.3.

and $^{143}\text{Nd}/^{144}\text{Nd}$ (0.5125) with the Nila-Teon-Damar group (Morris et al., 1984). The cordierite-bearing lavas of Ambon in the northern extinct segment are characterized by extreme values: $^{87}\text{Sr}/^{86}\text{Sr}=0.7158-0.7175$, $^{143}\text{Nd}/^{144}\text{Nd}=0.51215$ (Magaritz et al., 1978; Morris, 1984), ratios not found in the active Banda Arc. One Ambon basalt (Magaritz et al., 1978; Morris, 1984) has $^{87}\text{Sr}/^{86}\text{Sr}$ (0.7044) and $^{143}\text{Nd}/^{144}\text{Nd}$ (0.51275), these ratios are similar to those of the Banda Archipelago.

3.3.3. Pb isotopic compositions

Pb isotopes results are given in Appendix 6 and illustrated in Figs. 3.3a-d and 3.4. The Banda Arc samples have higher radiogenic Pb-isotope ratios (e.g. $^{206}\text{Pb}/^{204}\text{Pb}=18.6-19.4$) than other island arcs. Values for the southwestern part are the most radiogenic, and are comparable to those of the Lesser Antilles (White and Dupre, 1986). The overall range is extremely large and covers some two-thirds of the compositions of global marine sediments (e.g. White et al., 1985; Ben Othman et al., 1989).

Individual volcanoes have distinct Pb-isotope signatures. In contrast to the Sr-Nd trends found, there are hardly any within-suite variations. Also, there is a more systematic along-arc increase in $^{206}\text{Pb}/^{204}\text{Pb}$, $^{207}\text{Pb}/^{204}\text{Pb}$ and $^{208}\text{Pb}/^{204}\text{Pb}$ in the active centres from NE to SW. A parallel along-arc increase is observed in the local sediments (cf. Fig. 3.3 and 3.5), although it is of interest to note that the volcanics tend to have higher $^{208}\text{Pb}/^{204}\text{Pb}$ for a given $^{207}\text{Pb}/^{204}\text{Pb}$ than the sediments (Chapter 5).

The lavas from (1) The *Banda Archipelago* have the lowest $^{206}\text{Pb}/^{204}\text{Pb}$ (18.6-18.7) which is comparable to other oceanic-arc values (Barreiro, 1983; Meijer, 1976; Woodhead et al., 1987).

(2) *Manuk and Serua* have values between the Banda Archipelago and the Southern Banda Arc, but Manuk has $^{206}\text{Pb}/^{204}\text{Pb}=18.75$ and is isotopically closer to the Banda Archipelago than to Serua. Serua is the only volcano with a significant within-suite variation in $^{206}\text{Pb}/^{204}\text{Pb}$ (19.02-19.08), which correlates negatively with $^{87}\text{Sr}/^{86}\text{Sr}$ (cf. Morris, 1984).

(3) *Nila, Teon and Damar* show the highest $^{206}\text{Pb}/^{204}\text{Pb}$ (19.28-19.43). These values are also more radiogenic than those of the volcanoes on the other side of the inactive collision area in the easternmost Sunda Arc (Fig. 3.3a and 3.3c; Stolz et al., 1990; Vroon et al., 1990a). Romang is somewhat less radiogenic ($^{206}\text{Pb}/^{204}\text{Pb}=19.15-19.18$), and plots between Serua and the active volcanoes of the SW Banda Arc.

The Banda Arc includes the most radiogenic Pb-isotopic compositions of the SE-Asia arcs (Fig. 3.3a, 3.3c and 3.4), disregarding the anomalously high $^{207}\text{Pb}/^{204}\text{Pb}$ rocks of Java (Whitford, 1975b). The Philippines field (Mukasa et al., 1987) is closest to the I-MORB field, whereas Halmahera (Morris et al., 1983) includes more radiogenic values and overlaps with the NE centres of the Banda Arc. The intermediate values of Serua and Romang fall in or close to the fields of the Eastern Sunda Arc sectors (Stolz et al., 1990; Vroon et al., 1990a). Pb-isotope data for the inactive Banda Arc sectors are available for Ambon only (Morris, 1984). Acidic rocks plot between Banda-Manuk and Serua, while the Ambon basalt is comparable to the Banda Archipelago with regard to Pb isotopic ratios. Interestingly, the high-Mg basalt dredged north of Wetar yielded values (e.g. $^{206}\text{Pb}/^{204}\text{Pb}=19.46$) that are even more radiogenic than found in the entire active arc (Morris et al., 1984).

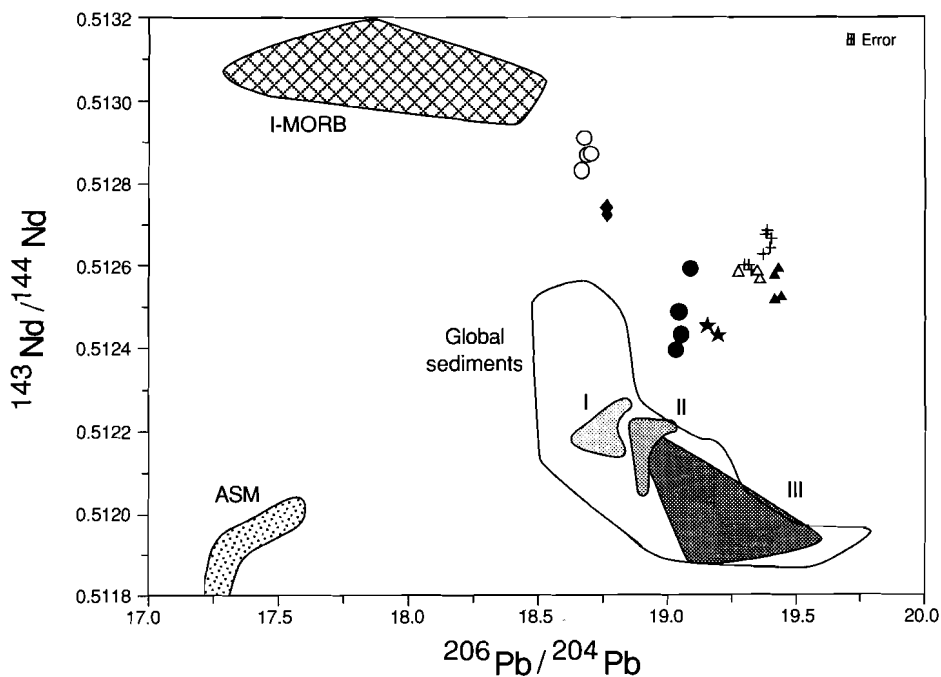


Fig. 3.5. $^{206}\text{Pb}/^{204}\text{Pb}$ - $^{143}\text{Nd}/^{144}\text{Nd}$ diagram for Banda Arc volcanics, I-MORB, global sediment, local sediments of Tracks I, II and III, see also Fig. 2.1. Note the NE-SW trend in $^{206}\text{Pb}/^{204}\text{Pb}$ of the volcanics follows that of the local sediments. Errors are 2 sd. I-MORB from: Hamelin and Allegre (1985), Hamelin et al. (1986), Michard et al. (1986), Price et al. (1986), Ito et al. (1987), Dosso et al. (1988), anomalous samples not plotted; Global sediment from: White et al. (1985), Ben Othman et al. (1989); ASM from: McCulloch et al. (1983), Fraser et al. (1986) and Nelson et al. (1986).

3.4. DISCUSSION

3.4.1. Introduction

The most important question concerning the origin of the marked continental signatures of the Banda Arc volcanics is how to distinguish between deep, subducted and shallow, assimilated terrigenous material. According to the regional configuration the subducted component can be either the continental crust or detrital sediments derived from it. Because of the difficulty in differentiating between the two with the isotopic data presented here, we shall use the term 'subducted continental material' (SCM).

The following observations are consistent with the involvement of subducted continent derived material:

- (1) The high $^{87}\text{Sr}/^{86}\text{Sr}$ and low $^{143}\text{Nd}/^{144}\text{Nd}$ ratios for an intra-oceanic island arc.
- (2) The steep $^{206}\text{Pb}/^{204}\text{Pb}$ - $^{207}\text{Pb}/^{204}\text{Pb}$ trend (cf. Gill, 1981).
- (3) The observation that Pb isotopes of the volcanics closely follow the NE-SW trend of increasing $^{206}\text{Pb}/^{204}\text{Pb}$, $^{207}\text{Pb}/^{204}\text{Pb}$ and $^{208}\text{Pb}/^{204}\text{Pb}$ ratios in the local sediments.

Furthermore, low $^3\text{He}/^4\text{He}$ ratios that characterise the Banda and East Sunda Arc, in contrast to the normal arc values in the Western Sunda Arc (Poreda and Craig, 1989; Hilton and Craig, 1989), also point to the involvement of SCM.

However, before addressing the role of deep source components, it is necessary to investigate the large within-suite ranges in some of the Banda Arc volcanoes, since they provide clear evidence for assimilation of portions of the up to ≈ 2 km thick sediments that cover the oceanic crust of the Banda Sea (e.g. Hartono, 1990).

3.4.2. Evidence for local effects of assimilation

The large Sr-Nd isotopic variation at Serua, Nila and Teon points to the involvement of several isotopically distinct components. For Nila and Teon, positive correlations between Sr-Nd isotope ratios and differentiation indices such as SiO_2 (Fig. 3.6a) are qualitative indications for shallow-level assimilation. The Serua suite lacks such co-variations.

The high-K calc-alkaline lavas of *Nila* provide the best starting point for an evaluation of the various options for open-system behaviour, given its wide chemical and isotopic range. The lavas contain mafic inclusions which have lower $^{87}\text{Sr}/^{86}\text{Sr}$ ratios than their hosts (Fig. 3.6b). The occasional presence of (meta-)sedimentary inclusions in some samples provides evidence for assimilation at shallow levels in the arc crust, probably of sea-floor sediments. The inclusions contain quartz- and carbonate-bearing associations showing variable degrees of thermometamorphic overprints (e.g. hedenbergitic pyroxene) as indicators of incomplete assimilation.

Carbonate-bearing sediments have been found in box cores close to Nila (Chapter 5), and a satisfactory mixing curve can be constructed between such a sediment (G5-4-99B) and a Manuk-type magma in terms of Sr-Nd isotope relations (Fig. 3.7). Sediment types with less carbonate (e.g. G5-1-2P) or terrigenous sediments (e.g. G5-4-106B), which have also been recovered from this region, are unlikely assimilants. The composition of the medium-K basaltic andesite of Manuk may be a plausible end member, because: (1) there is no chemical or isotopic evidence for assimilation in the Manuk series; (2) a high-K calc-alkaline Damar-type magma is not a reasonable alternative because it does not produce fitting mixing curves.

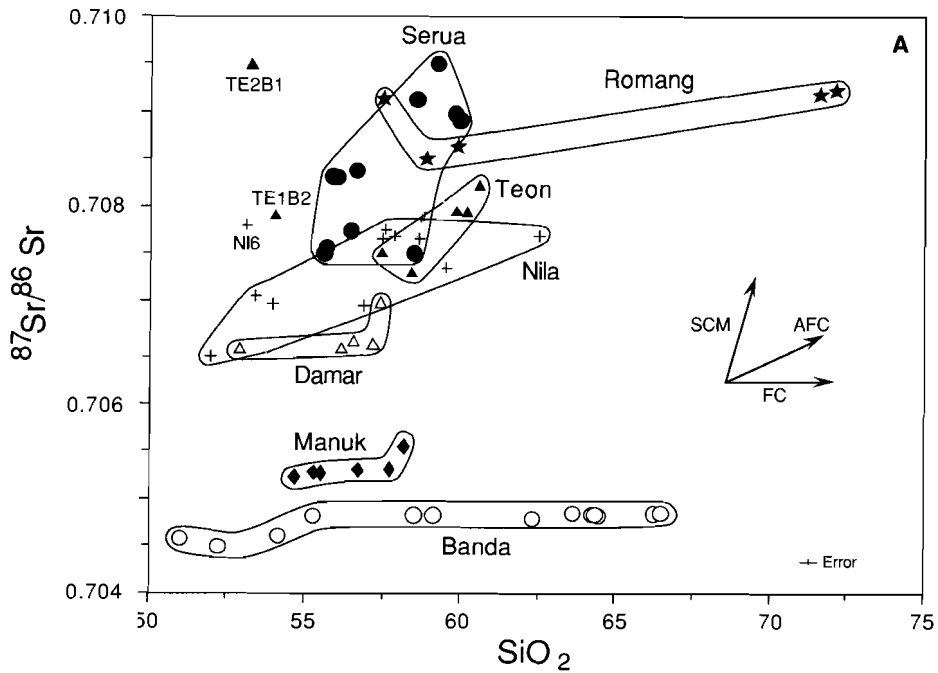


Fig. 3.6a. SiO_2 - $^{87}\text{Sr}/^{86}\text{Sr}$ diagram of the Banda Arc volcanics. Symbols as in Fig. 3.2b. Nila (NI6) and Teon (TE1B2) samples plotting outside the fields are inclusions with cumulate textures. Teon sample TE2B1 is omitted (see text). Note the positive trends of Nila and Teon, the constant $^{87}\text{Sr}/^{86}\text{Sr}$ ratios of Banda, Manuk and Damar, and the large range of Serua with only a limited spread in SiO_2 . SCM = Subducted Continental Material, AFC = Assimilation-Fractional Crystallization and FC = Fractional Crystallization.

The calculated maximum amount of assimilation by bulk mixing is quite large: 20%. However, the isotopic disequilibrium between the mafic inclusions and their hosts indicates that magmas with different isotopic signatures coexisted within single reservoirs. It is conceivable that the mafic inclusions are in composition closest to SCM-influenced mantle magmas, whereas only the more acid host rocks are dominated by assimilation. Starting from mafic inclusion NI18AI, it is possible to model the Nila trends by combined assimilation and fractional crystallization (AFC; DePaolo, 1981a), using the same carbonate-rich sedimentary end member (G5-4-99B) as in the Sr-Nd bulk mixing model. The maximum amount of assimilant is then less than 13%, depending on the distribution coefficients and the assimilant/crystallization mass ratio taken. The AFC models were tested for Sr isotopes and incompatible trace elements (Ba, Rb, Th and Hf), and yielded consistent results (Table 3.1). Although the most extreme Sr-isotopic compositions can therefore be explained by assimilation, the Nila magmas were probably already relatively high in $^{87}\text{Sr}/^{86}\text{Sr}$ prior to

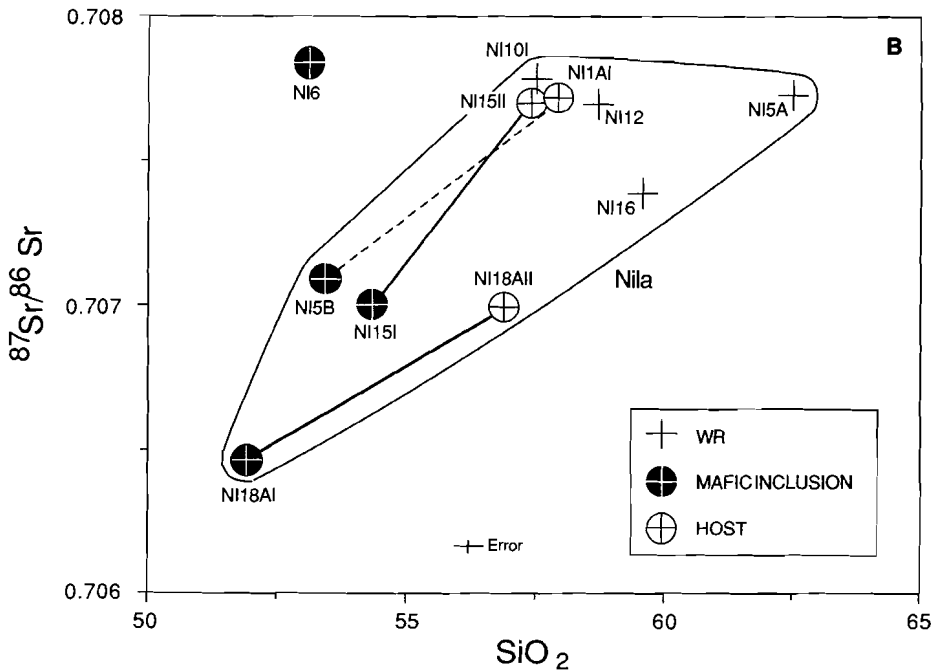


Fig. 3.6b. SiO₂ - ⁸⁷Sr/⁸⁶Sr diagram of the Nila volcanics (detail of Fig. 3.6a). Tie lines connect mafic inclusions and their hosts. One is dashed because the inclusion was found separate from the lava. Labels indicate sample numbers. WR=Whole Rock.

shallow-level contamination, given the SCM signatures of Manuk and of the mafic inclusions.

Teon volcanics displays features comparable to those of Nila, and tends to show a positive correlation between ⁸⁷Sr/⁸⁶Sr and SiO₂ (Fig. 3.6a), if samples with cumulate textures are omitted. In terms of Sr-Nd isotopes (Fig. 3.7) *Teon* lavas could have assimilated more than 30% of sediment 99B, starting from a Damar-type composition. More likely, the starting isotopic compositions were derived from carbonate poor SCM and only the within-suite trend was influenced by assimilation.

Serua is the most intriguing volcano in the Banda Arc. It combines an extremely wide range in Sr-Nd isotopic ratios with little chemical spread in compatible and incompatible elements. These features are difficult to reconcile with conventional low-pressure evolution models. Assimilation of a single sedimentary rock with a fixed Sr/Nd ratio starting from a Manuk-type magma would not explain the isotopic range. A strong heterogeneity of the local sediment pile (i.e. with variable carbonate contents), and high amounts of assimilation (20-50% in the case of bulk addition) would have to be invoked. Although it has been

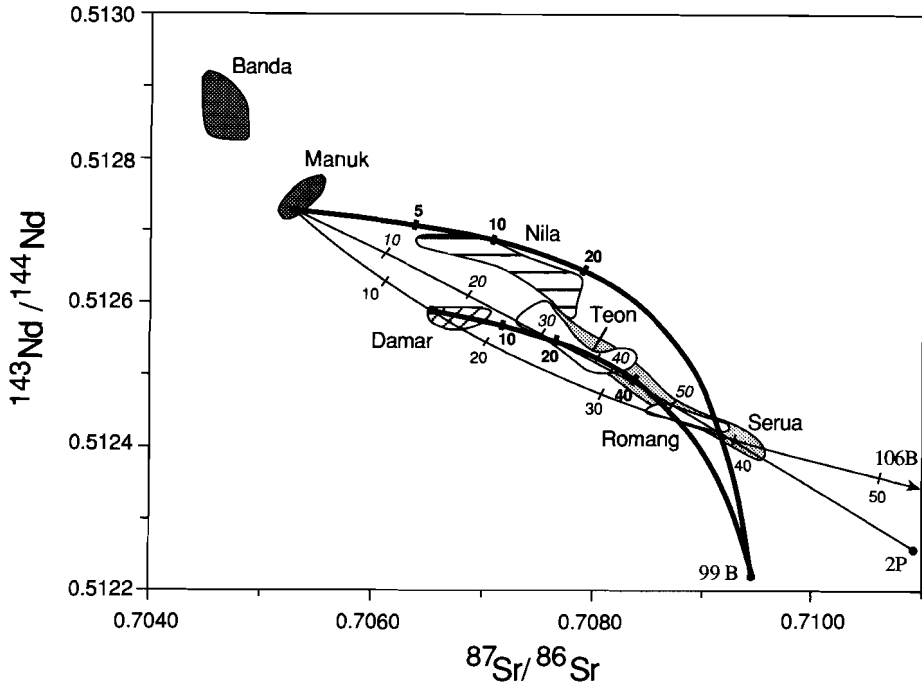


Fig. 3.7. $^{87}\text{Sr}/^{86}\text{Sr}$ - $^{143}\text{Nd}/^{144}\text{Nd}$ bulk-mixing models to illustrate hypothetical options for assimilation of local sediments (Chapter 5) by Manuk- or Damar-type magmas. The Manuk magma is assumed to have Sr=220 ppm, Nd=15 ppm, $^{87}\text{Sr}/^{86}\text{Sr}$ =0.70528, $^{143}\text{Nd}/^{144}\text{Nd}$ =0.51273; Damar: Sr=600 ppm, Nd=23 ppm, $^{87}\text{Sr}/^{86}\text{Sr}$ =0.70654, $^{143}\text{Nd}/^{144}\text{Nd}$ =0.51259. Sediments G5-4-99B and G5-4-106B are taken from the Weber Deep on Track II (see Fig. 2.1) and G5-1-2P from the Banda Ridges. G5-1-2P has Sr=344 ppm, Nd=20.4 ppm, $^{87}\text{Sr}/^{86}\text{Sr}$ =0.71092, $^{143}\text{Nd}/^{144}\text{Nd}$ =0.51226, CaCO_3 =13.0%; G5-4-99B: Sr=1527 ppm, Nd=12.0 ppm, $^{87}\text{Sr}/^{86}\text{Sr}$ =0.70944, $^{143}\text{Nd}/^{144}\text{Nd}$ =0.51222, CaCO_3 =49.8%; G5-4-106B: Sr=106 ppm, Nd=29.5 ppm, $^{87}\text{Sr}/^{86}\text{Sr}$ =0.72169, $^{143}\text{Nd}/^{144}\text{Nd}$ =0.51217, CaCO_3 =0%. Tick marks indicate percentages of sediment added. Nila compositions would require 5-20% addition of sediment 99B to a Manuk magma, and Teon compositions 10-30% addition of the same sediment to a Damar magma. For Serua a single assimilant cannot explain the Sr-Nd trend. For the samples with the highest $^{87}\text{Sr}/^{86}\text{Sr}$ at least 40-50% of sediments 106B or 2P would be required. See text for discussion of more complex alternatives.

suggested that high assimilation proportions and variability of arc crustal material may explain extreme isotopic signatures of volcanoes in other SCM-influenced arcs (Davidson and Harmon, 1989; Ellam and Harmon, 1990), this seems unlikely in the case of Serua.

We consider a subducted component a more plausible alternative, at least for the high $^{87}\text{Sr}/^{86}\text{Sr}$ group, because of the similarity between the major- and trace-element compositions of Serua and Manuk (cf. Fig. 3.1). Much larger differences would be expected than observed, if up to 50% sediment with a dominant terrigenous fraction (e.g. G5-1-2P) had

Table 3.1. AFC calculations

Element	K_d	NI18AI	G5-4-99B
Rb	0.01	46	51
Ba	0.01	322	450
Th	0.001	4.4	5.1
Hf	0.2	1.6	1.7
$^{87}\text{Sr}/^{86}\text{Sr}$		0.70519	0.70944

End-member compositions in AFC calculations for Nila. NI18AI from this Chapter and Chapter 4; composition of G5-4-99B sediment from Chapter 5. K_d values are from Gill (1981).

Sample	NI15I	NI5B	NI15II	NI18AII	NI12	NI1A1	NI16	NI5A
R	0.5	0.2	0.1	0.1	0.2	0.2	0.15	0.15
	F A	F A	F A	F A	F A	F A	F A	F A
Rb	- -	78 6	64 4	60 4	52 12	60 14	53 8	44 11
Ba	75 21	71 6	55 4	60 4	50 13	50 13	50 8	44 13
Th	78 22	89 7	53 4	57 4	57 14	55 13	46 8	39 11
Hf	77 23	75 6	57 4	53 3	42 10	39 10	46 6	42 11
mean-% assim.	22	8	4	4	12	13	8	12

Results for the Assimilation Fractional Crystallization (AFC) model (DePaolo, 1981a) using NI18AI as starting composition and carbonate-rich sediment G5-4-99B as assimilant. Abbreviations: R=mass assimilant/mass fractional crystallization; F=percentage of liquid remaining and A=percentage of assimilated rock, in this case sediment G5-4-99B. Note the quite consistent results for each sample.

been added to a Manuk-type parental magma. Incompatible trace-element abundances (e.g. LREE, see Chapter 4) are far too low compared to calculated Manuk-sediment mixtures. AFC instead of bulk mixing would make this difference even worse.

The cases of Nila and Serua suggest that assimilation and source contamination may have affected the individual Banda Arc volcanoes to variable extents. Other examples presenting evidence for two-stage source and arc crust contamination are Martinique, Lesser

Antilles (Davidson, 1986; Davidson and Harmon, 1989) and the Eolian Arc, Italy (Ellam and Harmon, 1990). The arc-wide variation in Sr isotopes at relatively constant SiO₂ (Fig. 3.6a) is probably largely a source mixing effect, whereas assimilation generated superimposed trends that show stronger correlations between SiO₂ and ⁸⁷Sr/⁸⁶Sr (Nila, Teon).

The distinction between 'deep' and 'shallow' contamination is often based on correlations between oxygen isotopes, SiO₂ and radiogenic isotopes, and on the requirement that assimilation should generate mixing lines in Sr-O isotope diagrams distinct from subduction mixtures (e.g. James, 1981). Magaritz et al. (1978) reported δ¹⁸O values of 5.6-9.2‰ for the active Banda volcanoes (with highest values of 7.4-9.2‰ for Serua samples). They found a positive correlation with ⁸⁷Sr/⁸⁶Sr, which they interpreted in terms of up to 50% contamination by subducted sediments. We would like to emphasize, however, that the concave-convex criterion of mixing lines in Sr-O isotope diagrams may not be conclusive to distinguish 'deep' from 'shallow' contamination. The curvature depends mainly on the relative Sr contents of end members. If, as will be hypothesized below, SCM melt is added to arc magma in the mantle wedge or arc crust, rather than to a solid mantle source, the Sr contrast will be considerably different, and the result of magma mixing may be indistinguishable from bulk assimilation of terrigenous sediment.

Given the large variations in Sr-Nd isotopes, the near constancy of Pb isotopic compositions within individual volcanoes of the Banda Arc is remarkable. It may suggest little influence of assimilation on Pb-isotopic compositions and a strong curvature of mixing lines connecting mantle and SCM sources in Pb-Sr or Pb-Nd plots (see below). Serua is the only volcano with a detectable variation in ²⁰⁶Pb/²⁰⁴Pb (19.02-19.10), which tends to correlate positively with ¹⁴³Nd/¹⁴⁴Nd (Fig 3.5), a trend that cannot be generated by simple two-component mixing between a mantle source and SCM.

Our preferred scenario for Serua is that of mixing between magmas with different imprints of assimilated and subducted material. One is the least contaminated by SCM. It has the least radiogenic strontium and most radiogenic Pb isotopes, and may have obtained its final isotopic signature from sediment assimilation, similar to nearby Nila volcano. The other contains the largest proportion of SCM, which generated the highest ⁸⁷Sr/⁸⁶Sr and lowest ¹⁴³Nd/¹⁴⁴Nd ratios of the series. Mixing of these magmas may explain why the wide Sr-Nd isotopic range of Serua is coupled with a much more limited range in major- and trace-element contents.

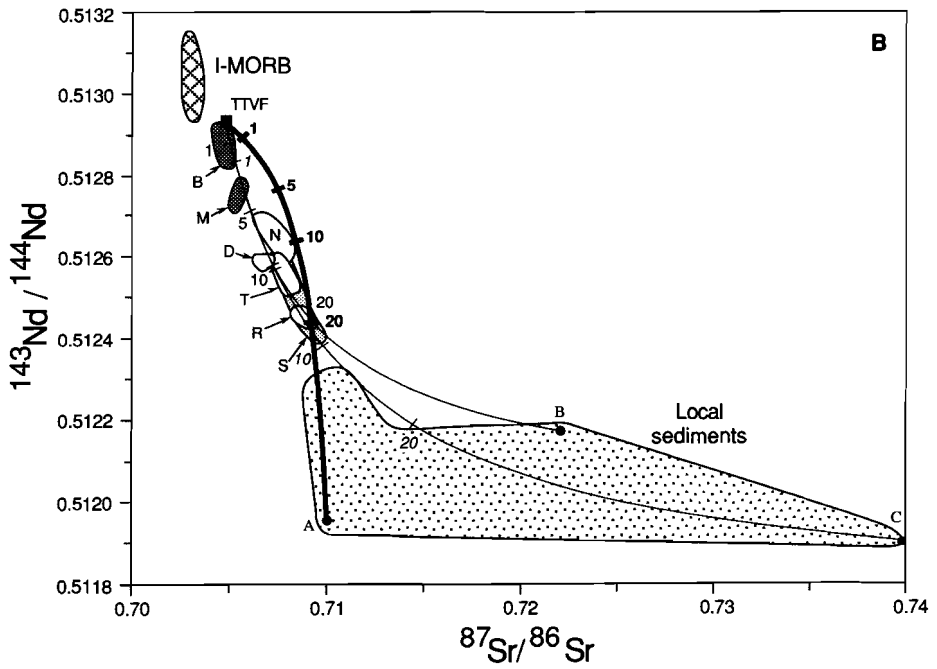
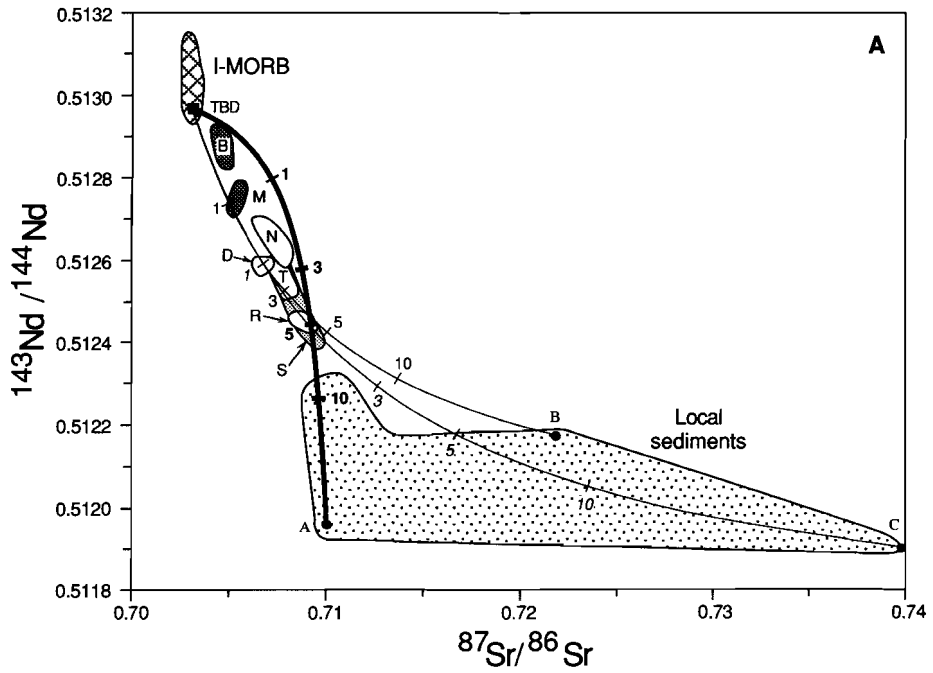
We conclude that assimilation was important for Nila, and probably also occurred at Teon and Serua, but that magmas were already characterized by high ⁸⁷Sr/⁸⁶Sr and low ¹⁴³Nd/¹⁴⁴Nd before reaching shallow levels in the arc crust.

3.4.3. Geological arguments against large-scale effects of assimilation

Geological arguments also favour SCM as the principle cause of the along-arc increasing involvement of continent-derived material. Low-K *Banda* and high-K *Damar*, the volcanoes at the NE and SW ends of the arc, are the extremes in terms of isotopic and trace-element ratios, but each shows little within-suite spread. Constant isotope compositions could be generated by MASH (Melting Assimilation Storage and Homogenisation) processes, as hypothesized for the Southern Volcanic Zone in the Andes (Hildreth and Moorbath, 1988). However, continental crust is absent in the Banda Arc and the only 1-2 km thick sediment layer on the sea floor does not seem capable of producing the same extent of assimilation and homogenisation as in the Andes. Furthermore, if the along-arc trends were caused by assimilation, it would require a shift in Pb-isotopic compositions of the assimilant, similar to that observed in the volcanics, and a concomitant NE-SW increase in the amount of assimilation towards the collision zone. Subduction of continental material is clearly a more plausible option. The shelf sediments show the corresponding shift, and the amount of SCM can be expected to increase towards the collision zone.

3.4.4. Acidic melts derived from subducted continental material?

All volcanoes in the Banda Arc display petrographical and mineral-chemical evidence for mixing between acidic magmas and more mafic magmas (e.g. Hutchison and Jezek, 1978; Van Bergen et al., 1989), and many lavas may be intermediate hybrids. The acidic end members probably originated from a variety of different processes. Crystal fractionation can largely explain the horizontal trend of Banda (Fig. 3.6a), whereas shallow-level contamination is most plausible for Nila, as discussed above. A third option is that acidic melts derived from SCM reached shallow levels in the arc crust. Cordierite-bearing rhyolitic rocks with high $^{87}\text{Sr}/^{86}\text{Sr}$ and low $^{143}\text{Nd}/^{144}\text{Nd}$ occur on Wetar in the southern extinct sector (Abbot and Chamalaun, 1981; McCulloch et al., 1982; see. Fig. 3.2), and we speculate that these represent pure SCM melts. Rhyodacitic rock types with appropriate compositions are also found at *Romang*. These rocks are associated with basaltic andesites, both having Sr-Nd signatures suggesting a large SCM component ($^{87}\text{Sr}/^{86}\text{Sr}=0.7085\text{-}0.7093$, $^{143}\text{Nd}/^{144}\text{Nd}=0.51243\text{-}0.51246$).



3.4.5. Source mixing models assuming an I-MORB mantle wedge

3.4.5.1. I-MORB source + bulk SCM

In order to define the contribution of SCM to magma genesis we first consider two end-member models in Sr-Nd-Pb mixing diagrams (Fig. 3.8a, 3.9, 3.10a). The composition of the SCM is assumed to be represented by box- and piston-cored sediments from the Australian-shelf in front of the arc and from the accretionary wedge (see Chapter 5). Samples from these two morpho-tectonic environments do not show systematic geochemical differences. Although these sediments are younger than those involved in magma genesis and have relatively high carbonate contents, the terrigenous fraction they contain is representative for the continental material subducted. Data on the shelf stratigraphy show that pre-Tertiary formations contain increasing amounts of terrigenous components (Veevers, 1984; Butcher, 1989). Nd-model ages (depleted mantle) of 1500-2200 Ma indicate that the recent sediments consist largely of material eroded from the Australian craton. Because of their systematic isotopic variation along the arc (see Chapter 5), three different compositions of the SCM end member -D, E and F (Table 3.2)-, closely corresponding to the sampling tracks (Fig. 2.1), are used.

As a mantle component, we shall first assume an Indian ocean MORB (I-MORB) source in the wedge. A MORB-type mantle is also considered to be one of the source components in the Sunda-Arc (Wheller et al., 1987; Varekamp et al., 1989; Stolz et al., 1990). Furthermore, as the Southern Banda Basin probably consists of an entrapped piece of Indian Oceanic crust (e.g. Bowin et al., 1980), the Banda Arc may also be underlain by a depleted I-MORB-residue. A 9 Ma I-MORB-type diabase was dredged on the eastern margin of the Tukang Besi platform east of Buton (Silver et al., 1985). It is a back-arc basalt in trace-element ratios (Schwartz et al., 1984) with high $^{143}\text{Nd}/^{144}\text{Nd}$ (0.51296) and I-MORB Pb isotopes (Morris et al., 1984). We use this Tukang Besi Diabase (TBD) to anchor the isotopic compositions of the mantle component in the mixing models, and assume that this end member has Pb, Sr and Nd concentrations 10 times lower than N-MORB (cf. White and Dupre, 1986). It should be realized, however, that its isotopic compositions, though overlapping or being close to I-MORB values, may not be entirely devoid of a minor slab-

Fig. 3.8a and 3.8b. Sr-Nd isotopic bulk-mixing models for I-MORB (Fig. 3.8a) and OIB-type mantle (Fig. 3.8b) with local sediments. B=Banda Archipelago, M=Manuk, S=Serua, N=Nila, T=Teon, D=Damar and R=Romang. End-member compositions are given in Table 3.2. Sediment compositions A, B and C were selected to show the influence of the Sr/Nd ratio (90, 3.3 and 2.5 respectively). Note that average upper continental crust has a Sr/Nd ratio of 13.5 (Taylor and McLennan, 1985). Tick marks indicate percentages of sediment added.

Table 3.2. End-member compositions used in mixing calculations

	TBD	TTVF	Sediment compositions					
	MORB source	OIB source	A	B	C	D	E	F
$^{87}\text{Sr}/^{86}\text{Sr}$	0.7030	0.7047	0.7100	0.7220	0.7400	0.71500	0.71500	0.72500
$^{143}\text{Nd}/^{144}\text{Nd}$	0.51297	0.51293	0.51195	0.51217	0.51190	0.51220	0.51215	0.51195
$^{208}\text{Pb}/^{204}\text{Pb}$	18.28	18.88	-	-	-	18.70	19.05	19.57
$^{207}\text{Pb}/^{204}\text{Pb}$	15.58	15.59	-	-	-	15.65	15.70	15.79
$^{206}\text{Pb}/^{204}\text{Pb}$	38.29	39.20	-	-	-	38.80	39.00	39.75
Sr (ppm)	9.0	66	1350	100	100	-	-	-
Nd (ppm)	0.73	3.85	15	30	40	27	27	27
Pb (ppm)	0.03	0.32	-	-	-	21	21	21

I-MORB source (based on TBD for $^{143}\text{Nd}/^{144}\text{Nd}$ and Pb-isotopes (Morris et al., 1984); $^{87}\text{Sr}/^{86}\text{Sr}$ based on data sources in Fig 3.2. N-MORB concentration data are from Sun and McDonough (1989), assuming 10% melting), OIB (based on TTVF with OIB concentration data of Sun and McDonough (1989), assuming 10% melting). Sediment compositions A, B and C are based on data from Chapter 5 and are selected to show the influence of the Sr/Nd ratio (indicative of the carbonate content of the sediment). Average compositions D, E, F are based on sediments from Chapter 5, corresponding to the shift in Nd and Pb-isotopic composition along the arc (see Fig. 2.1). Nd and Pb concentrations for sediments are based on average carbonate free sediment.

derived contribution.

As shown in Figs. 3.8a, 3.9 and 3.10a, about 0.5-5% of sediment is required to generate the isotopic signatures of the volcanics. Banda (< 1%) and Manuk (1-2%) in the NE part of the arc reflect the lowest SCM input, while Nila, Teon and Damar in the SW (1-3%) contain clearly higher proportions. Similar values have been found in other arcs that provide evidence of subducted sedimentary material, e.g. the Lesser Antilles, Aleutian, Eolian and South Sandwich Arcs (White and Dupre, 1986; Ellam et al., 1988, 1989; Barreiro, 1983; McCulloch and Perfit, 1981; Von Drach et al., 1986). The extinct volcanic island of Romang requires somewhat more continental material (> 5%), which is consistent with its position close to the collision area where continental crust could have been involved in magmagenesis. Also, the Serua high- $^{87}\text{Sr}/^{86}\text{Sr}$ group would have > 5% if, as argued above, assimilation has been of minor importance.

It is important to note that a shift in the Pb and Nd isotopic compositions of the sediments from Track I to III (see Chapter 5) is required to match the corresponding NE-SW variation in the volcanics along the arc, even if changes in the I-MORB composition were allowed. Therefore, this parallel trend of volcanics and sediments is considered as compelling evidence for the involvement of subducted continental material.

3.4.5.2. I-MORB source + fluid/melt derived from SCM

The above bulk-mixing model is based upon the assumption that mechanical mixing occurs prior to melting. However, it is widely believed that magma sources in the mantle wedge are infiltrated by slab-derived fluids or melts before they give rise to primary magmas (e.g. Gill, 1981; Tatsumi, 1989). If such a fluid is involved in magma genesis of the Banda Arc it would have enriched sources in Sr and Pb relative to Nd, which is expected to be less mobile (Tatsumi et al., 1986). As a consequence, the SCM imprint would be more enhanced for $^{87}\text{Sr}/^{86}\text{Sr}$ and radiogenic Pb than for $^{143}\text{Nd}/^{144}\text{Nd}$. Nevertheless, Sr-Nd mixing models (Fig. 3.8a) are inconsistent with a major role for fluid transfer. Mixing lines starting from I-MORB compositions fit all of the Banda Arc volcanoes if one uses the lowest Sr/Nd ratios (<5) found in the local sediments (i.e. those that are carbonate free, see Chapter 5). Good fits cannot be obtained with higher Sr/Nd ratios that would be expected in the case of an Sr-enriched fluid.

The low Sr/Nd ratio required for the SCM is even lower than 13.5 of average Upper Continental Crust (Taylor and McLennan, 1985). Hence, if it is assumed that continental crust rather than terrigenous sediments represent the SCM component, fluids may have played a role but only for the preferential removal of Sr during the earlier stages of subduction *before* arc source regions were reached. As an alternative to hydrous fluids, SCM-derived melts could have metasomatized the mantle sources. In this case fractionation between Sr, Pb and Nd is expected to be different. If all three behave as incompatible elements during partial melting, mixing curves would be virtually indistinguishable from bulk mixing lines in Figs. 3.8a and 3.10a, but proportions of the SCM end member are less than in the bulk-mixing models.

On the basis of the Sr/Nd ratio of the SCM, derived from the Sr-Nd mixing model, we conclude that SCM fluids did not play a dominant role in determining the isotopic signatures. This does not imply, however, that no slab-derived fluids have influenced magma compositions. The Banda Arc volcanics still have the high Sr/Nd ratios typical of island-arc volcanics, a feature generally ascribed to dehydration of the subducted basaltic oceanic crust (e.g. DePaolo and Johnson, 1978). If SCM is represented by sediments, they may have

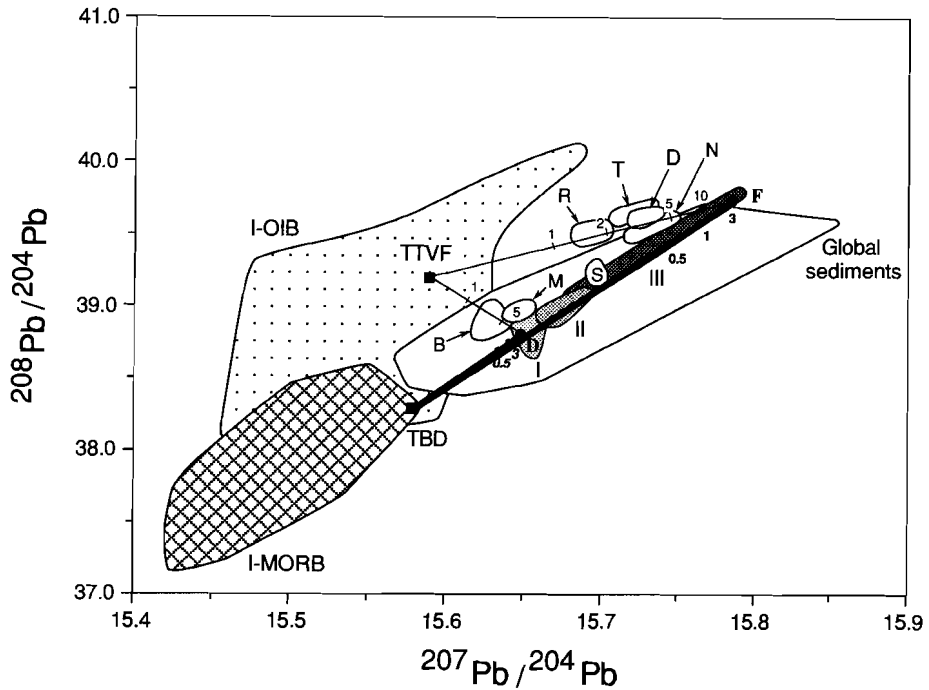


Fig. 3.9. $^{207}\text{Pb}/^{204}\text{Pb}$ - $^{208}\text{Pb}/^{204}\text{Pb}$ bulk mixing models for I-MORB (TBD) and OIB-type (TTVF) mantle with local sediments (bold D and F). B=Banda Archipelago, M=Manuk, S=Serua, N=Nilu, T=Teon, D=Damar and R=Romang. End-member compositions are given in Table 3.2. Tick marks indicate percentages of sediment. Note that the SW Banda Arc volcanoes (R,T,D,N) fall on a mixing line between an OIB-type mantle (TTVF) and sediment F.

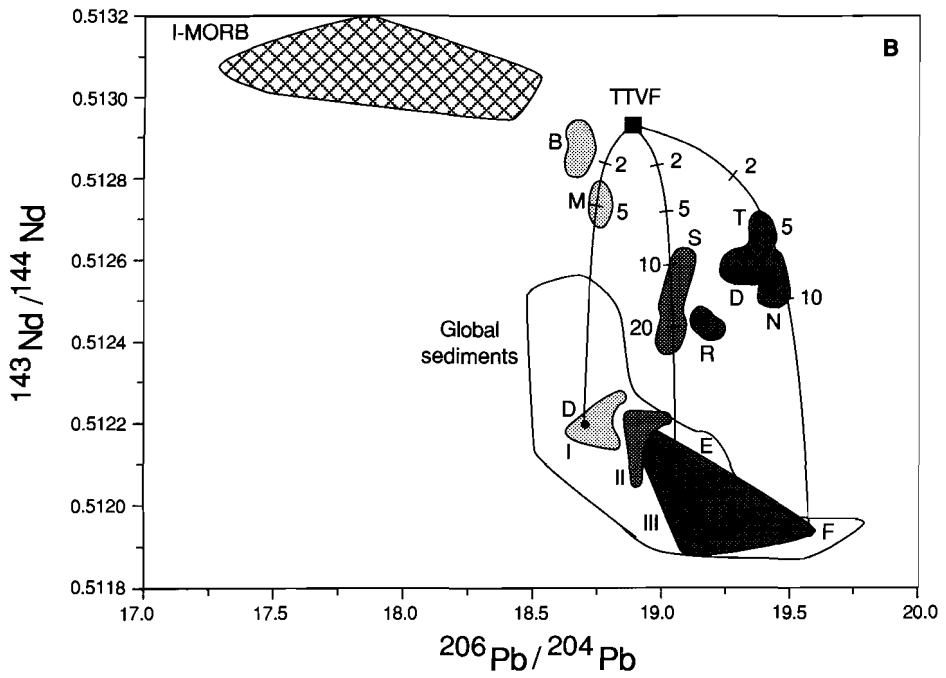
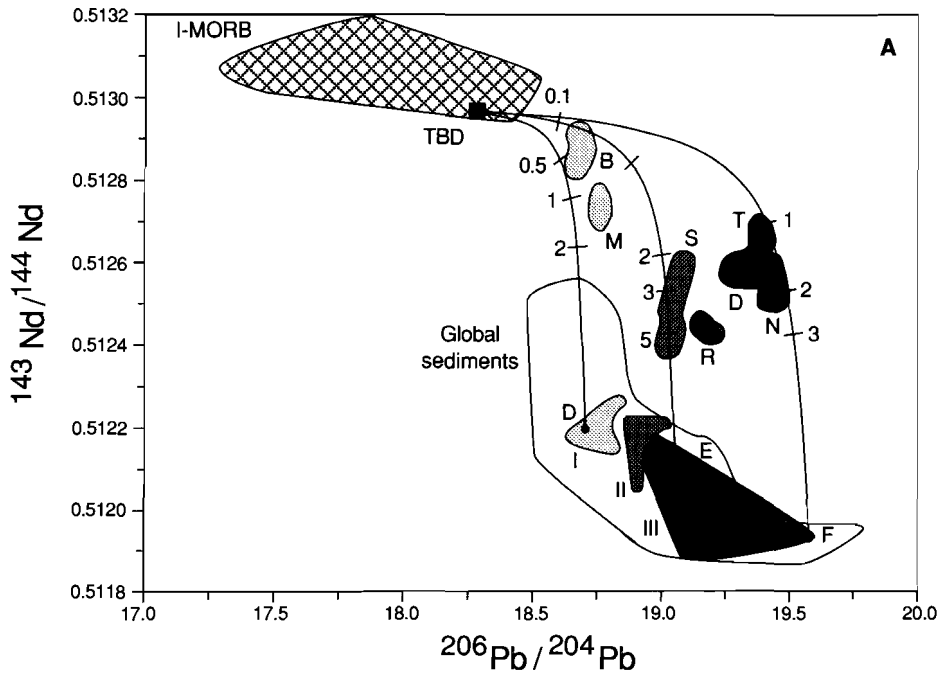
been infiltrated by fluids from underlying altered oceanic crust before they metasomatized the wedge. A plausible alternative is that fluids metasomatized the mantle source during earlier stages of subduction before SCM became involved. This would imply a mantle end member with higher $^{87}\text{Sr}/^{86}\text{Sr}$ and Sr/Nd than the assumed I-MORB source in Fig. 3.8a, and with a composition close to the TTVF source plotted in Fig. 3.8b. This diagram shows Sr-Nd mixing curves that agree well with the Banda Arc volcanics. A similar two-stage (fluid+bulk sediment) source-contamination model for island arcs was discussed by Ellam and Hawkesworth (1988).

3.4.6. Source mixing models assuming an OIB-type mantle wedge

In the previous section we considered an I-MORB source as the major mantle wedge component. However, OIB-type sources are believed to play a role in island-arc magma genesis (e.g. Morris and Hart, 1983; Gill, 1984), and should also be considered in this case, based primarily on the Pb isotope data. For the SE Banda Arc centres in particular, a $^{207}\text{Pb}/^{204}\text{Pb}$ - $^{208}\text{Pb}/^{204}\text{Pb}$ diagram illustrates best that an OIB source is a more plausible mantle end member, since mixing lines between these occurrences and I-MORB would require a sediment composition not found in any of the three tracks across the Australian shelf-outer Banda Arc (see Chapter 5) or anywhere else in the world (Figs. 3.4 and 3.9). Instead, a mixing curve connecting even the most radiogenic shelf sediment found (see Chapter 5) and the SE centres points to an end member in the OIB field. The most conspicuous characteristic of this end member is its high $^{208}\text{Pb}/^{204}\text{Pb}$ for a given $^{207}\text{Pb}/^{204}\text{Pb}$ or ($^{206}\text{Pb}/^{204}\text{Pb}$), which it shares with the Sunda Arc (Stolz et al., 1990; Vroon et al., 1990a) and other South East Asian arcs, e.g. Halmahera (Morris et al., 1983), Philippines (Mukasa et al., 1987), and is consistent with the position within the realm of the Dupal anomaly (Hart, 1984). The Australian subcontinental mantle, another enriched reservoir, and proposed by Varne (1985) as one of the source components in the Eastern Sunda arc on the basis of Ba/Nb and Sr- and Nd-isotopes, is an unlikely end member in the light of the currently available Pb isotope data (Fig. 3.3a-d and 3.4).

Our isotopically most extreme sample (TTVF) in the Banda Sea Region is the 6-7 Ma pillow lava (Abbott and Chamalaun, 1981; Carter et al., 1976) with $\text{SiO}_2=53\%$ and $\text{MgO}=5.74$, from Manamas on the north coast of Timor (Fig. 2.1), which has high $^{143}\text{Nd}/^{144}\text{Nd}$ (0.51293) and $^{87}\text{Sr}/^{86}\text{Sr}=0.7047$, $^{206}\text{Pb}/^{204}\text{Pb}=18.87$ and low $^{207}\text{Pb}/^{204}\text{Pb}$ (15.59) for its $^{208}\text{Pb}/^{204}\text{Pb}$ (39.20). These values are not far from Indian OIBs such as Kerguelen (e.g. Storey et al., 1988) and Christmas Island, south of the Java trench (Hart, 1988). In terms of Pb isotopic composition, the sample TTVF is similar to samples from Muriah, a potassic volcano on Java with a considerable OIB-type signature (Edwards et al., 1991). Abbott and Chamalaun (1981) refer to rocks from the Timor formation as arc tholeiites, but trace-element compositions (Appendix 4) indicate that the source of the TTVF sample was close to MORB and only little affected by subduction-related components.

The high $^{208}\text{Pb}/^{204}\text{Pb}$ end-member is least evident or absent at Banda, and it seems likely that the mantle component involved in magmagenesis changes from I-MORB in the NE to OIB in the SW. This trend coincides with a gradual steepening of the subduction zone towards the extinct sector (Cardwell and Isacks, 1978; McCaffrey, 1989), and possibly with a slight increase in depth of the Benioff zone (Table 2.1). On the western side of this sector, the high $^{208}\text{Pb}/^{204}\text{Pb}$ component can be recognized in the volcanics across the active AP sector



(see Fig. 2.1) irrespective of the depth of the Benioff zone (Stolz et al., 1990; Vroon et al., 1990a).

In summary, the Banda Arc volcanics can be described as mixtures involving two mantle end-members and an SCM component (Figs. 3.8, 3.9, 3.10), without counting the superimposed effects of assimilation. Both the relative proportions of the mantle components and the composition of the SCM change along the arc. Since OIB sources are enriched in Pb, Sr and Nd compared to N-MORB sources (Sun and McDonough, 1989), more SCM is required to obtain the isotopic signatures in mixing models than the values given above. Nevertheless, except for Serua and Romang, the proportion of SCM is at most 10%. On the other hand, the 'OIB' component may have been depleted by a previous melting event (McCulloch and Gamble, 1991); therefore only its isotopic composition would make it distinct from MORB-type sources (see also Chapter 4).

3.4.7. Models involving mantle wedge magma mixing (MWMM)

The $^{87}\text{Sr}/^{86}\text{Sr}$ and $^{143}\text{Nd}/^{144}\text{Nd}$ systematics of Romang indicate a relatively large SCM component (> 5% assuming bulk mixing). However, in the $^{207}\text{Pb}/^{204}\text{Pb}$ - $^{208}\text{Pb}/^{204}\text{Pb}$ diagram (Fig. 3.9) the Romang lavas do not plot close to the sediment field as one would expect, because they are clearly displaced towards higher $^{208}\text{Pb}/^{204}\text{Pb}$ (compared to Serua with similar $^{207}\text{Pb}/^{204}\text{Pb}$). In the previous section we discussed mixing between sediment and an OIB-type mantle component which is most pronounced in the SW Banda Arc, near the collision area, where also the largest amounts of SCM are involved. On a Pb isotope mixing line between the most radiogenic sediment and the mantle (TTVF) end member (Fig. 3.9), Romang plots closer to the latter than the other South Banda Arc volcanoes. Possible explanations are:

- (1) None of the isotopic compositions of Australian shelf sediments (see Chapter 5) is representative of the SCM at Romang. We consider this explanation unlikely because even in the global sediment data set an appropriate composition is lacking.
- (2) The high $^{208}\text{Pb}/^{204}\text{Pb}$ ratios are caused by the mantle component rather than by the SCM. This option is plausible since it fits in with the regional characteristics (Sunda Arc, Halmahera, Philippines, Fig. 3.4), irrespective of any subducted component postulated. Because the high Pb concentrations in the SCM (average 21 ppm) would have swamped the Pb-isotopic mantle signature in the case of mixing with solid OIB-type mantle containing

Fig. 3.10a and 3.10b. $^{206}\text{Pb}/^{204}\text{Pb}$ - $^{143}\text{Nd}/^{144}\text{Nd}$ bulk mixing models for I-MORB (TBD) and OIB type mantle (TTVF) and local sediments (D, E and F). End-member compositions are given in Table 3.2. B=Banda Archipelago, M=Manuk, S=Serua, N=Nilu, T=Teon, D=Damar and R=Romang. Tick marks indicate percentages of sediment added. Note the along-arc correspondence in Pb isotopes.

some 0.1 ppm Pb (cf. Ben Othman et al., 1989; Sun and McDonough, 1989; assuming 10% melting), mechanisms other than simple bulk mixing are required. The most likely process seems that of mixing between a melt from an SCM-modified mantle source and a low-degree(?) melt from a high $^{208}\text{Pb}/^{204}\text{Pb}$ mantle.

Models invoking different melting regimes in the mantle wedge have been discussed by Arculus and Powell (1986), Reagan and Gill (1989) and Carr et al. (1990). The mantle-wedge magma mixing (MWMM) model of Reagan and Gill (1989), introduced to explain variable HFSE signatures, assumes mixing between melts created at different levels in the mantle wedge. One is a small-degree melt from a hydrated mantle above the slab, the other a large-degree melt with MORB-like characteristics generated in the upwelling limb of a convecting cell in the wedge. Carr et al. (1990) emphasize the importance of the subduction geometry in the Central American arc, and proposed that the degree of melting of mantle above the slab depends on the flux of slab-derived fluids which is controlled by the dip angle. Such melts could subsequently mix in different proportions with small-degree melts formed in an incompatible-element rich asthenospheric mantle by decompression in the upward moving counterflow of the wedge cell.

These models are attractive in that they are able to explain variations in both trace-element and isotopic signatures of closely associated arc magmas. The isotopic data of the Romang lavas are consistent with an MWMM model, with the specification that the mantle source above the slab is infiltrated by SCM melts rather than fluids. Isotopically, this mantle component is not necessarily distinct from the mantle source in the counterflow, but incompatible trace-element contents may have been lowered as a result of previous melt extraction. McCulloch and Gamble (1991) noted that even the input of depleted residual material from back-arc basalts into the mantle wedge should be taken into account.

If MWMM has occurred in the Banda Arc, the amounts of SCM required to generate the isotopic signatures could be markedly different from those calculated for the case of simple bulk mixing. If the SCM-bearing end member is a melt originating from the metasomatized mantle above the slab, the amount of SCM is difficult to quantify, but it would not necessarily deviate substantially from the above percentages in the single-stage bulk mixing result (cf. Van Bergen et al., 1992). It is conceivable, however, that SCM melts mixed directly with the high- $^{208}\text{Pb}/^{204}\text{Pb}$ melt without previous interference of wedge peridotite in places where melts escaping from the slab are sufficiently voluminous, or where the mantle has been modified to a large degree after prolonged interaction with slab-derived material. Mixing lines in the $^{206}\text{Pb}/^{204}\text{Pb}$ - $^{143}\text{Nd}/^{144}\text{Nd}$ diagram (Fig. 3.10b) would be the same, but the amounts of SCM would increase by about one order of magnitude (e.g. some 50% for Romang), assuming Pb and Nd concentrations in TTVF equal to those of average OIB (Sun and McDonough, 1989), and mixing with completely melted SCM. Centres close to the

inactive sector north of Timor where large amounts of sediment and the leading portions of the continental crust have been subducted over a significant period of time are locations where large volumes of 'pure' SCM magmas can be expected. The high $^{87}\text{Sr}/^{86}\text{Sr}$ amphibole-bearing rhyodacites of Romang are SCM-rich but still contain a mantle contribution. Possibly the best representatives are the acidic cordierite-bearing lavas of Wetar.

3.5. CONCLUSIONS

The Banda Arc magmas carry Sr-Nd-Pb isotopic signatures that reflect the incorporation of subducted continent-derived source components as well as the assimilation of arc-crust sediments.

Within-suite Sr-Nd isotopic ranges are highly variable, and point to marked differences between the individual volcanic centres as far as the local controls of assimilation processes are concerned. The case of Nila illustrates that quartz-carbonate bearing assemblages play an important role. After correction for these shallow contamination effects, the remaining isotopic compositions are still 'continental' to various degrees, and point to a deep origin. Parallel Pb-isotope trends of volcanics and shelf sediments along the arc provide the strongest argument for the involvement of a subducted terrigenous source component derived from the Australian continent. Pb isotopes also signal a change in the nature of the mantle wedge component along the arc from I-MORB in the NE to an enriched (OIB-type) mantle in the SE. These spatial systematics correlate with apparent variations in subduction geometry and dynamics, and with the progressive stages of collision between the surrounding continental margins and the arc system.

Calculated proportions of SCM involved in magma genesis strongly depend on the mixing mechanism adopted. Selective element mobility by fluid transfer is clearly of minor importance compared to wholesale incorporation. A conventional bulk-mixing approach points to an addition of about 0.5-5% to a MORB-type source. These values are minimum estimates, since the proportions may be higher in the case of an OIB-type mantle, whereas they can be up to ten-fold higher if SCM melts mixed with mantle magma rather than metasomatized solid wedge domains above the slab. Such a magma mixing scenario seems inescapable from the isotopic 'visibility' of mantle Pb, despite the substantial SCM contributions detected.

Irrespective of the mixing models applied, the proportion of SCM is 2-5 times higher in the SW part of the arc than in the NE sector, which coincides with a greater supply at the locus of collision near Timor. In addition to melting of slab sediments, mobilization of the leading portions of subducted Australian continental lithosphere is a conceivable origin of

acidic SCM melts that were sufficiently voluminous to rise as discrete magma batches until they hybridized with basaltic magma or reached the arc-crusts surface. In general, the Banda Arc volcanics call for the occurrence of magma mixing processes in the mantle wedge and/or the arc crust, involving mantle end members with variable slab-derived imprints as well as SCM melts. The precise significance of the latter is difficult to establish, given the masking influence of the substantial sediment assimilation in various centres.

CHAPTER 4

TRACE-ELEMENT CONSTRAINTS ON THE ROLE OF SUBDUCTED CONTINENTAL MATERIAL IN THE BANDA ARC

4.1. ABSTRACT

The Banda Arc is situated in a favourable setting to evaluate the role of subducted continental material (SCM) in magma genesis, since the arc is constructed on oceanic crust, and is surrounded by continental areas from which source components can be derived. We determined major- and trace-element compositions of rock suites from all six islands with active volcanoes and from an adjacent island where volcanic activity has ceased, presumably due to the collision between the Australian continent and the arc. These centres cover the entire 500 km length of the arc, which forms the eastern end of the Sunda-Banda Arc.

The volcanics are mainly quite evolved ($\text{SiO}_2 > 52\%$, Mg-number < 59). Incompatible trace-element ratios and REE patterns show little within-suite systematics, and are thought to approximate source characteristics. There is a general along-arc increase in the LILE, LREE and Nb from NE-SW towards the extinct sector that marks the collision. Variations in the HREE, Zr, Hf and Y are limited or absent. N-MORB normalized abundance patterns and ratios of incompatible trace elements are strikingly similar to those of terrigenous sediments in front of the arc. Hence, on the basis of the trace-element data, the Banda Arc shows greater affinities with continental arcs than with other island arcs.

Source mixing-melting models indicate that the observed REE systematics can be generated if magmas originate from amphibole- (and/or phlogopite-) bearing mixtures of MORB mantle and bulk subducted continental material, and if proportions of the latter increase from NE to SW. Most incompatible trace-element ratios are consistent with mixing of these end members. The SCM also influences the HFSE signatures, as appears from along-arc changes in Zr/Nb which follow the main trend, and from the similarity of negative Nb-Ta anomalies in volcanics and sediments.

However, two-component source mixing cannot explain all of the trace-element features observed. Local contributions of more components at shallow levels in the arc crust (e.g. at Nila) or at greater depth (Serua?), cause detectable deviations from the geographical systematics for some element pairs.

Furthermore, some LILE/HFSE ratios are too high for bulk SCM+MORB-mantle mixtures, which suggests an additional role of fluids, possibly derived from dehydrating

SCM. It is suggested that source regions in the sub-arc mantle were infiltrated by hydrous fluids, either by dehydrating slab material in the shallower parts of the subduction zone, or during earlier episodes of subduction. Nevertheless, bulk addition of (melted) SCM seems to be the dominating transfer mechanism, particularly in the SE where more voluminous contributions are expected from subducted leading portions of the continental margin.

4.2. INTRODUCTION

Evidence from an array of isotopic systems (Sr-Nd-Pb-He-Hf-O) has shown that subducted continental material (SCM) is an important magma-source component of the Banda Arc (Chapter 3; Whitford, 1977; Magaritz et al., 1978; Whitford et al., 1979; Whitford et al., 1981; Morris, 1984; Morris and Hart, 1980; Morris et al., 1984; White and Patchett, 1984; Poreda and Craig, 1989; Hilton and Craig, 1989; Poorter et al., 1991; Hilton et al., 1992; Vroon et al., 1990b). The Sr-Nd-Pb isotopic evidence for the subduction of continent-derived material (Chapter 3) has given rise to an important argument from the correspondence between volcanics and sediments on the adjacent Australian-New Guinean shelves surrounding the Banda Arc. The parallel along-arc trends in Pb-isotopes of both the volcanics and the sediments was regarded as strong support for the involvement of subducted terrigenous material. It was also concluded that the amount of SCM increases along the arc from NE to SW towards the collision zone north of Timor.

Despite these isotopic arguments, very few major and trace-element data are available to test the SCM hypothesis (Whitford and Jezek, 1979; Van Bergen et al., 1989). Whitford and Jezek (1979) reported concentration data for a number of LIL elements, and demonstrated that K, Rb, Cs, Ba and Sr abundances increase along the arc from NE to SW. They found an absence of 'mixing line' effects between Sr-isotopes and major and trace-element abundances, but noted that this did not necessarily preclude source contamination.

Here we present major and trace-element data (including LILE, HFSE and REE) for all of the Banda Arc volcanoes. By comparing the compositions with those of the shelf sediments (Chapter 5), we use the results to define the role of SCM in determining the trace-element signatures. It will be demonstrated that along-arc variations in REE patterns and incompatible trace-element ratios are broadly consistent with source mixing between bulk SCM and MORB mantle. Explanations for the observed decouplings between trace-elements and isotope ratios (e.g. transfer mechanism at the slab-wedge interface and shallow-level contamination) will be discussed.

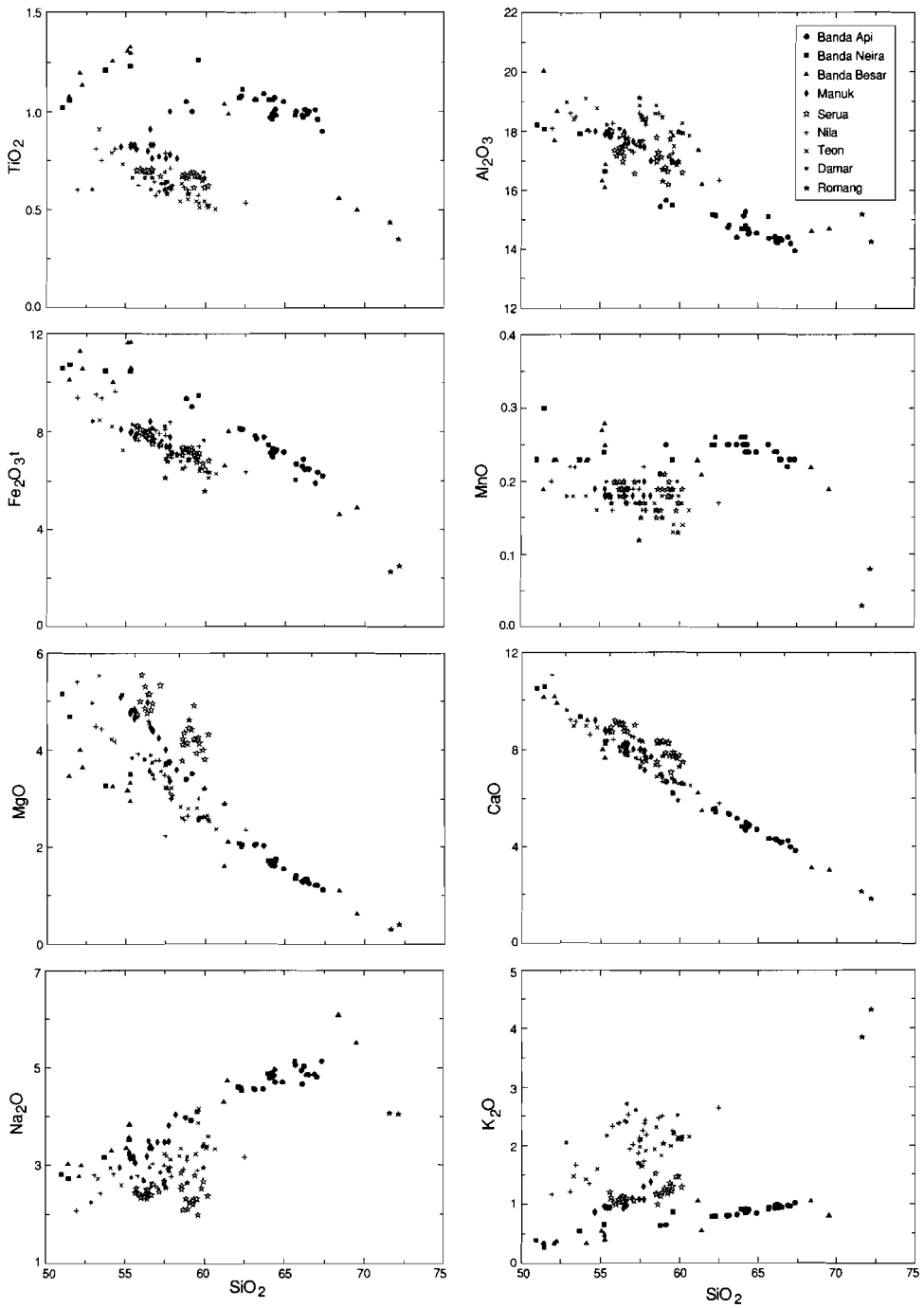


Fig. 4.1. SiO_2 variation diagrams for the major elements of the Banda Arc volcanics. Note the deviating CaO and Na_2O trends of Serua and Romang compared to the other volcanoes.

4.3. RESULTS

4.3.1. Major elements

Major elements are given in Appendix 4 and illustrated in variation diagrams against SiO_2 in Fig. 4.1. Basalts ($\text{SiO}_2 < 52\%$) are scarce and were found only on Banda and Nila. Andesite is the most common rock type, whereas acidic rocks were found only on Banda Api (dacites) and Romang (rhyodacites). MgO is generally low (< 5.5 wt. %), Mg numbers < 59 , and Cr contents < 128 ppm. These compositional features reflect the lack of primary mantle magmas in the arc, if it is assumed that standard criteria are applicable.

As documented earlier (Jezek and Hutchison, 1978; Whitford and Jezek, 1979; Van Bergen et al., 1989), the Banda Arc volcanoes display conspicuous along-arc compositional changes, with potassium increasing from NE to SW (Fig. 4.1 and 3.1). The active volcanoes can be divided into three groups on the basis of SiO_2 - K_2O systematics (cf. Van Bergen et al., 1989; see Fig. 3.1):

(1) *Banda Archipelago* has $K_{57.5}$ (wt. % K_2O at 57.5% SiO_2) of 0.60 and forms a low-K group, which displays the largest range in SiO_2 (51-70%) of the arc. Dacites are the dominant rock type at the active Banda Api cone. Basaltic and andesitic rocks occur mainly on the adjacent islands of Banda Neira and Banda Besar. Rhyodacitic pumices were found on the latter island as well. The Banda group is characterized by the highest Fe_2O_3 (as well as MnO and TiO_2) enrichment of the arc, in agreement with its tholeiitic nature (cf. Jezek and Hutchinson, 1978; Whitford and Jezek, 1979), whereas Al_2O_3 tends to be relatively low.

(2) *Manuk and Serua* have $K_{57.5} = 1.14$ -1.15 and define a medium-K group with a limited spread in SiO_2 (54-58% and 55-60% respectively) and in other major elements. Although these volcanoes are similar in terms of petrography and potassium content, there are marked differences in other major elements. For a given SiO_2 , Serua has higher CaO and MgO and lower Na_2O contents than Manuk and the other volcanoes (Fig. 4.1). There is little or no systematic relation between major elements and the large range of $^{87}\text{Sr}/^{86}\text{Sr}$ ratios of the Serua lavas (Chapter 3; Whitford and Jezek, 1979).

(3) *Nila, Teon and Damar* form a high-K group with $K_{57.5} = 1.89$ -2.43. Damar, at the SW end of the arc, is the most potassic active volcano. Within-suite ranges are larger than in the medium-K group: $\text{SiO}_2 = 51$ -63% for Nila, 53-62% for Teon and 52-60% for Damar. Al_2O_3 tends to be higher and TiO_2 lower for a given SiO_2 content than in the other groups. Nila and Romang have steep within-suite trends, crossing the boundaries of the medium and high-K series (cf. Fig. 3.1). Samples from the extinct volcanic island of *Romang* are medium- to high-K and are bimodally distributed between andesites ($\text{SiO}_2 = 57$ -60) and rhyodacites ($\text{SiO}_2 = 71$ -72).

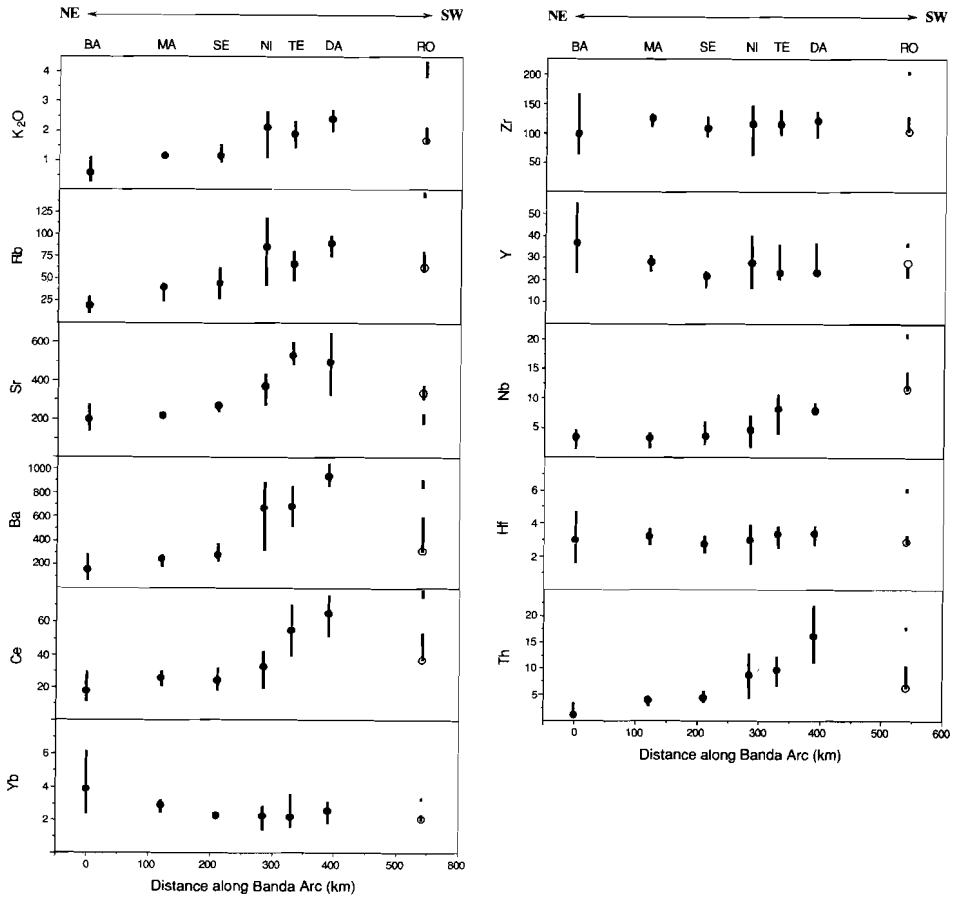


Fig. 4.2. Along-arc variations of potassium and selected trace-element contents, taken at 57.5% SiO₂ (filled circles for active volcanoes, open circle for extinct Romang). Abbreviations: BA=Banda Archipelago, MA=Manuk, SE=Serua, NI=Nila, TE=Teon, DA=Damar and RO=Romang. The bars indicate the total range within each volcano. The 57.5 SiO₂ symbols of the Banda Archipelago only represent Banda Api, whereas the range is for the entire archipelago. Romang is splitted into an andesitic group (open circle shown for this group) and a rhyodacitic group.

4.3.2. Trace elements

Trace-element concentrations are listed in Appendix 4. In general, within-suite variations are large for low-K Banda and high-K Nila, and relatively small for medium-K Manuk and Serua, which is consistent with the major element trends. Along-arc systematics are illustrated in Fig. 4.2.

4.3.2.1. Large ion lithophile elements

The LILE (Cs, Rb, Ba, Pb and Sr, here including U and Th) behave as incompatible elements, except for Sr, apparently due to plagioclase fractionation. Within-suite ranges are large for Nila (about 2-3 times those of the other high-K volcanoes of Teon and Damar), but are relatively small for medium-K Manuk and Serua. The abundances of LILE (including Sr) increase along the arc from NE to SW (Fig. 4.2 and cf. Whitford and Jezek, 1979). This trend is not gradual but follows the pattern of the three groups with different potassium levels. For example, $Ba_{[57.5]}$ (Ba content at $SiO_2=57.5\%$) increases from 150-180 in the Banda Archipelago to 240-280 for Manuk and Serua, and further to 670-940 for Nila, Teon and Damar. All LILE show a relatively large jump between the medium- and high-K groups. The LILE contents of the andesites from Romang plot between the medium- and high-K groups. The rhyodacitic samples have the highest K_2O and Rb contents of the arc.

4.3.2.2. Rare earth elements and Yttrium

Within-suite REE variations are consistent with incompatible behaviour, whereas Y generally remains relatively constant. A significant range in Yb was found for the Banda Archipelago; the other volcanoes show only a limited spread. In contrast, the largest within-suite variations for Ce were found in the SW Banda Arc volcanoes. The LREE contents increase along the arc from NE to SW, comparable to the LIL elements, whereas $Yb_{[57.5]}$ and $Y_{[57.5]}$ tend to decrease (Fig. 4.2). The limited change in $Yb_{[57.5]}$ compared to the NE-SW increase in $Ce_{[57.5]}$ (Fig. 4.2 discarding Banda) is not common in arc volcanics, but tends to be restricted to continental arcs (Gill, 1981).

Fig. 4.3 shows REE patterns of representative samples and the fields of N-IMORB and local sediments for comparison. The Banda Arc patterns generally overlap those of other oceanic arcs (cf. White and Patchett, 1984). In detail, there is a systematic change from MORB-like shapes of the patterns in the NE to greater similarity with the sediments in the SW.

The low-K *Banda Archipelago* is characterized by flat REE patterns ($[La/Yb]_n=0.9-1.6$) and relatively high HREE contents: $Yb_n=11-20$ ($Yb_n=Yb$ content normalized on chondrite). Some samples show small Eu anomalies: $Eu/Eu^*=0.90-1.04$. The REE patterns largely overlap the N-IMORB field, except for the La-Nd parts in some samples.

Medium-K *Manuk and Serua* are characterized by parallel REE patterns with flat HREE, high HREE contents ($Yb_n=9-15$) and slightly enriched LREE ($[La/Yb]_n=2.3-3.6$). They overlap only partly with N-IMORB and local sediments. Eu anomalies are small:

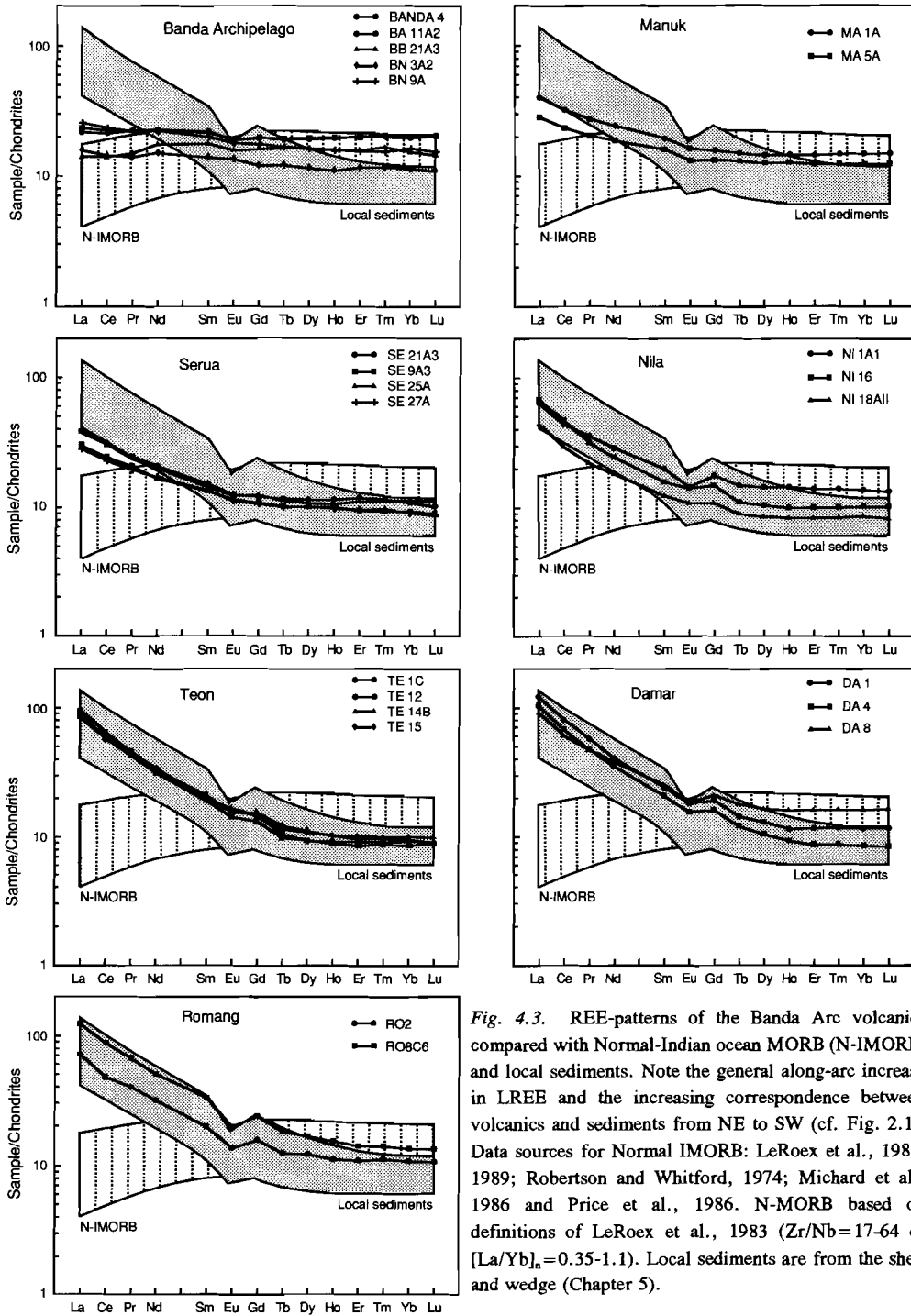


Fig. 4.3. REE-patterns of the Banda Arc volcanics compared with Normal-Indian ocean MORB (N-IMORB) and local sediments. Note the general along-arc increase in LREE and the increasing correspondence between volcanics and sediments from NE to SW (cf. Fig. 2.1). Data sources for Normal IMORB: LeRoex et al., 1983; 1989; Robertson and Whitford, 1974; Michard et al., 1986 and Price et al., 1986. N-MORB based on definitions of LeRoex et al., 1983 ($Zr/Nb=17-64$ or $[La/Yb]_n=0.35-1.1$). Local sediments are from the shelf and wedge (Chapter 5).

$\text{Eu}/\text{Eu}^* = 0.90\text{-}0.95$. HREE contents of Serua samples are lower than for Manuk and similar to the high-K volcanics.

High-K *Nila*, *Teon* and *Damar* still have flat HREE at relatively high levels ($\text{Yb}_n = 9\text{-}16$) but they are more enriched in LREE ($[\text{La}/\text{Yb}]_n = 4.6\text{-}12.2$) and have deeper Eu anomalies ($\text{Eu}/\text{Eu}^* = 0.77\text{-}0.96$) than the medium-K rocks. The patterns largely overlap the local sediment field, particularly those of *Teon*. Within the suites of *Nila* and *Damar* (e.g. sample DA8) the patterns of individual samples occasionally cross, which suggests involvement of magmas with different melting and/or crystallization histories.

The samples from *Romang* are also characterized by flat HREE with high HREE contents ($\text{Yb}_n = 11\text{-}13$) and large enrichments in LREE ($[\text{La}/\text{Yb}]_n = 6.7\text{-}9.1$), comparable to the high-K group. The two samples have large negative Eu anomalies: $\text{Eu}/\text{Eu}^* = 0.70\text{-}0.77$). The *Romang* patterns largely overlap with the local sediment field. The only significant Ce anomaly of the Banda Arc was found in the basaltic-andesite (RO2: $\text{Ce}/\text{Ce}^* = 0.89$).

4.3.2.3. High field strength elements

Zr, Hf and Nb trends in the Banda-Arc suites are consistent with incompatible behaviour during fractionation. Within-suite ranges are largest for Banda and *Nila* and only minor for the medium-K volcanoes. In terms of along-arc variations there is a clear distinction between Nb and the other HFSE (excluding Ti, which is generally depleted, probably as a result of magnetite fractionation). There is an almost three-fold increase in $\text{Nb}_{[57.5]}$, but Zr and Hf do not systematically vary along the arc and $\text{Y}_{[57.5]}$ even tends to decrease (Fig. 4.2).

4.3.2.4. Scandium, Chromium and Cobalt

Abundances of Sc, Cr and Co are low compared to MORBs and IABs in all of the Banda Arc lavas, consistent with compatible behaviour and the evolved character of the rocks. Only in the least evolved samples of the low-K Banda Archipelago does Sc increase (up to 55 wt. % SiO_2), after which a decrease is observed, similar to TiO_2 . Medium-K Serua and Manuk rocks are higher in Cr at a given SiO_2 content than the low- and high-K series.

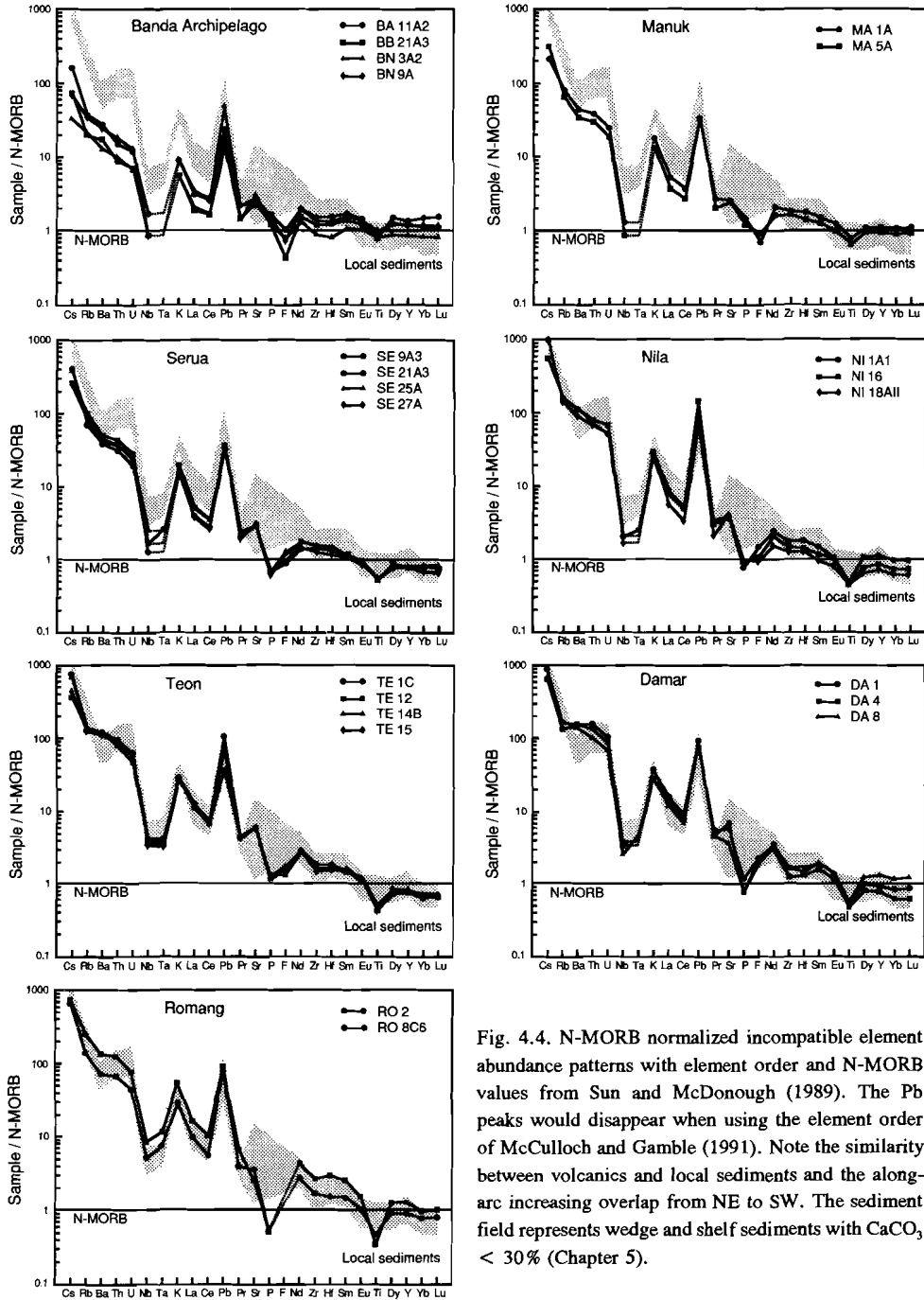


Fig. 4.4. N-MORB normalized incompatible element abundance patterns with element order and N-MORB values from Sun and McDonough (1989). The Pb peaks would disappear when using the element order of McCulloch and Gamble (1991). Note the similarity between volcanics and local sediments and the along-arc increasing overlap from NE to SW. The sediment field represents wedge and shelf sediments with $\text{CaCO}_3 < 30\%$ (Chapter 5).

4.3.3. Correspondence with trace-element signatures of local sediments

A compilation of the incompatible trace-element signatures is given in Fig. 4.4, using N-MORB normalized abundance patterns (order of elements and normalization factors from Sun and McDonough, 1989). These diagrams show a striking correspondence between the patterns of volcanics and local sediments. For the high-K volcanoes in the SW part of the Arc (Nila, Teon, Damar and Romang), the patterns are almost identical. This observation points to the major role of continental material in determining the chemical characteristics of the magmas.

4.4. DISCUSSION

4.4.1 Introduction

In the following discussion rare-earth-element patterns and incompatible-trace-element ratios are interpreted in terms of source-contamination processes. Because the Banda Arc lavas are generally not primary mantle-derived magmas according to standard criteria, shallow-level evolution may have modified original signatures. Differentiation by fractional crystallization could have some effect when phenocryst assemblages include amphibole and biotite (Nila, Teon, Damar), which to some extent preferentially incorporate the middle REE, Nb, K, Rb and Ba relative to other incompatible elements (cf. distribution coefficients in Gill, 1981). Fractionation of significant amounts of these minerals would be required to cause detectable changes. However, with only a few exceptions, there are no within-suite correlations between differentiation indices (e.g. SiO_2) and trace-element ratios, nor are there significant changes in REE patterns, which suggests that any modifications of primary signatures were of minor importance.

Some correlations were found in the series of Nila and Serua. As discussed in Chapter 3, a positive correlation between $^{87}\text{Sr}/^{86}\text{Sr}$ and SiO_2 in the Nila lavas can be explained by assimilation of arc-crust sediments. $^{87}\text{Sr}/^{86}\text{Sr}$ also tends to correlate positively with Ba/La and negatively with Sr/Nd, which is consistent with assimilation of arc-crust sediment (see Chapter 3 for discussion of AFC), and/or mixing between magmas of different origin. Other correlations are weak or absent.

The Serua lavas show a weak positive correlation between $^{87}\text{Sr}/^{86}\text{Sr}$ and Zr/Nb. Other trace-element ratios are remarkably constant, given the wide range of $^{87}\text{Sr}/^{86}\text{Sr}$ ratios (0.7075-0.7095). The lavas may represent hybrids of magmas with SCM-derived signatures that are

Table 4.1. Source compositions used in REE mixing-melting models

Element	MORB-source	SCM	S1	S3	S5	S10
SiO ₂	45.64	66.0	45.84	46.25	46.66	47.68
TiO ₂	0.12	0.50	0.12	0.13	0.14	0.16
Al ₂ O ₃	2.70	15.20	2.83	3.08	3.33	3.95
FeO	8.02	4.50	7.99	7.91	7.84	7.69
MgO	40.75	2.20	40.37	39.59	38.82	36.90
CaO	2.40	4.20	2.42	2.45	2.49	2.58
Na ₂ O	0.23	3.90	0.27	0.34	0.41	0.60
K ₂ O	0.05	3.40	0.08	0.15	0.22	0.39
La	0.206	48.0	0.68	1.64	2.60	4.99
Ce	0.722	90.5	1.62	3.41	5.21	9.69
Pr	0.143	10.8	0.25	0.46	0.68	1.21
Nd	0.815	39.4	1.20	1.97	2.75	4.68
Sm	0.299	7.54	0.37	0.52	0.66	1.02
Eu	0.155	1.58	0.13	0.16	0.19	0.26
Gd	0.419	7.30	0.49	0.63	0.76	1.11
Tb	0.077	0.94	0.09	0.10	0.12	0.16
Dy	0.525	5.80	0.58	0.68	0.79	1.05
Ho	0.12	1.13	0.13	0.15	0.17	0.22
Er	0.347	2.97	0.37	0.43	0.48	0.61
Tm	0.054	0.39	0.057	0.064	0.071	0.088
Yb	0.347	2.80	0.37	0.42	0.47	0.59
Lu	0.054	0.426	0.058	0.065	0.073	0.091

Source compositions used in REE mixing melting models. S1=1% SCM +99% MORB-source, S3=3% SCM + 97% MORB-source, S5= 5% SCM + 95% MORB-source, S10=10% SCM + 90% MORB source. MORB-source major elements are the Bulk Earth values of McKenzie and O’Nions (1991). SCM (Subducted Continental Material): major elements are the Upper Continental Crust estimate of Taylor and McLennan (1985) and the REE concentrations are from sediment G5-4-134B (see Chapter 5).

different in nature and/or proportions. Whitford and Jezek (1979) suggested that Serua’s location above the intersection of two subducted slabs may explain some of the peculiarities of its rocks.

We conclude that the regional systematics in REE trends and trace-element ratios must be attributed to source characteristics. Shallow-level processes had a subordinate influence and affected primary trace-element signatures only locally and to a limited extent.

Table 4.2. Mineral proportions used in melting calculations

Rocktype	Chemistry	Olivine	Opx	Cpx	Garnet	Phlogopite	Amphibole	SSR
GPP	S1	0.591	0.191	0.084	0.134	-	-	0.272
GPP	S3	0.552	0.216	0.083	0.142	0.007	-	0.336
GPP	S5	0.512	0.241	0.083	0.150	0.014	-	0.414
GPP	S10	0.415	0.304	0.081	0.169	0.032	-	0.667
AP	S1	0.590	0.243	0.053	-	-	0.114	0.496
AP	S3	0.551	0.276	0.048	-	-	0.126	0.559
AP	S5	0.512	0.309	0.042	-	-	0.137	0.638
AP	S10	0.414	0.391	0.291	-	-	0.167	0.914
PP	S1	0.600	0.199	0.126	-	0.075	-	1.671
PP	S3	0.561	0.225	0.128	-	0.086	-	1.898
PP	S5	0.522	0.251	0.129	-	0.098	-	2.148
PP	S10	0.424	0.315	0.134	-	0.126	-	2.872

Mineral proportions used in melting-mixing models which were calculated by a least-squares method with mineral compositions reported in McKenzie and O'Nions (1991). See text for details. Opx=orthopyroxene, Cpx=clinopyroxene, GPP= garnet-phlogopite peridotite, AP=amphibole peridotite and PP=phlogopite peridotite. SSR=sum of residuals.

4.4.2. REE mixing-melting models

The along-arc variations in incompatible-element abundances and ratios could reflect changes in (1) melting degree, (2) source mineralogy, and (3) proportions of subducted and mantle-wedge components. Because the shelf and wedge sediments do not show a systematic along-arc change in trace-element characteristics (Chapter 5), important changes in the compositions of SCM is an unlikely alternative explanation.

We tested options (1), (2) and (3) with mixing-melting models applied to the REE. Magma generation was considered as a two-step process: first, creation of a 'modified mantle' by addition of SCM to 'pre-subduction' MORB-source mantle; subsequently, generation of primary arc magmas by melting this 'modified mantle' source. REE concentrations in the magmas, predicted from forward modelling of this mixing-melting process, were compared with the observed compositions of the low-, medium- and high-K volcanoes (Figs. 4.5 and 4.6). The approach is similar to that used by Nicholls et al. (1980).

The models were applied to the REE, because their distribution coefficients and abundances in the mantle are better known than for other trace elements. We use the REE distribution coefficients of McKenzie and O'Nions (1991), but it should be noted that other sets of distribution coefficients would not change the general conclusions.

Table 4.3. Distribution coefficients used in REE mixing-melting calculations

Element	Olivine	Opx	Cpx	Phlogopite	Garnet	Amphibole
La	0.00040	0.00200	0.05400	0.03400	0.01000	0.17000
Ce	0.00050	0.00300	0.09800	0.03400	0.02100	0.26000
Pr	0.00080	0.00480	0.15000	0.03300	0.05400	0.35000
Nd	0.00100	0.00680	0.21000	0.03200	0.08700	0.44000
Sm	0.00130	0.01000	0.26000	0.03100	0.21700	0.76000
Eu	0.00160	0.01300	0.31000	0.03100	0.32000	0.88000
Gd	0.00150	0.01600	0.30000	0.03100	0.49800	0.86000
Tb	0.00150	0.01900	0.31000	0.03000	0.75000	0.83000
Dy	0.00170	0.02200	0.33000	0.03000	1.06000	0.78000
Ho	0.00160	0.02600	0.31000	0.03200	1.53000	0.73000
Er	0.00150	0.03000	0.30000	0.03400	2.00000	0.68000
Tm	0.00150	0.04000	0.29000	0.03600	3.00000	0.64000
Yb	0.00150	0.04900	0.28000	0.04200	4.03000	0.59000
Lu	0.00150	0.06000	0.28000	0.04200	5.50000	0.51000

REE distribution coefficients used in mixing-melting models. Distribution coefficients are from McKenzie and O'Nions (1991), except those of phlogopite, which are from Schnetzler and Philpotts (1970), Philpotts and Schnetzler (1970). La, Pr, Eu, Gd, Tb, Ho, Tm and Lu were estimated by interpolation and extrapolation.

4.4.2.1. Assumptions for the mixing step

For calculations of the REE concentrations in the 'modified mantle' source, it was assumed that mixing occurred by bulk addition of SCM to the wedge. Compositions of the hypothetical end members are given in Table 4.1. Because sediments on the Australian shelf are a good representative of SCM (see Chapter 5), a local (low-carbonate) sediment with a high terrigenous fraction (and hence a relatively high REE content) was taken as end member. It should be noted that other compositions (e.g. average sediment) would not change the conclusions arrived at below. The REE concentrations in the mantle end member are those used by McKenzie and O'Nions (1991) for depleted mantle. Evidence for the involvement of depleted N-MORB type mantle in the East-Indonesian arcs has been discussed in various earlier studies (e.g. Stolz et al., 1990; Wheller et al., 1987; and see Chapter 3). The synthetic 'modified-mantle' compositions (S1-S10) were calculated for 1, 3, 5 and 10% sediment addition.

4.4.2.2. Assumptions for the melting step

Modal compositions of 'modified mantles' from which melts were extracted, were calculated from estimated major element compositions, using a least-squares routine and the mineral compositions in McKenzie and O'Nions (1991). Three different mineral assemblages were considered: garnet-phlogopite peridotite (GPP), phlogopite-peridotite (PP) and amphibole peridotite (AP). The calculated modal proportions are given in Table 4.2. The major-element compositions of these 'modified-mantle' sources were obtained by mixing SCM and MORB mantle in the same proportions as chosen for the REE, using the compositions of average Upper Continental Crust (Taylor and McLennan, 1985) and Bulk Earth (McKenzie and O'Nions, 1991) respectively.

Partial melting models have been discussed by Williams and Gill (1989). For high degrees of partial melting there is little difference between various models, but significant differences can be expected for small melting degrees ($X < 5\%$). Dynamic melting models are commonly applied to MORB genesis (e.g. Williams and Gill, 1989; and cf. Klein and Langmuir, 1987) for physical reasons, but are also appropriate for arc magma genesis (Reagan and Gill, 1989). Here we used a dynamical melting model after McKenzie (1985), which assumes that fertile material (undepleted by melt extraction) constantly moves into the source region, and that refractory material is left after undergoing some maximum degree of melt extraction.

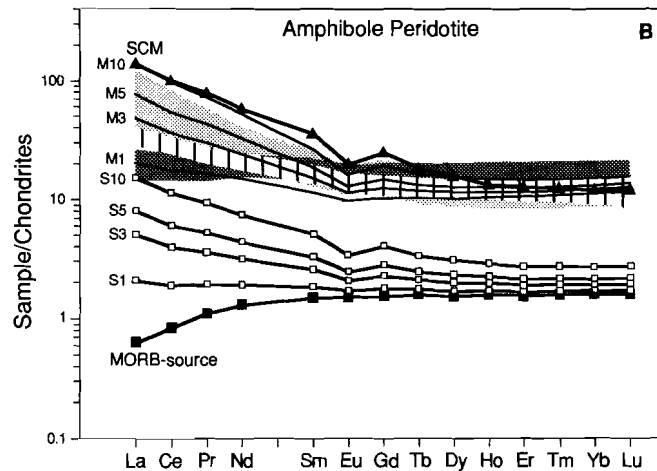
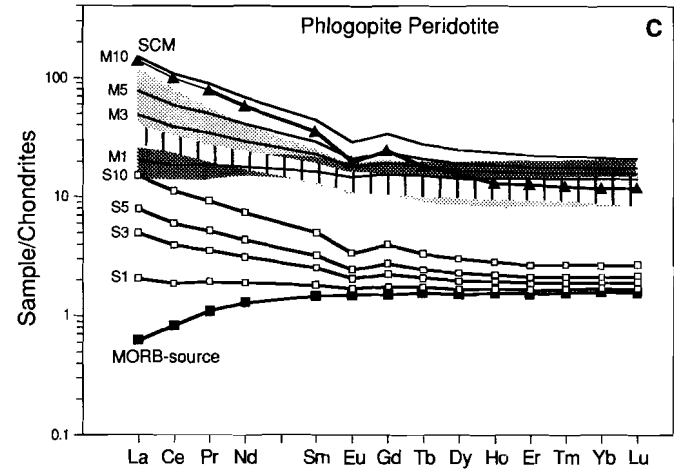
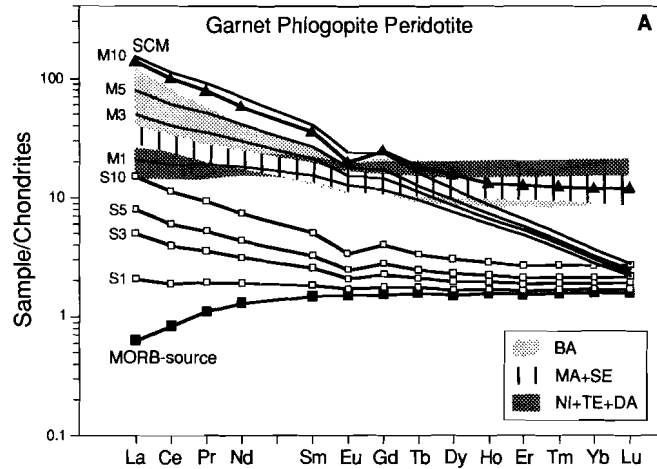


Fig. 4.5a,b,c. REE mixing-melting models. Patterns of five hypothetical melts (M1-3-5-10) from source compositions (S1-3-5-10) were calculated for three mantle mineralogies: Garnet Phlogopite Peridotite (a); Amphibole Peridotite (b) and Phlogopite Peridotite (c). The dynamic melting model of McKenzie (1987) was used with a mantle porosity $\phi=0.5\%$, and the melt was assumed to have a density 0.95 times that of the source (cf. Reagan and Gill, 1989). The melting degree is 10%. Fields of volcanics: BA = Banda Archipelago, MA + SE = Manuk + Serua, NI + TE + DA = Nila + Teon + Damar. Source compositions (S) were calculated by 1-3-5-10% bulk addition of SCM to MORB source. Compositions and distribution coefficients used are given in Tables 4.1, 4.2 and 4.3. Note that increasing amounts of SCM can generate the REE patterns of the volcanics for amphibole and phlogopite-bearing sources, and that garnet is an unlikely residual mineral in all cases.

4.4.2.3. Evaluation of mixing-melting models

Variations in residual minerals?

The shape of calculated REE patterns strongly depends on whether garnet, amphibole or phlogopite is taken as a residual phase (Fig. 4.5). Garnet-bearing residual assemblage would yield satisfactory LREE trends, but much more depleted HREE relative to the LREE than observed in any of the rock suites, irrespective of the amount of SCM added to the mantle (as illustrated for the garnet-phlogopite peridotite in Fig. 4.5). Amphibole and phlogopite produce patterns of which the shapes correspond much better to the observed trends. Either of these minerals (or both) could be residual phases in the magma sources. The NE-SW increase in potassium may imply an increasing phlogopite control, but this cannot be substantiated by the REE models.

Sekine and Wyllie (1982) pointed out that amphibole could be stabilized during fluid transfer to the wedge, whereas phlogopite is formed when siliceous melts derived from the subducted oceanic crust/sediments react with mantle peridotite. The generation of magmas below the volcanic front has been ascribed to the pressure-dependent break-down of amphibole in metasomatized peridotite, dragged down during the subduction, whereas destabilization of phlogopite at higher pressure could control melting behind the front (e.g. Tatsumi, 1989). However, Foley (1991) demonstrated that the stability of amphibole strongly depends on its fluorine content, and is higher for fluorine amphibole than for hydroxy amphibole, which implies that the break-down of amphibole may occur over a depth interval of 45 km. Although the K/F ratios of the Banda Arc volcanics (Vroon et al., 1989) are consistent with residual phlogopite, a possible role for fluorine- and potassium-bearing amphiboles cannot be discarded.

Variations in melting degree?

If the along-arc trends in incompatible elements reflected changes in the degree of melting of one compositionally constant source, the melt fractions would decrease from the low-K series in the NE to the high-K series in the SW. The results of mixing-melting models for amphibole and phlogopite peridotites with a fixed composition S1 (Table 4.1) are shown in Fig. 4.6. The observed increase in LREE enrichments from NE to SW can be generated from each peridotite by decreasing the melting degree from $X=10\%$ to about $X=0.1\%$.

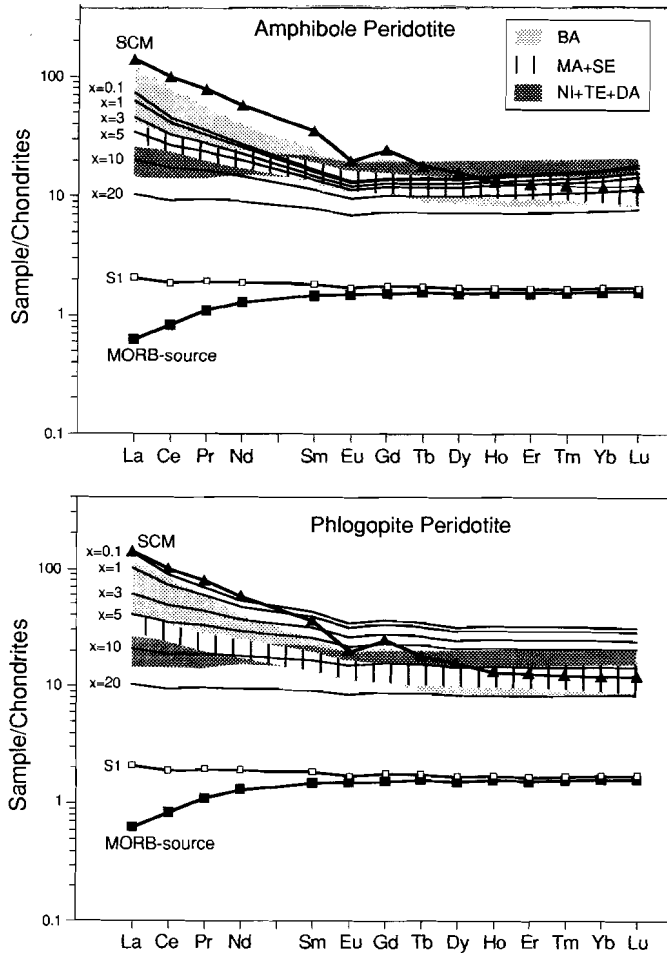


Fig 4.6a and b. REE mixing-melting models. Parameters and symbols are the same as in Fig. 4.5, except that the melting degree (x) varies from 0.1 to 20%, and that only source composition S1 is used. The calculated patterns suggest that a systematic variation of the melting degree is an unlikely explanation for the NE-SW change in REE patterns of the volcanics. See text for further discussion.

However, the models predict an NE-SW increase in the HREE, contrary to the observed decrease. The HREE contents calculated from the phlogopite-bearing source in particular become too high. Hence, although small variations cannot be ruled out, it seems unlikely that different melting degrees caused the along-arc variations in the REE.

Variations in the amount of SCM?

Fig. 4.5 shows the results of models used to investigate the effects of variations in the proportions of SCM. Sources S1-S10 were calculated by adding 1-10% SCM to the MORB mantle. The REE patterns were calculated for amphibole and phlogopite peridotites, assuming a fixed degree of melting ($X=10\%$). The shapes of the model patterns (M1-M10) correspond well to the observed compositions. The results indicate that the along-arc REE trend can be explained by a NE-SW increase in SCM. This applies to both the amphibole- and phlogopite-bearing source assemblages. Residual amphibole yields smaller variations in the HREE, and is probably a more ubiquitous phase than phlogopite, which may only occur in the high-K sources.

Although the uncertainties inherent in these models preclude precise quantitative constraints on the mixing-melting process, we believe that the REE signatures of the Banda Arc volcanoes largely reflect mantle sources which were contaminated by SCM in increasing amounts from NE (about 1%) to SW (about 10%) along the arc. Amphibole (and/or phlogopite) is a likely residual mineral in peridotitic source rocks. Partial melting controls cannot be excluded but were probably less significant.

4.4.3. Evidence for SCM from incompatible trace-element ratios: comparison with local sediments, MORB, OIB and other island arcs

The main conclusions from the REE models are supported by along-arc trends in incompatible trace elements. Fig. 4.7 shows these trends for various ratios of different element groups, and compares the volcanics with the local sediments, other island arcs and average MORB and OIB. The island-arcs used for comparison are all constructed on oceanic crust.

LILE/LILE ratios (K/Rb, Rb/Ba, Ba/Th)

The K/Rb and Ba/Th ratios of the volcanics generally overlap with the sediment field. These ratios are nearly constant along the Banda Arc, which suggests that any mantle component is swamped by the SCM contribution. Only for the Banda Archipelago does the SCM influence seem less. Ba/Th ratios in other oceanic arcs are at least four times higher than in the Banda Arc. The Rb/Ba values of Manuk, Serua and Romang plot within the sediment field, but the SW Banda Arc volcanoes fall between MORB and the sediments.

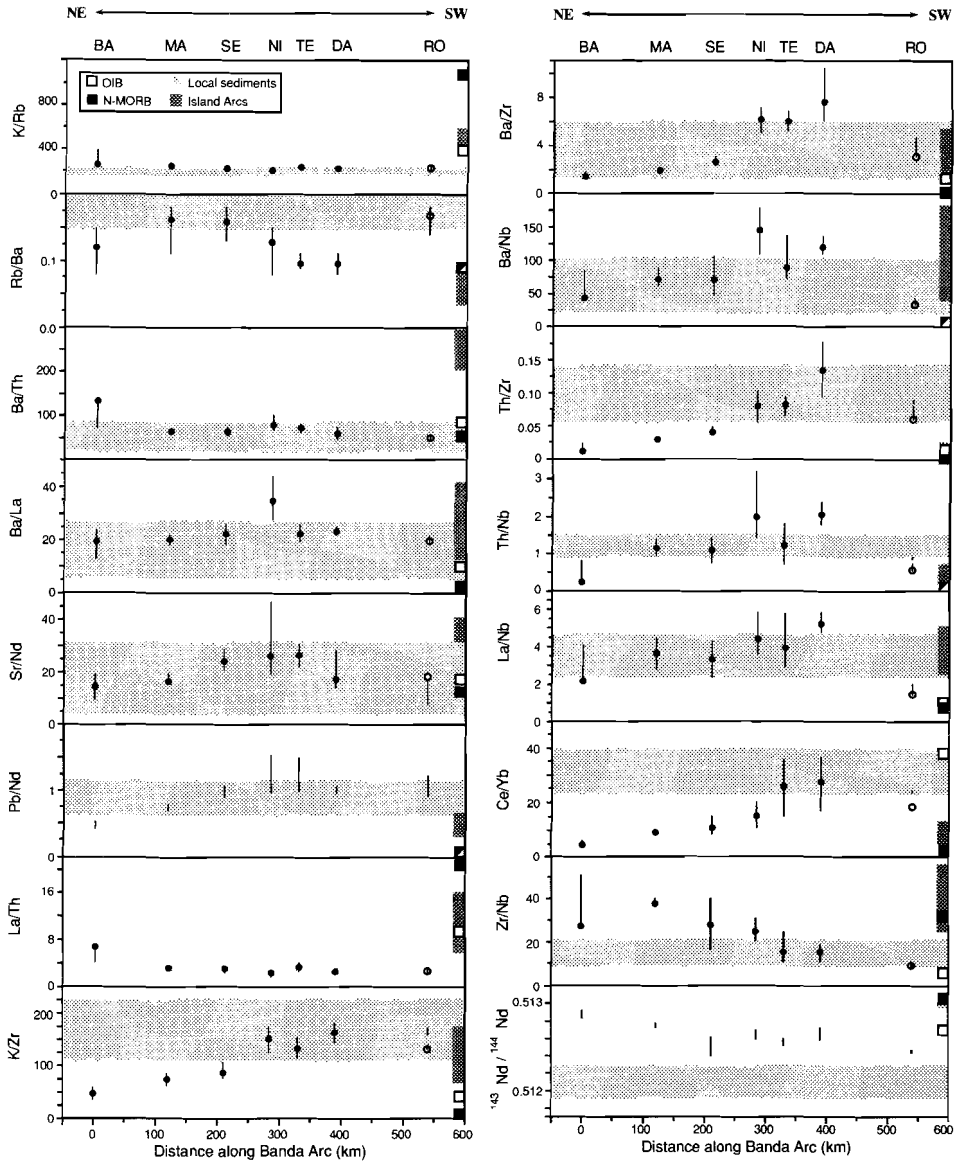


Fig. 4.7. Selected trace-element ratios of the Banda Arc volcanics. Solid circles indicate ratios at $\text{SiO}_2=57.5\%$ as determined by linear regression. Bars represent total ranges within individual suites. Abbreviations as in Fig. 4.2. Romang is displayed as open circle, which is the average of four andesites. The two bars for Romang are for andesites and rhyolites. Ranges for sediments are from Chapter 5, Table 5.3. The average N-MORB and OIB values are from Sun and McDonough (1989). The range for average island-arcs is based on the oceanic New Britain, Vanuatu, Marianas, and Aleutian Arcs. References are cited in McCulloch and Gamble (1991).

The Rb/Ba ratios of other island arcs are still lower. Ellam and Hawkesworth (1988) discussed LIL element fractionations in subduction-related basalts, and suggested that small degree partial melting of a relatively Rb-poor mantle source could account for variations in Rb/Ba, if Ba is slightly less incompatible than Rb. The low Rb/Ba ratios of Nila-Teon-Damar relative to the other volcanoes (despite the higher SCM proportions deduced from the other trace-element ratios, see Fig. 4.7) could thus be due to higher degrees of partial melting.

However, this is difficult to reconcile with: (1) the higher Rb contents in these high-K volcanoes, (2) the conclusions from the REE models, and (3) the lack of evidence from other trace-element ratios which would also be sensitive to small-degree partial melting effects (e.g. K/Rb). Hence, the deviations from bulk SCM-mantle mixing, which appear when element pairs with barium are considered, are probably due to a greater flux of this element when fluids escape from the slab. The distinct behaviour of Ba also appears in the N-MORB normalized abundance diagrams (Fig. 4.4). Whereas conspicuous negative Ba anomalies relative to other LIL elements characterize the sediments, the anomalies are less pronounced or absent in the volcanics. Assimilation effects may be superimposed, as is most evident in the case of Nila.

REE-LILE ratios (Ba/La, Pb/Nd, Sr/Nd, La/Th)

The Ba/La ratios show little variation and plot within the sediment field, except for the slightly higher value of Nila. The Sr/Nd ratios also fall within the sediment field and show a maximum in the central part of the arc (Serua, Nila, Teon). The Pb/Nd ratios increase along the arc from island-arc values (Banda Archipelago) to sediment values. The La/Th ratios are almost constant. They plot within or close to the narrow sediment field, which is strong evidence that they are almost completely controlled by SCM. The Banda Arc volcanics are lower in Sr/Nd and La/Th and higher in Pb/Nd than other island arcs. These deviations are all consistent with involvement of SCM.

LILE,LREE,HFSE/HFSE ratios (K/Zr, Ba/Zr, Ba/Nb, Th/Zr, Th/Nb, La/Nb, Zr/Nb)

All volcanoes show the characteristic island-arc signature of high LILE/HFSE relative to MORB. The LILE/HFSE ratios increase from values between N-MORB and the sediments in the NE to sediment values in the SW (only the Th/Nb and Ba/Nb ratios of Nila deviate from this trend), which indicates that these ratios also reflect increasing proportions of SCM. The K/Zr, Ba/Zr, Ba/Nb and La/Nb ratios show overlaps with other island arcs, but Th/Zr

and Th/Nb are generally higher. The La/Nb ratios plot in the sediment field except for Damar and Romang. There may be a slight NE-SW increase. The La/Nb ratios of other island arcs are similar. The Zr/Nb ratios decrease from island-arc values in the NE to sediment values in the SW. This trend is important since it provides support for the conclusion that also the HFSE/HFSE ratios to a large extent reflect the increasing amounts of SCM in this direction.

High LILE/HFSE or LREE/HFSE ratios in island arcs are conventionally explained by the addition of LILE enriched fluids (compared to the HFSE) and/or retention of HFSE in residual minerals (see Foley and Wheller, 1991 for a recent discussion). However, the NE-SW along-arc increase in $Nb_{[57.5]}$ (Fig.4.2), the decrease in Zr/Nb, and the broad correspondence between volcanics and sediments for LILE/HFSE and LREE/HFSE (Fig. 4.7) strongly suggest that HFSE were mobilized from the slab and supplied to magma sources, confirming experimental evidence that residual titanate phases are unlikely in the subduction zones (Green and Pearson, 1986; Ryerson and Watson, 1987). It is further important to emphasize that negative Nb-Ta anomalies characterize both the sediments and the volcanics (Fig. 4.4). The Banda Arc thus shows that this typical island-arc signature can be largely inherited from continent-derived subducted source components, an option not considered by Foley and Wheller (1991).

LREE/HREE ratio (Ce/Yb)

The along-arc behaviour of the REE was discussed above. It can further be noted that only the Ce/Yb ratios of Banda, Manuk and Serua fall within the range of other island arcs, whereas the ratios of the high-K volcanoes in the SW are higher. The slight NE-SW decrease in HREE contents of the volcanics (at $SiO_2=57.5\%$, Fig. 4.2) is difficult to reconcile with increasing proportions of SCM and melting of mineralogically similar sources at any constant melting degree. We speculate that magmas, generated by the mixing-melting process modelled above, subsequently mixed with SCM melts, particularly in the SW, where larger volumes of continental material may have been subducted. Garnet may be stable in SCM-type lithologies up to the PT conditions where the SCM is expected to melt in subduction zones, as suggested by the experimental results of Stern and Wyllie (1973a,b). Nevertheless, the observed depletions in HREE relative to the LREE are not as large as would be expected if garnet is a residual phase. Therefore, it is conceivable that any melting of SCM near magma source regions occurred to such a large degree that garnet was no longer present. The incompatible trace-element ratios thus corroborate the evidence derived from the REE models and isotope data for the involvement of SCM in magma genesis. They are also consistent

with a NE-SW increase in the proportion of SCM along the arc, which is clearly shown by ratios which trend towards the sediment field (e.g. K/Zr, Ba/Nb, Ba/Zr, Zr/Nb, Th/Zr).

Ratios tending to remain constant (e.g. K/Rb, Ba/Th, Ba/La, La/Th) do not contradict this, because their correspondence with the sediment ratios suggests that SCM had swamped magma sources for these elements, even where its contribution was low. The La/Th- $^{143}\text{Nd}/^{144}\text{Nd}$ bulk mixing curve between MORB mantle and average sediment (AS) in (Fig. 4.8a) is illustrative. The La/Th ratios of the volcanics remain constant and equal to the sediment value for any amount of sediment greater than about 1%.

4.4.4. Comparison with isotope evidence

Decoupling between Sr-Nd-Pb isotopes from trace-element abundances is a common feature in island arcs (Kay et al., 1980). The above conclusions from the trace-elements systematics in the Banda Arc are consistent with the Sr-Nd-Pb-He-Hf-O isotopic results (Chapter 3, and references therein), in the sense that all these tracers point to the involvement of continental material. Furthermore, the isotope data (notably Pb and Nd isotopes) agree with the trace-element evidence for smallest contributions of SCM to sources in the NE Banda Arc (Banda Archipelago and Manuk) and largest amounts in the SW (Nila, Teon, Damar, Romang). Thus, a crude correlation exists between isotopic data and incompatible trace-element abundances and ratios on the scale of the entire arc (note the along-arc $^{143}\text{Nd}/^{144}\text{Nd}$ trend in Fig. 4.7).

The coupling between isotopes and trace elements is not maintained in all details, which indicates that simple two-component source mixing can only be considered as a first-order approximation (e.g. see discussion on fluids below). Medium-K Serua forms an obvious example. Situated in the central part of the arc, it fits within the along-arc trends of trace-element ratios, but deviates in Sr- and Nd-isotopes, which suggests that some of its lavas contain the highest proportions of SCM, comparable to the high-K lavas from Romang in the SW (Chapter 3). Involvement of at least one more component, at depth and/or at shallow levels, must be invoked to explain such behaviour. In the case of Serua, it can be speculated that melts from subducted slivers of continental crust are involved, given the isotopic similarity with Romang where the leading edge of the Australian continent may have been subducted (Hilton et al., 1992).

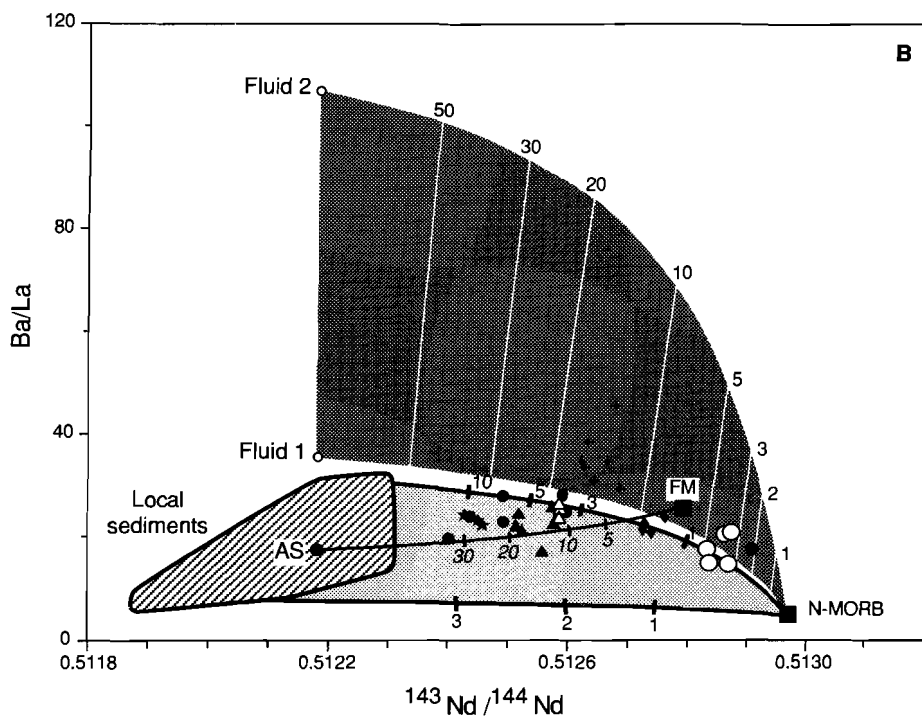
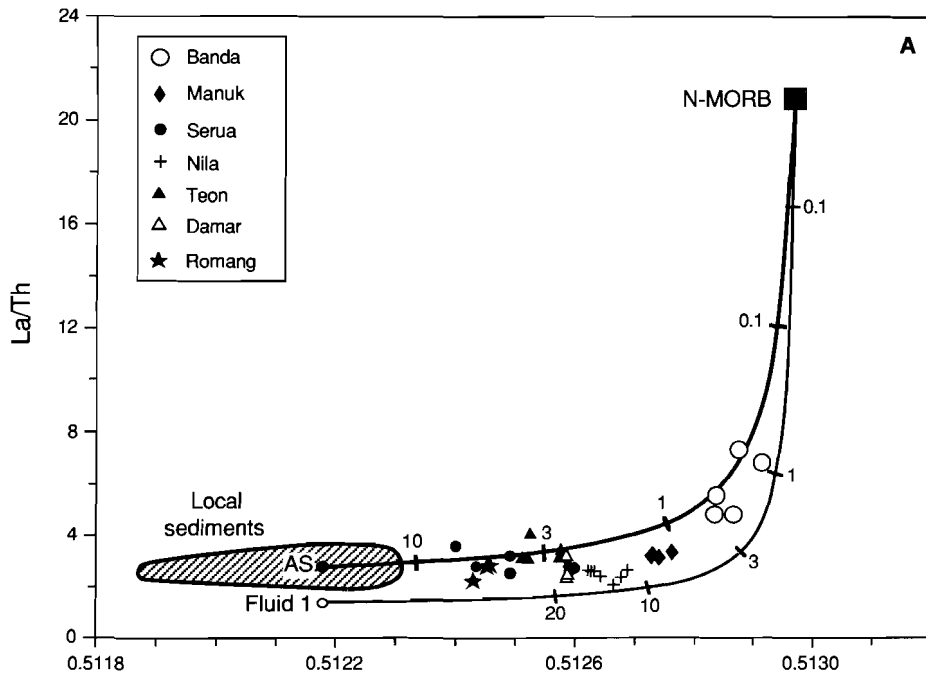
As discussed in Chapter 3, the high-K volcanics of the SW Banda Arc are characterized by high $^{208}\text{Pb}/^{204}\text{Pb}$ compared to $^{206}\text{Pb}/^{204}\text{Pb}$ and $^{207}\text{Pb}/^{204}\text{Pb}$, which cannot be explained by simple mixing between N-MORB mantle and the local sediments. Because these Pb-isotope signatures are typical for many Indian Ocean Island basalts, an OIB-type mantle

may be involved (cf. Morris and Hart, 1983). Some trace-element ratios may distinguish between MORB- and OIB- mantle in island arcs, provided that slab influences are minimal. For this reason, the Zr/Nb ratio has been employed as a diagnostic parameter in island-arcs (e.g. Ellam et al., 1988; 1989; Edwards et al., 1991), since Zr/Nb is lower in OIBs than in MORBs. Using such arguments, Van Bergen et al. (1992) suggested that an ultrapotassic suite in the adjacent Eastern Sunda Arc originated by mixing between OIB-melt and melt from SCM-contaminated MORB mantle. From inspection of Fig. 4.7, it seems that addition of bulk sediment to a MORB-mantle can largely account for the trace-element ratios of the high-K volcanics of the SW Banda Arc (including low Zr/Nb), without the need to invoke an OIB-type mantle. Alternatively, a mantle component may be involved which has OIB-type (Pb) isotopic characteristics, but does not necessarily have the trace-element signatures of OIBs.

4.4.5. Additional role of fluids

The above trace-element evidence suggests that bulk addition of SCM to mantle source without fractionation of elements is the dominant source-mixing mechanism in the Banda Arc. However, some ratios (Ba/Zr, Ba/Nb, Th/Nb) point to a possible additional role of fluids, since they occasionally plot above the sediment field (Fig. 4.7), and cannot be explained by simple SCM-mantle mixing. High Ba/HFSE and Th/HFSE ratios in island arcs are generally explained by preferential transport of the LIL elements by fluids (e.g. Gill, 1981; Arculus and Powell, 1986). Interestingly, the Th/HFSE and Ba/Nb ratios of the SCM-contaminated Banda Arc volcanoes are higher than in other oceanic arcs, from which we infer that, if fluids have transported LIL- and other mobile-elements to some extent, they may originate from SCM rather than from underlying basaltic oceanic crust.

The possible role of fluid metasomatism versus bulk mixing is illustrated by mixing curves in $^{143}\text{Nd}/^{144}\text{Nd}$ against La/Th and Ba/La diagrams (Fig. 4.8). The fluid compositions were calculated from average local-sediment compositions, using the element mobilities of Tatsumi et al. (1986). Because these mobilities were experimentally determined for the partitioning between fluid and serpentine, the fluid compositions can only be considered as rough estimates. The mixing lines between MORB source and fluids represent the hypothetical cases of source contamination by sediment-derived fluid, without addition of bulk sediment.



There is little difference between the MORB-SCM mixing curves for bulk sediment and fluid in the case of La/Th, because of the small difference in La/Th between sediment and fluid, and the low Th content of MORB source (0.012ppm) relative to both. The datapoints for the Banda Arc volcanoes plot close to both curves, which emphasizes the importance of SCM, irrespective of the transfer mechanism. Other ratios that show a similar behaviour are K/Rb and Ba/Th.

The significance of fluids in island-arc petrogenesis is commonly inferred from high Ba/La ratios, since Ba is considered to be more mobile than La (cf. Tatsumi et al., 1986). The $^{143}\text{Nd}/^{144}\text{Nd}$ -Ba/La diagram (Fig. 4.8b) demonstrates that most of the Banda Arc volcanoes have relatively low Ba/La ratios and plot within the field of bulk sediment-MORB source mixing. Only for Nila and the Banda Archipelago are the Ba/La ratios mostly too high. Shallow-level assimilation of carbonate-rich sediment, poor in terrigenous components, is a plausible explanation for Nila, as discussed in Chapter 3. For the low-K Banda Archipelago a fluid-controlled contribution seems most likely.

The range of Ba/La in the Banda Arc is limited (15-25, excluding Nila, Fig. 4.8b), and much higher ratios have been reported from other island arcs with more conspicuous evidence for fluids. For example, Ba/La ratios of 20-75 characterize the Mariana lavas (Lin et al. 1990). The extreme Ba/La ratio of fluid 2 (Fig. 4.8b) is the ratio these authors proposed for the fluid which may have generated the Marianas signatures. In contrast, moderately low Ba/La ratios have been found in the Luzon arc, where subducted continental material may have contaminated magma sources (Defant et al., 1991) in a similar way as in the Banda Arc. This correspondence also holds for the rapid increase of La/Sm ratios at almost constant (Banda Arc, cf. Fig. 4.3) or slightly increasing (Luzon Arc) Ba/La ratios, which is an uncommon feature in island arcs.

Fig. 4.8a. $^{143}\text{Nd}/^{144}\text{Nd}$ -La/Th diagram showing bulk mixing between Average Sediment (AS), AS-derived fluid and N-MORB source. End-member compositions are given in Table 4.4. Note that addition of more than 1% sediment or 3% fluid is sufficient to generate approximately the same La/Th ratios in the volcanics as in the sediment.

Fig. 4.8b. $^{143}\text{Nd}/^{144}\text{Nd}$ -Ba/La diagram illustrating source contamination by fluids versus bulk sediment addition. Compositions of local sediments, fluids and MORB-source are given in Table 4.4. Note that Nila and the Banda Archipelago plot outside the lower shaded field of N-MORB-sediment mixtures and fall partly in the darker shaded field of N-MORB-fluid mixtures (see text for discussion). Fluid 1 is derived from Average Sediment, and Fluid 2 is a 'Marianas-Arc fluid' (Lin et al., 1990). The AS-FM mixing line illustrates a possible scenario for the Banda Arc where AS melts mix with fluid-modified mantle (FM) or melts from this mantle (tick marks are for melt-melt mixtures).

Table 4.4. End-member compositions used in Fig. 4.8

Element/ ratio	MORB source	G5-2 19B	G5-6 134B	Average sediment	Fluid 1	Fluid 2	FM
$^{143}\text{Nd}/^{144}\text{Nd}$	0.51297	0.51229	0.51190	0.51218	0.51218	0.51218	0.51274
La/Th	20.8	3.00	2.62	2.73	1.36		
Ba/La	2.52	28.7	6.05	17.6	33.3	105	24.0
Nd (ppm)	0.73	24.4	38.2	27	2.97	2.97	9.27
Th (ppm)	0.012	10.5	20.3	11.2	3.37		
La (ppm)	0.25	31.5	53.2	30.5	4.57	3.8	5.25

MORB source: ratios and concentrations from Sun and McDonough (1989), assuming 10% melting, $^{143}\text{Nd}/^{144}\text{Nd}$ ratio taken similar as a back-arc rock TBD (Morris, 1984, cf. Chapter 3). The extremes of the local sediments are G5-2-19B and G5-6-134B (see Chapter 5) which are used to construct the field of possible sediment-MORB-source bulk-mixtures. Average Sediment (AS) was calculated from wedge and shelf sediments with less than 30% CaCO_3 (Chapter 5). Fluid 1 is calculated from AS using the mobility data from Tatsumi et al. (1986) and assuming a mobility of 11% for Nd (cf. Lin et al., 1990) and 30% for Th. Fluid 2 is a fluid composition calculated by Lin et al. (1990) for the Marrianas using the Pacific Authigenic Weighted Mean Sediment (PAWMS) of Hole et al. (1984) and the mobility data of Tatsumi et al. (1986), but assuming it has Nd-isotopes similar to Average Sediment (AS). The melt from the fluid modified mantle (FM) was calculated by mixing 10% Fluid 1 plus 90% N-MORB source and melting this mixture for 10%, assuming the following K_d 's: Ba=0.01; La=0.05; Nd=0.05.

4.4.6. Two-stage source contamination?

The evidence for a (subordinate) role of fluids in the entire arc, in addition to the (NE-SW increasing) importance of bulk SCM, leads to the hypothesis that the Banda Arc magmas result from source-mixing of (at least) three components: a mantle component, SCM and fluid (cf. Ellam and Hawkesworth, 1988). We envisage the addition of SCM to a mantle source which was previously metasomatized by fluids. Fig. 4.8b shows a mixing curve between a fluid-modified mantle (FM) and average local sediment (AS). The curve serves to illustrate the possibility that SCM is added to a mantle which was previously metasomatized by SCM-derived fluids. (Note that same curve is valid if FM represented a 'fluid-dominated' arc-type melt).

The fluid-modified mantle can be generated (1) when fluids escape from the slab at relatively shallow levels in the subduction zone before SCM starts to melt, or (2) during earlier periods of subduction in this region. Fig. 4.9 schematically illustrates the first option.

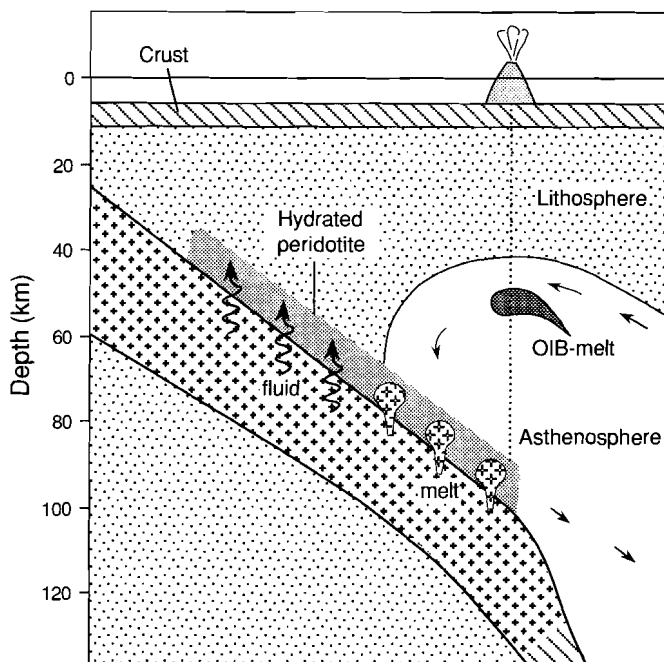


Fig. 4.9. Schematic cross section in the southern Banda Arc, illustrating the model discussed in Chapter 4. SCM-derived fluids infiltrate the mantle wedge at shallow levels, whereas SCM melts are generated at deeper levels. See text for discussion.

Fluids from dehydrating SCM create a hydrated peridotite in the overlying wedge, which is dragged down by the slab to depths where the SCM starts to melt and causes a second stage of metasomatism. The net result will be close to bulk addition of SCM to the mantle wedge. Subsequent melting of this mantle produces the typical SCM-dominated Banda Arc magmas.

It is also conceivable that hydrated peridotite starts to melt and yields 'fluid-dominated' arc magma without previous addition of SCM melt. This situation would be similar to the model proposed by Tatsumi (1989), except that hydrous fluids are not (only) derived from hydrated oceanic crust, but escape from SCM (probably sediments rather than solid continental crust).

Ascending batches of acidic melts from (dehydrated) SCM could mix with 'fluid-dominated' arc magma in the mantle wedge, yielding hybrid products that are geochemically difficult to distinguish from melts formed in a two-stage metasomatized peridotite. If the acidic melts are sufficiently voluminous, they even may reach shallow crustal levels, as might be the case in the southern extinct sector (Wetar, Romang). These melts may originate in the subducted leading edge of the Australian continental crust. The uncommonly low $^3\text{He}/^4\text{He}$

ratios that characterize this part of the Banda Arc may be attributed to the presence of crystalline continental crust below the volcanic front, rather than to fine-grained terrigenous sediments (Hilton et al., 1992; cf. Charlton, 1991).

Whether final magma compositions carry a 'bulk-SCM' dominated signature will depend on the volumes of SCM that are mobilized from the slab by melting. Fluid-dominated magmas will originate only where sediment volumes are relatively small, as shown by the compositions of the Banda Archipelago.

The second alternative, that of fluid enrichment during previous stages of subduction (e.g. before SCM entered the arc system), may also be valid. In this case, SCM-(melt) infiltrates mantle regions which were hydrated independent of the current subduction configuration. The assumption of an overlying mantle wedge being dragged-down is not required, and fluids could have originated from basaltic oceanic crust, which was subducted previously.

A three-component mantle-sediment-fluid mixing was previously suggested by Ellam and Hawkesworth (1988) as an explanation of the trace-element and isotopic variations in subduction-related basalts. They considered the origin of the fluid to be in subducted basaltic ocean crust. We cannot rule this out for the Banda Arc (particularly in the NE, where SCM contributions are minimal), but dehydration of SCM seems to be an important alternative here. Mixing of a fluid-modified mantle with bulk SCM is consistent with the Sr-Nd isotope systematics, as discussed in Chapter 3.

4.5. CONCLUSIONS

(1) Despite the fact that the Banda Arc is constructed on oceanic crust, the volcanics are characterized by trace-element signatures (e.g. low K/Rb, Ba/Th, La/Th ratios and high Th/Zr, Th/Nb and Ce/Yb ratios), which are more typical for continental arcs than for intra-oceanic arcs. These signatures correspond to the compositions of local sediments in front of the arc, which strongly indicates that Subducted Continental Material (SCM) is an important component in the magma sources. This conclusion agrees with isotopic evidence (Chapter 3), and corroborates the earlier hypothesis of Whitford and Jezek (1979). Along-arc variations in incompatible trace-element ratios are consistent with increasing contributions of SCM from NE to SW, where collision has led to the cessation of volcanic activity.

(2) Mixing-melting models favour the role of SCM in determining the REE patterns, and confirm the general NE-SW increase in the proportions of SCM involved. These models further suggest that amphibole (and/or phlogopite) are residual phases during partial melting, whereas garnet is probably absent. Variations in the degree of melting may have occurred,

but are not the principal cause of along-arc systematics.

(3) Negative Nb-Ta anomalies in N-MORB normalized abundance diagrams are to a large extent inherited from subducted sediments, and the observed along-arc trend in Zr/Nb ratios is consistent with changing proportions of SCM. Hence, SCM also controls the behaviour of HFSE (Nb, Ta, Zr and Hf), which are commonly considered as immobile when slab-derived fluids metasomatize arc mantle sources. In the Banda Arc, bulk addition of SCM, probably as melt, seems more important than selective transport of elements, particularly in the SW.

(4) Most trace-element ratios are consistent with two-component mixing of bulk SCM and MORB-source mantle. However, some ratios (e.g. Ba/HFSE and Th/HFSE) suggest that fluid transfer played an additional role. These ratios are often higher than in other island-arcs, which may imply that fluids are largely derived from dehydrating SCM (sediments), rather than from basaltic oceanic crust. Source regions in the mantle wedge were probably modified by subduction-related contributions in two ways: by infiltrating fluids and by addition of bulk SCM, probably as melts. Bulk transfer dominates over the role of fluids, particularly in the central and southwestern parts of the arc.

(5) Trace-element trends are not in all cases consistent with a systematic NE-SW increase in SCM. Assimilation of arc-crust material locally caused detectable deviations, and is most obvious in the Nila suite. Conversely, Serua, in the central part of the arc, follows the along-arc trend for many incompatible-element ratios, but some of its lavas contain the highest proportion of SCM in terms of Sr-Nd isotopes. Thus, the effects of local controls are superimposed on the general systematics, and are an additional cause of major deviations from simple two-component source mixing.

(6) The involvement of an OIB-type mantle component, the presence of which is suggested by Pb isotope data, does not have to be invoked to explain the trace-element systematics, although a minor contribution cannot be ruled out. Alternatively, if a mantle component with OIB-type isotopic signature is (locally) involved, it is conceivable that it has MORB-like trace-element signatures.

CHAPTER 5

SR, ND AND PB ISOTOPIC AND TRACE-ELEMENT SIGNATURES OF THE EAST INDONESIAN SEDIMENTS: PROVENANCE AND GEODYNAMICAL IMPLICATIONS

5.1. ABSTRACT

We present new trace-element and Pb-Sr-Nd isotope data for 127 surface sediments and 5 sediments from DSDP Site 262, distributed along and across the arc-continent collision region of the Banda Arc (East Indonesia). The results are used to evaluate the role of subducted continental material (SCM) in the genesis of the Banda Arc magmas, and to assess the extent to which geochemical and isotopic signatures of SCM are controlled by sediment provenance. In the surface sediments Pb and Nd isotope ratios are variable: $^{206}\text{Pb}/^{204}\text{Pb} = 18.65\text{-}19.57$, $^{143}\text{Nd}/^{144}\text{Nd} = 0.51230\text{-}0.51190$; with an increase in Pb isotope ratios and a decrease in the $^{143}\text{Nd}/^{144}\text{Nd}$ ratio from NE to SW along the Banda Arc. DSDP Site 262 sediments, farthest to the west in the Timor Trough, overlap with the surface sediments and have $^{206}\text{Pb}/^{204}\text{Pb} = 18.89\text{-}19.23$ and $^{143}\text{Nd}/^{144}\text{Nd} = 0.51200\text{-}0.51220$. In contrast, the trace-element ratios and REE patterns of the sediments do not show systematic along-arc variations, and largely overlap with estimated values for Upper Continental Crust, Post Archean Australian Shale and ODP Site 765 sediments from the Argo Abyssal Plain.

From the combined isotopic and trace-element ratios in the terrigenous fraction of the sediments two major sources can be distinguished: Phanerozoic New Guinea in the NE and Proterozoic Australia which is predominant in the SW. A further subdivision can be made on the basis of Th/Sc ratios, $^{147}\text{Sm}/^{144}\text{Nd}$ and Pb-Nd isotopes into: North New Guinea and Seram, South New Guinea, Timor and Northern Australia.

The Pb isotopic variations in the shelf and wedge sediments along the Banda Arc are parallel to similar variations in the volcanics; this is considered to be strong evidence for the incorporation of subducted continental material in the arc magmas. The hinterland of the sediments is responsible for isotopic signatures created in the Banda Arc mantle through recent subduction. This suggests that some of the mantle heterogeneities that are inferred from oceanic basalts can be explained by differences in the provenance of (ancient) subducted terrigenous sediment.

5.2. INTRODUCTION

Recycling of continental material is an important issue in many models concerning the evolution of continental crust (e.g. McLennan, 1988), oceanic island basalts (e.g. Zindler and Hart, 1986) and arc magmatism (e.g. Armstrong, 1981; Arculus and Powell, 1986). Generally, such models rely on estimates of the average composition of continental crust or sedimentary mass. However, trace-element and isotopic compositions cannot be considered as constant in space and time. For example, sediments from many ocean basins show a wide range in Sr-, Nd- and Pb-isotope ratios depending on provenance and age (e.g. Taylor and McLennan, 1985; White et al., 1985; Ben Othman et al., 1989; McLennan, 1990).

There is strong geochemical and isotopic evidence for the involvement of subducted continental material in the Banda Arc volcanics (Chapter 3 and references therein). In order to obtain better insight into the compositional variation of the subducted continental material (crustal and/or sedimentary), we have studied 127 box and piston cores from the Banda Sea region as well as 5 samples from DSDP Site 262 in the Timor Trough. Most of the samples come from three across-arc tracks in the NE, central and SW parts of the arc (Fig. 5.1 and Appendix 1.2). These tracks include all morphotectonic environments between the shelf and back-arc regions. The sediments are (sub-)recent (DSDP Site 262 sediments up to late Pliocene), and therefore too young to be the equivalent of the continent-derived components detected in the volcanics. Furthermore, the upper parts of the shelf sediments can be scraped off as they enter the trench, so that it may only be the underlying sediment sequences which have been subducted. However, we consider the Sr-Nd-Pb isotope ratios of the terrigenous fractions in the surface sediments to be representative for the continental masses of Northern Australia and New Guinea, and hence for earlier subducted continent-derived sediments (and crust) for the following reasons:

- (1) Sediments on the wedge are derived from older (Paleozoic-Tertiary) formations outcropping on uplifted islands (e.g. Seram).
- (2) The Northern Australian shelf has shown only little variation in depositional patterns from the late Cretaceous onwards. The Great Western Plain in Northern Australia has supplied clastic sediments since Precambrian times without undergoing major tectonic changes (Veveers, 1984).
- (3) Nd-depleted mantle ages (DePaolo, 1981b) of the sediments are > 1600 Ma, which suggests that all sediments are 'recycled' (see section 5.5.3.3).

Because the REE, Th, Sc are completely transferred to the sedimentary mass during weathering, transport and deposition, the REE/Th and Th/Sc ratios are indicative of the sediment provenance (McLennan et al., 1980). We compare the element ratios and the isotope data with the literature data on sediment geochemistry (e.g. McLennan et al., 1990,

Taylor and McLennan, 1985) and discuss the following topics:

- (1) Is there any variation in the trace elements and isotopes between New Guinea (NG) and Northern Australia (AS)?
- (2) What is the average chemical composition of Northern Australia and how does it compare with estimates of the average composition of upper continental crust?
- (3) What are the implications of this study for the involvement of subducted crustal material in magma genesis of the Banda and Eastern-Sunda-Arc volcanics?

5.3. TECTONIC FRAMEWORK AND LITHOFACIES OF THE BANDA SEA AREA

5.3.1. General

The area studied here belongs to an arc-continent collision complex (e.g. Hamilton, 1979). The passive Australian continental margin collided about 3 Ma ago with the Banda Arc. The volcanic Banda Arc is strongly curved and bends over nearly 180 degrees (see Fig. 5.1). The subduction trenches along the Banda Arc, the Timor, Aru and Seram troughs, are underlain by the Australian-New Guinea continental crust. Two plates are subducted beneath the Banda Arc: The Australian-Indian plate from the south and the New Guinea (Bird's Head) plate from the north.

The sediment samples studied here were obtained from the following morphotectonic environments (e.g. Hamilton, 1979; Situmorang, 1992): back-arc basin, volcanic arc, fore-arc basin, structural high, collision complex, trench, continental slope and continental shelf. In the next section, we shall describe the general characteristics of sediments from these morphotectonic environments. Detailed information on sediment cores and lithofacies descriptions can be found in Situmorang (1992), and for DSDP Site 262 in Veveers et al. (1974).

5.3.2. The back-arc basin

The Banda Sea back-arc region (water depth 5000 m) consists mainly of entrapped oceanic crust, probably Indian Oceanic crust (Bowin et al., 1980; Lee and McCabe, 1986), except for the Banda and Lucipara Ridges (water depth less than 2000 m). Dredge samples from these ridges reveal andesite, phyllite, amphibolite and meta-diorite with ages ranging from 6 to 22.5 Ma (Silver et al., 1985). Because these rocks are comparable with formations on Bird's Head, New Guinea (Silver et al., 1985), they are interpreted as 'continental slivers'

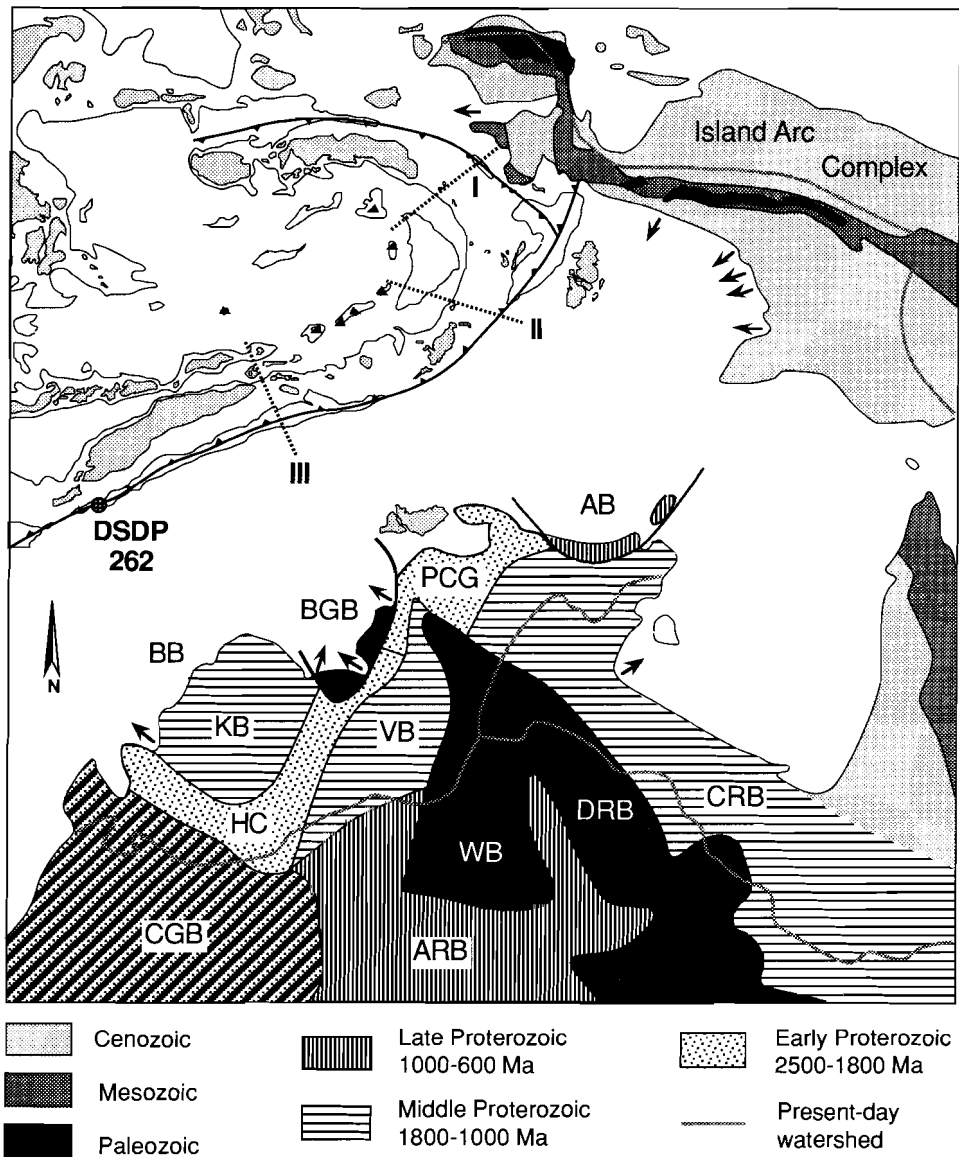


Fig. 5.1. Locations of sediment samples (Tracks I,II,III, DSDP-Site 262, cf. Fig. 2.1) and potential provenance areas of terrigenous sediments as shown by generalized age distributions in northern Australia and western New Guinea (Hamilton, 1979). Dashed lines on shelves and wedges are the borders of heavy-mineral provinces from Situmorang (1992): 1=Seram, 2=New-Guinea-Aru, 3=East Australia, 4=West Australia and 5=Kisar-Leti-Timor. Arrows indicate major rivers (those in northern Australia have mean discharges $> 150 \text{ m}^3/\text{sec}$ (Davies, 1977). Watersheds in Australia are from Warner (1977), in New Guinea from the Times World Atlas (1989). Abbreviations: CGB=Canning Basin; HC=Halls Creek; KB=Kimberly Basin; BB=Browse Basin; BGB=Bonaparte Gulf Basin; PCG=Pine Creek Geosyncline; VB=Victoria River Basin; ARB=Arunta Block; WB=Wisio Basin; DRB=Daly River Basin; CRB=Carpentaria Gulf Basin, AB=Arafura Basin.

derived from New Guinea. Sediment thicknesses on the Banda Sea floor are not well known. The irregular topography of the Banda Sea floor suggests that they are variable; this is also indicated by the seismic reflection data summarized in Bowin et al. (1980). From this data Hartono (1990) calculated a thickness of 1.7 km.

Pelagic sediments characterize the back arc basin. They consist of clay and calcareous clay, whereas terrigenous muds and sands are found closer to the islands of Buru and Seram (Situmorang, 1992). Only one sample, piston core G5-1-2P, was studied from this area.

5.3.3. The volcanic Banda Arc

The volcanic Banda Arc consists of six active volcanoes and a number of inactive volcanic islands: Alor-Wetar-Romang in the south and Ambon and neighbouring islands (The Uliassers) in the north. The Banda Archipelago stands upon a triangular platform, whereas the other active volcanoes emerge from a small ridge which rises 5000 m from the Banda Sea floor in the west and from 5000-7000 m in the Weber Deep.

Sediments from the volcanic arc are characterized by black unsorted sands, muddy sands and sandy muds near the Banda Archipelago (Track I) and Manuk-Serua (Track II). Calcareous clay, foram clay and mud, with some volcanic gravels were recovered between Wetar and Romang (Track III).

5.3.4. The fore-arc basins

The Weber Deep is deeper than the subduction trenches (> 7000 m). The sediment cover is thin (Hamilton, 1979) and is underlain by oceanic crust (Purdy et al., 1977, Bowin et al., 1980). The sediments include turbiditic deposits (silt-gravel size) and pelagic clay in the central parts of the basin.

The Wetar Strait is situated between Wetar and Timor Islands. Sediments in this basin are composed of ooze and calcareous sediments, with occasional gravel occurrences on the northern slope of the basin.

5.3.5. The structural highs and collision complex

The outer Banda Arc consists of an accretionary-wedge complex (Hamilton, 1979). This complex comprises a Tertiary subduction melange and imbricated complexes.

Lithologies include sedimentary and crystalline rocks. The sedimentary rocks show a wide variety in facies, ranging from abyssal pelagic sediments (red clays) to shelf deposits (platform limestones). The crystalline rocks include serpentinite, gneisses, schists and basalts. Most of this material was derived from the continental margins of New Guinea and Australia (Hamilton, 1979). Many islands of the structural highs and collision complex show large, highly variable uplift rates during Quaternary time (e.g. Chappell and Veeh, 1978; DeSmet et al., 1989). Timor, for example, shows uplift rates of 120-500 mm/ka in the northeast, and 20-40 mm/ka for the northwest (Chappell and Veeh, 1978).

The structural highs are characterized by the occurrence of gravels in all three Snellius II tracks. The gravels consist of sedimentary, volcanic and metamorphic clasts. The dominant sediment type of the structural high and the collision complex is calcareous pelagic clay.

5.3.6. The subduction trenches

The Seram, Aru and Timor troughs are the subduction trenches of the Banda Arc system and are characterized by relatively shallow water depths (1500-3500 m). For comparison, the Java Trench farther to the west and the fore-arc basins show water depths of 6000-7000 m. The subduction trenches are underlain by Australian-New Guinea continental crust which is covered by shallow-water continental shelf strata (Shor et al., 1977). The subduction trenches are filled with thick deep-water ponded sediments (Hamilton, 1979). For example, DSDP Site 262 in the western Timor Trough (Fig. 5.1) shows a 400 m thick fill of ooze, containing nannofossils, foraminifers and radiolaria, which overlies the shallow water shelf strata (dolomites/limestones, see Appendix 2.2). Surface sediments from the Seram, Aru and Timor troughs are composed mainly of (calcareous) clay and silty clay.

5.3.7. The North Australian and New Guinea continental slope and shelf

The depositional patterns and the position of the North Australian coastline have remained similar from Late Cretaceous until Recent (Veveers, 1984). Calcareous sediments (CaCO₃ content: 30-80%) are deposited away from the coastline, whereas quartz sediments are deposited close to the coastline. Four sedimentary basins are found on the shelf: the Canning, Browse (sediment thickness 5000 m) Bonaparte (6500 m) and Arafura (2000 m) basins (Hamilton, 1979). They comprise Phanerozoic sediments, except for the Arafura basin which is filled with Proterozoic sediments. The continental slope is composed of clay and

calcareous clay, while the shelves are composed of biogenic gravel/sand and silt. In some box-cores (e.g. G5-4-71/75) well-rounded basaltic pebbles were recovered.

5.3.8. Outline of the North Australia-West New Guinea geology

Extensive descriptions of the geology of Australia and references are given by Veveers (1984) and Hamilton (1979). Only a brief summary, relevant for the provenance of the East Indonesian sediments, is given here.

Northern Australia is characterized by ancient outcropping formations of Middle Proterozoic age. Phanerozoic formations occur in the Wiso, Daly River, Bonaparte Gulf and Canning basins (see Fig. 5.1). Archean rocks outcrop in small areas in the Pine Creek Syncline, and their significance for the EIS sediments can be neglected. The pattern of drainage to the Timor Sea (see Fig. 5.1) is such that most of the sediments ($\pm 80\%$) supplied to the Timor Sea should be derived from Early and Middle Proterozoic formations.

In contrast to Northern Australia, Western New Guinea is characterized by Phanerozoic formations. Paleozoic rocks are found in Bird's Head and in the Snow Mountains. The other rocks have a Mesozoic and Cenozoic age. The northern part of New Guinea is composed of an arc complex which collided with southern New Guinea during the Miocene (Hamilton, 1979). This arc-continent collision caused the uplift of the medial mountains of New Guinea and the sedimentation in the foreland basins of Southern New Guinea. The watershed on the medial mountains causes the material from the accreted arc to run off to the Pacific ocean. This implies that young immature sediments from this arc complex are currently not deposited in the Arafura and Seram Seas.

In summary, the western part of New Guinea is characterized by Phanerozoic rocks (600-0 Ma) in contrast to the northern part of Australia, which is dominated by Proterozoic rocks (2200-1400 Ma). Currently, the run-off from New Guinea to the Arafura and Timor sea is much larger than from North Australia.

5.3.9. Previous geochemical work

Organic carbon and carbonate contents of sediments obtained by the Snellius I expedition in the studied area were reported by Neeb (1943). Three piston-cores from this area were analysed by Ben Othman et al. (1989). They analysed REE, Th, U, K and Sr-Nd-Pb isotopes. Cook (1974) reported 15 analyses of the DSDP Site 262 core, including major elements and trace elements (Sr, Ba, Li, Cu, Pb, Zr, Co, Ni, Cr and V).

5.4. Sample selection and analytical techniques

Sediments for this study were obtained from box and piston cores which were sampled during the 1984-1985 Dutch-Indonesian Snellius II expedition. Figure 5.1 shows the sample tracks along which most of the samples were taken, and the position of sediment samples MB1, MB7, G5-1-2P and G5-3-69P. The individual sample locations of the samples along the tracks are shown in Appendix 1.2. The techniques used for sampling are described in Situmorang (1992). Core descriptions are given in Appendix 2.2.

Because our emphasis is on the (average) composition of the continental crust we tried to avoid ash layers and turbidites with a high percentage of volcanoclastic material. Dispersed volcanoclastics and scattered pumice pieces were difficult to avoid. Ninkovich (1979) demonstrated for the Lesser Sunda Arc, west of the Banda Arc, that ash falls extent some 500 km south of the arc. However, the fraction of volcanic material (<5%, on-board sample descriptions) in shelf and wedge sediments does not influence the results. As White et al. (1985) pointed out, the concentrations of most indicative elements in volcanoclastics are much lower than in the terrigenous fraction. Box-core samples were obtained preferentially from 20-30 cm depth, below the 'oxidation/reduction layer'. For the piston cores, we created a composite by sampling 2 cm³ of sediment every 50 cm. These samples were thoroughly mixed after drying. In addition, 5 core samples of DSDP Site 262 from different depths (see Appendix 1.2 and 2.2) were obtained from the Ocean Drilling Program repository. This core was described by Veveers et al., 1974). Further analytical details are given in Appendix 3.

5.5. RESULTS

This section describes variations in carbonate content, organic carbon, trace element characteristics and Sr, Nd and Pb isotopes of the Eastern Indonesian sediments (EIS). Carbonate and organic carbon contents are given in Appendix 2.2, together with sample locations and a description of the sediment cores. The major- and trace-element abundances of selected box- and piston-core samples are given in Appendix 5, Sr-Nd-Pb isotopes are given in Appendix 7, together with Sm, Nd, Th, U and Pb isotope dilution concentrations and the calculated T_{Nd} (Depleted Mantle Nd-model ages, DePaolo, 1981b).

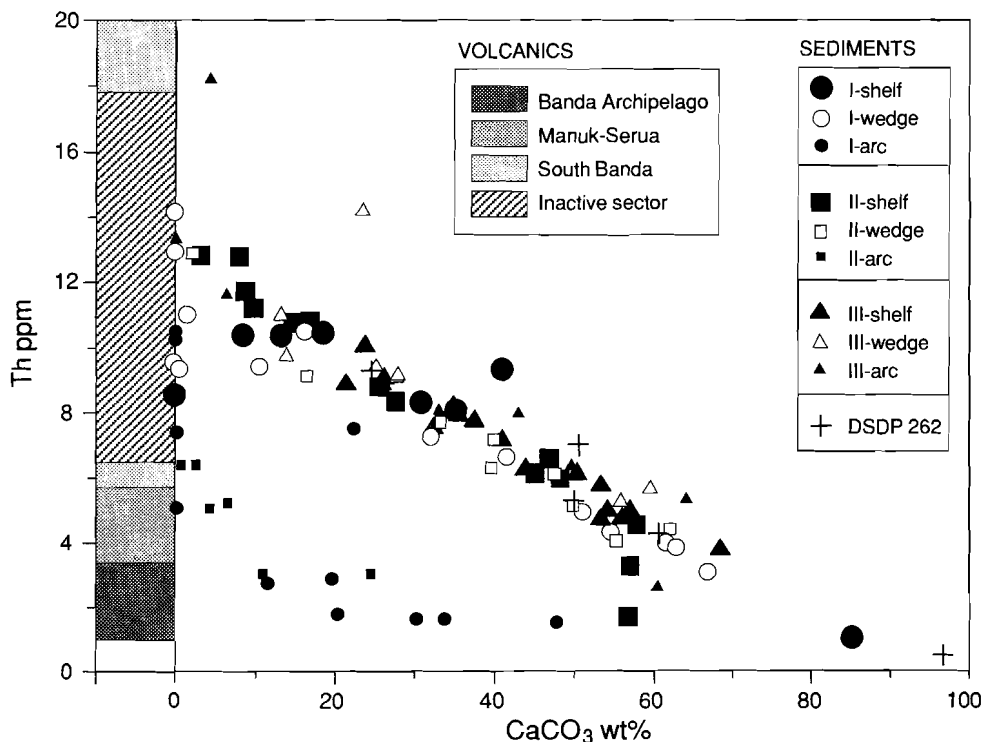


Fig. 5.2. CaCO_3 -Th diagram illustrating the effects of dilution by carbonate and volcanogenic material on the composition of terrigenous sediments ($\text{Th} > 8$ ppm, $\text{CaCO}_3 < 30\%$). Volcanogenic material is characterized by variable Th contents (low in Track I-II and high in Track III, corresponding to along-arc compositional changes of the volcanoes), and lowers the Th contents only near Banda, Manuk and Serua.

5.5.1. General geochemical characteristics of sediment types

First-order variations in the abundances of many trace elements (e.g. REE, Th, Zr, Nb, K) in the East Indonesian Sediments (EIS) are caused by dilution with carbonate and volcanic material. Figure 5.2 shows CaCO_3 versus Th. The compositional variation reflects mixing between three different sediment types: low-Th carbonate, a high-Th, low- CaCO_3 terrigenous sediments and low- CaCO_3 volcanoclastic sediments which have variable Th contents depending on the position along the arc (low Th in Track I and high Th in Track III).

Carbonate sediments are found mainly on the shelf. Sediments with a high carbonate fraction are also characterized by high organic carbon (cf. Neeb, 1943) and low trace-element contents (except Sr). For the purpose of this study, the carbonate sediments are defined as

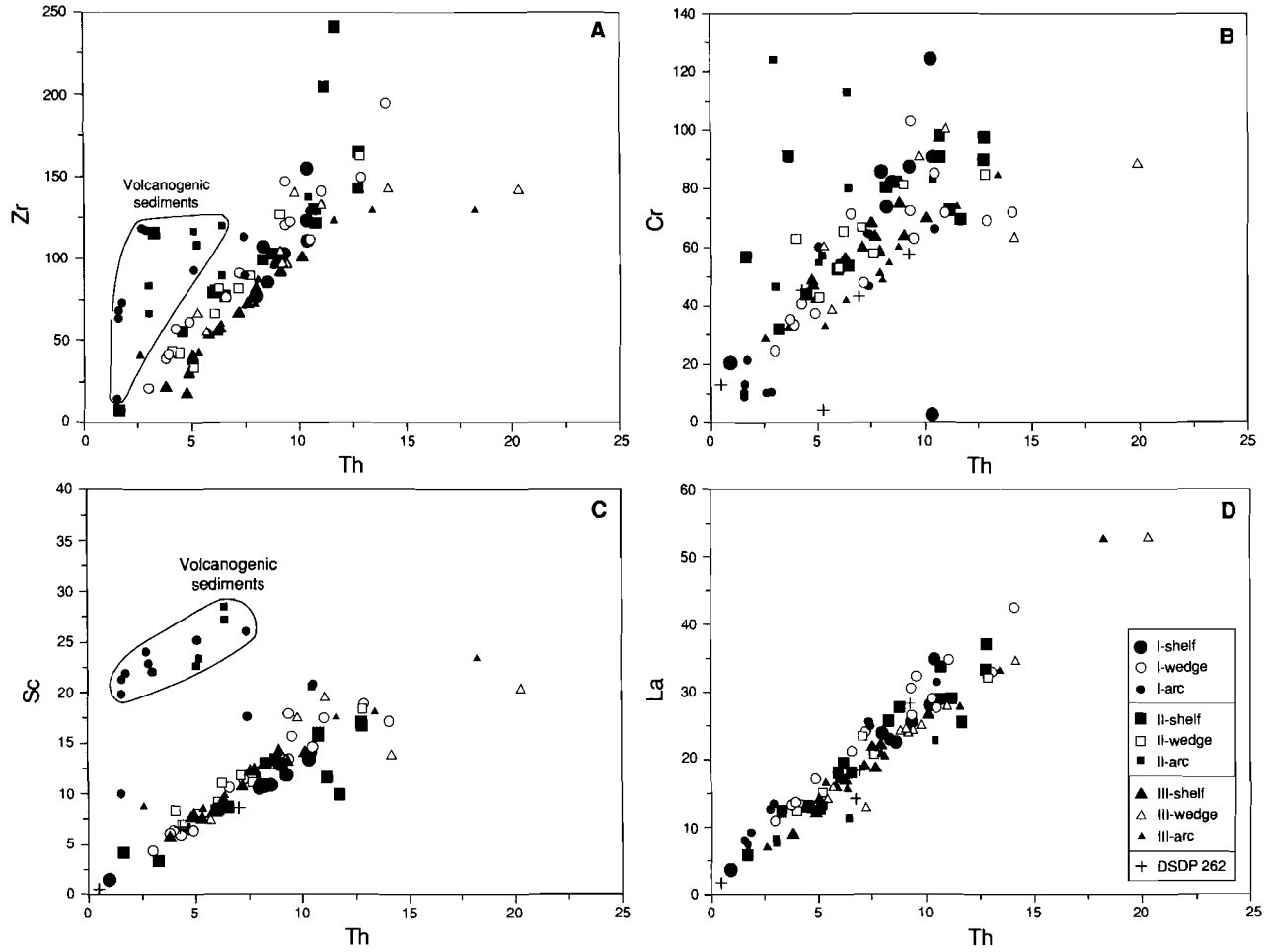


Fig. 5.3a-d. Th-variation diagrams: (a) Th-Zr, (b) Th-Cr, (c) Th-Sc, (d) Th-La.

having $\text{CaCO}_3 > 30\%$

The *volcanogenic sediments* are characterized by variable Th and other trace-element compositions, due to the changes compositions of the Banda Arc volcanics (Chapter 4). Although nearly all samples with a high volcanoclastic fraction are found close to the Banda volcanic arc, some samples with basaltic pebbles were also recovered from the Australian shelf (e.g. G5-4-75B). It should be noted that not all samples near the volcanic arc are dominated by volcanic material. The volcanoclastic sediments are characterized by high Sc and Zr at a given Th (see Fig. 5.3a and 5.3c) and by $\text{Th/Sc} < 0.5$ (see Fig 5.4a).

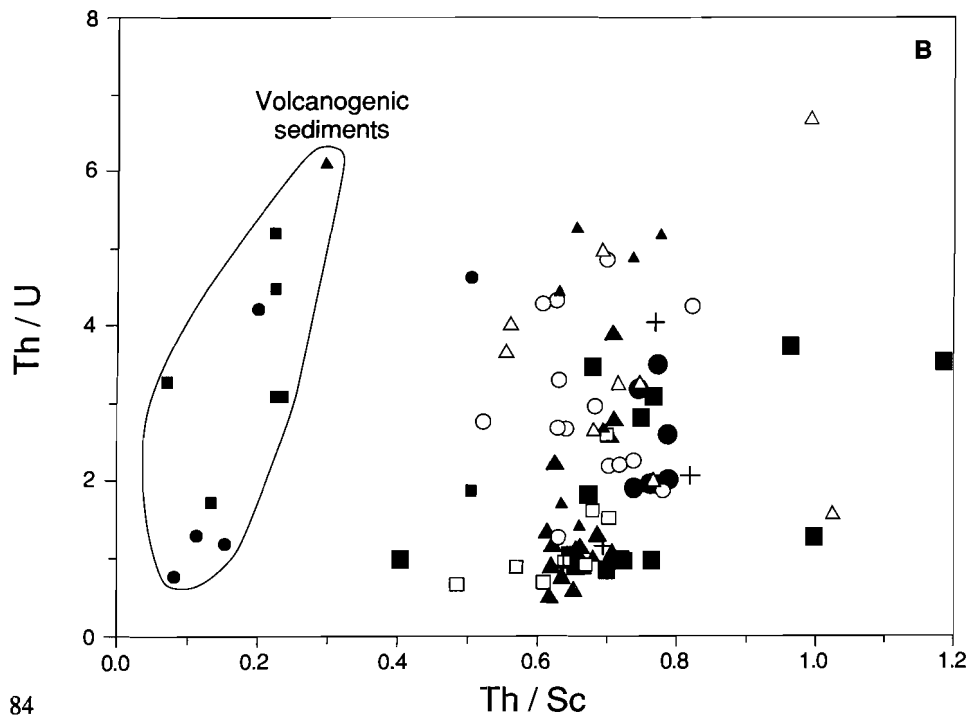
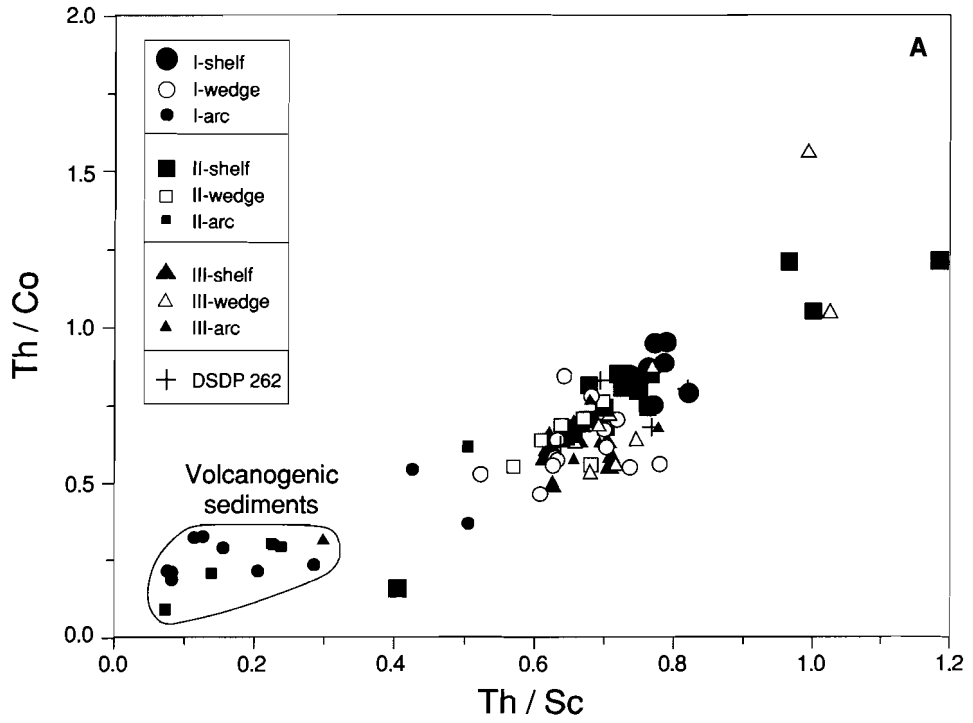
We distinguish *terrigenous sediments* from the other sediment types by low carbonate contents ($\text{CaCO}_3 < 30\%$ and $\text{Th/Sc} > 0.5$). When mixed with the other sediment types, the terrigenous fraction carries the bulk of the REE, HFSE and Th, and determines the Nd- and Pb-isotopic composition of the mixture, due to its high Pb and Nd contents.

5.5.2. Trace-element variations in the East Indonesian Sediments

Variation diagrams versus Th and ratio-ratio diagrams are shown in Fig. 5.3 and 5.4 for selected elements. Trace-element variations in the terrigenous sediments are illustrated in N-MORB normalized abundance diagrams (Fig. 5.5). They are compared with the Upper Continental Crust estimate of Taylor and McLennan (1985), Post Archean Australian Sediment and ODP Site 765 (Plank and Ludden, 1992). The trace-element characteristics of the EIS are described below for the following groups of elements: LILE, HFSE, REE and transitional elements.

5.5.2.1. LILE

Compared to N-MORB, EIS are characterized by high abundances of most LILE, especially Cs, Rb, Th and U (Fig. 5.5). Ba is low relative to Rb and Th. Sr varies widely (between 106-2981 ppm), and correlates positively with the carbonate content.



5.5.2.2. REE

REE patterns normalized on chondritic values and on Post Archean Australian Shale (PAAS, McLennan, 1989) are shown in Fig. 5.6. All chondrite-normalized patterns have a identical shapes, with $[La]_N$ (lanthanum normalized on chondrite) varying between 40-105 and $[Yb]_N \approx 6-10$. They are characterized by LREE enrichment (average $[La/Yb]_N = 8-10$) and fairly flat HREE (average $[Gd/Yb]_N = 1.59$). There is no difference in the shape of the REE patterns of the three tracks, the northern samples (MB-1, MB-7) and the DSDP Site 262 sediment. Some samples show a slight negative or positive Ce anomaly, just outside analytical error. A negative Eu anomaly is observed in all samples. Eu/Eu^* varies between 0.63-0.75, averaging at 0.70, which is a typical value for Post-Archean sediments (McLennan, 1989). The PAAS-normalized patterns are flat, except for Eu and Gd which are higher in the EIS sediments. Gd can be explained analytically by a BaF interference (see Appendix 3), and could be up to 10-20% too high. Eu contents agree well with those of INAA, suggesting that this is a real feature.

5.5.2.3. HFSE (Nb, Ta, Zr, Hf)

An important feature of the N-MORB normalized abundance patterns (Fig. 5.5) is the existence of a negative Nb-Ta anomaly, which is a typical characteristic of arc volcanics (e.g. Arculus and Powell, 1986). The depth of the 'trough' is comparable to those of the Banda Arc volcanics (Chapter 4). This anomaly is observed in all three tracks, and there is no systematic variation in the depth of the 'trough' along and across the arc. In contrast, there is no anomaly for Zr and Hf in the N-MORB normalized abundance diagrams (Fig. 5.5). Scatter in the Th-Zr variation diagram (Fig. 5.3a) probably reflects the effect of zircon fractionation. Zr in Track III is lower at a given Th content than in Track I and II. Situmorang (1992) has shown that sediments from Track I and II contain significant amounts of zircon, whereas it is almost absent in Track III, which is consistent with our data. The influence of the volcanogenic fraction in box cores close to the Banda Arc volcanoes is shown by higher Zr values at given Th contents (Fig. 5.3a) compared to cores from the wedge and shelf.

Fig. 5.4a and b. Ratio diagrams: (a) Th/Sc-Th/Co; (b) Th/Sc-Th/U. Note the large spread in Th/U and lack of correlation with depositional environment (wedge, shelf, arc).

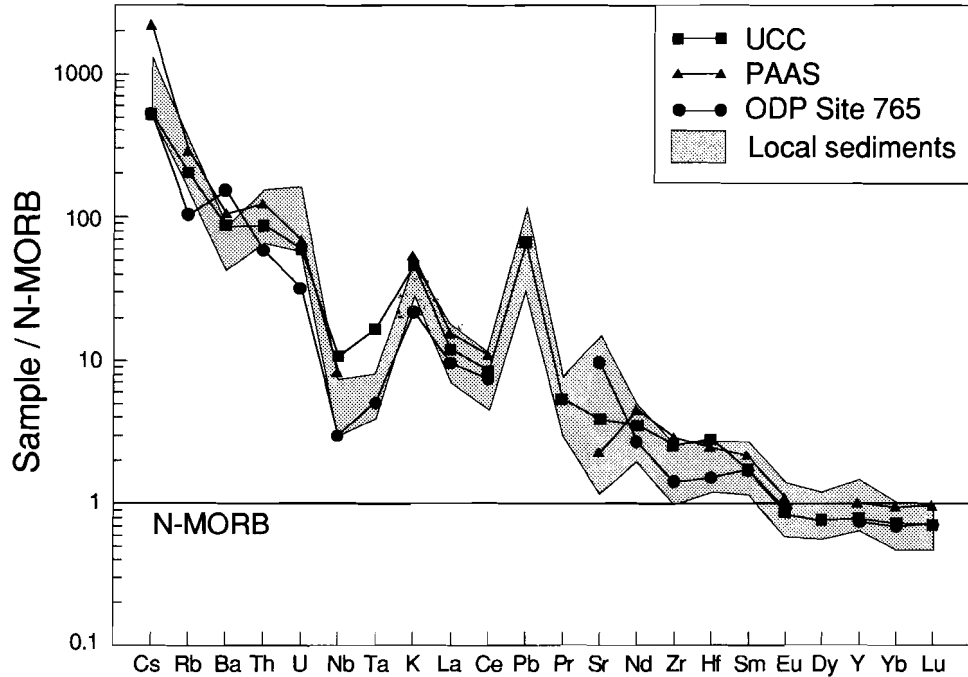
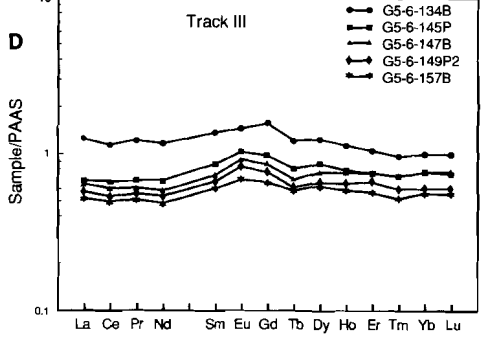
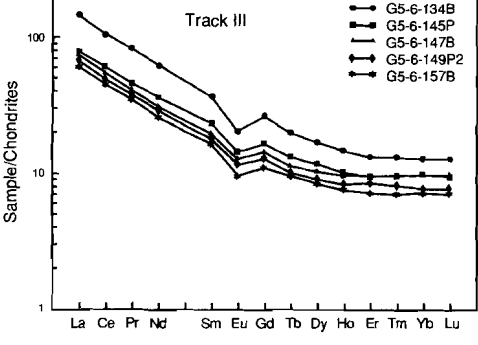
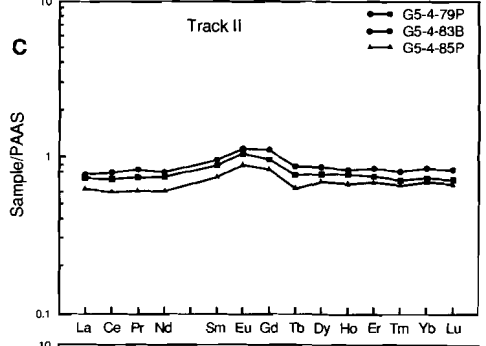
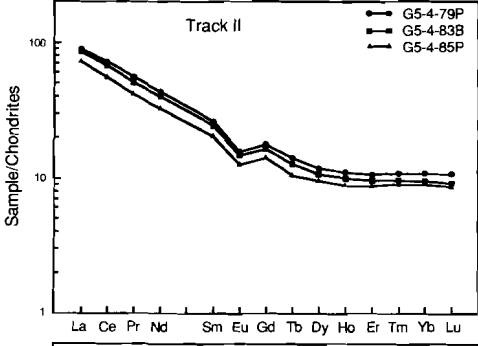
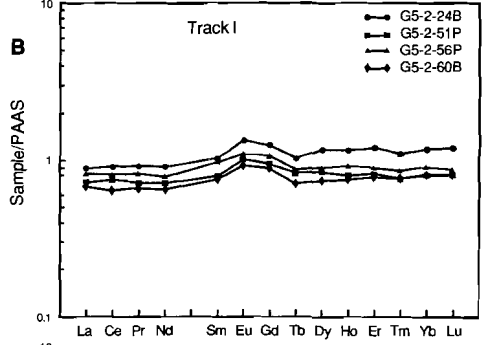
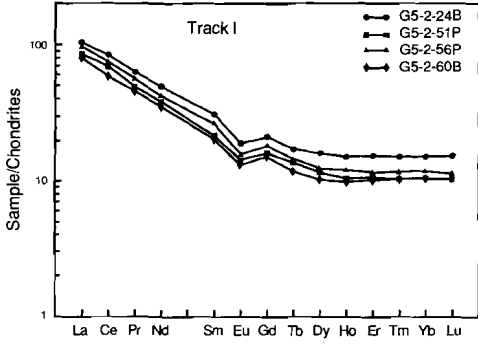
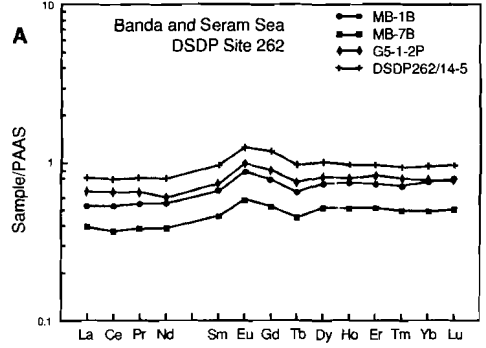
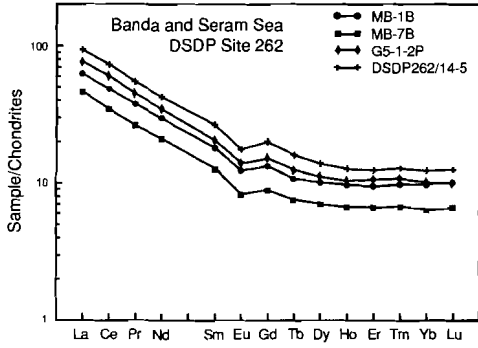


Fig. 5.5. N-MORB normalized abundance pattern for East Indonesian Sediments from the wedge and shelf (including all Tracks and one DSDP Site 262 sample), compared with Upper Continental Crust (Taylor and McLennan, 1985), Post Archean Australian Shale (PAAS) and average ODP Site 765 sediments (Plank and Gradstein, 1992). Note the negative Nb-Ta anomaly in the sediments, which is similar to that of the Banda Arc volcanics (see Chapter 4). Element order and normalizing values are from Sun and McDonough (1989).

5.5.2.4. Transitional elements (Sc, Co, Cr)

Scandium, cobalt and chromium correlate positively with Th (Fig. 5.3b and 5.3c, Co not shown). Sediments from the vicinity of the volcanic arc often have higher Sc and Co, and tend to have lower Cr contents at given Th concentrations than the sediments from the wedge and shelf. On the bases of Th/Sc and Th/Co ratios (Fig 5.4a) volcanoclastic sediments can be easily separated from the terrigenous sediments.

Fig. 5.6. a-d. Chondrite- and PAAS-normalized REE patterns of sediments from (a) Seram+Banda Seas and DSDP Site 262; (b) Track I; (c) Track II and (d) Track III. Chondritic values are from Nakamura (1974) as modified by White and Patchett (1984), and PAAS values are from McLennan (1989).



5.5.3. Isotopes

5.5.3.1. General ranges and correlations

$^{87}\text{Sr}/^{86}\text{Sr}$ ratios show a large variation between 0.7081 and 0.7394. Most of the samples have an $^{87}\text{Sr}/^{86}\text{Sr}$ value around 0.7092, close to the present-day seawater value of 0.709175 (Hoddle et al., 1991), which reflects the high carbonate content of the sediments. The range in $^{143}\text{Nd}/^{144}\text{Nd}$ ratios is much smaller (0.51189-0.51242). There is no correlation with carbonate content. The lowest values occur in three samples of Track III (0.51189-0.51195). On average, the piston-core samples are lower in $^{143}\text{Nd}/^{144}\text{Nd}$ than the box-core samples from the same track. There tends to be an NE-SW decrease in $^{143}\text{Nd}/^{144}\text{Nd}$ from Track I to Track III, but the DSDP Site 262 samples are intermediate between Track II and III (see Fig. 5.7).

The EIS display a large range in Pb-isotopes (Fig. 5.8a-b): $^{206}\text{Pb}/^{204}\text{Pb}=18.65-19.57$, $^{207}\text{Pb}/^{204}\text{Pb}=15.65-15.79$, $^{208}\text{Pb}/^{204}\text{Pb}=38.70-39.76$. The Pb-isotopes become more radiogenic from Track I in the NE to Track III in the SW. For example, the $^{206}\text{Pb}/^{204}\text{Pb}$ ratio increases from Track I (18.65-18.81) to Track II (18.87-19.01) to Track III (18.93-19.57). The DSDP Site 262 samples have intermediate values between Track II and Track III ($^{206}\text{Pb}/^{204}\text{Pb}=18.89-19.23$). The Pb isotopes, like the Nd isotopes, do not correlate with CaCO_3 contents.

Ben Othman et al. (1989) studied a piston core (V28-341) from a location between Track II and III (see Fig. 5.1). It has comparable values to those of Track II and III sediments: $^{87}\text{Sr}/^{86}\text{Sr}=0.7100$, $^{143}\text{Nd}/^{144}\text{Nd}=0.51216$ and $^{206}\text{Pb}/^{204}\text{Pb}=18.96$.

5.5.3.2. Comparison with Indian-, Pacific- and Atlantic-Ocean sediments

The EIS span a large range of the currently available isotope database of global sediments. The $^{87}\text{Sr}/^{86}\text{Sr}$ - $^{143}\text{Nd}/^{144}\text{Nd}$ systematics (Fig. 5.7) of the EIS overlap with Pacific-, Atlantic- and Indian-Ocean sediments. Only sample G5-6-134B is higher in $^{87}\text{Sr}/^{86}\text{Sr}$ than the most radiogenic sediments from the Indian and Atlantic Oceans. Pacific-Ocean sediments generally have higher $^{143}\text{Nd}/^{144}\text{Nd}$ and lower $^{87}\text{Sr}/^{86}\text{Sr}$ than EIS.

Pb-isotopes (Fig. 5.7) show a large overlap with Indian- and Atlantic-Ocean sediments. In general, the EIS have higher $^{207}\text{Pb}/^{204}\text{Pb}$ ratios at a given $^{206}\text{Pb}/^{204}\text{Pb}$ than the Pacific-Ocean sediments. The EIS sediments tend to be higher in $^{208}\text{Pb}/^{204}\text{Pb}$ than the Atlantic-Ocean sediments for $^{206}\text{Pb}/^{204}\text{Pb} > 19.0$.

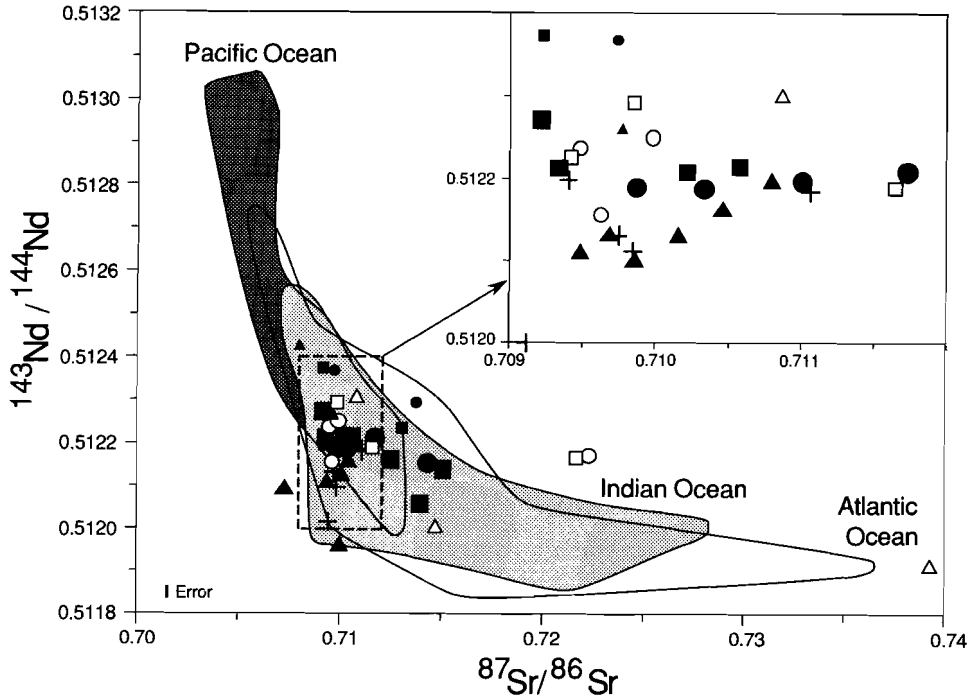
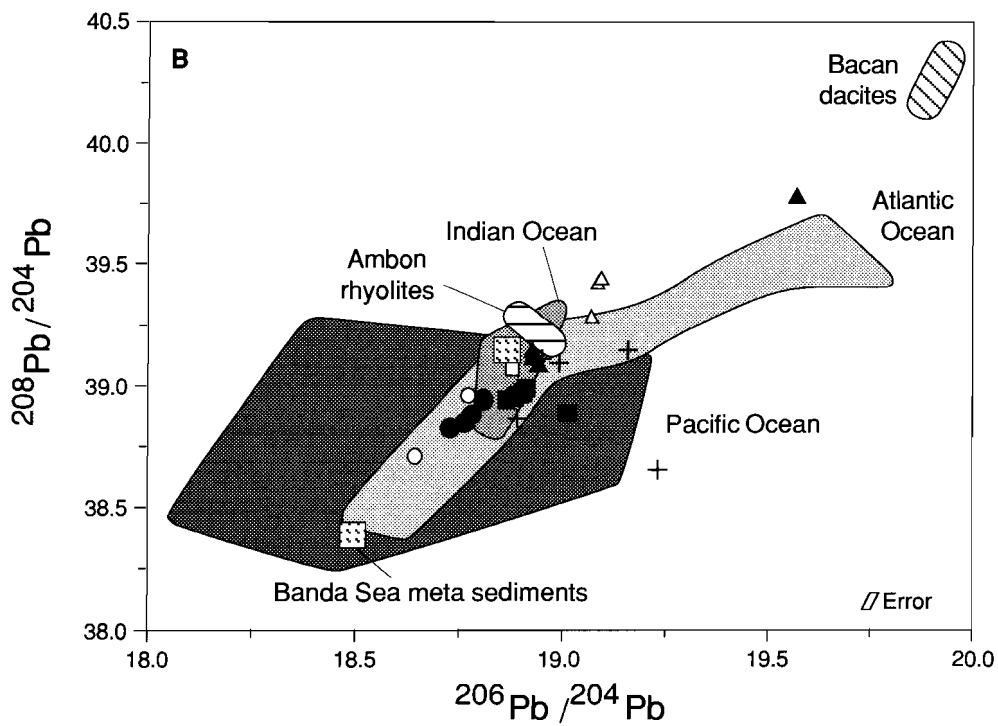
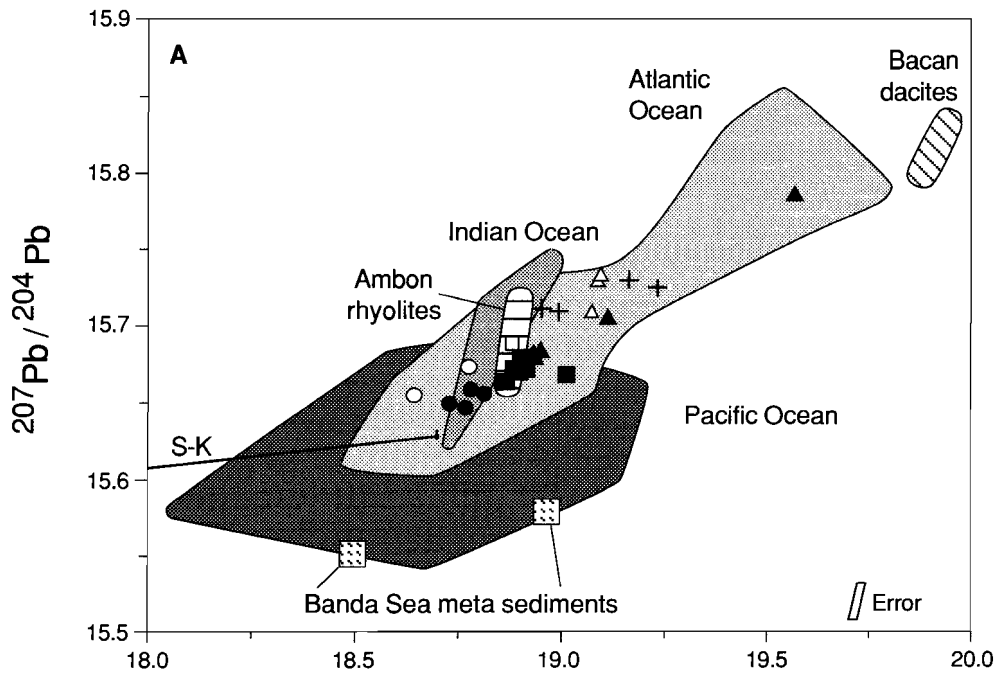


Fig. 5.7. Sr and Nd isotope ratios of East Indonesian Sediments compared with Indian, Atlantic and Pacific Ocean sediments. Data sources: Goldstein et al. (1981); White et al. (1985); Von Drach et al. (1986); Ben Othman et al. (1989).

5.5.3.3. $^{147}\text{Sm}/^{144}\text{Nd}$ ratios and Nd model ages

The $^{147}\text{Sm}/^{144}\text{Nd}$ ratio varies between 0.1073 and 0.1375, both extreme values being found in sediments from the volcanic arc region. If we only consider the shelf and wedge data, we obtain an average $^{147}\text{Sm}/^{144}\text{Nd}$ ratio of 0.1202 ± 0.0042 (1 sd). This value is slightly higher than the mean crustal value (0.112) and averaged continental shales (0.115, Goldstein et al., 1984). DSDP Site 262 sediments also show high ratios: $^{147}\text{Sm}/^{144}\text{Nd} = 0.1224 \pm 0.0019$. Samples with high $^{147}\text{Sm}/^{144}\text{Nd}$ (>0.13) always have a volcanogenic component. For example, shelf sample G5-4-75B, which consists of mud and basaltic pebbles, has $^{147}\text{Sm}/^{144}\text{Nd} = 0.1362$. If we discard the samples with a volcanogenic fraction, we obtain an average value of 0.1184 for wedge and shelf sediments.

Nd model ages based on the depleted mantle model of DePaolo (1981b), hereafter referred to as T_{Nd} , range from 1161 to 2264 Ma. The oldest ages are all found in Track III.



There is a tendency to older model ages towards the south: averages for Track I, II and III are 1626 ± 68 , 1665 ± 90 and 1811 ± 198 Ma respectively (1 sd from the mean). The DSDP Site 262 sediments average around 1817 ± 160 Ma. Most of the model ages are in the range of 1600-1800 Ma, which is similar to the Nd model ages of modern fluvial sediment from a variety of rivers (≈ 1700 Ma; Goldstein et al., 1984). The oldest ages are also close to an Australian period of crust addition of 2300-2100 Ma (McCulloch, 1986). The average EIS values tend to fall in or between the two Australian crust forming periods of 1900-1700 Ma and 1550-1500 Ma (Compston and Arriens, 1968). These are based on U-Pb ages of zircons. Sr model ages for sediments with $\text{CaCO}_3 < 3\%$ are much lower ($T_{\text{Sr}} = 267\text{-}599\text{Ma}$) than the T_{Nd} , which is a common feature for sediments (e.g. Goldstein, 1988).

5.6. DISCUSSION

5.6.1. Introduction

Because the main objective of this study is to obtain insight into the composition and variation of subducted continental material, the following discussion will concentrate on the terrigenous sediments. We shall first consider the provenance of these sediments, then compare our data with published estimated compositions of (upper) continental crust, and finally discuss some of the implications for Banda Arc volcanism.

5.6.2. The provenance of East Indonesian sediments

The large variations in Pb isotopes of the EIS suggest that the terrigenous fraction is derived from areas with different compositions, or from areas with a different age. The T_{Nd} of the non-volcanogenic EIS displays a small range (1600-2250 Ma) compared to the age variation of possible origins in Australia and New Guinea, which vary from 0-2000 Ma. This suggests that large amounts of the sediments are cannibalistic (e.g. Veizer and Jansen, 1985). On average, there is a small increase from Track I to Track III. The Track III sediments

Fig. 5.8. (a) $^{206}\text{Pb}/^{204}\text{Pb} - ^{207}\text{Pb}/^{204}\text{Pb}$ and (b) $^{206}\text{Pb}/^{204}\text{Pb} - ^{208}\text{Pb}/^{204}\text{Pb}$ systematics for East Indonesian sediments, compared with Indian, Atlantic and Pacific Ocean sediments, dacites from Bacan Island, rhyolites from Ambon and meta-sediments from the Banda Sea. S-K is the Stacey and Kramer (1975) curve for continental growth. Data sources: Meijer (1976), Church (1976), Sun (1980), Barreiro (1983), White et al. (1985), Woodhead et al. (1987), Ben Othman et al. (1989), Morris et al. (1983, 1984), Morris (1984).

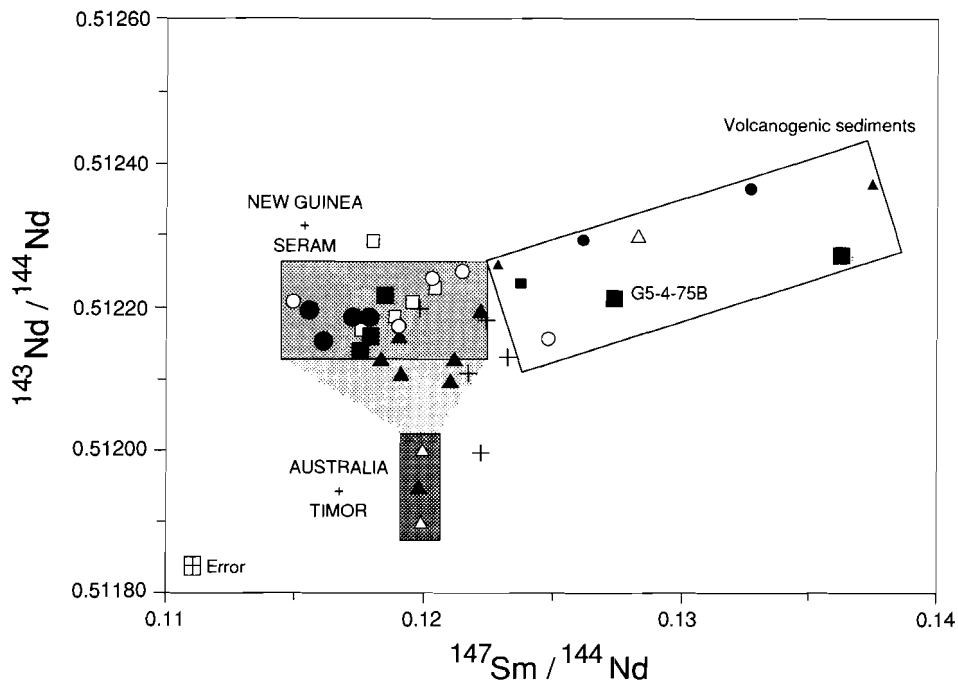


Fig. 5.9. $^{147}\text{Sm}/^{144}\text{Nd}$ - $^{143}\text{Nd}/^{144}\text{Nd}$ diagram illustrating different provenances of East Indonesian sediments. Note that volcanogenic sediments have high $^{147}\text{Sm}/^{144}\text{Nd}$ (>0.125).

have T_{Nd} close to the average age (Early and Middle Proterozoic) of Northern Australia (see Fig. 5.1).

The almost linear correlation of the sediment data in the $^{206}\text{Pb}/^{204}\text{Pb}$ - $^{207}\text{Pb}/^{204}\text{Pb}$ diagram (Fig. 5.8a) could be interpreted as a single isochron with an age of about 2500 Ma. However, this contradicts the T_{Nd} which suggests variable ages. The Pb isotope trend is most easily explained by the mixing of less radiogenic sediments ($^{206}\text{Pb}/^{204}\text{Pb} \approx 18.7$) with radiogenic sediments ($^{206}\text{Pb}/^{204}\text{Pb} \approx 19.5$). This trend in Pb isotopes is also observed in $^{143}\text{Nd}/^{144}\text{Nd}$ variations. The low Pb isotopes are characterized by relatively high $^{143}\text{Nd}/^{144}\text{Nd}$ (0.51215-0.51225), whereas the radiogenic Pb isotopes are characterized by the lowest $^{143}\text{Nd}/^{144}\text{Nd}$ (0.51189-0.51195).

However, the Th/Sc versus $^{206}\text{Pb}/^{204}\text{Pb}$ and $^{147}\text{Sm}/^{144}\text{Nd}$ versus $^{143}\text{Nd}/^{144}\text{Nd}$ diagrams (Figs. 5.11b and 5.9) show that a two-component mixing is too simple, and that more components are involved. The non-volcanogenic sediments can be separated into three groups: (1) a low $^{143}\text{Nd}/^{144}\text{Nd}$ (<0.51200) component with $^{147}\text{Sm}/^{144}\text{Nd} \approx 0.120$; (2) a component with high $^{143}\text{Nd}/^{144}\text{Nd}$ (0.51215-0.51225) and low $^{147}\text{Sm}/^{144}\text{Nd}$ (0.115-0.118),

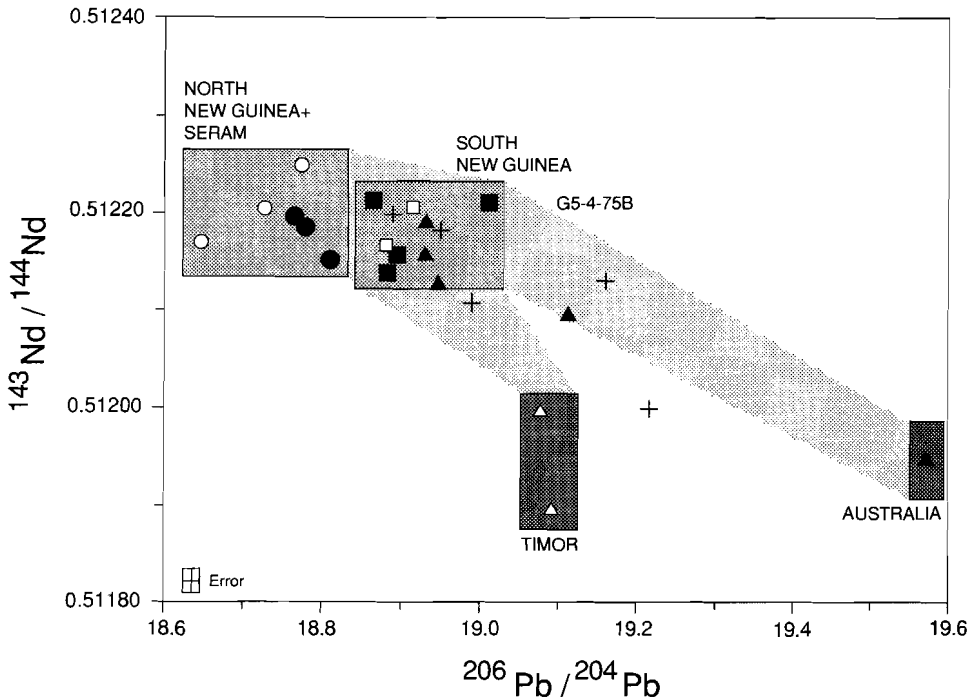
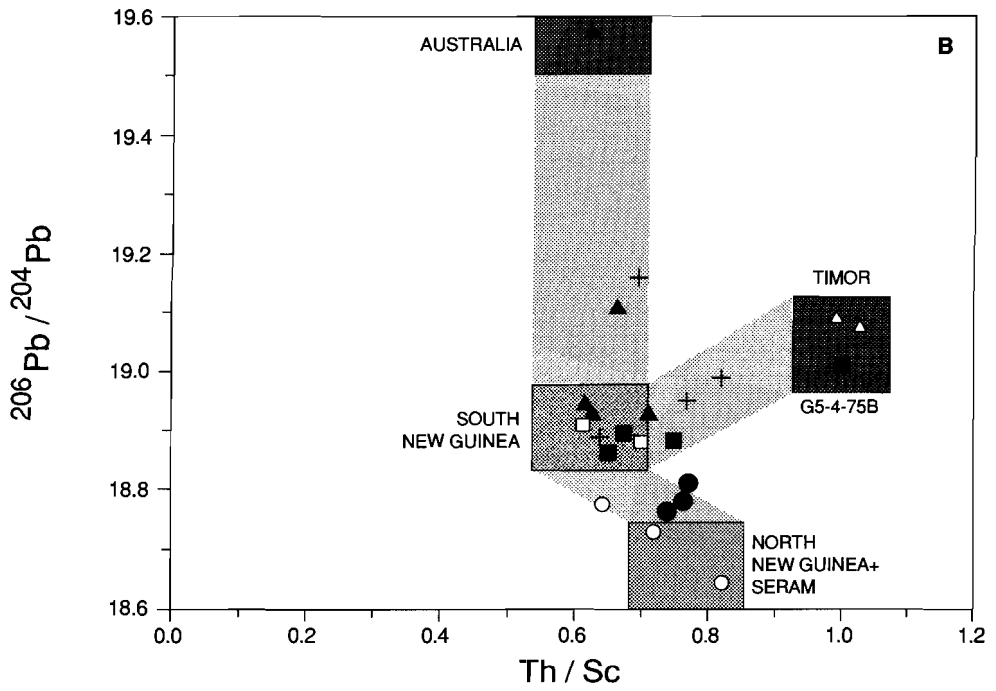
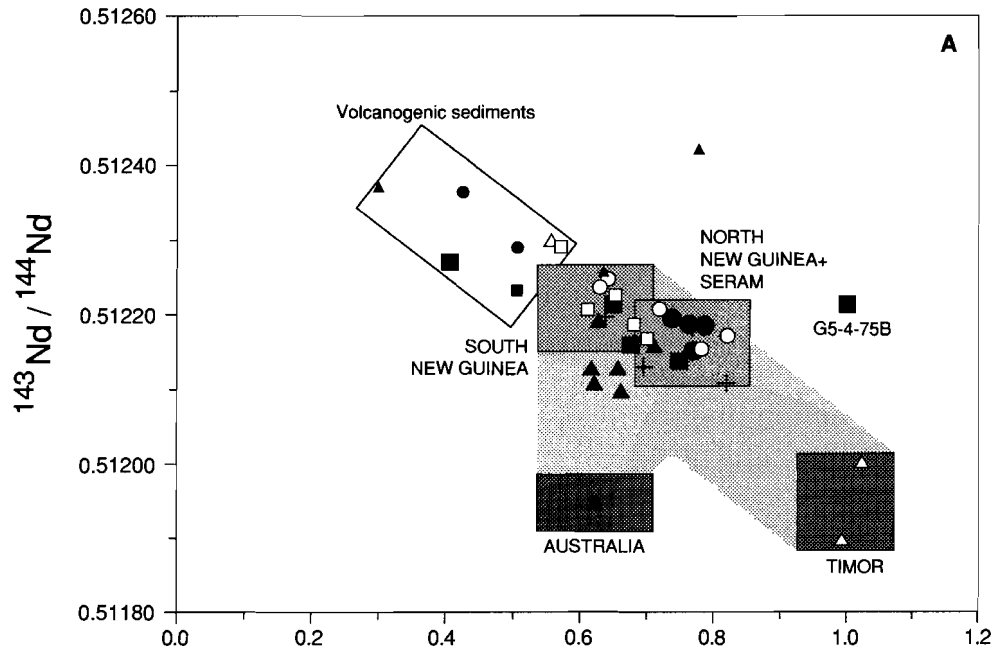


Fig. 5.10. $^{206}\text{Pb}/^{204}\text{Pb}$ - $^{143}\text{Nd}/^{144}\text{Nd}$ diagram. The geographical distribution of the sediment samples suggest four possible provenance areas: North New Guinea + Seram, South New Guinea, Timor and Australia. Inferred end members are given as boxes (see text for discussion).

represented mostly by sediments of Track I; (3) a component similar to (2) in $^{143}\text{Nd}/^{144}\text{Nd}$ but with higher $^{147}\text{Sm}/^{144}\text{Nd}$ (0.119-0.125), which is found mainly in Tracks II+III and in the DSDP Site 262 samples.

The same components appear in the Th/Sc versus $^{143}\text{Nd}/^{144}\text{Nd}$ and $^{206}\text{Pb}/^{204}\text{Pb}$ (Fig. 5.11a+b), but an extra subdivision is suggested in the samples with low $^{143}\text{Nd}/^{144}\text{Nd}$ (Fig. 9). One sample has high $^{206}\text{Pb}/^{204}\text{Pb}$ (19.57) and relatively low Th/Sc (0.6), and two samples have moderate $^{206}\text{Pb}/^{204}\text{Pb}$ (19.0-19.1) and Th/Sc \approx 1. These three samples with $^{143}\text{Nd}/^{144}\text{Nd}$ $<$ 0.51200 are probably the end-members of mixing trends visible in the other samples (e.g. the DSDP Site 262 samples). These chemical and isotopic groups within the EIS, combined with geographical considerations, point to at least two, but probably four different source regions that have contributed to the terrigenous fractions. The low Pb isotopes ($^{206}\text{Pb}/^{204}\text{Pb} \approx 18.6-18.8$), high Nd isotopes ($^{143}\text{Nd}/^{144}\text{Nd} \approx 0.51218-0.51225$) and moderate Th/Sc (0.6-0.8) are found close to Western New Guinea, and are most probably derived from the Paleozoic/Mesozoic complexes of New Guinea and Seram. The Pb isotopes and



Th/Sc ratios can distinguish between two provenance areas: North New Guinea + Seram and South New Guinea. The Track I sediments are derived from North New Guinea + Seram (cf. Situmorang, 1992). Although Palaeozoic rocks (Fig. 5.1) are more dominant in Seram and Bird's Head than in Southern New Guinea, the lowest Pb isotope values ($^{206}\text{Pb}/^{204}\text{Pb}=18.6-18.8$) are found in Track I. These values overlap with Pacific Ocean sediments (Fig. 5.8). The present watershed (Fig. 5.1) precludes that the sediments contain a component from the immature accreted arc complex in Northern New Guinea. Material from this complex currently runs off into the Pacific Ocean. Whether this situation was different in the recent past, given the rapid tectonic movements in this region, is not known.

The higher $^{206}\text{Pb}/^{204}\text{Pb}$ ratios ($\approx 19.0-19.6$) and less radiogenic $^{143}\text{Nd}/^{144}\text{Nd}$ ratios (0.51189-0.51195) are found in Track III and DSDP Site 262, which points to North Australian sources. A 'Timor' component with $^{206}\text{Pb}/^{204}\text{Pb}=19.0-19.1$ and $\text{Th}/\text{Sc} \approx 1$ is found on the wedge in the vicinity of Timor, and is probably derived from this island. An 'Australia' component with very high $^{206}\text{Pb}/^{204}\text{Pb}$ (19.57) and lower Th/Sc ratios (0.6) is found on the north Australian shelf, and must be derived from Proterozoic complexes on the mainland. The $^{143}\text{Nd}/^{144}\text{Nd}$ of this component is consistent with the results of one sample from the Canning Basin (Fig. 5.1) which has $^{143}\text{Nd}/^{144}\text{Nd}$ ratio of 0.51179 and $T_{\text{Nd}}=1890$ Ma (Allègre and Rousseau, 1984). One sample from DSDP Site 262 is characterized by exceptionally low $^{208}\text{Pb}/^{204}\text{Pb}$ compared to the other sediments. Its Pb isotope composition is close that of the Kimberley igneous rocks (McCulloch et al., 1983; Frasnier et al., 1986; Nelson et al., 1986), which could be a plausible provenance.

The four provenance regions distinguished above compare well with evidence from heavy mineral assemblages in the EIS (see Table 5.1). Situmorang (1992) distinguished the following heavy mineral provinces in the wedge and shelf regions: Seram, New-Guinea-Aru, East Australia, Molu-Babar-Tanimbar, Kisar-Leti-Timor and West Australia (Fig. 5.1). The wedge and shelf sediments of Track I contain the Seram-Manowoka-New Guinea and New Guinea-Aru assemblages. The geochemical evidence for mixing between these assemblages can be seen in Fig. 5.11. The shelf and wedge of Track II are completely within the New Guinea-Aru heavy mineral province, which also fits with the geochemical data.

The wedge and shelf sediments of Track III contain the West Australian and Kisar-Leti-Timor assemblages. Our Timor component is equivalent to the Kisar-Leti-Timor heavy-mineral province and our Northern Australia component to the West Australian province. Situmorang (1992) also identified an East Australian heavy mineral province on the shelf

Fig. 5.11a and b. (a) Th/Sc- $^{143}\text{Nd}/^{144}\text{Nd}$ and (b) Th/Sc- $^{206}\text{Pb}/^{204}\text{Pb}$ diagrams showing the same division in four provenance areas as in Fig. 5.10.

Table 5.1. Components in terrigenous East Indonesian sediments and their provenance

No	Th/Sc	T _{Nd} (Ma)	²⁰⁶ Pb/ ²⁰⁴ Pb	Provenance	Heavy mineral province
1	0.8	1600	18.65	Seram + North New Guinea	Seram + NewGuinea-Aru
2	0.6-0.7	1600	18.9	South New Guinea	New Guinea-Aru
3	1.0	2250	19.1	Timor (N-Australia)	Kisar-Leti-Timor
4	0.65	2000	19.6	Northern Australia	West Australia

Components in terrigenous East Indonesian sediments and their provenances, see text for discussion. Heavy mineral provinces from Situmorang (1992).

between the Track II and III, but this has no geochemical equivalent. The most likely explanation is that the New-Guinea-Aru and East Australian heavy mineral provinces are chemically and isotopically identical. This is supported by piston-core V28-341 (Ben Othman et al., 1989) which was taken in the East Australian heavy mineral province, and has Pb- and Nd isotopes similar to our South New Guinea component.

The Th/Sc-²⁰⁶Pb/²⁰⁴Pb and ¹⁴⁷Sm/¹⁴⁴Nd-¹⁴³Nd/¹⁴⁴Nd diagrams (Figs. 5.9 and 5.11b) suggest mixing between sediments from different provenances. Sediments from North New Guinea + Seram mixed with those from South New Guinea, whereas South New Guinea also mixed with the 'Timor' and 'Australia' components. The latter two components probably did not mix with sediments from North New Guinea.

5.6.3. Some implications for continental fragments in East Indonesia

Eastern Indonesia is a complex tectonic region. Continental break-up and major collisions between New Guinea and an oceanic arc, and between the Australian continent and the Banda Arc have led to the formation of a number of individual continental fragments. Tectonic transport of these fragments sometimes occurred over large distances (e.g. Hamilton, 1979; Silver et al., 1985). Therefore, their origin is sometimes difficult to assess and has been widely debated (see Hartono, 1990 for an overview). The main question is: are these continental slivers derived from Australia or New Guinea? The difference in the Pb- and Nd-isotopes in New Guinea and northern Australia may provide some of the answers for Bacan (west of the south arm of Halmahera, just north of the map of Fig. 5.1), the Banda Ridges in the Banda Sea and Buru-Seram-Ambon continental fragments.

The island of Bacan is a curious block in the Halmahera arc. Its southern part is believed to be composed of metamorphic Late Paleozoic basement derived from New Guinea (e.g. Hamilton, 1979). Morris et al. (1983) published isotopic data for two Quaternary dacites, which were interpreted as having assimilated large amounts of continental arc crust. The Pb isotopes are highly radiogenic (see Fig. 5.8a+b), and if these are representative for the Bacan crust, it is more likely that this block originates from Northern Australia than from New Guinea, or alternatively, contains old Precambrian basement from New Guinea which is similar to the northern Australian surface composition.

Meta-sediments dredged from the Banda ridges display clear characteristics of arc volcanoclastics ($^{87}\text{Sr}/^{86}\text{Sr}=0.7047\text{--}0.7073$, $^{143}\text{Nd}/^{144}\text{Nd}=0.5126\text{--}0.5129$, Morris et al., 1984). Because of their similarity with rocks in Bird's Head, Silver et al. (1985) suggested that the Banda ridges were derived from New Guinea. Their $^{206}\text{Pb}/^{204}\text{Pb}$ and $^{208}\text{Pb}/^{204}\text{Pb}$ ratios largely overlap with the Track I values, but $^{207}\text{Pb}/^{204}\text{Pb}$ is much lower than observed in the sediments from any of the three tracks. Therefore, it seems likely that the origin of the Banda Ridges lies in the northern part of New Guinea rather than in the Paleozoic area of New Guinea. Northern New Guinea is composed of an accreted island-arc complex and may have the appropriate Pb isotopic compositions, if they are comparable to the sediments in the nearby parts of the Pacific Ocean (cf. Karig and Kay, 1981; their Fig. 5).

Buru, Ambon and Seram islands are considered to form a micro-continental fragment derived from the north-east sector of the former Australian continental margin which rifted away during the Middle Jurassic (cf. Pigram and Panggabean, 1984; Hamilton, 1979; Linthout et al., 1989). Acidic rocks (ambonites) from Ambon, which assimilated large amounts of continental basement, have Pb-isotope compositions (Morris, 1984) overlapping with the Track II sediments. This correspondence suggests a similar South New Guinea origin for this microcontinent.

5.6.4. Geochemical comparison between the East Indonesian sediments and Average Upper Continental Crust

Because trace-element ratios in the East Indonesian sediments display only limited variation, irrespective of sample locations, a reasonable estimate of averaged ratios can be made for comparison with literature data for Upper Continental Crust (UCC). The average ratios of non-volcanogenic EIS with $\text{CaCO}_3 < 30\%$ are given in Table 5.2, together with data for UCC, Post Archean Australian Shale (PAAS) and some Australian sedimentary basins. Our mean ratios for EIS generally compare well with the estimates for UCC from Taylor and McLennan (1985). This similarity is particularly obvious for the *La/Th* ratio,

Table 5.2. Trace-element ratios in Eastern Indonesian Sediments (EIS) compared with estimates for Upper Continental Crust and NW Australian sedimentary basins

Ratio	This study	Taylor & McLennan UCC	Canada	PAAS	Canning	Pine Creek	ODP-765
La/Th	2.78 ± 0.30	2.80	3.20	2.62	3.42	2.86	3.43
Th/Sc	0.72 ± 0.14	0.97	1.4	0.93			0.71
Th/Co	0.76 ± 0.23	1.07	0.83	0.63			0.33
Ce/Yb	27.1 ± 3.8	29.1	43.3	28.7	24.0	47.4	26.7
Zr/Nb	14.7 ± 3.7	7.6	9.2	11.1		11.1	14.3
La/Nb	3.32 ± 0.71	1.20	1.23	2.01		3.07	3.24
Th/Nb	1.19 ± 0.16	0.43	0.38	2.01		1.14	0.95
Th/Zr	0.086 ± 0.017	0.056	0.042	0.069		0.118	0.066
Zr/Hf	36.1 ± 2.5	32.8	41.4	42.2			28.9
K/La	789 ± 113	933	807	809	886	805	553
K/Rb	208 ± 21	250	235	193			229
K/Zr	183 ± 33	147	108	147	232	232	125
Rb/Zr	0.89 ± 0.17	0.59	0.46	0.76			0.55
Ba/La	16.7 ± 6.6	18.3	33.4	17.0	12.3	17.3	40.1
Ba/Zr	4.01 ± 1.64	2.89	4.46	3.09		4.98	9.1
Ba/Th	46.2 ± 19.3	51.4	107	44.6	40.1	42.1	138
Th/U	2.88 ± 1.18	3.82	4.00	4.65	3.88	4.40	4.67
Sr/Nd	13.6 ± 8.3	13.5	12.2	6.2			43.6
Pb/Nd	0.81 ± 0.14	0.80	0.65			0.83	

Average ratios are from wedge and shelf sediments with $\text{CaCO}_3 < 30\%$. Errors are 1 sd. The Upper Continental Crust (UCC) estimate is from Taylor and McLennan (1985), Canada from Shaw et al. (1967, 1976), PAAS and ODP Site 765 averages from Plank and Gradstein (1992), the Canning basin from Nance and Taylor (1976), Pine Creek average from McLennan and Taylor (1980) and McLennan (1982).

confirming the observation that La and Th are transferred completely to the sediment during weathering and transport (McLennan and Taylor, 1980).

On the other hand, some notable differences between EIS and UCC are found for element ratios with Nb in the denominator. The Zr/Nb and La/Nb ratios in the EIS are 2-2.5 times higher than the UCC ratios. The difference is probably due to the Nb contents (see also Fig. 5.5). Taylor and McLennan (1985) reported a value of 25 ppm for Nb in the UCC, whereas our average value for carbonate-free sediment is 11 ppm. This could imply that: (1) source rocks of EIS are characterized by lower Nb contents and deviate from UCC, or (2) Nb was fractionated in shelf/wedge sediments compared to UCC, or (3) the Nb estimate of Taylor and McLennan (1985) is too high.

Only limited data are available for Northern Australian (meta-)sedimentary basins (Table 5.2). The data for Pine Creek Early Proterozoic sediments (McLennan and Taylor, 1980) indicate Zr/Nb and La/Nb ratios similar to our data within one standard deviation, which suggests that the Nb contents could have already been low in the source rocks of the EIS, at least in the case of Track III. Nb fractionation in sediments has not been documented so far. Nb is presumably bound to the clay fraction, since it correlates perfectly with Th in our data set (not shown). Furthermore, its residence time in seawater is short: <250 yr (Taylor and McLennan, 1985). It is therefore assumed to be completely transferred to the sediment during weathering and transport, similar to the REE, Sc and Th (McLennan and Taylor, 1981). The third option of too high Nb content in the UCC estimate of Taylor and McLennan seems likely in view of our EIS data. The Zr/Nb ratio of the EIS fits better with the UCC estimate of Weaver (1991), who reported a Zr/Nb value of 16.2. In addition, it of interest to note that PAAS and ODP 765 sediments (Plank and Gradstein, 1992) also have Zr/Nb ratios which overlap the EIS data.

Our average Th/U ratio is lower than the UCC estimate of Taylor and McLennan (1985) and the generally accepted value of 3.8 for bulk earth. This can be explained by enrichment of U at the oxidation/reduction zone in the sediment and by the absorption of U on organic matter, causing a decrease in the Th/U ratio (cf. Ben Othman et al., 1989). The highest Th/U values of 4.0 were found in samples with the lowest organic carbon contents and are close to the estimated 3.8 for UCC.

Ce/Yb ratios (measured by INAA, but identical to the ICP-MS values) correspond well to the UCC values of Taylor and McLennan (1985). Fractionation between HREE and LREE, as recently suggested for continental shelf sediments (Sholkovitz, 1988), therefore seems unlikely. This fractionation strongly depends on the minerals that preferentially host the REE. HREE can be hosted in zircons (Sholkovitz, 1990), whereas all REE are taken up by clays (Condie, 1991). Situmorang (1992) found significant amounts of the mineral zircon only in the shelf and wedge areas of Track I and II (cf. Fig. 5.1). This explains the shift

towards higher Zr contents at a given Th content in the Track I and II samples relative to the shelf sediments of Track III. All non-volcanogenic EIS are characterized by low Zr contents (Fig. 5.3a). We assume that the largest part of the REE in EIS is bound to clay minerals since La and Yb correlate much better with Th than with Zr (cf. Condie, 1991). Furthermore, the low Zr contents (maximum 200 ppm) suggest that, if all Zr is present in zircon having an average Yb content of 1000 ppm (Klaver pers. com.), only 0.1 ppm Yb can be accounted for by this mineral (cf. Condie, 1990). A final argument against a dominant zircon control on the HREE in EIS is the lack of a negative correlation between Ce/Yb and Yb/Hf ratios. The minor influence of zircon is probably due to the fact that most sediments studied are in the clay fraction.

5.6.5. Implications for the recycling of continental material in the Banda Arc

The provenance of the EIS sediments from several, isotopically distinct regions has important implications for the isotopic compositions and variations in the Banda Arc volcanics. The following observations have provided strong evidence for the involvement of subducted continental material in the magma genesis:

- (1) The volcanics are characterized by high $^{87}\text{Sr}/^{86}\text{Sr}$ (0.7045-0.7095), high $^{206}\text{Pb}/^{204}\text{Pb}$ (18.7-19.4) and low $^{143}\text{Nd}/^{144}\text{Nd}$ (0.51295-0.51245). The Pb isotope ratios decrease and the neodymium isotopes increase along the arc from NE to SW (see Chapter 3)
- (2) The ratios of incompatible trace elements largely overlap with the EIS ranges (see Chapter 4).
- (3) Oxygen isotope compositions of the volcanics are generally consistent with the involvement of large quantities of continental material (Magaritz et al., 1978).
- (4) $^3\text{He}/^4\text{He}$ ratios of volcanics are exceptionally low ($R_s=1-5$), and provide evidence for the involvement of subducted continental crust (Hilton et al., 1990; 1992).

The most convincing argument for the subduction of continental material is the similarity of along-arc Pb-isotope shifts between the sediments and the volcanics (Chapter 3; Fig. 3.11a). As shown in this chapter, these isotopic shifts can be explained by the provenance of the sediments. Therefore, the Banda Arc provides strong evidence that isotopic anomalies in sub-arc mantles can be created by recent subduction of isotopically heterogeneous continental material. In Chapter 6 we shall discuss further implications of this study for the generation of OIB-type signatures by the subduction of continental material.

5.7. CONCLUSIONS

(1) The terrigenous fractions in the East-Indonesian sediments are derived from four provenance areas, as based on Pb-Nd isotope compositions, Th/Sc ratios and geographic distributions: (1) North New Guinea and Seram with Th/Sc (≈ 1.0) and low $^{206}\text{Pb}/^{204}\text{Pb}$ (> 18.65); (2) South New Guinea with Th/Sc (≈ 0.8) and higher $^{206}\text{Pb}/^{204}\text{Pb}$ (≈ 18.8); (3) Northern Australia: low Th/Sc (≈ 0.7) and high $^{206}\text{Pb}/^{204}\text{Pb}$ (≈ 19.57) and (4) Timor with Th/Sc ≈ 1.0 , low $^{206}\text{Pb}/^{204}\text{Pb}$ (≈ 19.1) and extremely low $^{143}\text{Nd}/^{144}\text{Nd}$ (≈ 0.51190).

(2) An estimate of the average composition of the northern Australia Upper Continental Crust in terms of trace-element ratios has been made from the EIS data. Most ratios agree well with published values for upper continental crust, as do the REE patterns. The EIS thus confirm that variations in trace-element ratios of continental masses are limited, in contrast to the isotopic variations.

(3) From the correspondence between the isotopic signatures of EIS and the Banda Arc volcanics, it is concluded that the hinterland of sediments has exerted an important control in generating the isotopic compositions and variations of magma source regions in the sub-arc mantle.

(4) From a comparison of Pb isotope signatures of microcontinents and shelf sediments, it is suggested that the Banda Ridges are derived from a Pacific Arc, Bacan island from Precambrian Australia and the Ambon-Seram block from Paleozoic New Guinea.

CHAPTER 6

IMPLICATIONS FOR ISLAND-ARC MAGMATISM, THE NATURE OF THE SUBDUCTED CONTINENTAL MATERIAL AND OIB SOURCES

6.1. INTRODUCTION

In this Chapter some implications of the isotopic and trace-element results are discussed. Some general remarks on island-arc magma genesis are presented in section 6.2. The nature of the subducted continental crust (i.e. is it either continent-derived sediment or continental crust?) will be examined in section 6.3. Finally, some trace-element implications for the involvement of continent-derived sediment in the sources of some Ocean Island Basalts (OIBs) are evaluated in section 6.4.

6.2. IMPLICATIONS FOR ISLAND-ARC MAGMATISM

At least three *variable* components contribute to the composition of arc magmas: (1) the mantle wedge; (2) the subducted component (e.g. oceanic crust and/or sediments); (3) arc crust. The extreme isotopic composition and the large amounts of continental material involved in the Banda Arc clearly demonstrate the important role played by the subducted component in magma genesis. As shown in Chapter 3, the isotopic and geochemical along-arc variations of the Banda arc can be largely explained by two effects: (1) variation in the Pb (and Nd) isotopic composition of the continental material along the arc; (2) variations in the amount of the subducted continental material from NE to SW.

Although changes in the nature of the mantle wedge and the extent of arc-crust assimilation are detectable, they had only a limited effect on the final geochemical signatures. Therefore, nearly all systematic along-arc variations can be explained by the subducted component. The results of this study further emphasize that the 'decoupling' of isotopes and trace elements can not be used as an argument against sediment subduction (Arculus and Johnson, 1981). This decoupling may be explicable when data on critical elements (e.g. Ba, Nb) from local sediments are taken into account, and when the details of slab-mantle transfer mechanisms are better evaluated. Studies that attempt to model island-arc magma genesis on the basis of generalized end-member compositions are unlikely to solve some of the 'island-

arc' problems (e.g. the negative Nb-Ta anomalies). Detailed studies of individual arcs, using the compositions of potentially involved *local* end members, are essential to solve these complexities. Furthermore, more experimental data on the distribution of element between solid, fluid and melt phases for the the whole spectrum of conditions in subduction zones are required.

6.3. THE NATURE OF SCM: SUBDUCTED CONTINENTAL CRUST OR CONTINENT-DERIVED SEDIMENTS?

The evidence for SCM in the Banda Arc pertains directly to the question of how far the Australian continental margin has been subducted. This question has been debated for many years, and conflicting tectonic models have been proposed. Geological arguments against subduction have emphasized the importance of crustal shortening and deformation in the fore-arc, arc and back-arc (e.g. Audley-Charles, 1981), but several observations suggest that the continental crust has at least reached the inner margin of the outer arc (cf. Hamilton, 1979): (1) the strong recent uplift in the outer arc which can be interpreted as a result of rebounding subducted continental crust (e.g. Chappell and Veeh, 1979; DeSmet et al., 1989); (2) gravity interpretations (e.g. Chamalaun et al., 1976; Schluter and Fritsch, 1985); (3) geometric considerations based on the subduction velocity and the time elapsed since the collision started (ca. 3 Ma, Abbott and Chamalaun, 1981), which indicate that some 250 km of continental crust must have entered the subduction zone (e.g. McCaffrey, 1989); (4) seismological evidence for slab detachment (Charlton, 1991), which suggests that the recent uplift and fore-arc extension is caused by the rebound of continental crust, which would have been subducted to a depth of approximately 100 km. The latter two arguments would imply that the continental crust has reached the magma generation zone of the Eastern Sunda and western part of the Banda Arc.

Sr-Nd-Pb and trace-elements as used in this study cannot distinguish between subducted continent-derived sediments and continental crust. However, the following mass-balance considerations provide evidence that continental crust may well be involved, in particular in the southern part of the Banda Arc. This evidence is based on a comparison between the calculated minimum thickness of SCM that must have been subducted in order to generate the volcanic arc and the sediment thickness on the Argo Abyssal Plain. This 300-1000 m sediment sequence in front of the trench close to the Australian Continent covers oceanic crust just west of the collision zone (DSDP Sites 260-261 (Veveers et al., 1974); ODP Site 765 (Gradstein et al., 1992); and the tectonic map of the Indonesian region (Hamilton, 1979). Hence, it may be equivalent to the leading oceanic portion of the

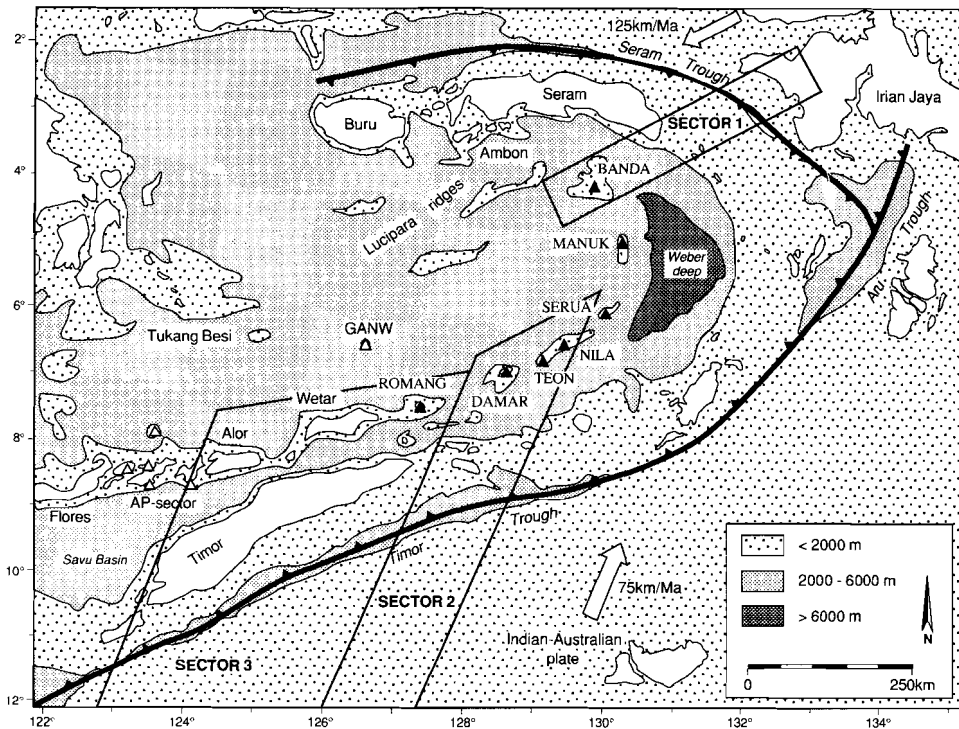


Fig. 6.1. Map of Eastern Indonesia showing the three sectors for which mass-balance calculations were performed (see Table 6.1 for details). Subduction velocities and -directions are from Jordan and Minster (1978) and DeSmet et al. (1989). Other details are given in Fig. 2.1.

Indo-Australian plate that was subducted below the southern Banda Arc before the collision. As will be shown, the calculated SCM thickness was probably considerably larger, which implies the involvement of the continental margin.

The time-averaged minimum thickness of the SCM-sequence that has reached the magma generation zone in a given arc sector can be estimated as follows. We first calculate the total volume of contaminated mantle source from which the total volume of the arc crust has been generated since the onset of volcanism. The arc-crust volume is considered to be twice the volume of the volcanics above the sea floor, and a melting percentage of 10% is assumed. Subsequently, the SCM volume is calculated from the percentage derived from the Sr-Nd-Pb systematics (assuming that the density of the mantle is twice that of SCM). This volume of SCM is then converted to a thickness, depending upon the subduction velocity, the total subduction time (approximately the age of the arc sector) and the length along the

trench over which SCM was subducted.

Estimates are presented for the Banda Archipelago sector, the south Banda Arc sector and the inactive sector North of Timor (Fig. 6.1) in Table 6.1. In the absence of sufficiently detailed geochronological constraints, three different ages were used in each case: 1, 5 and 10 Ma. The calculated SCM thicknesses range from a minimum of 25 m (10 Ma) to a maximum of 7350 m (1 Ma). The lowest calculated values are found in the Banda Archipelago sector (25-240 m), whereas the highest values are found in the inactive sector (735-7350 m).

It should be stressed that the calculations are rough and based on the assumption of a steady-state contribution of SCM during the build up of the arc. Nevertheless, the calculated SCM thicknesses may well be only *minimum* values. For example, the volume of intrusives in the arc crust is probably much larger than assumed in these calculations (e.g. Bowin et al., 1980, crust thickness approximately 6-17 km). Furthermore, the amount of SCM which was supplied to the trench was significantly larger than calculated, considering that sediment must have been scraped off in order to form the accretionary wedge (see Table 6.1). It should be noted that high extrusion rates are implied for an age of 5 Ma: 16.6, 19.7, and 34.4 km³/arc km/Ma for sectors 1, 2 and 3 respectively. Sigurdsson et al. (1980) reports an estimate of 7 km³/arc km/Ma for the Lesser Antilles.

If we assume that the Banda Archipelago in the NE has a maximum age of 1-5 Ma, SCM here is more likely to consist of sediment than continental crust. For sector 2, the southern Banda Arc, the result is more ambiguous. If the age is closer to 1 Ma than to 5 Ma, continental crust is a likely component in this sector. However, if this arc sector is older than 5 Ma, sediments dominate the SCM component.

For sector 3, the inactive segment, subduction of continental crust is likely if the 10% SCM component in the source, which was obtained from Romang, is representative for the entire volume of the inactive island arc volume. It should be noted that the large Sr and Nd isotopic variations (McCulloch et al., 1982) indicate that this assumption may not be valid. However, rocks which have a much larger (>50%) SCM component also occur on Wetar (McCulloch et al., 1982; Vroon and Hoogewerff, unpublished data). If material which is scraped off is taken into account, it is likely that subducted continental crust has reached the magma-generation zones.

The inferred subduction of continental crust in this sector agrees with the He isotope results as presented by Hilton et al. (1992) for the Eastern Sunda and Banda Arcs. They explained the unusually low ³He/⁴He ratios of the volcanics in this sector by the degassing of the subducted continental crust. On the basis of argument that fine-grained sediments are not capable of retaining sufficient helium when entering the subduction zone, the low ³He/⁴He ratios must be due to crystalline crust.

Table 6.1. Mass-balance estimates of the amounts of subducted continental material

		Sector 1 Banda Archipelago	Sector 2 South Banda Arc	Sector 3 Inactive segment
Wedge volume ¹⁾		70200 km ³	66800 km ³	230500 km ³
Volume arc extrusives ¹⁾		10400 km ³	22600 km ³	68900 km ³
Total arc volume ²⁾		20800 km ³	45000 km ³	135000 km ³
Width of sector ³⁾		135 km	185 km	490 km
Subduction velocity ⁴⁾		125 km/Ma	75 km/Ma	75 km/Ma
SCM % bulk mixing ⁵⁾		1	5	10
Estimated age		1-5 Ma	1-5 Ma	3-12 Ma
Thickness	1 Ma	240 m	3250 m	7350 m
SCM ⁶⁾	5 Ma	50 m	650 m	1470 m
	10 Ma	25 m	325 m	735 m
Total CM	5 Ma	900 m	1600 m	3100 m
thickness ⁷⁾	10 Ma	440 m	800 m	1500 m
Ratio SCM/ACM ⁸⁾		0.06	0.4	0.5

Estimate minimum amounts of subducted continental material (SCM) (1) Volumes of wedge and arc extrusives were calculated from the map of Hamilton (1979). (2) The total arc volume (intrusives and extrusives) is twice the volume of the extrusives. (3) See Fig. 6.1. (4) The velocities are from Jordan and Minster and De Smet (1989). (5) The amounts by bulk mixing are from this study (cf. Chapter 3). (6) Calculated thickness of SCM for three different periods (1, 5 and 10 Ma) since collision started. (7) Total thickness of Continental Material (CM) transported to the trench=Subducted + Accreted CM. (8) Ratio of accreted and subducted continental material for the three sectors for the 5 Ma case. See text for details about the calculations.

6.4. IS THE EMII OIB SOURCE GENERATED BY SEDIMENT SUBDUCTION?

The large along-arc variations in Sr, Nd and Pb isotopes in the Banda Arc indicate that subduction of continental material can generate significant heterogeneities in the mantle. In Figure 6.2, the isotopic variations of the Banda Arc and oceanic basalts are compared for different scale lengths within which they occur. On the scale of 10 km (the single Serua volcano), 100-200km (arc segments=Northern and Southern Banda Arc) and 700 km (the whole arc) the variations, normalized to the maximum variation (amplitude ratio), largely overlap with those of the oceanic basalts. This implies that a Banda-Arc type subduction system is capable of generating isotopic variations on the same length scales as observed in present-day oceanic basalts.

Sr-Nd-Pb isotopic evidence has led to the hypothesis that certain OIBs (e.g. Kerguelen, Gough, Tristan and Samoa) contain an old (1-2.5 Gyr) recycled component of sediment or (altered) oceanic crust with or without sediment (e.g. Chase, 1981; Hofmann and White, 1982; Zindler and Hart, 1986; Weaver, 1991). The 'Enriched Mantle II' (EMII) is the OIB-type thought to contain a fraction of recycled sediment (Zindler and Hart, 1986). The effects of Pb isotopic evolution in old recycled bulk sediments has been discussed by Ben Othman et al. (1989) and Weaver (1991). On the basis of U/Pb and Th/Pb ratios in recent sediments, they concluded that recycling of old sedimentary material can explain the Pb isotopic compositions of EMII OIBs. Their Sr-Nd isotope systematics suggest that the recycled sedimentary component must have mixed with a low Sr and Nd component. Ben Othman et al. (1989) estimated the amount of sediment involved in OIB sources to be less than 1%. Although this is a small fraction, incompatible element abundances and ratios will be determined by the sedimentary component if it mixes with mantle material.

Could the Banda Arc subduction system be a present-day example of the ancient settings where EMII sources were generated? In order to answer this question, it must be assumed that the compositions of sediments subducted in ancient times (> 1 Gyr) were similar to those of the recent sediments. As pointed out by McLennan (1988) and Ben Othman et al. (1989), the abundances of some elements (e.g. U, Rb, Sr, Pb, Ba) could have changed due to changes in oxidation conditions and in the biological fractionation in sediments. However, it is reasonable to assume that the trace-element compositions of recent sediments are generally close to those of ancient recycled sediments (Taylor and McLennan, 1985).

Most source-mixing models for EMII OIB use 'bulk' sediments as an end member. However, as shown in Chapter 4, deep subduction of sediment without chemical modifications is unlikely. If these are taken into account, EMII sources could conceivably be created by the mixing of mantle material with (Fig 6.3):

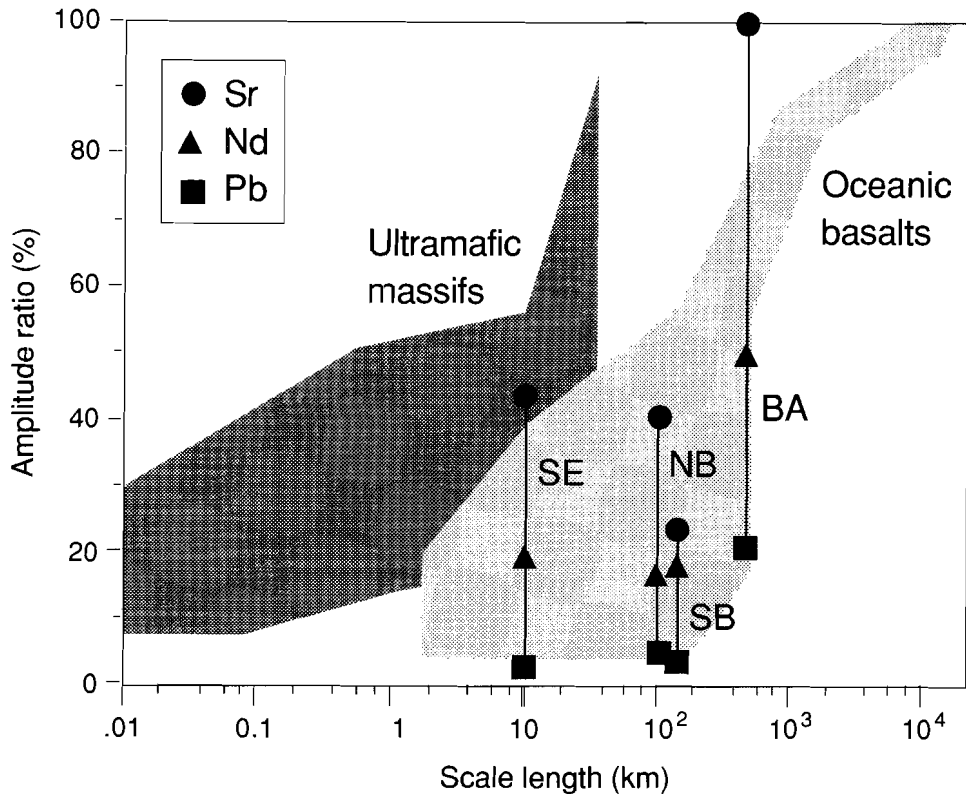


Fig. 6.2. Amplitude ratios of Sr-Nd-Pb isotopes versus scale lengths for the Banda Arc volcanoes, compared with oceanic basalts and ultramafic massifs (Zindler and Hart, 1986). Amplitude ratios were obtained by normalizing the isotopic variations in the Banda Arc to the maximum variations found in oceanic basalts (amplitude ratio of 100%). Scale lengths indicate the geographical distances within which the isotopic variations occur. NB=Banda Archipelago+Manuk, SE=Serua, SB=Nila+Teon+Damar. Note that the isotopic variations in the Banda Arc are similar to the variations in oceanic basalts on 10-700 km scale lengths.

- (1) bulk continental crust and/or sediments (SCM)
- (2) a mantle which was chemically modified by fluids derived from SCM
- (3) SCM which was chemically modified by dehydration.

1. Bulk continental crust and/or sediments

If 'bulk' terrigenous sediments are involved in the source of EMII OIBs, this should be visible in corresponding LILE, HFSE and LREE signatures. Abundance diagrams for EMII and sediments are compared in Fig. 6.4. The sediments are characterized by negative

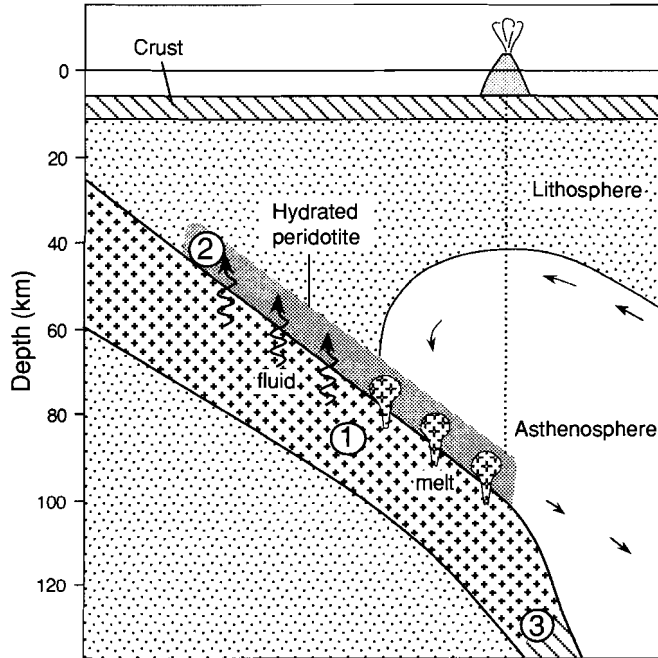


Fig. 6.3. Schematic diagram showing various options for subducted components potentially involved in the generation of EMII OIB: (1) bulk continental crust and/or sediments (SCM), (2) peridotite which is chemically modified by SCM-derived fluids, (3) SCM which is chemically modified by dehydration. See text for discussion.

Nb-Ta anomalies in contrast to the EMII OIBs (Weaver, 1991). Hence, if sediments are involved, a process which decreases the LILE and LREE abundances relative to the HFSE must be invoked, or the sediments must have mixed with a component that had a positive Nb-Ta anomaly. Weaver (1991) suggested that bulk continental crust may have mixed with an HIMU-type OIB end-member. This end member could be composed of dehydrated altered oceanic crust which has a positive Nb-Ta anomaly (e.g. Weaver, 1988).

2. Fluid-modified mantle

Because SCM-derived hydrous fluids are probably even more enriched in LILE and LREE compared to HFSE than bulk sediment (cf. Tatsumi, 1986), a fluid-modified mantle is an unlikely source component of EMII OIB. The addition of dehydrated altered oceanic crust to cancel the negative Nb-Ta anomaly is considered to be less likely, because such crust will probably be physically separated from the fluid-modified mantle which rises as

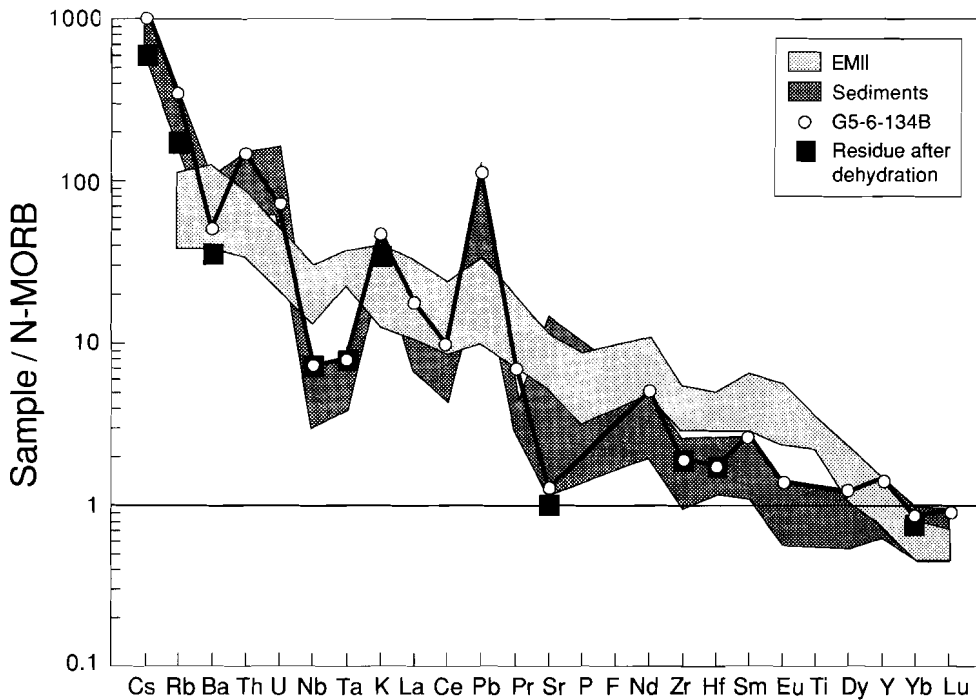


Fig. 6.4. N-MORB normalized trace-element abundance patterns of East Indonesian Sediments ($\text{CaCO}_3 < 30\%$, Chapter 5), compared to EMII OIBs, which include Tutulia and Upula Islands (Samoa) and Tahaa (Society Islands). Element order and normalizing values from Sun and McDonough (1989). Sediment G5-6-134B is from Chapter 5, the solid squares represent the dehydrated residue of G5-6-134B if Tatsumi et al. (1986) mobility data are used. Note that the residue would still have a large negative Nb-Ta anomaly which would be visible in EMII like magmas, even if small ($< 1\%$) quantities are added to a MORB source. Data sources for EMII OIBs: Dostal et al. (1982), Palacz and Saunders (1986), Devey et al. (1990).

diapirs to shallower levels before melting (e.g. Kay, 1980; Tatsumi, 1989).

It is of interest to note that a fluid-modified mantle could be the origin of certain continental lithosphere-derived basalts. Because the Banda Arc will become incorporated into the Australian lithosphere within 10 Ma (McCaffrey, 1991), the future subcontinental mantle will inherit the large isotopic anomalies and the trace element-signature of the Banda Arc mantle. This process of lateral accretion may explain some 'subduction-type' signatures (e.g. negative Nb-Ta anomalies) of 'continental' alkali basalts, such as those observed in the Western United States (Omrod and Hawkesworth, 1990).

3. Dehydrated SCM.

The third possible explanation for the recycled component in the EMII OIB source is the dehydrated sediment left after the expulsion of fluids at shallow depths (see Fig. 6.3). This component will be enriched in HFSE compared to LILE, because the LILE are preferentially transported by the fluid phase (cf. Tatsumi et al., 1986). LILE/HFSE and LREE/HFSE ratios like those observed in EMII OIBs can only be generated if LILE and REE escape in large quantities and the HFSE are retained in the subducting slab. We illustrate this for Th and La versus Nb. The average Th/Nb and La/Nb in the East Indonesian Sediments are 1.19 and 3.32, respectively (Chapter 5, Table 5.2). Assuming no Nb transfer, and Th/Nb to be 0.14 and La/Nb to be 1.00 for EMII OIB (Weaver, 1991), one concludes that more than 88% of the Th and 70% of the La must have been released by the fluid.

If dehydrated sediments are the recycled component in EMII OIB sources, much larger mobilities for the LILE and LREE are required than those experimentally determined by Tatsumi et al. (1986). Figure 6.4 shows a trace element pattern of dehydrated sediment as calculated from sample G5-6-134B and the mobility data of Tatsumi et al. (1986). This dehydrated sediment is not sufficiently depleted in LILE and LREE compared to EMII OIB. Mixing with an HIMU-type OIB end member could be an additional mechanism in this case too.

A final but quite conceivable option is that dehydrated subducted continental material melts and metasomatizes the deeper portions of the mantle wedge. Small-degree melting of this mixture could produce basalts with EMII OIB characteristics. This evidence for the transfer of SCM from the slab to the wedge in the form of melt has been discussed in Chapter 4.

From the above considerations, it is concluded that subduction of continental material in Banda Arc type settings could have generated EMII OIB sources, provided that progressive chemical modifications during the subduction process are taken into account.

REFERENCES

- Abbott, M.J., and Chamalaun F.H., 1981, Geochronology of some Banda arc volcanics. In: *Geology and Tectonics of Eastern Indonesia* (ed. A.J. Barber), *Indonesian Geological Research and Development Center Special Publication No. 2*, pp. 253-268.
- Allègre, C.J., and Rousseau, D., 1984, The growth of the continent through geological time studied by Nd isotope analysis of shales. *Earth Planet. Sci. Lett.*, **67**, 19-34.
- Arculus, R.J., and Johnson, R.W., 1981, Island-arc magma sources: a geochemical assessment of the roles of slab-derived components and crustal contamination. *Geochem. J.*, **15**, 109-133.
- Arculus, R.J., and Powell R., 1986, Source component mixing in the regions of arc magmagenesis. *J. Geophys. Res.*, **91**, 5913-5926.
- Armstrong, R.L., 1968, A model for Sr and Pb isotope evolution in a dynamic earth. *Rev. Geophys.*, **6**, 175-199.
- Armstrong, R.L., 1971, Isotopic and chemical constraints on models of magma genesis in volcanic arcs. *Earth Planet. Sci. Lett.*, **12**, 137-143.
- Armstrong, R.L., 1981, Radiogenic isotopes: The case for crustal recycling on a near steady-state no-continental-growth Earth. *Phil. Trans. R. Soc. Lond.*, **A301**, 443-472.
- Audley-Charles, M.G., 1981, Geometric problems and implications of large scale overthrusting in the Banda Arc-Australian margin collision zone. In: *Thrust and Nappe Tectonics* (ed. K.R. McClay and N.J. Price); *Geol. Soc. London Spec. Publ.*, **9**, 407-418.
- Audley-Charles, M.G., Carter, D.J., Barber, A.J., Norvick, M.S., and Tjokrosapeetro S., 1979, Reinterpretation of the geology of Seram: implications for the Banda Arcs and northern Australia. *J. Geol. Soc. London*, **136**, 547-568.
- Barreiro, B., 1983, Lead isotopic compositions of South Sandwich Island volcanic rocks and their bearing on magmagenesis in intra-oceanic island arcs. *Geochim. Cosmochim. Acta*, **47**, 817-822.
- Ben Othman, D., White, W.M., and Patchett, J., 1989, The geochemistry of marine sediments, island arc magma genesis, and crust-mantle recycling. *Earth Planet. Sci. Lett.*, **94**, 1-21.
- Bowin, C.O., Purdy, G.M., Johnston, C., Shor, G.G., Lawver, L., Hartono, H.M.S., and Jezek, P., 1980, Arc-continent collision in Banda Sea region. *Bull. Am. Assoc. Pet. Geol.*, **64**, 868-915.
- Brown, L., Sacks, I.S., Tera, F., Klein, J., and Middletown, R., 1981, Beryllium-10 in continental sediments. *Earth Planet. Sci. Lett.*, **55**, 370-376.

- Brown, L., Klein, J., Middletown, R., Sacks, I.S., and Tera, F., 1982, ^{10}Be in island-arc volcanoes and implications for subduction, *Nature*, **299**, 718-720.
- Butcher, B.P., 1989, Northwest shelf of Australia, In: *Divergent/passive margin basins* (eds. J.D. Edwards, and Santagrossi). *AAPG Memoir*, **48**, pp. 81-116.
- Cameron, A.E., Smith, D.H., and Waler, R.L., 1969, Mass spectrometry of nanogram-size samples of lead. *Anal. Chem.*, **41**, 525-526.
- Carr, M.J., Feigenson, M.D., and Bennett, E.A., 1990, Incompatible element and isotopic evidence for tectonic control of source mixing and melt extraction along the Central American Arc. *Contrib. Mineral. Petrol.*, **105**, 369-380.
- Cardwell, R.K., and Isacks, R.L., 1978, Geometry of the subducted lithosphere beneath the Banda Sea in eastern Indonesia from seismicity and fault plane solutions. *J. Geophys. Res.*, **83**, 2825-2838.
- Chappell, J., and Veeh, H.H., 1978, Late Quaternary tectonic movements and sea-level changes at Timor and Atauro Island. *Geol. Soc. America Bull.*, **89**, 356-368.
- Charlton, T.R., 1991, Postcollision extension in arc-continent collision zones, eastern Indonesia. *Geology*, **19**, 28-31.
- Chase, C.G., Oceanic island Pb: two stage histories and mantle evolution. *Earth Planet. Sci. Lett.*, **52**, 277-284.
- Chauvel, C., Hofmann, A.W., Vidal, P., 1992, HIMU-EM: The French-Polynesian connection. *Earth Planet. Sci. Lett.*, **110**, 99-119.
- Chen, C.H., Jahn, B.M., Lee, T., Chen, C.H., and J. Cornichet, 1990, Sm-Nd isotopic geochemistry of sediments from Taiwan and implications for the tectonic evolution of southeast China. *Earth Planet. Sci. Lett.*, **88**, 317-332.
- Coats, R.R., 1962, Magma type and crustal structure in the Aleutian Arc. In: *The Crust of the Pacific Basin* (eds. G.A. McDonald, and H. Kuno), *Am. Geoph. Un.*, Washington, pp. 99-109.
- Cohen, R.S., and O'Nions, R.K., 1982, Identification of recycled continental material in the mantle from Sr, Nd, Pb isotope investigations. *Earth Planet. Sci. Lett.*, **61**, 73-84.
- Condie, K.C., 1991, Another look at rare earth elements in shales. *Geochim. Cosmochim. Acta*, **55**, 2527-2531.
- Cook, P.J., 1974, Major and trace element geochemistry of sediments from deep sea drilling project, leg 27, sites 259-263, Eastern Indian Ocean; In: *Initial reports on the Deep Sea Drilling Project* (eds. Z.J.J. Veevers, J.R. Heirtzler, et al.), **27**, Washington, U.S. Government Printing Office, pp. 481-497.
- Compston, W., and Arriens, P.A., 1968, The Precambrium geochronology of Australia. *Canadian Jour. Earth Sci.*, **5**, 561-583.

- Church, S.E., 1976, The Cascade Mountains revisited: A reevaluation in light of new lead isotope data. *Earth Planet. Sci. Lett.*, **29**, 175-188.
- Davidson, J.P., 1986, Isotope and trace element constraints on petrogenesis of subduction-related lavas from Martinique, Lesser Antilles. *J. Geophys. Res.*, **91**, 5943-5962.
- Davidson, J.P., Harmon, R.S., 1989, Oxygen isotope constraints on the petrogenesis of volcanic arc magmas from Martinique, Lesser Antilles. *Earth Planet. Sci. Lett.*, **95**, 255-270.
- Davies, J.L., 1977, The coast. In: *Australia: a geography* (ed. D.N. Jeans), Sydney University Press, pp. 134-151.
- De Bruin, M., Instrumental neutron activation analysis - a routine method, 1983, Delftse Universitaire Press, Delft, 270p.
- Defant, M.J., Maury, R.C., Ripley, E.M., Feigenson, M.D., and Jacques, D., 1991, An example of island-arc petrogenesis: geochemistry and petrology of the southern Luzon Arc, Philippines. *J. Petrol.*, **32**, 455-500.
- DePaolo, D.J., 1981a, Trace element and isotopic effects on combined wallrock assimilation and fractional crystallization. *Earth Planet. Sci. Lett.*, **53**, 189-202.
- DePaolo, D.J., 1981b, A Neodymium and Strontium isotopic study of Mesozoic calc-alkaline granitic batholiths of the Sierra Nevada and Peninsular Ranges, California. *J. Geophys. Res.*, **86**, 10470-10488.
- DePaolo, D.J., and Johnson, R.W., 1979, Magma genesis in the New Britain island arc: Constraints from Nd and Sr isotopes and trace element patterns. *Contrib. Mineral. Petrol.*, **70**, 367-379.
- DeSmet, M.E.M., Fortuin, A.R., Tjokrosapoetro, S., and Van Hinte, J.E., 1989, Late Cenozoic vertical movements of non-volcanic islands in the Banda Arc area. *Neth. J. Sea Res.*, **24**, 263-275.
- Devey, C.W., Albarede, F., Cheminée, J.-L., Michard, A., Mühe, R., and Stoffers, P., 1990, Active Submarine Volcanism on the Society Hotspot Swell (West Pacific): A Geochemical Study. *J. Geophys. Res.*, **95**, 5049-5066.
- Dosso, L., Bougault, H., Beuzart, P., Calvez, J.-Y. and Joron, J.L., 1988, The geochemical structure of the South-East Indian Ridge. *Earth Planet. Sci. Lett.*, **88**, 47-59.
- Dostal, J., Dupuy, C., Lotard, J.M., 1982, Geochemistry and Origin of Basaltic Lavas from Society Islands, French Polynesia (South Central Pacific Ocean). *Bull. Volcanol.*, **45**, 51-62.
- Dupre, B., and Allegre, C.J., 1983, Pb-Sr isotope variations in Indian Ocean basalt and mixing phenomena. *Nature*, **303**, 142-146.

- Edwards, C., Menzies, M., and Thirlwall, M., 1991, Evidence from Muriah, Indonesia, for the interplay of supra-subduction zone and intraplate processes in the genesis of potassic alkaline magmas. *J. Petrol.*, **32**, 555-592.
- Ellam, R.M. and Hawkesworth, C.J., 1988, Elemental and isotopic variations in subduction related basalts: evidence for a three component model. *Contrib. Mineral. Petrol.*, **98**, 72-80.
- Ellam, R.M., Menzies, M.A., Hawkesworth, C.J., Leeman, W.P., Rosi, M., and Serri, G., 1988, The transition from calc-alkaline to potassic orogenic magmatism in the Aeolian Islands, southern Italy. *Bull. Volcanol.*, **50**, 386-398.
- Ellam, R.M., Hawkesworth, C.J., Menzies, M.A., and Rogers, N.W., 1989, The volcanism of southern Italy: the role of subduction and the relationship between potassic and sodic alkaline magmatism. *J. Geophys. Res.*, **94**, 4589-4601.
- Ellam, R.M., and Harmon, R.S., 1990, Oxygen isotope constraints on the crustal contribution to the subduction-related magmatism of the Aeolian Islands, southern Italy. *J. Volcanol. Geotherm. Res.*, **44**, 105-122.
- Foley, S.F., 1991, High-pressure stability of the fluor- and hydroxy-endmembers of pargasite and K-richterite. *Geochim. Cosmochim. Acta*, **55**, 2689-2694.
- Foley, S.F., and Wheller, G.E., 1990, Parallels in the origin of the geochemical signatures of island-arc volcanics and continental potassic igneous rocks: The role of residual titanates. *Chem. Geol.*, **85**, 1-18.
- Fraser, K.J., Hawkesworth, C.J., Erlank, A.J., Mitchell, R.H., and Scott-Smith, B.H., 1986, Sr, Nd and Pb isotope and minor element geochemistry of lamproites and kimberlites. *Earth Planet. Sci. Lett.*, **76**, 57-70.
- Gill, J.B., 1981, Orogenic andesites and plate tectonics. New York, Springer-Verlag, 370 pp.
- Gill, J.B., 1984, Sr-Pb-Nd isotopic evidence that both MORB and OIB sources contribute to oceanic island arc magmas in Fiji. *Earth Planet. Sci. Lett.*, **68**, 443-458.
- Goldstein, S.L., and O'Nions, R.K., 1981, Nd and Sr isotopic relationships in pelagic clays and ferromanganese deposits. *Nature*, **292**, 324-327.
- Goldstein S.L., O'Nions, R.K., and Hamilton, P.J., 1984, A Sm-Nd isotopic study of atmospheric dusts and particles from major river systems. *Earth Planet. Sci. Lett.*, **70**, 221-236.
- Goldstein, S.L., 1988, Decoupled evolution of Nd and Sr isotopes in the continental crust and the mantle. *Nature*, **336**, 733-738.
- Govindaraju, K., 1989, Compilation of working values and sample descriptions for 272 geostandards. *Geostandards Newsletter*, **13**, 1-113.

- Gradstein, F.M., Ludden, J.N., et al., 1992, *Proceedings of the Ocean Drilling Program, Scientific Results*, Vol., **123**, in press.
- Green, D.H., Pearson, N.J., 1986, Ti-rich accessory phase saturation in hydrous mafic-felsic compositions at high P, T. *Chem. Geol.*, **54**, 185-201.
- Green, D.H., Pearson, N.J., 1987, An experimental study of Nb and Ta partitioning between Ti-rich minerals and silicate liquids at high pressure and temperature. *Geochim. Cosmochim. Acta*, **51**, 55-62.
- Hamelin, B., and Allegre, C.J., 1985, Large scale regional units in the depleted upper mantle revealed by an isotope study of the South-West Indian Ridge. *Nature*, **315**, 196-199.
- Hamelin, B., Dupre, B., and Allegre, C.J., 1986, Pb-Sr-Nd isotopic data of Indian Ocean ridges: new evidence of large-scale mapping of mantle heterogeneities. *Earth Planet. Sci. Lett.*, **76**, 288-298.
- Hamilton, W., 1979, Tectonics of the Indonesian region. *U.S. Geol. Surv. Prof. Pap.*, **1078**, 345 pp.
- Hart, S.R., 1984, A large-scale isotope anomaly in the southern hemisphere mantle. *Nature*, **309**, 753-757.
- Hart, S.R., 1988, Heterogeneous mantle domains: signatures, genesis and mixing chronologies. *Earth Planet. Sci. Lett.*, **90**, 273-296.
- Hartono, H.M.S., 1990, Late Cenozoic tectonic development of the Southeast Asian continental margin of the Banda Sea area. *Tectonophysics*, **181**, 267-276.
- Hawkesworth, C.J., Hergt, J.M., McDermott, F., and Ellam, R.M., 1991, Destructive margin magmatism and the contributions from the mantle wedge and subducted crust. *Austr. J. Earth Sc.*, **38**, 577-594.
- Hebeda, E.H., Andriessen, P.A.M., and Belle, J.C., 1988, Simultaneous isotope analysis of Nd and Sm with a fixed multicollector mass spectrometer. *Fresenius Z. Anal. Chem.*, **331**, 114-117.
- Hickey, R.L., Frey, F.A., Gerlach, D.C., and Lopez-Escobar, L., 1986, Multiple sources for basaltic arc rocks from the southern volcanic zone of the Andes (34-41 S): trace element and isotopic evidence for contributions from subducted oceanic crust, mantle, and continental crust. *J. Geophys. Res.*, **91**, 5963-5983.
- Hilde, T.W.C., 1983, Sediment subduction versus accretion around the Pacific. *Tectonophysics*, **99**, 381-397.
- Hildreth, W., and Moorbath, S., 1988, Crustal contributions to arc magmatism in the Andes of Central Chile. *Contrib. Mineral. Petrol.*, **98**, 455-489.
- Hilton, D.R., and Graig, H., 1989 A helium isotope transect along the Indonesian archipelago. *Nature*, **342**, 906-908.

- Hilton, D.R., Hoogewerf, J.A., Van Bergen, M.J., and Hammerschmidt, K., 1992, Mapping magma sources in the east Sunda-Banda arcs, Indonesia: Constraints from helium isotopes. *Geochim. Cosmochim. Acta*, **56**, 851-859.
- Hodde, D.A., Muller, P.A., and Garrido, J.R., 1991, Variations in the Sr-isotopic composition of seawater during the neogene. *Geology*, **19**, 24-27.
- Hofmann, A.W., and White, W.M., 1981, Mantle plumes from ancient oceanic crust. *Earth Planet. Sci. Lett.*, **57**, 421-436.
- Hutchinson, C.S., 1982, Indonesia. In: *Andesites*. (ed. R.S. Thorpe), John Wiley & Sons, pp. 307-325.
- Hutchison, C.S., and Jezek, P.A., 1978, Banda arc of eastern Indonesia: Petrography, mineralogy and chemistry of the volcanic rocks. In: *Proceedings of the third regional conference on geology and mineral resources of S.E. Asia* (ed. Prinya Nutalaya), pp. 607-619. Asian Institute of Technology, Bangkok.
- Ito, E., White, W.M., and Gospel, C., 1987, The O, Sr, Nd and Pb isotope geochemistry of MORB. *Chem. Geol.*, **62**, 157-176.
- Jacobson, R.S., Shor, G.G., Kieckhefer, R.M., and Purdy, G.M., 1978, Seismic refraction and reflection studies in the Timor-Aru Trough system and Australian continental shelf. *Am. Ass. Petrol. Geol. Mem.*, **29**, 209-222.
- James, D.E., 1981, The combined use of the oxygen and radiogenic isotopes as indicators of crustal contamination. *Ann. Rev. Earth. Planet. Sci.*, **9**, 311-344.
- Jezek, P.A., and Hutchinson, C.S., 1978, Banda arc of eastern Indonesia: Petrography and geochemistry of the volcanic rocks. *Bull. Volc.*, **41**, 586-608.
- Jongsma, D., Huson, W., Woodside, J.M., Suparka, S., Sumantri, T., and Barber, A.J., 1989, Bathymetry and Geophysics of the Snellius-II Triple Junction and tentative seismic stratigraphy and neotectonics of the northern Aru Trough. *Neth. J. Sea Res.*, **24**, 231-150.
- Karig, D.E., Kay, R.W., 1981, Fate of sediments on the descending plate at convergent margins. *Phil. Trans. R. Soc. Lond.*, **A301**, 233-251.
- Katili, J.A., 1978, Past and present geotectonic position of Sulawesi, Indonesia. *Tectonophysics*, **45**, 289-322.
- Kay, R.W., 1980, Volcanic arc magmas: Implications of a melting-mixing model for element recycling in the crust-upper mantle system. *J. Geol.*, **88**, 497-522.
- Klein, E.M., and Langmuir, C.H., 1987, Global Correlations of Ocean Ridge Basalt Chemistry with Axial Depth and Crustal Thickness. *J. Geophys. Res.*, **82**, 8089-8115.
- Knittel, U., Defant, M.J., and Raczek, I., 1988, Recent enrichment in the source region of arc magmas from Luzon Island, Philippines: Sr and Nd isotopic evidence. *Geology*, **16**, 73-76.

- Kuenen, P.H., 1935, Contributions to the Geology of the East Indies from the Snellius Expedition. Part I, Volcanoes, *Leid. geol. Meded.*, **7**, 273-331.
- Lee, C.S., and McCabe, R., 1986, The Banda-Celebes-Sula basin: a trapped piece of Cretaceous-Eocene oceanic crust. *Nature*, **322**, 51-54.
- LeRoex, A.L., Dick, H.J.B., Erlank, A.J., Reid, A.M., Frey, F.A., Hart, S.R., 1983, Geochemistry, Mineralogy and Petrogenesis of lavas erupted along the Southwest Indian Ridge between the Bouvet Triple junction and 11 degrees East. *J. of Petrol.*, **24**, 267-318.
- LeRoex, A.L., Dick, H.J.B., and Fisher, R.L., Petrology and Geochemistry of MORB from 25 °E to 46 °E along the Southwest Indian Ridge: Evidence for contrasting styles of mantle enrichment. *J. of Petrol.*, **30**, 947-986.
- Lin, P.N., Stern, R.J., Morris, J., and Bloomer, S.H., 1990, Nd- and Sr-isotopic compositions of lavas from the northern Mariana and southern Volcano arcs: implications for the origin of island arc melts. *Contrib. Mineral. Petrol.*, **105**, 381-392.
- Linthout, K., Helmers, H., Sopaheluwakan, J., and Surya Nila, E., 1989, Metamorphic Complexes in Buru and Seram, Northern Banda Arc. *Neth. J. Sea Res.*, **24**, 345-356.
- Margaritz, M., Whitford, D.J., and James, D.E., 1978, Oxygen isotopes and the origin of high-⁸⁷Sr/⁸⁶Sr andesites. *Earth Planet. Sci. Lett.*, **40**, 220-230.
- McCaffrey, R., 1989, Seismological constraints and speculations on Banda Arc tectonics. *Neth. J. Sea Res.*, **24**, 141-152.
- McCaffrey, R., Abers, G.F., 1991, Orogeny in arc-continent collision: The Banda arc and western New Guinea. *Geology*, **19**, 563-566.
- McCulloch, M.T., and Perfit, M.R., 1981, ¹⁴³Nd/¹⁴⁴Nd, ⁸⁷Sr/⁸⁶Sr and trace element constraints on the petrogenesis of Aleutian island arc magmas. *Earth Planet. Sci. Lett.*, **56**, 167-179.
- McCulloch, M.T., Compston, W., Abbott, M., Chivas, A., Foster, J.J., and Nelson, D.R., 1982, Neodymium, strontium, lead and oxygen isotopic and trace element constraints on magma genesis in the Banda island-arc, Wetar. *Research School of Earth Sciences Annual Report 1982*, 236-238.
- McCulloch, M.T., Jaques, A.L., Nelson, D.R., and Lewis, J.D., 1983, Nd and Sr isotopes in kimberlites and lamproites from Western Australia: An enriched mantle origin. *Nature*, **302**, 400-403.
- McCulloch, M.T., 1986, Sm-Nd constraints on the evolution of Precambrian crust in the Australian continent. In: Proterozoic Lithospheric Evolution (ed. A. Kroner), *Amer. Geophys. Union Geodynamics Ser.*, Vol. **17**.
- McCulloch, M.T., and Gamble, J.A., 1991, Geochemical and geodynamical constraints on subduction zone magmatism. *Earth Planet. Sci. Lett.*, **102**, 358-374.

- McKenzie, D., 1985, ^{230}Th - ^{238}U disequilibrium and the melting processes beneath ridge axes. *Earth Planet. Sci. Lett.*, **72**, 149-157.
- McKenzie, D., and O'Nions, R.K., 1991, Partial Melt Distributions from Inversion of Rare Earth Element Concentrations. *J. Petrology*, **32**, 1021-1091.
- McLennan, S.M, and Taylor, S.R., 1980, Rare earth elements in sedimentary rocks, granites and Uranium deposits of the Pine Creek geosyncline. *Proceedings of the International Uranium Symposium on the Pine Creek Geosyncline*, 175-190.
- McLennan, S.M, Nance W.B., and Taylor, S.R., 1980, Rare Earth Element - Thorium correlations in sedimentary rocks, and the composition of the continental crust. *Geochim. Cosmochim Acta*, **44**, 1833-1839.
- McLennan, S.M, and Taylor, S.R., 1981, Role of subducted sediments in island-arc magmatism: constraints from REE patterns. *Earth Planet. Sci. Lett.*, **54**, 423-430.
- McLennan, S.M., 1988, Recycling of the Continental crust. *Pure and Applied Geoph.*, **128**, 683-724.
- McLennan S.M., 1989, REE in sedimentary rocks: influence of provenance and sedimentary processes. *Rev. Mineral.*, **21**, 170-199.
- McLennan, S.M., Taylor, S.R., McCulloch, M.T., and Maynard, J.B., 1990, Geochemical and Nd-Sr isotopic compositions of deep-sea turbidites: Crustal evolution and plate tectonic associations. *Geochim. Cosmochim. Acta*, **54**, 2015-2050.
- Meijer, A., 1976, Pb and Sr isotopic data bearing on the origin of volcanic rocks from the Mariana island-arc system. *Geol. Soc. Am. Bull.*, **87**, 1358-1369.
- Michard, A., Montigny, R., and Schlich, R., 1986, Geochemistry of the Mantle beneath the Rodriguez Triple Junction and the South-East Indian Ridge. *Earth Planet. Sci. Lett.*, **78**, 104-114.
- Miller R.G., O'Nions R.K., Hamilton, P.J., and Welin, E., 1986, Crustal residence ages of clastic sediments, orogeny and continental evolution. *Chem. Geol.*, **57**, 87-89.
- Minster, J.B., and Jordan, T.H., 1978, Present-day plate motions. *J. Geophys. Res.*, **83**, 5331-5354.
- Molengraaff, G.A.F., 1916, De vulkaan Woerlali op het Eiland Dammer. *Jaarb. Mijnw. Ned. Oost-Indie, Verh.* **I**, **45**, 3-10.
- Moorbath, S., 1978, Age and isotope evidence for the evolution of the continental crust. *Phil. Trans. R. Soc. Lond.*, **A288**, 401-433.
- Morris, J.D., and Hart, S.R., 1980, Lead isotope geochemistry of the Banda arc [abs.]. *EOS Trans. AGU*, **61**, 1157.

- Morris, J.D., Jezek, P.A., Hart, S.R., and Gill, J.B., 1983, The Halmahera island arc, Molucca Sea collision zone, Indonesia: a geochemical survey. In: *The Tectonic and Geologic Evolution of Southeast Asian Seas and Islands, Part 2* (ed. D.E. Hayes), *Am. Geophys. Union, Geophys. Monogr. Ser.*, **27**, 373-387.
- Morris, J.D., and Hart, S.R., 1983, Isotopic and incompatible element constraints on the genesis of island arc volcanics from Cold Bay and Amak Island, Aleutians, and implications for mantle structure. *Geochim. Cosmochim. Acta*, **47**, 2015-2030.
- Morris, J.D., Gill, J.B., Schwartz, D., and Silver, E.A., 1984, Late Miocene to Recent Banda Sea volcanism, III: Isotopic compositions [abstr.]. *EOS Trans. AGU*, **65**, 1135.
- Morris, J.D., 1984, Enriched geochemical signatures in Aleutian and Indonesian arc lavas: an isotopic and trace element investigation. *Ph.D. thesis, Mass. Inst. Technol., Cambridge*, 320 pp.
- Mukasa, S.B., McCabe, R., and Gill, J.B., 1987, Pb-isotopic compositions of volcanic rocks in the West and East Philippine island arcs: presence of the Dupal isotopic anomaly. *Earth Planet. Sci. Lett.*, **84**, 153-164.
- Murray, R.W., Buchholtz ten Brink, M.R., Gerlach, D.C., Russ III, G.P., and Jones, D.L., 1991, Rare earth, major, and trace elements in chert from the Franciscan Complex and Monterey Group, California: Assessing REE sources to fine-grained marine sediments. *Geochim. Cosmochim. Acta*, **55**, 1875-1895.
- Nakamura, N., 1974, Determination of REE, Ba, Fe, Mg, Na, and K. in carbonaceous and ordinary chondrites. *Geochim. Cosmochim. Acta*, **38**, 757-775.
- Neeb, G.A., 1943, The Snellius Expedition V. *Geological Results*; 3: The Composition and Distribution of the Samples. Brill, Leiden, pp. 55-265.
- Nelson, D., McCulloch, M.T., and Sun, S.S., 1986, The origins of ultrapotassic rocks as inferred from Sr, Nd and Pb isotopes. *Geochim. Cosmochim. Acta*, **50**, 231-245.
- Nicholls, I.A., Whitford, D.J., Harris, K.L., Taylor, S.R., 1980b, Variation in the geochemistry of mantle sources for tholeiitic and calc-alkaline mafic magmas, western Sunda volcanic arc, Indonesia, *Chem. Geol.*, **30**, 177-199.
- Ninkovich, D., 1979, Distribution, age and chemical composition of tephra layers in deep-sea sediments off western Indonesia. *J. Volc. Geotherm. Res.*, **5**, 67-86.
- Nishimura, S., Suparka, S., 1990, Tectonics of Eastern Indonesia. *Tectonophysics*, **181**, 257-266.
- Ormerod, N.W., Rogers, N.W., and Hawkesford, C.J., Melting in the lithospheric mantle: Inverse modelling of alkali-olivine basalts from the Big Pine Volcanic Field, California. *Contrib. Mineral. Petrol.*, **108**, 305-317.
- Palacz, Z.E., and Saunders, A.D., 1986, Coupled trace element and isotope enrichment in the Cook-Austral-Samoa islands. *Earth Planet. Sci. Lett.*, **79**, 270-280.

- Patchet, P.J., White, W.M., Feldmann, H., Kielinczuk, S., and Hofmann, A.W., 1984, Hafnium/rare earth element fractionation in the sedimentary system and crustal recycling into the Earth's mantle. *Earth Planet. Sci. Lett.*, **69**, 365-378.
- Philpotts, J.A., and Schnetzler, C.C., 1970, Phenocryst-matrix partition co-efficients for K, Rb, Sr and, Ba, with applications to anorthosite and basalt genesis. *Geochim. Cosmochim. Acta*, **36**, 1131-1166.
- Pigram, C.J., and Panggabean, H., 1984, Rifting of the northern margin of the Australian continent and the origin of some microcontinents in eastern Indonesia. *Tectonophysics*, **107**, 331-353.
- Plank, T. and Ludden, J., 1992, Geochemistry of sediments in the Argo abyssal plain at site 765: A continental margin reference section for sediment recycling in subduction zones. In: *Proceedings of the Ocean Drilling Program* (eds. Gradstein, F.M., and J.N. Ludden), *Scientific Results*, Vol. **123**, in press.
- Poorter, R.P.E., Varekamp, J.C., Poreda, R.J., Van Bergen, M.J., and Kreulen., R., Chemical and isotopic compositions of volcanic gases from the east Sunda and Banda arcs, Indonesia. *Geochim. Cosmochim. Acta*, **55**, 3795-3807.
- Poreda, R., and Craig, H., 1989, Helium isotope ratios in circum-Pacific volcanic arcs. *Nature*, **338**, 473-478.
- Potts, P.J., 1987, A handbook of silicate rock analysis. Blackie, Glasgow and London, 622 pp.
- Powell, D.E., and Mills, S.J., 1978, Geological evolution and hydrocarbon prospects of contrasting continental margin types, southwest Australia. In: *Regional conference on Geology and Mineral Resources of SE Asia, Proceedings, Jakarta, Indonesia* (eds. S. Wiryosujono and A. Sudradjat), *Association of Indonesian Geologists*, pp. 77-100.
- Price, R.C., Kennedy, A.K., Riggs-Sneeringer, M., and Frey, F.A., 1986, Geochemistry of basalts from the Indian Ocean triple junction: Implications for the generation and evolution of Indian Ocean ridge basalts. *Earth Planet. Sci. Lett.*, **78**, 379-396.
- Priem, H.N.A., Andriessen, P.A.M., Boelrijk, N.A.I.M., Hebeda, E.H.C.S., Hutchinson, Verdurme, F.A., and Verschure, R.H., 1978, Isotopic evidence for a Middle to Late Pliocene Age of the Cordierite Granite on Ambon, Indonesia. *Geologie en Mijnbouw*, **57**, 441-443.
- Purdy, G.M., Detrick, R.S. and Shor, G.G. Jr., 1977, Crustal structure of the Banda Sea and Weber Deep [abs.]. *EOS Trans. AGU*, **58**, 509.
- Reagan, M.K., and Gill, J.B., 1989, Coexisting calcalkaline and high-niobium basalts from Turrialba volcano, Costa Rica: Implications for residual titanates in arc magma sources. *J. Geophys. Res.*, **94**, 4619-4633.

- Ritsema, A.R., Sudarmo, R.P., and Putu Pudja, I., 1989, The generation of the Banda Arc on the basis of its seismicity. *Neth. J. Sea Res.*, **24**, 165-172.
- Robinson, P.T., and Whitford, D.J., 1974, Basalts from the Eastern Indian Ocean, DSDP Leg 27, In: *Initial Reports of the Deep Sea Drilling Project*, (Eds. J.J. Veevers, J.R. Heirtzler et al.), **27**, U.S. Government Printing Office, Washington, p. 551-560.
- Ryerson, F.J., and Watson, E.B., 1987, Rutile saturation in magmas: implications for Ti-Nb-Ta depletion in island-arc basalts. *Earth Planet. Sci. Lett.*, **86**, 225-239.
- Schnetzler, C.C., and Philpotts, J.A., 1970, Partition coefficients of rare-earth elements between igneous matrix-material and rock-forming mineral phenocrysts-II. *Geochim. Cosmochim. Acta*, **34**, 331-340.
- Schwartz, D., Gill, J.B., and Duncan, R.A., 1984, Late Miocene to Recent Banda Sea-volcanism, II: Petrology [abs.]. *EOS Trans. AGU*, **65**, 1135.
- Sekine, T., and Wyllie, P.J., 1982, The System Granite-Peridotite-H₂O at 30 kbar, with Applications to Hybridization in Subduction Zone Magmatism. *Contrib. Mineral. Petrol.*, **81**, 190-202.
- Sholkovitz, E.R., 1988, REE in sediments of the north Atlantic Ocean, Amazon delta and east China Sea: Reinterpretation of terrigenous input patterns to the oceans. *Amer. J. Sci.*, **288**, 236-281.
- Sholkovitz E.R., 1990, Rare-earth elements in marine sediments and geochemical standards. *Chem. Geol.*, **88**, 333-347.
- Shor, G.G. Jr. and Jacobson, R.S., 1977, Structure beneath the Timor-Tanimbar-Aru Trough system [abs.]. *EOS Trans. AGU*, **58**, 509.
- Sigurdsson, H., Sparks, R.S.J., Carey, S.N., and Huang, T.C., 1980, Volcanogenic sedimentation in the lesser Antilles Arc. *J. Geol.*, **88**, 523-540.
- Silver, E.A., Reed, D., McCaffrey, R., and Joyodiwiryo, Y., 1983, Back arc thrusting in the eastern Sunda arc, Indonesia: A consequence of arc continent collision. *J. Geophys. Res.*, **88**, 7429-7448.
- Silver, E.A., Gill, J.B., Schwartz, D., Prasetyo, H., and Duncan, R.A., 1985, Evidence for a submerged and displaced continental borderland, north Banda Sea, Indonesia. *Geology*, **13**, 687- 691.
- Simkin, T., Siebert, L., McClelland, L., Bridge, D., Newhall, C., and Latter, J.H., 1981, *Volcanoes of the World*. Smithsonian Institution, Washington D.C., pp. 1-232.
- Situmorang, M., 1992, Sedimentology and marine geology of the Banda Arc, Eastern Indonesia, *PhD thesis University of Utrecht, Geol. Ultraiectina*, no **84**. pp 191.
- Smedley, P.L., 1988, The geochemistry of Dinantian volcanism in south Kintyre and the evidence for Provincialism in the southern Scottish mantle. *Contrib. Mineral. Petrol.*, **99**, 374-384.

- Stern, C.R., and Wyllie, P.J., 1973a, Water-saturated and undersaturated melting relations of a granite to 35 kilobars. *Earth Planet. Sci. Lett.*, **18**, 163-167.
- Stern, C.R., and Wyllie, P.J., 1973b, Melting Relations of Basalt-Andesite-Rhyolite-H₂O and a pelagic red clay at 30 kb. *Contr. Mineral. Petrol.*, **42**, 313-323.
- Stolz, A.J., Varne, R., Wheller, G.E., Foden, J.D., and Abbott, M.J., 1988, The geochemistry and petrogenesis of K-rich alkaline volcanics from the Batu Tara volcano, eastern Sunda arc. *Contrib. Mineral. Petrol.*, **98**, 374-389.
- Stolz, A.J., Varne, R., Davies, G.R., Wheller, G.E., and Foden, J.D., 1990, Magma source components in an arc-continent collision zone: the Flores-Lembata sector, Sunda Arc, Indonesia. *Contrib. Mineral. Petrol.*, **105**, 585-601.
- Storey, M., Saunders, A.D., Tarney, J., Leat, P., Thirlwall, M.F., Thompson, R.N., Menzies, M.A., and Marriner, G.F., 1988, Geochemical evidence for plume-mantle interactions beneath Kerguelen and Heard Islands, Indian Ocean. *Nature*, **336**, 371-374.
- Sun, S.S., 1980, Lead isotopic study of young volcanic rocks from mid-ocean ridges, ocean islands and island arcs. *Phil. Trans. R. Soc. London*, **A297**, 409-445.
- Sun, S.S., and McDonough, W.F., 1989, Chemical and isotopic systematics of oceanic basalts: implications for mantle composition and processes, In: *Magmatism in the Oceanic Basins*, (eds. A.D. Saunders and M.J. Norry). *Geol. Soc. Spec. Publ.*, **42**, 313-145.
- Tatsumi, Y., Hamilton, D.L., and Nesbitt, R.W., 1986, Chemical characteristics of fluid phase released from a subducted lithosphere and origin of arc magmas: evidence from high-pressure experiments and natural rocks. *J. Volcanol. Geotherm. Res.*, **29**, 293-309.
- Tatsumi, Y., 1989, Migration of fluid phases and genesis of basalt magmas in subduction zones. *J. Geophys. Res.*, **94**, 4697-4707.
- Tatsumi, Y., Murasaki, M., Arsadi, E.M., and Nohda, S., 1991, Geochemistry of quaternary lavas from N.E. Sulawesi: transfer of subduction components into the mantle wedge. *Contrib. Mineral. Petrol.*, **107**, 137-149.
- Tatsumoto, M., and Knight, R.J., 1969, Isotopic composition of lead in volcanic rocks from central Honshu - with regard to basalt genesis. *Geochem. J.*, **3**, 53-86.
- Taylor, S.R., and McLennan, S.M., 1985, The continental crust: its composition and evolution, 312 pp., Blackwell, Oxford.
- Terra, F., Brown, L., Morris, J., Sacks, I.S., Klein, J., and Middleton, R., 1986, Sediment incorporation in island-arc magmas: inferences from ¹⁰Be. *Geochim. Cosmochim. Acta*, **50**, 535-550.
- Uyeda, S., 1983, Comparative subductology, *Episodes*, **2**, 19-24.

- Valbracht, P.J., 1991, The Origin of the continental crust of the Baltic shield, as seen through Nd and Sr isotopic variations in 1.89-1.85 Ga old rocks from Western Bergslagen, Sweden. *PhD thesis, GUA papers of geology, Series 1*, No. 29, pp. 222.
- Van Bemmelen, R.W., 1949, The geology of Indonesia, Volume 1A, Government Printing Office, The Hague, 732 pp.
- Van Bergen, M.J., Erfan, R.D. Sriwana, T. Suharyono, K., Poorter, R.P.E. Varekamp, J.C., Vroon, P.Z., and Wirakusumah, A.D., 1989, Spatial geochemical variations of arc volcanism around the Banda Sea. *Neth. J. Sea Res.*, 24, 313-322.
- Van Bergen, M.J., Vroon, P.Z., and Elburg, M.A., 1990, Petrological and geochemical evidence for open-system evolution of magmas in the Banda Arc, East Indonesia. *Geological Society of Australia Abstracts*, 27, 104.
- Van Bergen, M.J., Vroon, P.Z., Varekamp J.C., and Poorter, R.P.E., 1992, The Origin of the Potassic rock suite from Batu Tara volcano (East Sunda Arc, Indonesia), *Lithos* (in press).
- Varekamp, J.C., van Bergen, M.J., Vroon, P.Z., Poorter, R.P.E., Wirakusumah, A.D., Erfan, R., Suharyono, K., and Sriwana, T., 1989, Volcanism and tectonics in the Eastern Sunda Arc, Indonesia. *Neth. J. Sea Res.*, 24, 303-312.
- Varne, R., 1985, Ancient subcontinental mantle: a source for K- rich orogenic volcanics. *Geology*, 13, 405-408.
- Varne, R., and Foden, J.D., 1986, Geochemical and isotopic systematics of Eastern Sunda Arc volcanics: implications for mantle sources and mantle mixing processes. In: *The Origin of Arcs* (ed. F.C. Wezel), Elsevier, Amsterdam, pp. 159-189.
- Veevers, J.J., Heirtzler, J.R., et al., 1974, Site 262, In: *Initial reports on the Deep Sea Drilling Project* (eds. J.J. Veevers, J.R. Heirtzler, et al.), Vol. 27, Washington, U.S. Government Printing Office, pp. 193-278.
- Veevers, J.J., 1984, Phanerozoic earth history of Australia. Oxford University Press, Oxford, 418 pp.
- Veizer, J., and Jansen, S. L., 1985, Basement and sedimentary recycling-2: Time dimension to global tectonics. *J. Geology*, 93, 625-643.
- Verbeek, R.D.M., 1900, Geologische beschrijvingen van de Banda Eilanden. *Jaarb. Mijnw. Ned. Oost-Indie*, 29, 1-29.
- Verbeek, R.D.M., 1905, Geologische beschrijving van Ambon. *Jaarb. Mijnw. Ned. Oost-Indie*, 34, 1-308.
- Verbeek, R.D.M., 1908, Molukkenverslag. *Jaarb. Mijnw. Ned. Oost-Indie*, Wetensch. Gedeelte, 37, 1-826.

- Von Drach, V., Marsh, B.D., and Wasserburg, G.J., 1986, Nd and Sr isotopes in the Aleutians: Multicomponent parenthood of island-arc magmas. *Contrib. Mineral. Petrol.*, **92**, 13-34.
- Vroon, P.Z., Van Bergen, M.J., Poorter, R.P.E., and Varekamp, J.C., 1989, Fluorine geochemistry of tholeiitic to potassic-alkaline arc volcanics from the Banda Sea region, Eastern Indonesia. [abs.], *New Mexico Bureau of Mines and mineral resources*, Bulletin **131**, p. 283.
- Vroon, P.Z., van Bergen, M.J., Varekamp, J.C., and Poorter, R.P.E., 1990a, Across-arc Sr, Nd, Pb-isotopic signatures of active volcanism at the collision between the Australian continent and the Sunda-Banda Arc, East-Indonesia. *Abstract volume IAVCEI meeting Mainz 3-8 sept 1990*.
- Vroon, P.Z., van Bergen, M.J., White, W.M., 1990b, Source contamination versus high-level assimilation in the Banda Arc volcanics: Sr, Nd and Pb isotopic evidence. *Geological Society of Australia Abstracts*, **27**, 107.
- Warner, R.F., 1977, Hydrology. In: *Australia: A geography* (ed. D.N. Jeans), pp. 134-151. Sydney University Press.
- Weaver, B.L., 1991, The origin of ocean island basalt end-member compositions: trace-element and isotopic constraints. *Earth Planet. Sci. Lett.*, **104**, 381-397.
- Wheller, G.E., R. Varne, J.D. Foden, and M.J. Abbott, 1987, Geochemistry of Quaternary volcanism in the Sunda-Banda arc, Indonesia, and three-component genesis of island-arc basaltic magmas. *J. Volcanol. Geotherm. Res.*, **32**, 137-160.
- White, W.M., and Patchett, J., 1984, Hf-Nd-Sr isotopes and incompatible element abundances in island arc: Implications for magma origins and crust mantle evolution. *Earth Planet. Sci. Lett.*, **67**, 167-185.
- White, W.M., 1985, Sources of oceanic basalts: Radiogenic isotopic evidence. *Geology*, **13**, 115-118.
- White, W.M., Dupre, B., and Vidal, P., 1985, Isotope and trace element geochemistry of sediments from the Barbados Ridge - Demerara Plain region, Atlantic Ocean. *Geochim. Cosmochim. Acta*, **49**, 1875-1886.
- White, W.M., and Dupre, B., 1986, Sediment subduction and magma genesis in the Lesser Antilles: Isotopic and trace element constraints. *J. Geoph. Res.*, **91**, 5927-5941.
- Whitford, D.J., 1975a, Strontium isotopic studies of the volcanic rocks of the Sunda arc, Indonesia, and their implications. *Geochim. Cosmochim. Acta*, **39**, 1287-1302.
- Whitford, D.J., 1975b, Geochemistry and petrology of volcanic rocks from the Sunda arc, Indonesia. *Unpubl Ph.D. thesis, Australian National University*.

- Whitford, D.J., Compston, W., Nicholls, I.A., and Abbott, M.J., 1977, Geochemistry of late Cenozoic lavas from eastern Indonesia: Role of subducted sediments in petrogenesis. *Geology*, **5**, 571-575.
- Whitford, D.J., and Jezek, P., 1979, Origin of the late Cenozoic lavas from the Banda arc, Indonesia: Trace element and Sr isotope evidence. *Contrib. Mineral. Petrol.*, **68**, 141-150.
- Whitford, D.J., Nicholls, I.A., and Taylor, S.R., 1979, Spatial Variations in the Geochemistry of Quaternary Lavas Across the Sunda Arc in Java and Bali. *Contrib. Mineral. Petrol.*, **70**, 341-356.
- Whitford, D.J., White, W.M., and Jezek, P.A., 1981, Neodymium isotopic composition of Quaternary island arc lavas from Indonesia. *Geochim. Cosmochim. Acta*, **45**, 989-995.
- Williams, R.W., and Gill, J.B., 1989, Effects of partial melting on the uranium decay series. *Geochim. Cosmochim. Acta*, **53**, 1607-1619.
- Woodhead, J.D., 1989, Geochemistry of the Mariana arc (western Pacific): Source composition and processes. *Chem. Geology*, **76**, 1-24.
- Woodhead, J.D., and Fraser, D.G., 1985, Pb, Sr and ¹⁰Be isotopic studies of volcanic rocks from the Northern Mariana islands - Implications for magmagenesis and crustal recycling in the Western Pacific. *Geochim. Cosmochim. Acta*, **49**, 1925-1930.
- Woodhead, J.D., Harmon, R.S., and Fraser, D.G., 1987, O, S, Sr and Pb isotope variations in volcanic rocks from the Northern Mariana Islands. *Earth Planet. Sci. Lett.*, **83**, 39-52.
- Zindler, A. and Hart, S., 1986, Chemical Geodynamics. *Ann. Rev. Earth Planet. Sci.*, **14**, 493-571.

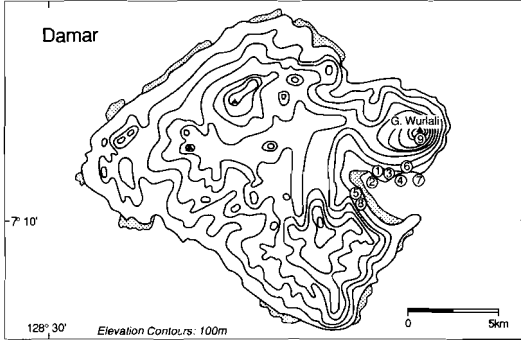
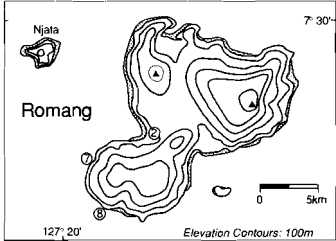
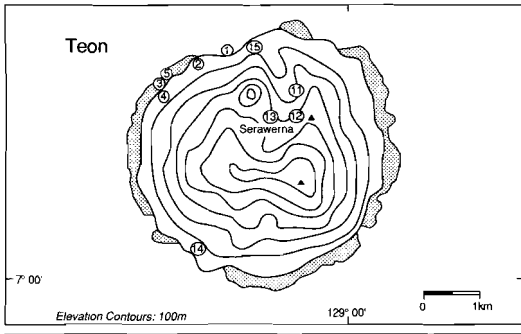
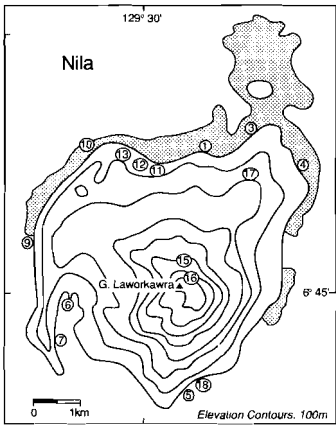
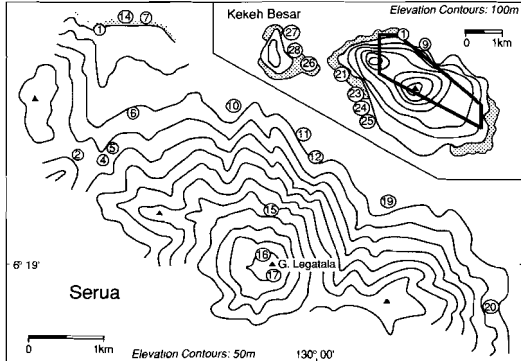
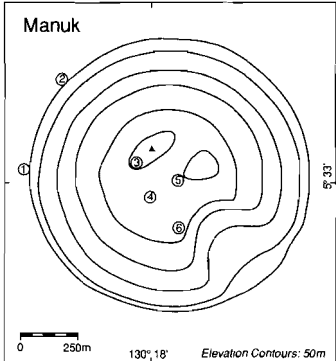
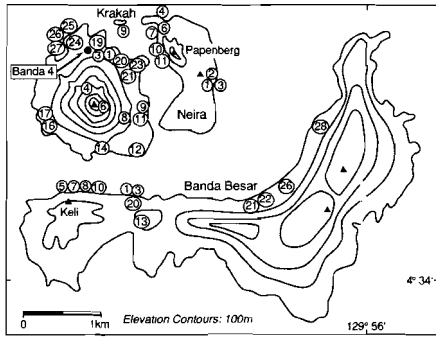
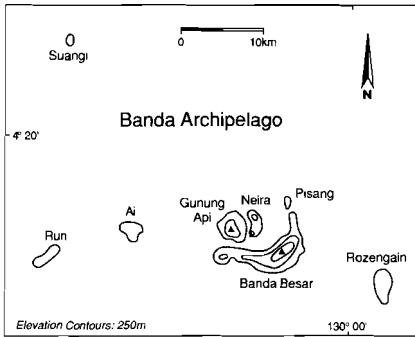
APPENDICES

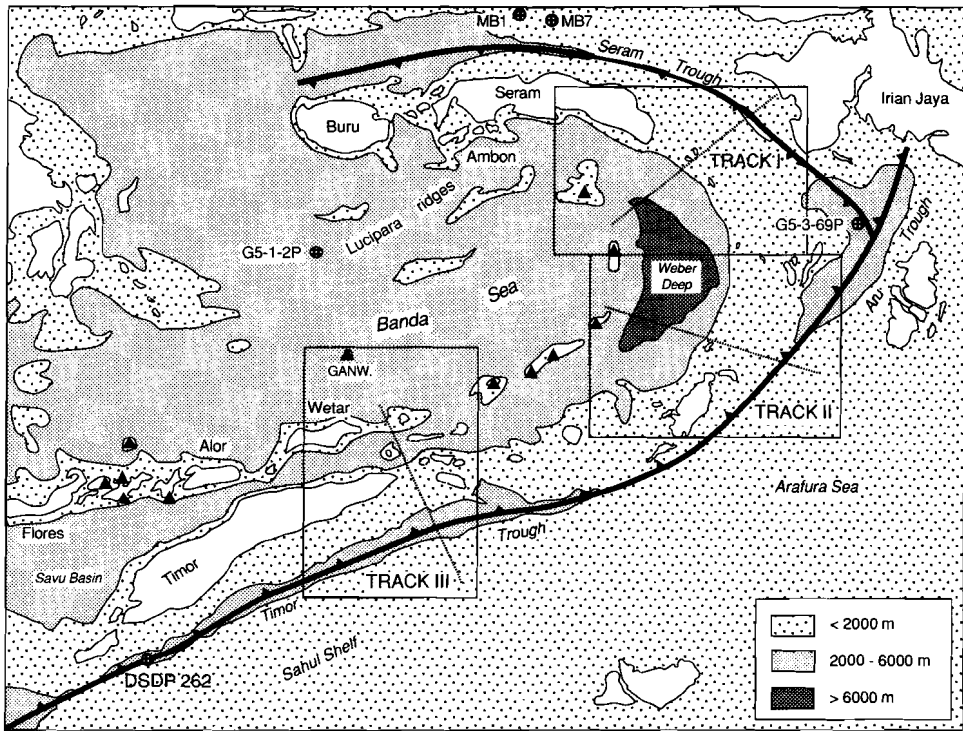
Appendix 1. Sample locations	131
1.1. Sample locations of the Banda Arc volcanics	132
1.2. Box-, Piston- and DSDP Site 262 core locations	
1.2a. Overview map	134
1.2b. Track I samples	135
1.2c. Track II samples	136
1.2d. Track III samples	137
1.2e. Lithology of DSDP Site 262 hole	138
Appendix 2. Sample descriptions	139
2.1. Description of Banda Arc volcanics	140
2.2. Description of Box-, Piston- and DSDP Site 262 cores	145
Appendix 3. Analytical techniques	149
3.1. Sample preparation	151
3.1.1. Volcanic rocks	151
3.1.2. Sediment cores	151
3.2. Carbonate and organic carbon determination in sediments	152
3.3. XRF	154
3.4. INAA	156
3.5. ICP-MS	158
3.5.1. Sample dissolution procedures for ICP-MS	158
3.5.2. REE and Cs determination by standard addition	158
3.5.3. Th, U and Pb determination by isotope dilution	161

3.6. Sr, Nd and Pb isotope ratios and Sm, Nd, Th and U isotope dilutions determinations	163
3.6.1. Sr and Nd isotopic composition determination of volcanic rocks	163
3.6.2. Sr and Nd isotopic composition determination of sediments	165
3.6.3. Pb isotopic composition determination of volcanic rocks	165
3.6.4. Pb isotopic composition determination of sedimentary rocks	165
3.6.5. Pb, U and Th isotope-dilution determination	166
Appendix 4. Major- and trace-element data of the Banda Arc volcanics	167
Appendix 5. Trace-element data of East Indonesian Sediments	181
Appendix 6. Sr-, Nd- and Pb-isotopes and parent-daughter elements of the Banda Arc volcanics	195
Appendix 7. Sr-, Nd- and Pb-isotopes and trace-elements of East Indonesian Sediments	201

APPENDIX 1

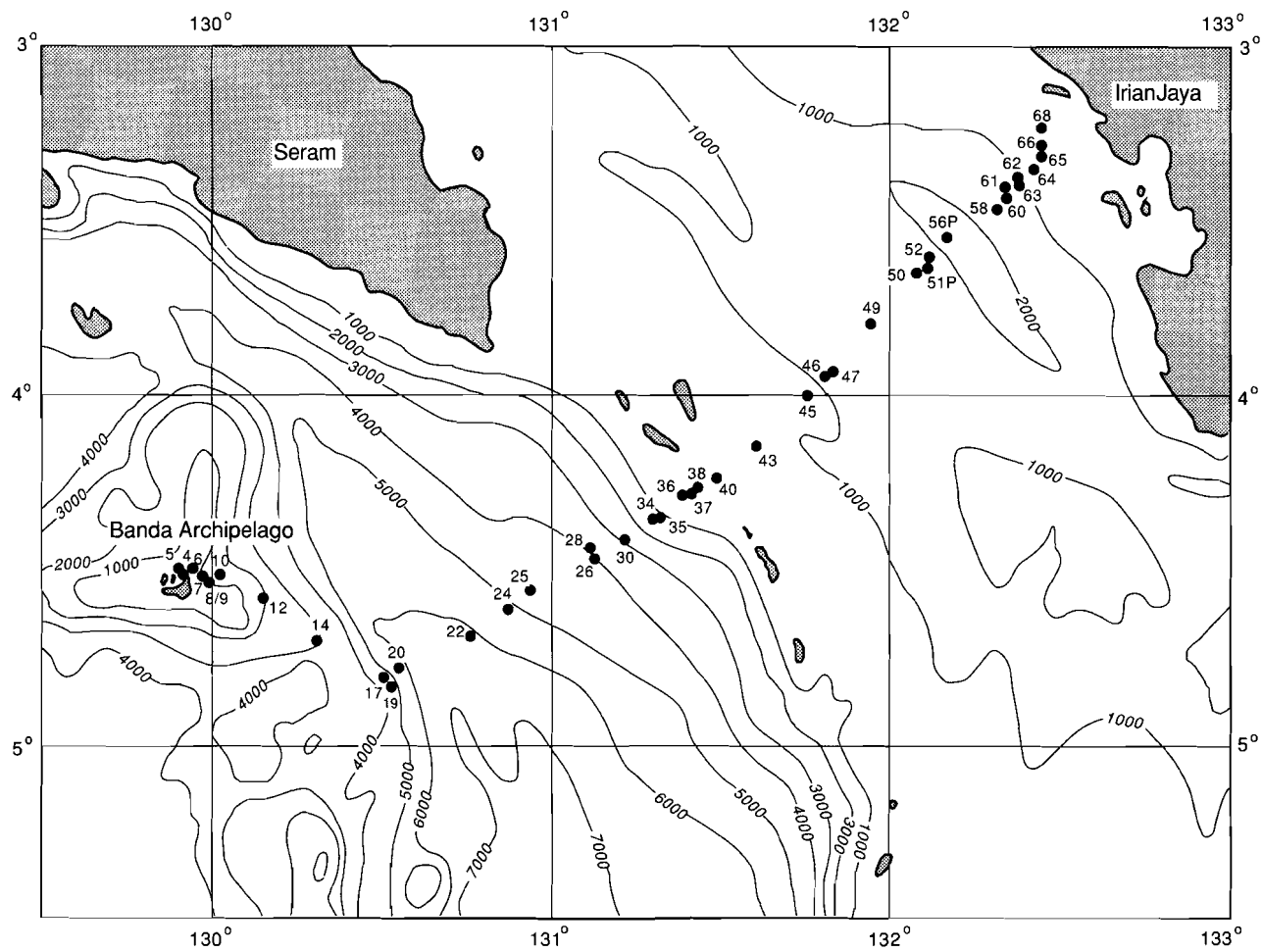
SAMPLE LOCATIONS

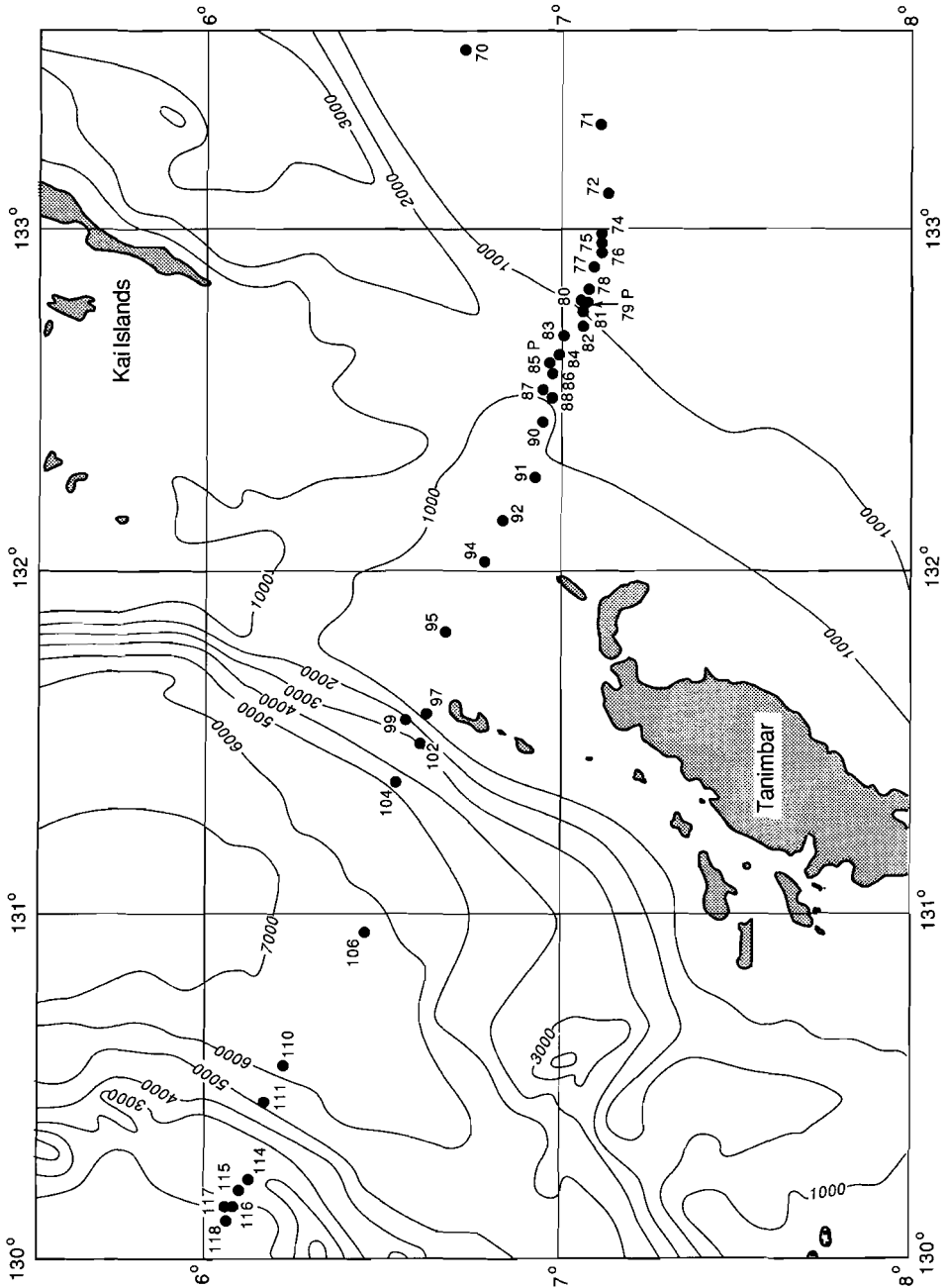




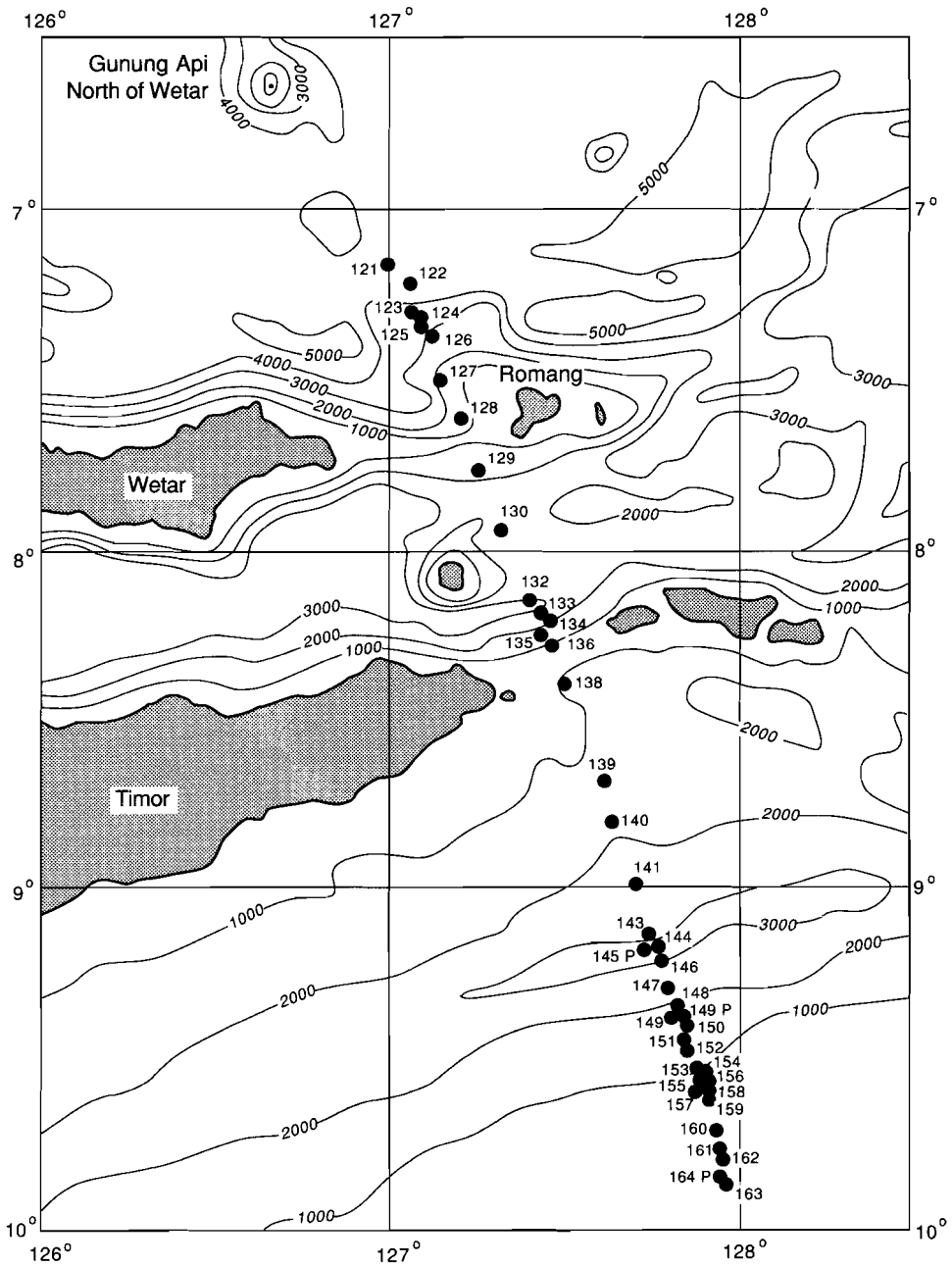
Appendix 1.2a. Overview with the locations of Tracks I, II, III, DSDP Site 262 and the locations of the cores G5-1-2P, MB1, MB7 and G5-3-69P.

Appendix 1.2b. Track I box- and piston-core locations (code G5-2).

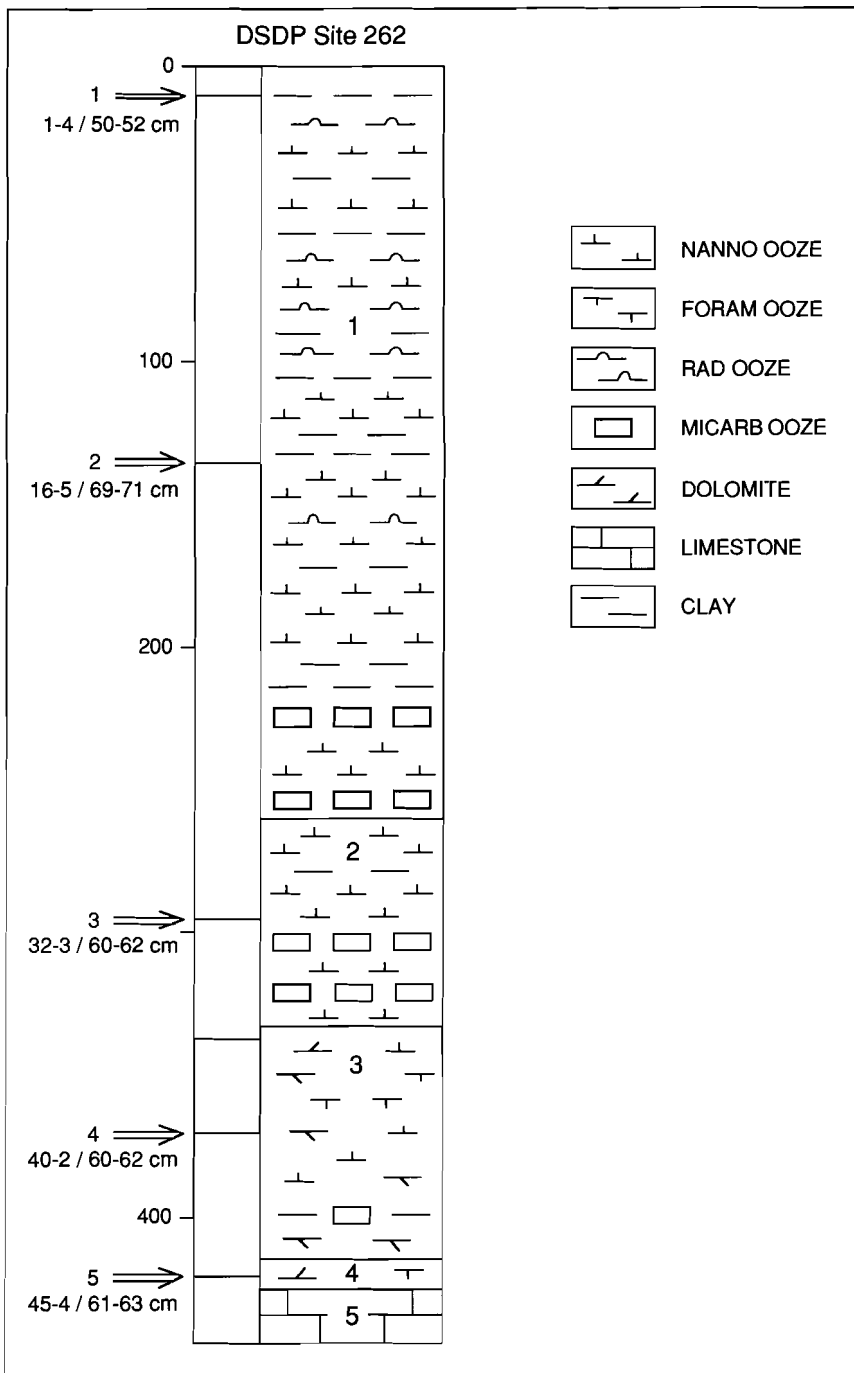




Appendix 1.2c. Track II box- and piston-core locations (code G5-4).



Appendix 1.2d. Track III box- and piston-core locations (code G5-6).



Appendix 1.2e. DSDP Site 262 Lithology and sample positions (Figure after Verweers et al., 1974).

APPENDIX 2

SAMPLE DESCRIPTIONS

Appendix 2.1. Petrographic description of the Banda Arc volcanics

Sample	Type	Name	OL	CPX	OPX	PLAG	HBL	BI	OX	AP	Remarks
BA 1A1	Lava	Dacite		●	●	●			●		porphyritic to glomeroporphyritic texture
BA 3A	Lava	Dacite		●	●	●			●		porphyritic to glomeroporphyritic texture
BA 4A	Lava	Dacite		●	●	●			●		porphyritic texture
BA Banda-4	Lava	Andesite	●	●	●	●			●		porphyritic to glomeroporphyritic texture
BA 6A	Lava	Dacite		●	●	●			●		porphyritic to glomeroporphyritic texture
BA 8A1	Lava	Dacite		●	●	●			●		porphyritic texture
BA 9A1	Lava	Dacite		●	●	●			●		porphyritic texture
BA 9B	Lava	Dacite		●	●	●			●		porphyritic texture
BA 11A2	Lava	Andesite	●	●	●	●			●		glomeroporphyritic texture
BA 12A	Lava	Dacite		●	●	●			●		porphyritic glomeroporphyritic texture
BA 14A2	Lava	Dacite		●	●	●			●		porphyritic to glomeroporphyritic texture
BA 16	Lava	Dacite			●	●			●		porphyritic texture
BA 17	Lava	Dacite									no thin section available
BA 19	Lava	Dacite		●	●	●			●		porphyritic to glomeroporphyritic texture
BA 20A	Lava	Dacite	●	●	●	●			●		porphyritic to glomeroporphyritic texture
BA 21A	Lava	Dacite		●	●	●			●		porphyritic to glomeroporphyritic texture
BA 23	Lava	Dacite		●	●	●			●		porphyritic to glomeroporphyritic texture
BA 24A	Lava	Dacite									no thin section available
BA 25A	Lava	Dacite	●	●	●	●			●		porphyritic to glomeroporphyritic texture
BA 26	Lava	Dacite		●	●	●			●		porphyritic to glomeroporphyritic texture
BA 27A	Lava	Dacite		●	●	●			●		porphyritic texture
BB 21A3	Lava	Basaltic-andesite	●	●		●					glomeroporphyritic texture
BB 22	Lava	Basaltic-andesite		●		●			●		porphyritic to glomeroporphyritic texture
BB 26	Lava	Basaltic-andesite	●			●					porphyritic texture
BB 28	Lava	Basaltic-andesite		●	●	●			●		porphyritic to glomeroporphyritic texture
BL 1B	Lava	Rhyodacite		●	●	●			●		porphyritic textures
BL 3	Lava	Andesite		●	●	●			●		porphyritic to glomeroporphyritic texture
BL 5	Pumice	Rhyodacite									no thin section available
BL 7A1	Lava	Basaltic-andesite		●	●	●			●		porphyritic texture
BL 8	Pumice	Andesite		●	●	●			●		no thin section available
BL 10	Lava	Basalt		●	●	●			●		cumulate
BL 13	Pumice	Basaltic-andesite									no thin section available

Appendix 2.1. Petrographic description of the Banda Arc volcanics

Sample	Type	Name	OL	CPX	OPX	PLAG	HBL	BI	OX	AP	Remarks
BN 1A2	Lava	Dacite		●	●	●			●		porphyritic to glomeroporphyritic texture
BN 1C4	Lava	Dacite		●	●	●			●		porphyritic to glomeroporphyritic texture
BN 2A1	Lava	Dacite		●	●	●			●		glomeroporphyritic texture
BN 3A2	Lava	Basalt		●	●	●					glomeroporphyritic texture
BN 4A1	Lava	Basaltic-andesite	●	●	●	●			●		glomeroporphyritic texture
BN 6A1	Lava	Andesite, dark part		●	●	●			●		porphyritic to glomeroporphyritic texture
BN 6A11	Lava	Andesite, light part									no thin section available
BN 7A	Lava	Andesite		●	●	●			●		porphyritic to glomeroporphyritic texture
BN 9A	Lava	Basaltic-andesite	?	●		●			●		glomeroporphyritic texture
BN 10A1	Lava	Andesite		●	●	●			●		porphyritic texture, pig in groundmass
BN 11D	Lava	Basalt	●	●		●			●		glomeroporphyritic texture
MA 1A	Lava	Andesite	●	●		●			●		glomeroporphyritic texture
MA 1B	Lava	Andesite	●	●		●			●		glomeroporphyritic texture
MA 2A	Lava	Basaltic-andesite	●	●	●	●			●		porphyritic texture
MA 2B	Lava	Andesite	●	●	●	●			●		porphyritic to glomeroporphyritic texture
MA 2C	Lava	Andesite	●	●	●	●			●		glomeroporphyritic texture
MA 2D	Lava	Andesite		●	●	●			●		glomeroporphyritic texture
MA 2E	Lava	Andesite	●	●	●	●			●		porphyritic to glomeroporphyritic texture
MA 2F	Lava	Andesite		●	●	●			●		glomeroporphyritic texture, altered
MA 3A2	Lava	Basaltic-andesite	●	●	●	●			●		glomeroporphyritic texture
MA 3B	Lava	Basaltic-andesite	●	●	●	●			●		porphyritic to glomeroporphyritic texture
MA 3C2	Lava	Basaltic-andesite	●	●	●	●			●		glomeroporphyritic texture
MA 3C4	Lava	Basaltic-andesite	●	●	●	●			●		glomeroporphyritic texture
MA 4A1	Lava	Andesite	●	●	●	●			●		glomeroporphyritic texture
MA 4B	Lava	Andesite	●	●	●	●			●		porphyritic texture
MA 5A	Lava	Basaltic-andesite	●	●	●	●			●		glomeroporphyritic texture
MA 5B	Lava	Basaltic-andesite	●	●	●	●			●		glomeroporphyritic texture
MA 6A1	Lava	Andesite	●	●	●	●			●		glomeroporphyritic texture

Appendix 2.1. Petrographic description of the Banda Arc volcanics

Sample	Type	Name	OL	CPX	OPX	PLAG	HBL	BI	OX	AP	Remarks
SE 1A1	Pumice	Andesite									no thin section available
SE 1B	Lava	Andesite									no thin section available
SE 1D	Lava	Andesite		●	●	●			●		glomeroporphyritic texture
SE 2A	Lava	Andesite		●	●	●			●		glomeroporphyritic texture
SE 2B	Lava	Basaltic-andesite		●	●	●			●		glomeroporphyritic texture
SE 4	Lava	Andesite		●	●	●			●		porphyritic texture
SE 5	Lava	Andesite		●	●	●			●		glomeroporphyritic texture
SE 6	Lava	Andesite		●	●	●			●		glomeroporphyritic texture
SE 7AI	Lava	Andesite		●	●	●			●		glomeroporphyritic texture
SE 7AII	Lava	Andesite		●	●	●			●		glomeroporphyritic texture
SE 7B	Lava	Andesite		●	●	●			●		glomeroporphyritic texture
SE 9A3	Lava	Andesite	●	●	●	●			●		glomeroporphyritic texture
SE 10	Lava	Andesite	●	●	●	●			●		glomeroporphyritic texture
SE 11Sc	Pumice	Basaltic-andesite		●	●	●			●		glomeroporphyritic texture
SE 12A3	Lava	Andesite		●	●	●			●		glomeroporphyritic texture
SE 14A1	Pumice	Andesite									no thin section available
SE 14A2	Pumice	Andesite									no thin section available
SE 15B	Lava	Andesite	●	●	●	●			●		glomeroporphyritic texture, some calcite
SE 16B	Lava	Andesite		●	●	●			●		porphyritic texture, altered
SE 17	Lava	Andesite		●	●	●			●		porphyritic to glomeroporphyritic texture
SE 19	Lava	Andesite		●	●	●			●		porphyritic to glomeroporphyritic texture
SE 20	Lava	Andesite		●	●	●			●		porphyritic to glomeroporphyritic texture
SE 21A3	Lava	Andesite		●	●	●			●		porphyritic to glomeroporphyritic texture
SE 23A	Lava	Andesite		●	●	●			●		porphyritic texture
SE 24A	Lava	Andesite		●	●	●			●		porphyritic texture
SE 25A	Lava	Andesite		●	●	●			●		porphyritic texture
SE 26A	Lava	Andesite	●	●	●	●			●		porphyritic texture
SE 27A	Lava	Basaltic-andesite		●	●	●			●		glomeroporphyritic texture
SE 28A	Lava	Andesite		●	●	●			●		glomeroporphyritic texture

Appendix 2.1. Petrographic description of the Banda Arc volcanics

Sample	Type	Name	OL	CPX	OPX	PLAG	HBL	BI	OX	AP	Remarks
NI 1A1	Lava	Andesite		●	●	●			●		glomeroporphyritic texture
NI 3A3	Lava	Andesite	●	●	●	●			●	●	glomeroporphyritic texture
NI 4A2	Lave	Andesite	●	●	●	●			●		glomeroporphyritic texture
NI 5A	Lave	Andesite		●	●	●	●		●		porphyritic texture
NI 5B	Blob	Basaltic-andesite		●	●	●	●		●		porphyritic texture
NI 6	Blob	Basaltic-andesite		●	●	●	●		●		equigranular
NI 7A	Lava	Basaltic-andesite	●	●	●	●	●		●		glomeroporphyritic texture
NI 7B	Lava	Andesite	●	●	●	●			●	●	glomeroporphyritic texture
NI 9A	Lave	Andesite		●	●	●			●		glomeroporphyritic texture
NI 10A1	Lava	Andesite		●	●	●			●		porphyritic texture, two types of incl.
NI 11	Lava	Andesite		●	●	●			●	●	porphyritic texture. bi in clusters
NI 12	Lava	Andesite		●	●	●			●	●	glomeroporphyritic texture
NI 13	Lave	Andesite	●	●	●	●			●		glomeroporphyritic texture
NI 15I	Host	Basaltic-andesite			●	●	●		●	●	porphyritic texture
NI 15II	Blob	Andesite			●	●	●		●		glomeroporphyritic texture
NI 16	Lava	Andesite	●	●	●	●	●		●		glomeroporphyritic texture
NI 17A	Lave	Andesite		●	●	●	●		●		glomeroporphyritic texture
NI 18AI	Blob	Basalt		●	●	●	●		●		porphyritic texture
NI 18AII	Host	Andesite		●	●	●	●		●		glomeroporphyritic texture
TE 1A	Lava	Andesite		●	●	●			●		glomeroporphyritic texture
TE 1B1	Blob	Andesite		●	●	●	●		●		glomeroporphyritic texture
TE 1B2	Blob	Basaltic-andesite		●	●	●	●		●	●	glomeroporphyritic texture
TE 1C	Lava	Andesite		●	●	●	●		●		glomeroporphyritic texture
TE 2A	Lava	Andesite		●	●	●			●		glomeroporphyritic texture
TE 2B1	Blob	Basaltic-andesite		●	●	●	●		●		glomeroporphyritic texture
TE 2B2	Blob	Basaltic-andesite		●	●	●	●		●		glomeroporphyritic texture
TE 3A	Lava	Andesite		●	●	●			●		glomeroporphyritic texture
TE 3C	Lava	Andesite		●	●	●			●		glomeroporphyritic texture
TE 3D	Lava	Andesite		●	●	●			●		glomeroporphyritic texture
TE 4B	Lava	Andesite		●	●	●			●		glomeroporphyritic texture
TE 5	Pumice	Andesite		●	●	●	●		●		glomeroporphyritic texture
TE 11	Lava	Andesite		●	●	●	●		●		glomeroporphyritic texture
TE 12	Lave	Andesite		●	●	●	●		●		glomeroporphyritic texture
TE 14A	Lava	Andesite		●	●	●	●		●	●	glomeroporphyritic texture
TE 14B	Lava	Andesite		●	●	●	●		●		glomeroporphyritic texture
TE 15	Lava	Andesite		●	●	●			●		glomeroporphyritic texture

Appendix 2.1. Petrographic description of the Banda Arc volcanics

Sample	Type	Name	OL	CPX	OPX	PLAG	HBL	BI	OX	AP	Remarks
DA 1	Lava	Andesite		●	●	●		●	●		porphyritic to glomeroporphyritic texture
DA 2	Lava	Andesite		●	●	●	●	●	●		porphyritic to glomeroporphyritic texture
DA 3	Lava	Andesite	●	●	●	●	●	●	●		porphyritic to glomeroporphyritic texture
DA 4	Blob	Basaltic-andesite	●	●	●	●	●	●	●		porphyritic to glomeroporphyritic texture
DA 5	Lava	Andesite		●	●	●	●		●		porphyritic to glomeroporphyritic texture
DA 6	Lava	Andesite		●	●	●	●	●	●		porphyritic to glomeroporphyritic texture
DA 7	Lava	Basaltic-andesite		●	●	●	●		●		porphyritic to glomeroporphyritic texture
DA 8	Lava	Andesite	●	●	●	●	●		●		porphyritic to glomeroporphyritic texture
DA 9A	Lava	Andesite				●					porphyritic to glomeroporphyritic texture
DA 9B	Lava	Andesite		●	●	●	●	●	●		porphyritic to glomeroporphyritic texture
RO 2	Lava	Andesite		●	●	●			●		porphyritic texture
RO 7B	Lava	Andesite		●	●	●			●		porphyritic to glomeroporphyritic texture
RO 7C2	Lava	Andesite		●	●	●			●		porphyritic to glomeroporphyritic texture
RO 8B	Lava	Andesite		●	●	●			●		porphyritic texture
RO 8C6	Lava	Rhyolite			●	●	●		●		glomeroporphyritic texture
RO 8E	Lava	Rhyolite			●	●	●		●		glomeroporphyritic texture
TI TTVF	Lava	Basaltic-andesite		●	●	●			●		porphyritic texture
TI TTVG	Lava	Basaltic-andesite		●	●	●			●		porphyritic texture

Appendix 2.2. Descriptions of box-, piston- and DSDP Site 262 cores

No	Sample	Depth (cm)	Latitude S	Longitude E	Water depth(m)	Environment	CaCO3 (wt%)	Org. C (wt%)	Description
1	MB-1	B	2°01.00'	128°26.50'	3000	Shelf	9.7	1.44	no description available.
2	MB-7	B	2°15.10'	128°50.70'	1730	Shelf	36.1	1.09	no description available.
3	G5-1 2	T	5°19.37'	126°10.81'	4282	Back-arc	1.7		Silty scaly clay.
4	G5-1 2	P	5°19.37'	126°10.81'	4282	Back-arc	13.0	1.02	Scaly clay alternating with diatomitic ooze clay.
5	G5-2 4	B	4-10	5°30.28'	129°54.05'	139	Volcanic arc	30.3	Volcanic sand.
6	G5-2 5	B	1-4	4°30.19'	129°56.17'	347	Volcanic arc	33.7	Volcanic sand with shell hash.
7	G5-2 6	B		4°29.72'	129°56.28'	170	Volcanic arc	20.5	Volcanic sand and gravel.
8	G5-2 7	B		4°30.91'	129°57.60'	0	Volcanic arc	16.5	Volcanic sand.
9	G5-2 8	B		4°31.71'	129°58.97'	661	Volcanic arc	11.7	Clayey volcanic sand.
10	G5-2 9	B		4°29.90'	129°53.44'	1142	Volcanic arc	22.7	Sandy clay with volcanic pebbles.
11	G5-2 10	B	1-5	4°30.50'	130°01.00'	1454	Volcanic arc	19.8	Grey brown silty sandy clay.
12	G5-2 12	B	1-9	4°35.00'	130.08.60'	1820	Volcanic arc	47.8	Volcanic sand with pumice pieces.
13	G5-2 14	B	1-3	4°42.20'	130°18.20'	2940	Volcanic arc	22.4	0.75 Oxidized zone, light brown, full of burrows.
14	G5-2 17	B	1-5	4°48.88'	130°30.20'	4561	Volcanic arc	0.0	Greyish green clay.
15	G5-2 19	B	1-4	4°50.07'	130°31.09'	4315	Inner deep	0.1	1.02 Light brown oxidized sandy clay with burrows.
16	G5-2 20	B	1-3	4°46.73'	130°33.03'	5334	Inner deep	0.3	Greyish green clay with stumpy layer.
17	G5-2 22	B	2.5-5.5	4°41.43'	130°45.70'	6073	Inner deep	6.6	Blue greyish very stiff clay.
18	G5-2 24	B	1-2.5	4°36.75'	130°52.06'	5056	Inner deep	0.0	0.72 Oxidized zone, brown clay.
19	G5-2 25	B	13-15	4°33.67'	130°56.61'	4647	Inner deep	0.0	Green soft clay with bioturbation.
20	G5-2 26	B	1-7	4°28.08'	131°07.90'	4068	Inner deep	0.5	Greenish grey clay, rather stiff with forams.
21	G5-2 28	B	2-5	4°26.13'	131°07.46'	3600	Wedge	1.7	Greenish green clay.
22	G5-2 30	B	1-5	4°23.70'	131°15.70'	2994	Wedge	0.0	Olive grey clay, homogeneous.
23	G5-2 34	B	2-4	4°19.80'	131°19.50'	1399	Wedge	32.2	0.51 Olive green foram ooze, homogeneous with open burrows.
24	G5-2 35	B	1-5	4°19.00'	131°20.80'	1091	Wedge	61.7	Brownish green sandy clay.
25	G5-2 36	B	2-3	4°17.70'	131°21.30'	671	Wedge	67.0	Brown grey foram ooze.
26	G5-2 37	B	1-8	4°17.60'	131°23.30'	505	Wedge	51.2	Greyish brown medium-fine sand.
27	G5-2 38	B	7-9	4°16.60'	131°25.10'	372	Wedge	41.6	Greyish green sandy silty clay with sandy pockets.
28	G5-2 40	B	5-11	4°14.80'	131°28.30'	618	Wedge	51.1	1.28 Greyish green sand with much shell hash, some small well rounded pebbles.
29	G5-2 43	B	1-3	4°10.80'	131°33.60'	823	Wedge	54.7	Yellow foram ooze.
30	G5-2 45	B	1-2	4°05.59'	131°39.91'	874	Wedge	62.9	0.85 Light brown oxidized foram ooze.
31	G5-2 46	B	8-15	3°59.80'	131°45.80'	1107	Wedge	34.4	Greenish grey homogeneous foram ooze.
32	G5-2 47	B	5-10	3°56.40'	131°49.10'	1476	Wedge	25.0	Very unconsolidated clay, silty/sandy green.
33	G5-2 49	B	8-13	3°47.90'	131°57.07'	1349	Wedge	33.2	Olive green clay homogeneous.
34	G5-2 50	B	10-11	3°38.95'	132°04.96'	1659	Wedge	13.8	Olive green homogeneous foram clay.
35	G5-2 51	P	0-347	3°37.36'	132°06.85'	1974	Trench	16.4	1.41 no description available.
36	G5-2 52	B	6-11	3°36.61'	132°06.88'	1967	Trench	10.7	no description available.
37	G5-2 56	P	0-804	3°34.56'	132°10.58'	2113	Trench	8.6	1.32 Clay and silty clay, calcereous, oxidized layer on calcereous clay.
38	G5-2 58	B	2-7	3°28.70'	132°18.80'	1816	Trench	13.5	Greyish green silty sandy clay.
39	G5-2 60	B	4-8	3°24.47'	132°20.94'	1564	Shelf	18.6	2.24 Olive green foram clay very soft.
40	G5-2 61	B	3-6	3°24.41'	132°20.78'	1402	Shelf	21.8	Olive green foram clay.
41	G5-2 62	B	2-7	3°23.54'	132°22.34'	1097	Shelf	30.9	Greenish grey sandy silty foram clay.
42	G5-2 63	B	4-9	3°22.74'	132°22.88'	919	Shelf	41.1	1.67 Greenish grey homogenous clay.
43	G5-2 64	B	1-5	3°17.80'	132°25.00'	684	Shelf		Greenish grey homogenous clay.
44	G5-2 65	B	1-4	3°17.00'	132°26.40'	486	Shelf	35.4	2.12 Brown clay oxidized very soft, coarse fraction made up of forams and glauconite.
45	G5-2 66	B	1-6	3°16.20'	132°26.66'	150	Shelf	85.2	Shell hash with silty clay patches.
46	G5-2 68	B	13-14	3°15.90'	132°25.70'	350	Shelf	45.0	Greyish green foram clay.
47	G5-4 69	B	9-15	5°09.39'	133°47.24'	3455	Shelf	9.9	Greenish grey clay with black lenses.
48	G5-4 69	P	0-722	5°10.91'	133°47.97'	3444	Trench	8.8	1.19 Volcanic sands and muds in alternating layers.
49	G5-4 70	B	15-22	6°43.45'	133°31.20'	87	Shelf	76.1	Olive green coarse shell sand.
50	G5-4 71	B	19-25	7°06.97'	133°18.38'	78	Shelf	57.0	1.89 Bioclastic sand olive grey.

Appendix 2.2. Descriptions of box-, piston- and DSDP Site 262 cores

No	Sample	Depth (cm)	Latitude S	Longitude E	Water depth(m)	Enviroment	CaCO3 (wt%)	Org. C (wt%)	Description
51	G5-4 72 B	10-19	7°08.19'	133°06.45'	59	Shelf	90.8		Grey calcereous sand with foraminifera and shell debris.
52	G5-4 74 B	11-22	7°07.40'	132°58.90'	141	Shelf	84.3		Greenish medium-coarse sand, ill sorted, abundant volcanic grains.
53	G5-4 75 B	1-6	7°07.20'	132°57.40'	249	Shelf	57.9		Coarse sand with shell debris.
54	G5-4 75 B	6-19	7°07.20'	132°57.40'	249	Shelf	56.8	0.19	Medium volcanic sand with finer shell debris, mottled appearance.
55	G5-4 76 B	31-35	7°06.90'	132°56.00'	346	Shelf	16.7		Blue grey clay with some forams.
56	G5-4 77 B	22-28	7°05.50'	132°53.20'	488	Shelf	3.4		Greasy clay with burrows filled with foram sand.
57	G5-4 78 B	17-23	7°04.69'	132°49.01'	713	Shelf	57.9		Grey green clay /silt with forams and little volcanic sand (<1%).
58	G5-4 79 P	0-527	7°04.02'	132°47.13'	848	Shelf	8.2	1.02	Foram ooze/clay on homogeneous calcereous clay.
59	G5-4 80 B	16-20	7°03.73'	132°47.50'	903	Shelf	46.9		Strongly bioturbated layer of foram sands and blue grey clay.
60	G5-4 81 B	25-30	7°03.82'	132°45.28'	1077	Shelf	48.2		Olive grey foram ooze with forams and glauconite.
61	G5-4 82 B	16-21	7°03.54'	132°42.90'	1311	Trench	45.0		Olive grey homogeneous clay with burrows.
62	G5-4 83 B	21-30	6°59.67'	132°38.19'	1654	Trench	27.7	1.61	Olive green homogeneous foram nanno ooze.
63	G5-4 84 B	11-20	6°58.38'	132°34.81'	1749	Trench	25.7		Green soft clay.
64	G5-4 85 P	0-422	6°58.43'	132°36.58'	1802	Trench	15.0	1.40	Foram ooze and foram clay on homogeneous clay.
65	G5-4 86 B	24-29	6°56.70'	132°31.79'	1391	Trench	47.5		Grey green foram sand mixed with clay.
66	G5-4 87 B	24-29	6°58.18'	132°30.33'	1171	Trench	62.0		Grey-green foram sand mixed with clay.
67	G5-4 88 B	28-31	6°58.40'	132°30.50'	1023	Trench	40.0	0.99	Olive grey clay.
68	G5-4 90 B	20-21	6°57.00'	132°26.50'	780	Wedge	71.2		Olive grey biogenic sand, homogeneous.
69	G5-4 91 B	21-29	6°55.50'	132°16.70'	592	Wedge	55.3		Greenish grey foram sand, homogeneous.
70	G5-4 92 B	12-17	6°49.80'	132°09.50'	481	Wedge	39.7	1.15	Greenish grey clay with few forams, homogeneous and stiff.
71	G5-4 94 B	12-14	6°47.30'	132°01.80'	460	Wedge	68.8		Foram coarse sand.
72	G5-4 95 B	29-34	6°40.80'	131°49.40'	681	Wedge	70.6		Olive grey foram ooze, homblende present?
73	G5-4 97 B	5-11	6°36.70'	131°34.10'	582	Wedge	84.0		Light yellowish brown foram sand with quartz and dark brown pebbles.
74	G5-4 99 B	20-29	6°35.00'	131°32.50'	2141	Wedge	49.8	1.73	Homogeneous olive green nanna foram ooze, very soft sediment.
75	G5-4 102 B	23-28	6°35.70'	131°29.50'	3272	Wedge	33.2		Grey clay, homogeneous, with some dark brown grains.
76	G5-4 104 B	9-11	6°31.90'	131°23.40'	4941	Inner deep	16.4	1.32	Grey brown sandy clay with black volcanics and foram sands.
77	G5-4 106 B	19-21	6°26.32'	130°56.80'	6241	Inner deep	2.3	0.96	Grey clay with some faint laminations.
78	G5-4 110 B	26-31	6°13.10'	130°33.30'	6251	Inner deep	0.0	0.77	Grey clay, fine laminated silt and terrigenous material.
79	G5-4 111 B	3-9	6°09.86'	130°26.56'	5199	Inner deep	0.9		Brownish grey sandy mud with abundant volcanoclastics (including pumices).
80	G5-4 114 B	14-19	6°06.00'	130°11.50'	3241	Volcanic arc	24.5		Grey green sandy clay with forams and black volcanogenic sand and gravel.
81	G5-4 115 B	20-23	6°03.90'	130°09.10'	3657	Volcanic arc	2.8		Black to dark grey loose volcanic sand.
82	G5-4 115 B	13-18	6°03.90'	130°09.10'	3657	Volcanic arc	11.0		Grey muddy tuffaceous sand (volcanoclastic).
83	G5-4 116 B	7-12	6°03.29'	130°06.42'	3886	Volcanic arc	4.5		Sandy clay with abundant volcanic grains.
84	G5-4 117 B	7-12	6°03.20'	130°09.10'	3181	Volcanic arc	6.6	0.59	Olive green sandy mud with mottled appearance.
85	G5-4 118 B	12-16	6°07.10'	130°13.30'	2541	Volcanic arc	60.5		Gl. Medardii ooze, grey brown, less than 5% volc material.
86	G5-6 121 B	20-25	7°09.80'	126°58.80'	4059	Volcanic arc	6.6		Dark greenish grey clay, homogeneous.
87	G5-6 122 B	17-24	7°13.20'	127°03.20'	4350	Volcanic arc	0.0		Olive grey and mud, volcanic grains present.
88	G5-6 123 B	11-16	7°18.70'	127°03.80'	3988	Volcanic arc	4.4	0.70	Brown-green-yellowish soft clay.
89	G5-6 124 B	28-35	7°19.00'	127°04.80'	3667	Volcanic arc	34.9		Greenish grey clay, slightly calcereous, rather stiff.
90	G5-6 125 B	29-34	7°20.20'	127°04.70'	2893	Volcanic arc	43.1		Olive green foram clay.
91	G5-6 126 B	20-29	7°22.50'	127°07.30'	2893	Volcanic arc	49.7		Olive green foram ooze.
92	G5-6 127 B	6-9	7°29.50'	127°08.30'	1911	Volcanic arc	65.1		Yellow grey muddy sand with foraminifera.
93	G5-6 128 B	4.5-10	7°37.00'	127°11.80'	1414	Volcanic arc	64.2		Greyish-yellow medium-coarse muddy sand.
94	G5-6 129 B	30-37	7°45.30'	127°14.80'	1777	Volcanic arc	33.2	0.78	Greyish olive foram ooze.
95	G5-6 130 B	25-30	7°57.80'	127°19.30'	2772	Inner deep	26.5		Greyish green coarse foram sand with shell fragments and forams.
96	G5-6 132 B	3-10	8°09.60'	127°23.80'	3070	Inner deep	73.0		Foram sand, very clean containing some quartz.
97	G5-6 133 B	23-28	8°11.00'	127°25.40'	2592	Inner deep	27.9		Greyish foram bearing clay.
98	G5-6 134 B	8-11	8°12.50'	127°26.80'	2181	Inner deep	1.6	0.38	Greyish yellow clay with abundant gravel including fragments of metamorphic rocks (phylite and slate?).
99	G5-6 135 B	0-3	8°14.70'	127°26.00'	1727	Wedge	84.5		Light yellow orange foram ooze (sand size) with very few pebbles of metamorphic rocks.
100	G5-6 136 B	15-20	8°17.00'	127°27.70'	1211	Wedge	23.7	0.46	Grey clay with pebbles (green sandstone, quartz, slates and phyllites), also mica.

Appendix 2.2. Descriptions of box-, piston- and DSDP Site 262 cores

No	Sample	Depth (cm)	Latitude S	Longitude E	Water depth(m)	Environment	CaCO3 (wt%)	Org. C (wt%)	Description
101	G5-6 138 B	12-18	8°23.30'	127°29.70'	1038	Wedge	55.9		Greyish olive clay with terrigenous pebbles.
102	G5-6 139 B	32-33	8°42.20'	127°37.50'	1570	Wedge	59.6		Grey green clayey foram sand.
103	G5-6 140 B	31-38	8°48.20'	127°38.00'	1936	Wedge	28.0		Olive grey calcareous clay.
104	G5-6 141 B	31-38	8°59.10'	127°41.70'	2294	Trench	25.4		Grey calcareous ooze.
105	G5-6 143 B	26-31	9°07.60'	127°44.00'	2870	Trench	14.2	0.70	Greenish clay with planktonic forams.
106	G5-6 144 B	33-39	9°07.87'	127°44.37'	3151	Trench	13.4		Grey clay, very soft and homogenous.
107	G5-6 145 P	0-968	9°10.14'	127°43.62'	3267	Trench	21.5	1.26	Calcareous clay with some forams.
108	G5-6 146 B	21-30	9°10.10'	127°45.21'	3000	Trench	24.0		Olive grey foraminiferal nanno ooze.
109	G5-6 147 B	34-39	9°12.70'	127°46.30'	2539	Trench	26.3	0.86	Grey-green clay.
110	G5-6 148 B	26-31	9°17.40'	127°47.10'	1951	Shelf	35.7		Greenish grey foram clay, rather stiff.
111	G5-6 149 B	15-20	9°22.46'	127°48.49'	1673	Shelf	83.0		Coarse to very coarse foramm sand, some olive green grains.
112	G5-6 149 P	0-1520	9°21.10'	127°49.30'	1699	Shelf	32.5	1.00	Homogeneous clay with forams.
113	G5-6 150 B	24-32	9°24.05'	127°50.49'	1832	Shelf	41.1	1.25	Dark olive grey nanno-foram ooze.
114	G5-6 151 B	29-34	9°26.60'	127°50.30'	1503	Shelf	53.5		Greenish grey foram clay, homogenous.
115	G5-6 152 B	23-28	9°27.97'	127°50.84'	1266	Shelf	50.5		Greenish grey foram clay.
116	G5-6 153 B	23-28	9°31.00'	127°52.30'	1088	Shelf	43.9	1.31	Olive grey foram clay, soft and homogenous.
117	G5-6 154 B	31-38	9°32.91'	127°53.61'	915	Shelf	54.3		Olive grey foram bearing nanno ooze, homogenous.
118	G5-6 155 B	21-30	9°34.33'	127°53.98'	711	Shelf	57.2		Greyish foram nanno ooze.
119	G5-6 156 B	32-36	9°35.06'	127°52.60'	547	Shelf	56.3		Dark olive grey nanno foram ooze.
120	G5-6 157 B	31-36	9°35.15'	127°54.25'	416	Shelf	37.7	0.98	Dark greenish grey nanno ooze.
121	G5-6 158 B	22-26	9°36.61'	127°54.70'	331	Shelf	68.6		Greenish dark grey clay, strongly bioturbated.
122	G5-6 159 B	22-26	9°41.70'	127°55.90'	210	Shelf	57.0		Greenish grey clay.
123	G5-6 160 B	?-?	9°44.90'	127°56.20'	150	Shelf	90.8		No description available.
124	G5-6 161 B	?-?	9°46.90'	127°56.70'	100	Shelf	92.3		Reef debris.
125	G5-6 162 B	11-14	9°50.73'	127°57.10'	90	Shelf	89.6		Grey yellow granule sized lamellibranchiate hash.
126	G5-6 163 B	6-12	9°50.36'	127°56.50'	71	Shelf	92.2		Yellow biogenic sands and gravels consisting of broken shells, molluscs, coral and some forams.
127	G5-6 164 P	0-885	9°33.50'	127°53.20'	885	Shelf	53.5		Calcareous siliceous silty clay.
128	Core 1-4 D	50-52	10°52.19'	123°50.78'	2298	Trench	50.6		Greyish olive nanno ooze with narrow bands (<1cm) and streaks of greyish black foram rich clay stiff.
129	Core 14-5 D	69-71	10°52.19'	123°50.78'	2298	Trench	24.6	0.53	Stiff greyish olive nanno ooze with dark layers and streaks and slight mottles.
130	Core 32-3 D	60-62	10°52.19'	123°50.78'	2298	Trench	60.5	0.82	Stiff greyish olive and pale olive nanno ooze with slight mottling.
131	Core 40-2 D	60-62	10°52.19'	123°50.78'	2298	Trench	49.9		Semi lithified greyish olive and yellow green foram ooze. Layered and slightly mottled.
132	Core 45-4 D	61-63	10°52.19'	123°50.78'	2298	Trench	96.6		Soft, stiff and semi-lithified grey and pale olive foram rich dolomite, generally massive.

APPENDIX 3

ANALYTICAL TECHNIQUES

3.1. SAMPLE PREPARATION

3.1.1. Volcanic rocks

Massive rock samples of 0.5-5 kg were sawn to small blocks of approximately 20 cm³. Only inclusion-free pieces with a fresh interior were selected. The blocks (typically about 300 g) were cleaned with distilled water in an ultrasonic bath for half an hour, rinsed with distilled water and dried at 80 °C for 24 hours.

Cleaned blocks were checked with a binocular microscope to avoid small inclusions and coatings (e.g. Fe-oxide and/or carbonate) on vesicles and cracks. The selected blocks were broken in a tungsten-carbide coated jaw-crusher to < 0.5 cm chips. Where many small inclusions were present, samples were further purified by handpicking. A split of those chips was used for the Pb-isotope determination. After homogenization, a split of approximately 100 g was ground in an agate or tungsten-carbide shatter-box to < 200 μ diameter.

3.1.2. Sediment cores

Box cores

Samples of approximately 200 g were taken from a selected depth interval of the box-cores and dried for three weeks at 50 °C. They were ground in an agate grinding-mill to a size of < 200 μ. These powders were used for XRF work. After homogenization, a split of about 2-4 g was dialyzed in distilled water for four days (refreshing water two times a day) to remove the seawater signal (e.g. Na, Cl and Sr). After decanting the water, samples were dry frozen. These dialyzed samples were used for INAA, ICP-MS and isotope work.

Piston cores

Composite samples were acquired from 10 selected piston-cores. Sub-samples of approximately 2 cm³ were taken at a spacing of 25 cm for the whole length of the piston-core and thoroughly mixed. The composite of every core was dried for three weeks at 50 °C, and ground in an agate grinding-mill to a size of < 200 μ. Samples were further treated by the same procedures as the box-cores.

DSDP Site 262 samples

The DSDP Site 262 samples were provided by the Ocean Drilling Program Depository. Due to the limited sample size (5-10 g), only INAA and isotope work were performed on these samples. Procedures were similar to those applied to the box cores.

3.2. CARBONATE AND ORGANIC CARBON DETERMINATION IN SEDIMENTS

Carbonate contents were determined on all sediment samples. About 1 g of (non dialyzed) sample powder was put in a furnace at 120 °C for at least eight hours to remove adsorbed water. Subsequently, 0.1 g was weighed and put into a plastic cup. This plastic cup was placed into a wash bottle containing 15 ml of 1N HCl and closed with a rubber cap with a tap. The sample was not yet in contact with the acid. Fifteen samples, together with one standard made up of a Na₂CO₃ standard-solution and one blank (containing 15 ml 1N HCl), were put on a vibrating table. During shaking, the acid came into contact with the sample and CO₂ was released. After shaking 30 minutes, the volumes of released CO₂ were measured. The blank and standard were measured first and subsequently the samples. Using the blank and standard, the CO₂ was recalculated to the amount of carbonate (CaCO₃) in the samples. Precision, as determined on duplicates, is in the order of 3%

Organic carbon was determined on the samples which were selected for isotopic analyses (45). About 3 g of (non-dialyzed) sample was weighed into a teflon flask. About 10 ml of 1N HCl was added to decarbonate the samples which were put on a vibrating table overnight. Subsequently, the samples were centrifuged and the liquid decanted. The residue was dried and weighed. About 0.1 g of decarbonated sample powder was put into a glass container. Organic carbon was determined by burning the sample in an oxygen atmosphere of 900 °C. All released carbon gases were converted to CO₂ by CuO. The CO₂ in the released gas was separated from H₂O by cold traps and measured by a Servomex infrared analyser 1490. Before every run it was calibrated with 2 ml CO₂ gas (1 atm). Duplicates indicate a precision of better than 5%.

Table I. XRF running conditions

Element	Filter	Collector	Detector	Crystal	Tube	PHS	kV	mA	Background		Counting Time (seconds)		
									Offsets (Degrees)		Peak	Background	
Si	K α	No	Coarse	Flow	PE	Cr	25-75	60	50	+3.50		20	20
Ti	K α	No	Fine	Flow	LiF200	Cr	25-75	60	50	+2.00	-2.00	20	20
Al	K α	No	Coarse	Flow	PE	Cr	25-75	60	50	+1.92		20	20
Fe	K α	No	Fine	Flow	LiF220	Cr	18-78	60	50	+2.00		20	20
Mn	K α	Yes	Coarse	Flow	LiF200	Cr	15-75	60	50	+2.00	-1.50	50	20
Mg	K α	No	Coarse	Flow	TLAP	Cr	40-60	60	50	+2.00	-0.60	100	50
Ca	K β	No	Fine	Flow	LiF200	Cr	26-70	60	50	+0.00	-4.22	20	20
Na	K α	No	Coarse	Flow	TLAP	Cr	20-80	60	50	+1.50	-1.50	100	50
K	K α	No	Fine	Flow	LiF200	Cr	19-75	50	40	+5.10		20	20
P	K α	No	Fine	Flow	PE	Cr	34-80	60	50	+3.00		100	50
Zn	K α	No	Fine	Flow+Sin.	LiF200	Rh	25-75	60	50	+0.70	-0.80	20	20
Cu	K α	No	Fine	Flow+Sin.	LiF200	Rh	24-75	60	50	+1.70	-1.00	50	20
K ²¹	K α	No	Fine	Flow	LiF200	Rh	20-80	50	40	+5.10		20	20
Rb	K α	No	Fine	Flow+Sin.	LiF200	Rh	25-75	60	50	+0.44	-0.76	50	20
Sr	K α	No	Fine	Flow+Sin.	LiF200	Rh	25-75	60	50	+0.60	-0.70	50	20
Ba	L α	No	Fine	F	LiF200	Cr	25-75	50	60	+1.50		100	50
Pb	L β	No	Fine	Flow+Sin.	LiF220	Rh	25-75	60	50	+0.50	-0.40	100	50
Y	K α	No	Fine	Flow+Sin.	LiF200	Rh	25-75	60	50	+0.26	-0.28	50	20
Nb	K α	No	Fine	Flow+Sin.	LiF200	Rh	25-75	60	50	+0.34	-0.34	50	20
Zr	K α	No	Fine	Flow+Sin.	LiF200	Rh	25-75	60	50	+0.44	-0.80	20	20
Rh ²	K α	No	Fine	Sin.	LiF200	Rh	25-75	60	50				

Table IIa. Major elements AGV-1

Element	No	X	S	Value	%P	%A
SiO ₂	6	59.99	0.09	58.79	0.2	2.0
TiO ₂	6	1.10	0.01	1.05	0.9	4.8
Al ₂ O ₃	6	17.63	0.05	17.14	0.3	2.9
Fe ₂ O _{3t}	6	6.76	0.03	6.76	0.4	0.0
MnO	6	0.12	0.00	0.092	0.0	30.4
MgO	6	1.51	0.04	1.53	2.7	1.3
CaO	6	5.02	0.03	4.94	0.6	1.6
Na ₂ O	6	4.30	0.05	4.36	1.2	1.4
K ₂ O	6	3.06	0.03	2.91	1.0	5.2
P ₂ O ₅	6	0.51	0.02	0.49	3.9	4.1

Table IIb. Major elements BHVO-1

Element	No	X	S	Value	%P	%A
SiO ₂	2	49.41	0.07	49.94	0.1	1.1
TiO ₂	2	2.82	0.01	2.71	0.4	4.1
Al ₂ O ₃	2	13.66	0.01	13.80	0.1	1.0
Fe ₂ O _{3t}	2	12.16	0.02	12.23	0.2	0.6
MnO	2	0.21	0.00	0.168	0.0	25.0
MgO	2	7.22	0.04	7.23	0.6	0.1
CaO	2	11.55	0.02	11.40	0.2	1.3
Na ₂ O	2	2.19	0.02	2.26	0.9	3.1
K ₂ O	2	0.53	0.01	0.52	1.9	1.9
P ₂ O ₅	2	0.28	0.01	0.27	3.6	3.7

Coefficient of variation ($[\%P]=X/S*100\%$) and accuracy (expressed as $[\%A]=(X-R)/R*100$, where R is the reported value, X is the average and S the standard deviation) of international standards AGV-1 (a) and BHVO-1 (b) of major elements determined by XRF. The reported values are from Govindaraju (1989).

3.3. XRF

Major elements

Loss on ignition (LOI) was first determined by the weight loss of adsorbed water by heating 4-5 g sample powder in a porcelain cup at 120 °C for one hour (M1). Subsequently, the weight loss was determined of the samples (in the same porcelain cup) by heating to 900 °C in a furnace for eight hours (M2). The reported LOI values in Appendix 4 are M2-M1. LOI of duplicates indicate a precision of better than 5%.

XRF analyses were made using a Philips PW 1400 XRF. Major elements were determined on glass beads, which were made by fusing 0.5000 g ignited rock powder with 5.00 g LiBO₂-LiB₄O₇ (66/34) at 1100 °C in a Herzog HAG 1200 automated furnace. Synthetic standards were used for calibration. Operational conditions are given in Table I.

The precision of the XRF was judged by running two fused disks of international standards AGV-1 and BHVO-1 with every batch. The precision, here expressed as the

Table IIIa. XRF trace elements AGV-1

Element	No	X	S	Value	%P	%A
Rb	8	73.0	1.20	67.3	1.6	8.5
Ba	4	1191.0	19.23	1226	1.6	2.9
Sr	8	664.3	4.68	662	0.7	0.3
Y	8	21.1	0.64	20	3.0	5.5
Zr	8	213.5	4.69	227	2.2	5.9
Nb	8	13.5	0.53	15	3.9	10.0
Pb	8	38.5	1.85	36	4.8	6.9
Cu	8	64.1	0.99	60	1.5	6.8
Zn	8	92.4	2.26	88	2.5	5.0

Table IIIb. XRF trace elements BHVO-1

Element	No	X	S	Value	%P	%A
Rb	8	12.0	0.53	11	4.4	9.1
Ba	4	128.3	7.93	139	7.9	7.7
Sr	8	401.6	5.07	403	1.3	0.3
Y	8	25.3	0.46	27.6	1.8	8.3
Zr	8	172.1	3.80	179	2.2	3.9
Nb	8	17.9	0.64	19	3.6	5.8
Pb	8	<dl	-	2.6	-	-
Cu	8	140.8	1.28	136	0.9	3.5
Zn	8	109.0	2.62	105	2.4	3.8

Coefficient of variation (%P) and accuracy of international standards AGV-1 (a) and BHVO-1 (b) for XRF trace-elements. See Table II for abbreviations and definitions. Reported values are from Govindaraju (1989).

coefficient of variation ($CV = sd/mean * 100\%$) is given in in Table II. The reproducibility of the whole XRF major element procedure (sample preparation and measurement) was estimated by running duplicate samples. These indicate a difference of less than 2%.

The accuracy, the deviation of the 'true' value, as determined on the international standards AGV-1 and BHVO-1 is reported for each major element in Table II. In general these are better than 3%, except for MnO, TiO₂ and P₂O₅.

Trace elements

Trace elements were determined on pressed powder pellets. These were made of 8.0 g sample powder mixed with 2 ml elvacite solution (1:5=elvacite:acetone) as binding agent and pressed under 20 ton/cm² for 1 minute. Calibration curves were made of up to 30 international standards.

The precision of the XRF measurement was judged by running two pressed powder pellets of international standards AGV-1 and BHVO-1 with every batch. The precision, also expressed as the coefficient of variation ($CV = sd/mean * 100\%$) is given in in Table III.

The precision was better than 5% for all elements, except for low levels of Ba in the BHVO-1 where it was 8%.

The reproducibility of the whole XRF trace element procedure (sample preparation and measurement) was estimated by running duplicate and triplicate samples. These indicate a difference of less than 5%, except for Nb < 5 ppm, Pb < 15 ppm and Rb < 10 ppm which are better than 10%.

The accuracy, the deviation of the 'true' value, as determined on the international standards AGV-1 and BHVO-1, is reported in Table III. The accuracy was better than 5% except for Rb, Y, Nb and Pb which were better than 10%.

3.4. INAA

The abundances of Cr, Co, Sc, Hf, Th, Ta and La, Ce, Sm, Eu, Tb, Yb and Lu were determined by standard Instrumental Neutron Activation Analysis (INAA) techniques (De Bruin, 1983) at IRI, Delft, The Netherlands. The CV and accuracy for three international standards are given in Table IV. The newly weighed international standards were run in every batch. The CVs are generally better than 10%, except for Tb, Lu and Ta. The accuracy is often better than 10% except for Tb, Lu and Ta.

Table IVa INAA trace elements BCR-1

Element	Number	X	S	Value	%P	%A
La	9	29.42	1.24	24.9	4.2	18.2
Ce	4	52.84	2.34	53.7	4.4	1.6
Sm	9	6.66	0.33	6.59	5.0	1.1
Eu	4	2.00	0.04	1.95	2.0	2.6
Tb	4	1.09	0.15	1.05	13.8	3.8
Yb	9	3.28	0.24	3.38	7.3	3.0
Lu	9	0.63	0.11	0.51	17.5	18.9
Sc	4	33.24	0.62	32.6	1.9	2.0
Cr	4	13.80	1.24	16	9.0	13.8
Co	4	37.63	0.25	37	0.7	1.7
Hf	4	5.08	0.09	4.95	1.8	2.6
Ta	3	0.56	0.12	0.81	21.4	30.9
Th	9	5.80	0.15	5.98	2.6	3.0
U	4	1.71	0.12	1.75	7.0	2.3
Cs	1	1.06	-	0.96	-	10.4

Table IVb. INAA trace elements BHVO-1

Element	Number	X	S	Value	%P	%A
La	10	17.33	1.29	15.8	7.4	9.7
Ce	7	38.87	1.27	39	3.3	0.3
Sm	10	6.03	0.17	6.2	2.8	2.7
Eu	7	2.07	0.03	2.06	1.5	0.5
Tb	7	0.91	0.06	0.96	6.6	5.2
Yb	10	1.93	0.17	2.02	8.8	4.5
Lu	9	0.38	0.08	0.29	21.1	31.0
Sc	7	32.13	0.66	31.8	2.1	1.0
Cr	7	292.63	8.13	289	2.8	1.3
Co	7	45.74	0.90	45	2.0	1.6
Hf	7	4.45	0.15	4.38	3.4	1.6
Ta	7	1.04	0.15	1.23	14.4	15.4
Th	10	1.12	0.08	1.08	7.1	3.7
U	10	-	-	0.42	-	-
Cs	5	-	-	0.13	-	-

Table IVc. INAA trace elements SCO-1

Element	Number	X	S	Value	%P	%A
La	5	29.21	1.96	29.5	6.7	1.0
Ce	5	57.92	3.06	62	5.2	6.6
Sm	5	5.38	0.22	5.3	4.1	1.5
Eu	5	1.19	0.05	1.19	4.2	0.0
Tb	5	0.72	0.07	0.7	9.7	2.9
Yb	5	2.12	0.05	2.27	2.6	6.6
Lu	5	0.37	0.03	0.34	8.1	8.8
Sc	5	12.00	0.38	10.8	3.2	11.1
Cr	5	71.17	2.12	68	5.1	4.7
Co	5	11.31	0.58	10.5	5.1	7.7
Hf	5	4.71	0.16	4.6	3.4	2.4
Ta	5	0.76	0.07	0.92	9.2	17.4
Th	5	9.47	0.28	9.7	3.0	2.4
U	5	3.36	0.32	3.0	9.5	12.0
Cs	5	8.57	0.27	7.80	3.2	9.9

Coefficient of variation (%P) and accuracy of international standards BCR-1 (a), BHVO-1 (B) and SCO-1 (c) for trace-elements obtained by INAA. See Table II for abbreviations and definitions. Reported values are from Govindaraju (1989).

3.5. ICP-MS

For selected samples Cs, a complete set of REE and Th-U-Pb concentrations were determined on a VG PlasmaQuad II ICP-MS at Cornell University.

3.5.1. Sample dissolution procedures for ICP-MS

Sample preparation of volcanic rocks

Weighed sample powders (0.10-0.15 g) were dissolved together with a mixed ^{206}Pb - ^{230}Th - ^{235}U spike in sealed 15 or 30 ml PFA beakers on a hotplate at 140 °C for more than two days, using 4 ml HF and 1 ml HClO_4 (all chemicals are subboiled or of suprapure quality). As an internal standard 1 ml of a 10 ppm In solution was added. After evaporating, the residues were redissolved in 0.5 ml HClO_4 , and dried. The remaining salts were taken up in 5 ml HNO_3 (concentrated) and evaporated. Finally the residue was dissolved in 5 ml HNO_3 and diluted with H_2O to a volume of 100 ml.

Sample preparation of sediments

Dialyzed sediment powders (0.10-0.15 g) were first digested in open teflon bombs to remove carbonate and organic matter (CO_2 gas) with 4 ml HF and 1 ml HClO_4 on a hotplate. After evaporation, similar amounts of HF and HClO_4 were added, the teflon bombs sealed into their steel jackets and put into a furnace (175-180 °C) for at least three days. After cooling, the bombs were opened and the HF- HClO_4 fumed off completely. The residues were redissolved in 0.5 ml HClO_4 , and dried, followed by 5 ml HNO_3 (conc.) and again evaporated. The residue was dissolved in 5 ml HNO_3 (conc.) and the ^{206}Pb - ^{230}Th - ^{235}U spike and 1 ml of a 1 ppm In solution were added. Finally the sample solutions were diluted with H_2O to a volume of 100 ml.

3.5.2. REE and Cs determination by standard addition

A standard-addition technique was employed for REE-Cs, using solutions containing about 0, 2, 5 and 10 times the REE and Cs concentrations of a typical Banda Arc andesite. In each case 1 ml of standard-addition solution was added to 10 ml sample solution. PlasmaQuad runs for each sample consisted of a blank followed by the spiked solutions

Table V. Masses used on the ICP-MS for the REE and Cs

Element	Mass	Interference?
Cs	133	
La	139	
Ce	140	
Pr	141	
Nd	145	
Sm	147	
Eu	153	
Gd	157	BaF ⁺ , CeOH ⁺
Tb	159	
Dy	162	
Ho	165	
Er	166	
Tm	169	
Yb	174	
Lu	175	

Masses used for the REE and Cs on the ICP-MS at Cornell University and their possible interferences.

in ascending order of concentrations. Together with the REE and Cs, ¹¹⁵In and ¹³⁸Ba were measured as internal standards (In was added before sample digestion). Before every run the instrument settings were optimized on the ¹¹⁵In peak, and peaks were 'centred' for each mass analyzed (Average settings and operation conditions are given in Table VI). The peak-jump mode was applied with seven points on every peak. Three 1-minute scans were made on every solution. Raw counts were collected and a self-written routine was used to perform the calculations. The three scans of one solution were averaged and the blank subtracted. The ¹¹⁵In of the 'zero'-addition was used to correct the spiked solutions for drift (generally < 1% for individual sample sets). The selected masses for Cs and REE are shown in Table V.

Duplicate samples suggest reproducibility better than 5%. Results for USGS international standards BCR-1, BHVO-1 and MAG-1 are given in Table VII and indicate an accuracy generally better than 5%. An analytical problem was encountered with Gd. In some REE patterns Gd seems upto 10% too high. This was especially the case if Ba was also high in the samples (southern Banda Arc and high-Ba sediments). This could suggest an interference of BaF⁺ on the ¹⁵⁷Gd mass. A similar problem with ¹⁵⁷Gd on an ICP-MS was noted by Murray et al. (1991), which they attributed to interference of ¹⁴⁰CeOH⁺ or ¹³⁸BaF⁺.

The accuracy can be estimated by several other techniques. Differences between ICP-MS and thermal ionization isotope dilution Nd and Sm data are within 5% for nearly all samples and often are better than 2%.

Table VI. ICP-MS running conditions

Cool flow	:	14.0 l/min
Aux flow	:	0.5 l/min
Nebulizer flow	:	0.78 l/min
Reflected power	:	<10 Watt
Sample uptake rate	:	20 (Gilson pump)
Lenses:		
Extraction	:	80-120
Collector	:	670-700
L1	:	850-870
L2	:	460-525
L3	:	530-555
L4	:	325-505
Pole bias	:	420-530

Operational conditions of VG PlasmaQuad II for REE, Cs and Th-U-Pb analysis

A comparison between ICP-MS and INAA data reveals some larger differences, especially for La (10%) and Tb (10-20%). On the other hand, the Cs, Ce, Sm, Eu and Yb data are generally within 5%.

Table VIIa. BCR-1 ICP-MS REE and Cs data (one run)

Element	Measured	Reported
Cs	0.93	0.96
La	25.85	24.9
Ce	52.6	53.7
Pr	6.83	6.8
Nd	28.89	28.8
Sm	6.50	6.59
Eu	2.17	1.95
Gd	6.80	6.68
Tb	1.00	1.05
Dy	6.51	6.34
Ho	1.25	1.26
Er	3.87	3.63
Tm	0.51	0.56
Yb	3.41	3.38
Lu	0.52	0.51

Table VIIb. BHVO-1 ICP-MS REE and Cs data (one run)

Element	Measured	Reported
Cs	n.d	n.d
La	15.96	15.8
Ce	38.61	39.0
Pr	5.59	5.70
Nd	25.81	25.2
Sm	6.28	6.20
Eu	2.22	2.06
Gd	6.22	6.4
Tb	0.91	0.96
Dy	5.53	5.2
Ho	0.93	0.99
Er	2.70	2.4
Tm	0.32	0.33
Yb	2.13	2.02
Lu	0.28	0.29

Table VIIc. MAG-1 ICP-MS REE and Cs data (one run)

Element	Measured	Reported
Cs	8.67	8.60
La	42.86	43
Ce	86.05	88
Pr	10.13	9.3
Nd	37.97	38
Sm	7.32	7.5
Eu	1.55	1.55
Gd	6.43	5.8
Tb	0.83	0.96
Dy	5.17	5.2
Ho	0.89	1.02
Er	2.82	3
Tm	0.35	0.43
Yb	2.49	2.6
Lu	0.37	0.409

BCR-1 (a), BHVO-1 (b) and MAG-1 (c) USGS international standards results for REE and Cs as determined with ICP-MS standard addition. Reported values are from Govindaraju (1989).

3.5.3. Th, U and Pb determination by isotope dilution

For U-Th-Pb isotope measurements 1 ml of a 1 ppm Tl solution was added to 10 ml sample solution prepared as in section 3.5.1. Measurements were done on the VG Plasmaquad ICP-MS at Cornell University using the Isotope Dilution software. The peak-jump mode was used and 7 points were measured on each peak. Eight scans of approximately 1 minute were made. In one batch of 7 samples the blank was measured first, followed by three samples, the external standard (described below) and four more samples, including at least one USGS international standard. No lens adjustments were made after optimizing the instrument. The stability was monitored with the $^{205}\text{Tl}/^{203}\text{Tl}$ ratio, measured on every sample. An example of one run on $^{205}\text{Tl}/^{203}\text{Tl}$ is given in Fig. I. The mass-fractionation corrections of the raw data were made based on the $^{205}\text{Tl}/^{203}\text{Tl}$ ratio of 2.38870, and on an external standard composed of BHVO-1, NBS981 and the spike solution. These varied from 0-3%.

The isotopic composition of this standard was measured on the VG sector thermal ionization mass spectrometer. Internal precision of the isotope ratios varies from 1-3%. Precision and accuracy on USGS international standards are reported in Table VIII. The precision, which is directly related to the precision on the isotope ratios, varies between 1-3.5% if we discard BHVO-1. The poor precision of BHVO-1 is due to a blank problem.

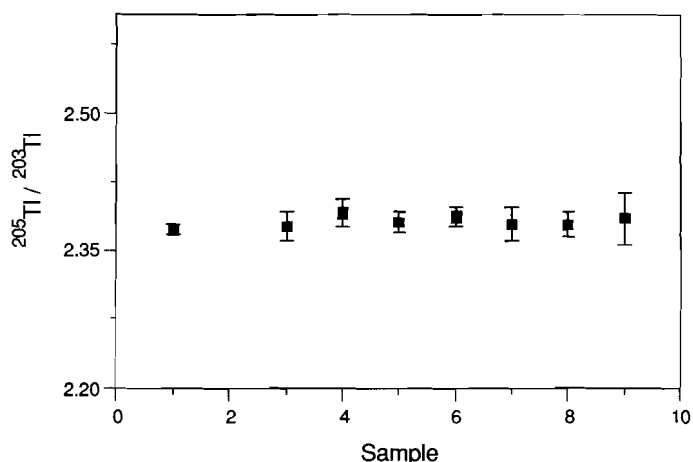


Fig. I. Typical example of the stability of the $^{205}\text{Tl}/^{203}\text{Tl}$ ratio during one run of the ICP-MS for Th-U-Pb isotope dilution analysis. Error bars represent 2σ .

Table VIII. ICP-MS Th-U-Pb isotope dilution**BCR-1**

Element	no	x	s	value	%P	%A	TIMS
Th	2	6.276	0.213	5.98	3.4	5.0	5.862
U	2	1.700	0.042	1.75	2.5	2.9	1.618
Pb	2	14.190	0.135	13.6	1.0	4.3	13.52

BHVO-1

Element	no	x	s	value	%P	%A	TIMS
Th	2	1.192	0.148	1.08	12.4	10.2	
U	2	0.416	0.032	0.42	7.7	1.0	
Pb	2	2.065	0.175	(2.6)	8.5	2.2	2.028

AGV-1

Element	no	x	s	value	%P	%A	TIMS
Th	2	6.272	0.146	6.5	2.3	0.2	6.26
U	3	1.914	0.018	1.92	0.9	0.3	
Pb	2	36.547	0.948	36	2.6	1.9	37.24

MAG-1

Element	no	x	s	value	%P	%A	TIMS
Th	8	11.844	0.147	11.9	1.2	0.1	11.85
U	8	2.718	0.037	2.7	2.7	1.2	2.687
Pb	8	26.578	0.540	24.0	2.0	1.4	26.95

Coefficient of variations (%P) and accuracies obtained on international standards BCR-1, BHVO-1, AGV-1 and MAG-1 for Th-U-Pb isotope dilution. Thermal Ionization Mass Spectrometer (TIMS) results are also displayed. For BHVO-1 the TIMS Pb concentration was used to calculate the accuracy. See Table II for abbreviations and definitions. Reported values are from Govindaraju (1989).

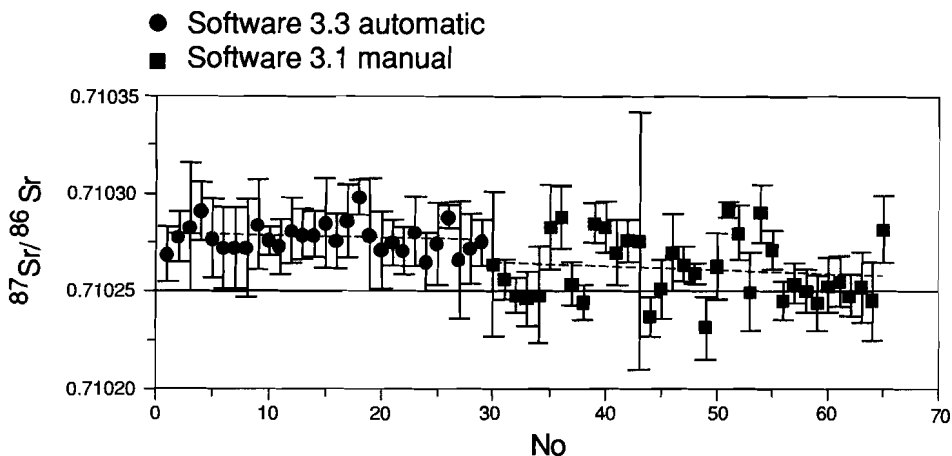


Fig II. NBS 987 Sr-isotope standard results during the course of this study. Note the slight difference between Finnegan software 3.1 and 3.3. No correction to the data was applied.

3.6. SR, ND AND PB ISOTOPE-RATIO AND SM, ND, TH AND U ISOTOPE-DILUTION DETERMINATIONS

3.6.1. Sr and Nd isotopic composition determination of volcanic rocks

For the Sr-isotopes in volcanic rocks approximately 450 mg of powder was dissolved in a HF-HClO₄ (5:1) mixture in open PTFE beakers and evaporated to dryness. This was repeated once, and the residue was dissolved in 3N HCl. An aliquot of this solution was evaporated to dryness and redissolved in 2 ml HClO₄ and 5 ml 3.25 M HCl, cooled in the fridge for at least one night to precipitate the Rb as (K,Rb)ClO₄. An aliquot of this solution was, after centrifuging, separated on AG50x16 (200-400 mesh) using two steps. The average total blank for this procedure is 0.5 ng Sr

Measurements were performed on a Finnigan MAT261 mass spectrometer at the Free University of Amsterdam, fitted with 10 fixed multicollectors. Double-jump experiments were applied (Smedley, 1988). The results of 68 runs of NBS 987 in the course of this study are displayed in Fig. 3.2 and yield a ⁸⁷Sr/⁸⁶Sr ratio of 0.710269 ± 26 (2 sd). There is a slight difference between two versions of software used on the Finnegan MAT261. Systematic higher ⁸⁷Sr/⁸⁶Sr ratios were obtained with software release 3.3 for the NBS 987 (Fig. II). The data (normalized to ⁸⁸Sr/⁸⁶Sr = 8.37521) are given uncorrected.

For Nd isotopes of volcanic samples approximately 250 mg was dissolved in an

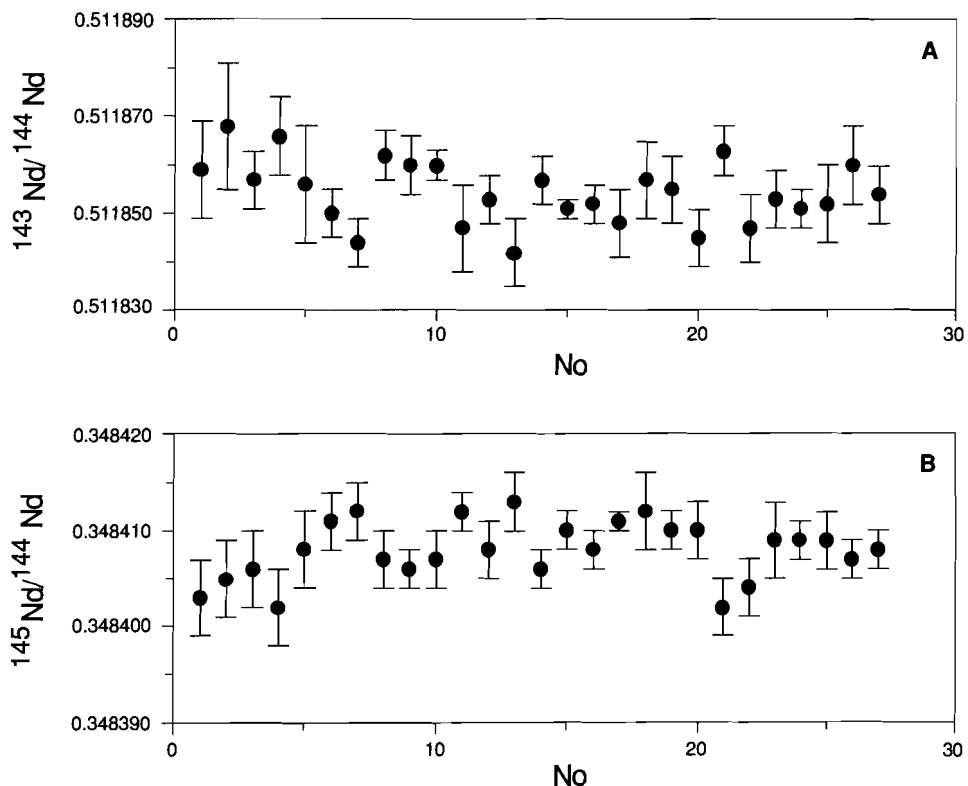


Fig 3a and b. La Jolla Nd-standard results for $^{143}\text{Nd}/^{144}\text{Nd}$ (a) and $^{145}\text{Nd}/^{144}\text{Nd}$ (b) during the course of this study.

$\text{HClO}_4\text{-HNO}_3\text{-HF}$ mixture in PFA screw-cap beakers. After dissolution, samples were evaporated to dryness, redissolved in 6.3N HCl and split into two fractions, one for Nd-isotopic composition and one for Sm, Nd concentrations. Sm and Nd were separated using standard ion-exchange techniques (cf. Valbracht, 1991). The average blank of the total procedure was 1 ng Nd and 0.6 ng Sm.

Nd was run as metal on double Re filaments with a double-jump experiment (see Smedley, 1988). The results of 38 runs of the La Jolla standard are shown in Fig. 3.3a and yielded a $^{143}\text{Nd}/^{144}\text{Nd}$ of 0.511853 ± 12 (2 sd). Data are normalized to $^{146}\text{Nd}/^{144}\text{Nd}$ of 0.7219 using a linear correction. The $^{145}\text{Nd}/^{144}\text{Nd}$ ratio (Fig. 3.3b) shows the high precision and long term stability of the Nd analyses.

Sm and Nd were measured simultaneously on the Finnigan MAT261 using the method of Hebeda et al. (1988). The precision on Sm and Nd concentrations as indicated on multiple

analysis of BHVO-1 and BCR-1 is better than 1% (Valbracht, 1991).

3.6.2. Sr and Nd isotopic composition determination of sediments

For the sediments one dissolution for Nd and Sr isotopes and Sm, Nd isotope dilution was used. Approximately 0.5 g of dialyzed sediment sample was dissolved in a 12 ml PFTE beaker and put on a hot plate for at least 1-2 weeks at 150 °C. After dissolution, the sample solution was split into a Sr fraction, a Nd isotope fraction and Sm, Nd isotope-dilution fraction which were treated as the volcanic rocks. The measurement on the Finnigan MAT261 mass spectrometer was also identical to those of the volcanic rocks.

3.6.3. Pb isotopic composition determination of volcanic rocks

Pb isotopic compositions were determined at Cornell University, following the method described in White and Dupre (1986), except that volcanic samples were digested in screw cap PFA. Pb (100 ng) was loaded using the H₃PO₄-silica gel technique on single Re-filaments (Cameron et al., 1969). The measurements were performed in static mode on a VG Sector equipped with variable multicollectors. The filament temperature was raised under computer control to 1300-1350 °C. All results were corrected for mass fractionation based on 21 replicate analyses of NBS-981: 1.37‰ per amu. The average blank of the total procedure of volcanic rocks was 300 pg Pb.

3.6.4. Pb isotopic composition determination of sedimentary rocks

Dialyzed sediment powders (0.10-0.15 g) were weighed directly into the teflon bombs. They were first digested in open teflon bombs to remove carbonate with 1 ml HF and 0.1 ml HNO₃ on a hotplate. After evaporation to dryness, 3 ml HF and 1 ml HNO₃ were added, the teflon bombs sealed into their steel jackets and put into a furnace (175-180 °C) for at least three days. After cooling, the bombs were opened and the solution evaporated. The residues were redissolved in 2 ml 6 N HBr, followed by column separation, using the method of White and Dupre (1986). The Pb blank of the sediment procedure was significantly higher (500-1000 pg) than those of the volcanic Pb procedure (300 pg) as larger quantities of acids and larger beakers (PFA teflon bombs) were used.

3.6.5. Pb, U and Th isotope-dilution determinations

A few samples, international standards and the external standard used for fractionation corrections with the Th-U-Pb ICP-MS determinations were analysed for Pb, U and Th by isotope dilution on the VG Sector. About 100 mg of sample was weighed out, spiked and digested in a 12 ml PFA beaker with 5 ml HF and 1 ml HNO₃. The sample was evaporated to dryness and 2 ml 6N HBr added. The solution was centrifuged and Pb separated from it using the method of White and Dupre (1986). The eluant of the Pb column separation and the residue from the sample were combined and dried down. Subsequently, the sample was dissolved in 1.5 ml 7N HNO₃. U-Th separation was done as described by White and Dupre (1986).

Pb was analysed in the same way as unspiked isotopic compositions (see section 3.6.4) on the VG sector. U and Th were loaded with H₃PO₄ and graphite on a Re filament. U was measured at 1800 °C and Th at 2000 °C using the Daly with peak hopping on the VG Sector.

APPENDIX 4

MAJOR- AND TRACE-ELEMENT DATA OF THE BANDA ARC VOLCANICS

Major- and trace-element data of the Banda Arc volcanics. Island codes: BA=Banda Api, BN=Banda Neira, BL+BB=Banda Besar, MA=Manuk, SE=Serua, NI=Nila, TE=Teon, DA=Damar, RO=Romang, WE=Wetar, TI=Timor (see Appendix 1.1 and Fig. 2.1 for sample locations). The major elements and Zn, Cu, Rb, Sr, Ba, Pb, Y, Nb, Zr were determined by XRF. The elements Sc, Cr, Co, Cs, La, Ce, Sm, Eu, Yb, Lu, Hf, Th and U were obtained by INAA. Complete REE sets were determined by ICP-MS, in that case the reported value for Cs was also determined by ICP-MS. Major elements and LOI in wt.%, all trace elements in ppm; <dl=below detection limit. See Appendix 3 for analytical techniques.

Appendix 4. Major- and trace-element data of the Banda Arc volcanoes

No Island Sample	1 BA 1A1	2 BA 3A	3 BA 4A	4 BA Banda-4	5 BA 6A	6 BA 8A1	7 BA 9A1	8 BA 9B	9 BA 11A2	10 BA 12A	11 BA 14A2	12 BA 16
SiO ₂	66.14	64.40	66.90	58.78	63.66	64.35	66.08	65.70	59.14	64.92	66.50	66.42
TiO ₂	0.97	1.01	1.01	1.05	1.09	1.07	0.98	1.00	1.00	1.05	1.00	0.99
Al ₂ O ₃	14.27	14.52	14.40	15.44	14.40	14.69	14.42	14.37	15.65	14.54	14.31	14.35
Fe ₂ O ₃	6.89	7.19	5.92	9.34	7.78	7.27	6.60	6.71	9.01	7.17	6.49	6.50
MnO	0.24	0.24	0.22	0.21	0.25	0.25	0.24	0.25	0.25	0.24	0.23	0.23
MgO	1.28	1.71	1.21	3.41	2.03	1.62	1.30	1.42	3.52	1.56	1.25	1.34
CaO	4.31	4.84	4.23	6.98	5.19	4.83	4.28	4.32	6.68	4.72	4.17	4.15
Na ₂ O	4.66	4.96	4.86	3.98	4.56	4.84	4.94	5.05	3.92	4.70	4.85	4.85
K ₂ O	0.97	0.90	0.97	0.63	0.81	0.87	0.91	0.93	0.64	0.84	0.94	0.93
P ₂ O ₅	0.27	0.24	0.29	0.20	0.23	0.22	0.25	0.24	0.19	0.25	0.26	0.25
Total	100.00	100.01	100.00	100.00	100.00	100.01	100.00	99.99	100.00	99.99	100.00	100.01
LOI	-0.20	-0.09	0.54	0.00	0.09	-0.13	-3.07	0.12	-0.30	-0.24	-0.22	-0.13
Sc		27.1			29.8	28.2	24.6		32.7	28.2	25.2	25.1
Cr		5.1			8.9	3.15	<dl		10.1	2.90	5.1	1.93
Co		11.1			43	10.0	8.6		21.1	10.4	13.3	25.0
Zn	98	103	110	92	105	104	101	105	102	98	93	95
Cu	10	16	11	27	18	21	15	13	33	11	10	8
Rb	25	26	28	18	25	26	25	27	21	21	25	22
Sr	171	180	173	184	184	183	178	180	195	183	175	167
Ba	257	230	254	178	212	231	255	251	174	239	254	258
Pb	8	11	11	9	12	11	11	12	8	10	10	9
Cs		1.68		1.14	1.24	1.84	0.64		1.13	0.57	0.76	<dl
La		12.4		7.2	10.5	10.8	13.4		7.7	12.0	13.2	13.6
Ce		25.3		18.5	22.6	25.9	28.5		19.3	27.9	29.1	27.8
Pr				2.92					2.92			
Nd				14.4					14.1			
Sm		6.1		4.48	5.4	6.0	6.3		4.40	6.1	6.6	7.1
Eu		1.80		1.45	1.70	1.85	1.88		1.45	1.85	1.85	1.81
Gd				5.5					5.4			
Tb		1.23		0.90	1.15	1.12	1.24		0.92	1.19	1.23	1.15
Dy				6.6					6.8			
Ho				1.50					1.53			
Er				4.53					4.45			
Tm				0.60					0.62			
Yb		5.6		4.34	4.60	5.1	5.1		4.45	5.5	5.8	6.1
Lu				0.69					0.69			
Y	51	51	55	40	46	50	51	54	38	49	53	51
Nb	4.36	2.91	4.49	3.84	2.96	4.07	2.91	4.35	4.00	3.83	4.45	4.26
Zr	159	146	155	109	138	145	149	152	111	143	157	151
Hf		4.10			3.88	4.07	4.39		3.16	4.26	4.63	4.43
Ta		<dl			<dl	<dl	<dl		<dl	<dl	0.30	0.30
Th		2.54			2.30	2.38	2.50		1.26	2.51	2.68	2.87
U		<dl			<dl	1.21	<dl		<dl	<dl	<dl	<dl

Appendix 4. Major- and trace-element data of the Banda Arc volcanoes

No	13	14	15	16	17	18	19	20	21	22	23	24
Island	BA	BA	BA	BA	BA	BA	BA	BA	BA	BN	BN	BN
Sample	17	19	20A	21A	23	24A	25A	26	27A	1A2	1C4	2A1
SiO ₂	67.05	64.22	64.44	67.36	64.09	64.21	63.09	63.17	66.24	64.22	63.96	65.67
TiO ₂	0.96	0.99	0.98	0.90	0.97	0.96	1.06	1.06	1.01	1.06	1.06	0.98
Al ₂ O ₃	14.19	14.80	14.56	13.94	15.13	15.28	14.73	14.82	14.22	14.69	14.70	15.11
Fe ₂ O ₃	6.36	7.14	7.27	6.21	7.14	6.99	7.84	7.72	6.49	7.32	7.47	6.05
MnO	0.23	0.24	0.24	0.23	0.25	0.25	0.25	0.25	0.24	0.26	0.26	0.25
MgO	1.21	1.72	1.76	1.12	1.66	1.65	2.04	2.07	1.34	1.63	1.73	1.35
CaO	3.97	5.02	4.91	3.83	4.81	4.69	5.39	5.36	4.24	4.81	4.84	4.31
Na ₂ O	4.81	4.80	4.70	5.13	4.79	4.85	4.57	4.55	5.02	4.88	4.87	5.13
K ₂ O	0.96	0.84	0.89	1.02	0.91	0.90	0.80	0.79	0.95	0.90	0.90	0.90
P ₂ O ₅	0.25	0.23	0.25	0.25	0.24	0.23	0.22	0.22	0.24	0.24	0.22	0.23
Total	99.99	100.00	100.00	99.99	99.99	100.01	99.99	100.01	99.99	100.01	100.01	99.98
LOI	0.00	-0.02	-0.05	-0.15	0.42	0.02	-0.13	-0.30	0.09	0.08	0.23	0.28
Sc		28.3	26.6		25.1		30.8		24.6	28.4		
Cr		7.0	4.44		4.44		11.2		2.27	2.71		
Co		38	12.0		34		40		22.3	11.1		
Zn	92	104	102	97	97	102	103	102	95	110	108	97
Cu	11	17	19	10	12	15	18	19	10	14	14	6
Rb	26	25	27	26	27	23	24	22	26	27	27	26
Sr	166	178	177	163	190	192	182	191	171	197	196	212
Ba	263	218	232	276	235	243	207	214	256	237	226	245
Pb	11	9	12	10	10	9	9	10	10	9	10	7
Cs		1.63	1.43		1.60		<dl		1.42	1.69		
La		12.5	12.4		12.8		10.5		13.9	13.1		
Ce		27.5	25.9		27.0				23.3	28.3		
Pr												
Nd												
Sm		6.3	5.9		5.7		5.6		6.8	5.6		
Eu		1.70	1.72		1.81				1.91	1.82		
Gd												
Tb		1.06	1.24		1.22				1.23	1.07		
Dy												
Ho												
Er												
Tm												
Yb		5.6	4.96		4.84		5.3		5.5	4.89		
Lu												
Y	52	49	51	54	49	50	46	46	51	46	47	46
Nb	3.96	3.06	4.37	3.28	4.60	3.90	2.78	3.05	3.46	2.54	4.42	3.35
Zr	161	139	148	167	144	143	130	135	152	130	132	131
Hf		4.00	4.06		4.40		4.20		4.38	3.68		
Ta		0.63	0.24		0.43		<dl		0.46	<dl		
Th		2.23	2.41		2.57		2.34		2.84	3.18		
U		<dl	<dl		<dl		<dl		<dl	<dl		

Appendix 4. Major- and trace-element data of the Banda Arc volcanoes

No	25	26	27	28	29	30	31	32	33	34	35	36
Island	BN	BN	BN	BN	BN	BN	BN	BN	BB	BB	BB	BB
Sample	3A2	4A1	6A1	6A11	7A	9A	10A1	11D	21A3	22	26	28
SiO ₂	50.99	53.70	62.12	62.25	62.30	55.26	59.54	51.44	52.24	55.10	52.09	54.15
TiO ₂	1.02	1.21	1.07	1.08	1.11	1.23	1.26	1.06	1.14	1.31	1.20	1.26
Al ₂ O ₃	18.21	17.92	15.18	15.17	15.14	16.65	15.49	18.07	18.69	16.35	17.71	18.05
Fe ₂ O ₃	10.59	10.46	8.14	8.08	8.11	10.44	9.48	10.73	10.58	11.65	11.32	10.03
MnO	0.23	0.23	0.25	0.25	0.26	0.24	0.23	0.30	0.23	0.27	0.23	0.23
MgO	5.14	3.27	2.09	2.02	2.06	3.50	2.59	4.68	3.66	3.19	4.02	3.27
CaO	10.50	9.35	5.56	5.58	5.47	8.34	6.22	10.56	9.93	8.04	10.18	9.23
Na ₂ O	2.80	3.15	4.60	4.58	4.52	3.52	4.09	2.72	3.00	3.36	2.77	3.30
K ₂ O	0.38	0.53	0.80	0.80	0.80	0.65	0.86	0.29	0.39	0.55	0.35	0.36
P ₂ O ₅	0.14	0.19	0.19	0.19	0.22	0.17	0.26	0.15	0.14	0.18	0.12	0.14
Total	100.00	100.01	100.00	100.00	99.99	100.00	100.02	100.00	100.00	100.00	99.99	100.02
LOI	-0.35	-0.38	-0.23	-0.23	-0.22	-0.26	0.73	0.91	0.01	0.33	0.11	0.35
Sc	40.3				31	40		40	37	40	43	41
Cr	42.4				4.06	14.2		40	15.8	9.4	19.4	6.7
Co	32.8				31.3	26.4		32	28.3	42	31	44
Zn	86	95	98	100	96	95	102	84	87	111	92	100
Cu	77	54	21	16	16	38	32	68	79	68	56	61
Rb	12	14	22	22	20	19	24	13	11	12	10	11
Sr	270	237	209	208	204	244	217	267	209	193	205	233
Ba	82	125	212	213	215	154	211	77	109	156	102	110
Pb	9	5	9	9	8	16	8	3	5	7	3	6
Cs	0.23				<dl	0.48		<dl	0.46	0.69	<dl	0.55
La	5.2				10.9	8.5		6.2	4.66	8.3	4.52	6.6
Ce	12.5				24.6	20.3		13.6	12.2	16.7	12.7	14.2
Pr	1.81					2.85			1.94			
Nd	9.5					14.0			11.1			
Sm	2.82				4.36	4.06		2.68	3.61	4.84	3.91	3.36
Eu	1.04				1.76	1.38		1.03	1.21	1.61	1.24	1.30
Gd	3.33					4.85			4.44			
Tb	0.57				0.96	0.79		0.52	0.78	1.06	0.80	0.79
Dy	3.97					5.6			5.6			
Ho	0.85					1.22			1.23			
Er	2.61					3.48			3.55			
Tm	0.35					0.46			0.50			
Yb	2.49				4.30	3.60		2.44	3.36	4.35	3.33	3.02
Lu	0.37					0.52			0.49			
Y	24	32	42	41	41	33	43	23	34	50	33	30
Nb	<dl	<dl	2.91	2.36	2.94	<dl	2.69	<dl	<dl	<dl	<dl	2.03
Zr	65	90	120	121	118	100	126	65	89	114	85	81
Hf	1.65				3.49	2.69		1.74	2.48	2.97	2.26	2.09
Ta	<dl				0.36	0.26		<dl	<dl	0.18	<dl	<dl
Th	1.13				2.66	2.08		1.01	1.02	1.42	0.84	1.07
U	<dl					1.23		<dl	<dl	<dl	<dl	3.87

Appendix 4. Major- and trace-element data of the Banda Arc volcanoes

No island Sample	37 BL 1B	38 BL 3	39 BL 5	40 BL 7A1	41 BL 8	42 BL 10	43 BL 13	44 MA 1A	45 MA 1B	46 MA 2A	47 MA 2B	48 MA 2C	
SiO ₂	69.52	61.19	68.39	55.29	61.43	51.41	55.27	57.77	57.77	54.68	58.19	57.07	
TiO ₂	0.50	1.04	0.56	1.30	0.99	1.08	1.33	1.00	0.78	0.82	0.76	0.77	
Al ₂ O ₃	14.71	17.38	14.62	16.89	16.23	20.06	16.11	17.47	17.47	18.01	17.00	17.66	
Fe ₂ O _{3t}	4.91	6.65	4.65	10.61	8.07	10.13	11.67	7.78	7.41	8.08	7.05	7.43	
MnO	0.19	0.23	0.22	0.25	0.21	0.19	0.28	0.20	0.18	0.19	0.18	0.18	
MgO	0.64	1.63	1.12	2.98	2.13	3.47	3.34	3.36	3.76	5.08	3.60	4.25	
CaO	3.03	6.25	3.12	8.27	5.54	10.16	7.69	7.16	7.96	9.21	7.70	8.01	
Na ₂ O	5.53	4.31	6.08	3.85	4.75	3.02	3.58	3.82	3.49	2.94	4.04	3.47	
K ₂ O	0.83	1.07	1.08	0.42	0.56	0.37	0.50	1.28	1.06	0.86	1.36	1.07	
P ₂ O ₅	0.13	0.25	0.17	0.14	0.09	0.10	0.22	0.17	0.12	0.12	0.12	0.11	
Total	99.99	100.00	100.01	100.00	100.00	99.99	99.99	100.01	100.00	99.99	100.00	100.02	
LOI	0.29	1.15	7.07	0.36	0.00	0.39	0.28	0.39	0.40	-0.10	4.17	0.10	
Sc	20.5	24.9	19.5	44.0				42.6	26.6		31.3	24.5	27.1
Cr	<dl	2.89	1.40	3.60			4.42	34		82	35	60	
Co	16.8	9.9	36	24.7				19.3		28.5	19.7	25.4	
Zn	90	95	105	109	114	84	134	80	74	74	77	68	
Cu	9	14	8	74	26	102	97	47	51	56	72	48	
Rb	17	29	20	10	14	10	17	44	40	32	43	40	
Sr	140	226	143	207	200	224	229	227	211	220	215	216	
Ba	251	218	226	112	165	108	157	274	235	187	260	234	
Pb	8	13	8	12	10	2	13	13	10	12	6	13	
Cs	0.43	1.78	1.53	0.64			0.96	1.47		2.14	3.21	2.24	
La	10.5	11.6	9.8	5.6			8.9	13.1		9.8	12.0	11.6	
Ce	24.4	24.4	20.6	12.1			17.7	27.6		20.9	24.4	26.4	
Pr								3.53					
Nd								15.3					
Sm	5.7	5.6	4.93	3.55			4.41	3.94		3.33	3.10	3.76	
Eu	1.80	1.94	1.78	1.38			1.49	1.25		1.08	0.97	1.11	
Gd								4.29					
Tb	1.24	1.29	1.14	0.74			0.96	0.70		0.73	0.69	0.68	
Dy								4.95					
Ho								1.12					
Er								3.26					
Tm								0.44					
Yb	5.7	4.57	5.1	3.47			4.00	3.25		2.48	2.74	2.80	
Lu								0.50					
Y	51	45	46	35	39	25	37	31	28	24	28	27	
Nb	2.03	<dl	2.76	<dl	<dl	<dl	<dl	3.07	3.66	2.46	3.35	4.12	
Zr	142	126	132	82	102	80	105	134	123	112	129	131	
Hf	4.15	3.64	3.76	2.23			2.89	3.63		2.74	3.13	3.22	
Ta	0.21	<dl	<dl	<dl			<dl	0.37		<dl	0.25	<dl	
Th	1.34	1.83	1.71	1.69			1.64	4.26		3.10	3.63	3.92	
U	<dl	<dl	<dl	<dl			<dl	<dl		<dl	6.62	<dl	

Appendix 4. Major- and trace-element data of the Banda Arc volcanoes

No	49	50	51	52	53	54	55	56	57	58	59	60
Island	MA	MA	MA	MA	MA	MA	MA	MA	MA	MA	MA	MA
Sample	2D	2E	2F	3A2	3B	3C2	3C4	4A1	4B	5A	5B	6A1
SiO ₂	56.63	57.49	56.50	55.31	55.54	55.54	55.65	56.53	56.72	55.29	55.27	56.35
TiO ₂	0.76	0.76	0.91	0.83	0.82	0.83	0.81	0.83	0.83	0.82	0.83	0.80
Al ₂ O ₃	17.64	17.50	17.98	17.95	17.86	18.05	17.83	17.60	17.62	17.90	17.91	17.45
Fe ₂ O ₃	7.80	7.39	8.41	8.00	7.79	7.74	7.88	7.66	7.55	7.97	7.95	7.70
MnO	0.17	0.17	0.20	0.18	0.18	0.18	0.18	0.18	0.19	0.19	0.18	0.19
MgO	4.42	4.01	3.57	4.80	4.83	4.65	4.77	4.48	4.40	4.78	4.75	4.97
CaO	8.09	8.01	7.86	8.73	8.79	8.77	8.78	8.25	8.22	8.75	8.80	8.15
Na ₂ O	3.39	3.47	3.50	3.14	3.13	3.18	3.04	3.34	3.34	3.21	3.25	3.17
K ₂ O	0.99	1.07	0.93	0.95	0.93	0.93	0.93	1.02	1.02	0.95	0.94	1.10
P ₂ O ₅	0.11	0.13	0.14	0.12	0.12	0.12	0.11	0.12	0.12	0.14	0.12	0.13
Total	100.00	100.00	100.00	100.01	99.99	100.01	99.98	100.01	100.01	100.00	100.00	100.01
LOI	0.41	0.14	0.27	0.16	0.28	0.13	0.20	0.08	-0.06	0.17	0.29	0.72
Sc		26.2					30.0			27.8	31	29.1
Cr		53					82			68	91	82
Co		22.1					26.0			46	62	24.4
Zn	55	72	76	72	72	73	68	73	75	73	73	72
Cu	35	45	24	56	55	57	69	60	53	55	55	46
Pb	23	40	33	36	36	34	34	38	39	36	35	37
Sr	207	222	216	215	217	221	210	213	217	219	218	224
Ba	217	222	220	212	210	208	226	224	230	211	212	233
Pb	5	14	10	11	12	11	8	13	11	12	13	10
Cs		2.87					2.46		2.61	2.13	2.45	
La		12.0					10.4		11.9	9.3	10.4	
Ce		22.2					24.5		22.8	20.2	22.3	
Pr										2.65		
Nd										11.8		
Sm		3.45					3.25		3.30	3.25	3.01	
Eu		1.05					1.05		1.05	1.01	1.02	
Gd										3.67		
Tb		0.75				0.75			0.62	0.61	0.79	
Dy										4.32		
Ho										0.98		
Er										2.78		
Tm										0.37		
Yb		2.70					2.82		2.81	2.72	2.72	
Lu										0.42		
Y	28	27	28	26	25	25	25	28	27	26	26	26
Nb	<dl	3.25	2.51	2.32	<dl	3.03	2.07	3.36	3.37	<dl	3.41	2.21
Zr	121	122	115	122	120	120	120	131	121	121	122	124
Hf		3.04				2.89			3.06	2.85	2.87	
Ta		<dl				<dl			0.50	<dl	<dl	
Th		3.75				3.63			3.53	3.69	3.18	
U		<dl				<dl			1.17	1.11	0.60	

Appendix 4. Major- and trace-element data of the Banda Arc volcanoes

No	73	74	75	76	77	78	79	80	81	82	83	84
Island	SE	SE	SE	SE	SE	SE	SE	SE	SE	SE	SE	SE
Sample	10	11Sc	12A3	14A1	14A2	15B	16B	17	19	20	21A3	23A
SiO ₂	56.22	55.89	56.35	58.56	58.56	59.53	56.58	56.67	59.28	60.18	59.81	59.94
TiO ₂	0.70	0.71	0.70	0.67	0.67	0.67	0.71	0.70	0.61	0.62	0.65	0.61
Al ₂ O ₃	17.26	17.37	17.31	17.13	16.98	17.00	17.51	17.67	16.20	16.62	16.89	16.99
Fe ₂ O ₃	7.83	8.10	7.97	7.27	7.37	7.00	7.86	7.51	7.07	6.84	6.73	6.46
MnO	0.20	0.20	0.19	0.15	0.15	0.19	0.19	0.19	0.18	0.19	0.16	0.17
MgO	5.31	5.00	4.77	4.13	4.24	4.27	4.83	4.96	4.92	4.34	4.02	3.82
CaO	9.05	9.21	9.05	8.30	8.36	7.74	8.80	8.74	8.30	7.51	7.69	7.79
Na ₂ O	2.34	2.41	2.50	2.58	2.51	2.31	2.40	2.39	2.21	2.37	2.52	2.67
K ₂ O	1.02	1.03	1.08	1.18	1.16	1.21	1.06	1.10	1.18	1.28	1.45	1.46
P ₂ O ₅	0.08	0.08	0.08	0.03	0.03	0.08	0.08	0.08	0.05	0.06	0.08	0.08
Total	100.01	100.00	100.00	100.00	100.00	100.00	100.02	100.01	100.00	100.01	100.00	99.99
LOI	0.17	0.25	-0.05			0.46	0.23	0.74	0.25	0.61	1.47	0.51
Sc		35		31				34			27.1	26.6
Cr		73		55				64			45	64
Co		26.5		31				23.2			22.0	21.3
Zn	69	74	69	66	75	66	70	68	65	63	64	62
Cu	64	69	68	62	48	51	58	25	34	32	39	37
Rb	42	40	41	42	44	47	41	41	45	49	56	52
Sr	269	267	272	253	277	264	269	263	250	240	268	280
Ba	253	236	239	298	280	318	258	253	300	331	318	357
Pb	12	19	14	14	16	14	13	13	12	13	13	26
Cs		3.20		3.53				1.85			1.82	1.98
La		11.4		14.4				9.7			13.0	16.1
Ce		23.9		31.7				18.1			27.1	25.0
Pr											3.26	
Nd											13.3	
Sm		2.82		3.11				2.63			3.10	2.80
Eu		0.97		0.99				0.89			0.97	0.92
Gd											3.36	
Tb		0.61		0.54				0.58			0.55	0.53
Dy											3.97	
Ho											0.89	
Er											2.67	
Tm											0.35	
Yb		2.24		2.15				2.24			2.42	2.19
Lu											0.34	
Y	21	22	23	22	23	22	22	21	22	21	22	21
Nb	2.86	3.99	3.18	6.0	4.60	4.82	2.09	2.70	3.51	4.26	4.16	4.54
Zr	103	107	108	105	110	129	108	107	114	123	114	114
Hf		2.47		3.05				2.58			2.76	3.14
Ta		<dl		0.55				<dl			0.35	0.36
Th		4.10		4.48				3.95			5.1	5.5
U		0.70		1.34				1.52			1.25	<dl

Appendix 4. Major- and trace-element data of the Banda Arc volcanoes

No Island Sample	85 SE 24A	86 SE 25A	87 SE 26A	88 SE 27A	89 SE 28A	90 N 1A1	91 N 3A3	92 N 4A2	93 N 5A	94 N 5B	95 N 6	96 N 7A
SiO ₂	58.94	59.26	56.45	55.71	58.53	57.92	57.77	58.89	62.53	53.44	53.10	55.78
TiO ₂	0.67	0.69	0.69	0.70	0.67	0.62	0.71	0.60	0.53	0.75	0.81	0.62
Al ₂ O ₃	16.71	16.65	17.89	18.02	17.81	18.45	17.39	18.51	16.34	18.49	18.60	18.27
Fe ₂ O ₃ ^{tot}	7.28	7.18	7.71	8.25	7.07	7.14	8.40	6.82	6.36	9.35	9.49	7.65
MnO	0.19	0.19	0.18	0.17	0.16	0.16	0.22	0.15	0.17	0.22	0.22	0.16
MgO	4.46	4.24	4.58	4.74	3.79	3.08	3.13	2.67	2.37	4.44	4.48	3.93
CaO	8.35	8.25	8.76	8.73	7.52	7.61	7.71	6.69	5.81	9.15	9.22	8.41
Na ₂ O	2.11	2.27	2.50	2.52	2.84	2.76	2.86	3.09	3.16	2.41	2.79	2.77
K ₂ O	1.19	1.19	1.14	1.10	1.52	2.17	1.72	2.49	2.64	1.65	1.21	2.32
P ₂ O ₅	0.10	0.08	0.10	0.07	0.09	0.09	0.08	0.09	0.09	0.10	0.08	0.09
Total	100.00	100.00	100.00	100.01	100.00	100.00	99.99	100.00	100.00	100.00	100.00	100.00
LOI	0.60	0.47	0.16	0.62	1.01	1.69	0.66	1.12	1.27	0.81	0.68	0.47
Sc	29.8	30.0	32	32	27.8	24.2			17.5	33	36.1	
Cr	72	61	69	47	35	12.5			5.3	12.4	11.0	
Co	27.0	30	29.0	28.5	23.1	23.5			16.1	28.3	28.6	
Zn	72	72	72	80	74	65	71	54	61	75	65	63
Cu	17	39	46	46	45	59	56	43	38	32	71	74
Rb	44	44	45	47	62	87	71	95	118	62	41	91
Sr	266	266	279	279	260	368	275	336	317	406	422	415
Ba	277	283	256	262	345	742	524	767	880	489	542	689
Pb	15	12	13	11	20	30	18	18	28	14	21	25
Cs	3.42	2.67	1.68	1.70	3.58	7.1			12.8	6.2	3.78	
La	15.4	12.5	13.6	9.4	13.2	20.8			23.2	11.2	14.9	
Ce	27.7	26.7	21.9	20.0	22.0	38			33	24.3	31	
Pr		3.12		2.55		4.68						
Nd		12.8		10.9		18.3						
Sm	3.13	2.93	2.98	2.77	3.09	4.06			2.86	2.65	3.24	
Eu	0.96	0.95	0.86	0.87	0.88	1.11			0.75	0.86	1.12	
Gd		3.44		2.96		4.89						
Tb	0.76	0.56	0.44	0.50	0.50	0.70			0.49	0.52	0.67	
Dy		3.73		3.50		4.95						
Ho		0.83		0.76		1.11						
Er		2.51		2.18		3.14						
Tm		0.34		0.29		0.42						
Yb	2.13	2.49	2.30	2.02	2.14	3.02			2.10	1.86	2.38	
Lu		0.38		0.29		0.45						
Y	23	23	22	22	23	32	29	38	23	20	23	26
Nb	4.21	5.7	2.25	3.32	2.67	4.99	3.82	5.7	4.00	<dl	3.97	5.5
Zr	118	119	94	94	118	136	105	146	124	83	80	138
Hf	3.13	3.13	2.59	2.39	2.84	3.85			3.53	2.07	2.10	
Ta	<dl	<dl	0.25	0.41	<dl	<dl			0.36	<dl	0.54	
Th	4.51	4.41	4.47	4.22	5.2	9.0			12.8	4.76	5.7	
U	<dl	<dl	<dl	<dl	1.95	<dl			<dl	1.53	1.09	

Appendix 4. Major- and trace-element data of the Banda Arc volcanoes

No	97	98	99	100	101	102	103	104	105	106	107	108
Island	N	N	N	N	N	N	N	N	N	N	N	N
Sample	7B	9A	10A1	11	12	13	15I	15II	16	17A	18AI	18AII
SiO ₂	56.77	57.68	57.47	57.85	58.67	57.08	57.43	54.30	59.57	57.80	51.93	56.87
TiO ₂	0.64	0.61	0.79	0.60	0.61	0.59	0.63	0.81	0.57	0.61	0.60	0.57
Al ₂ O ₃	17.78	17.68	18.61	18.21	18.61	17.29	17.61	18.01	17.27	18.38	18.09	17.35
Fe ₂ O _{3t}	7.69	7.31	7.84	6.96	6.57	7.91	8.09	9.62	7.41	7.05	9.37	8.05
MnO	0.17	0.16	0.19	0.16	0.16	0.19	0.19	0.23	0.18	0.17	0.20	0.19
MgO	3.41	3.45	2.24	3.01	2.57	3.80	3.49	4.17	3.02	3.01	5.39	3.79
CaO	7.90	7.88	7.60	7.73	7.34	8.50	7.98	8.62	6.75	7.59	11.07	8.56
Na ₂ O	3.02	2.92	2.99	2.95	2.92	2.53	2.60	2.81	2.88	2.94	2.07	2.58
K ₂ O	2.52	2.24	2.13	2.43	2.46	2.01	1.86	1.34	2.24	2.37	1.15	1.92
P ₂ O ₅	0.11	0.08	0.13	0.11	0.09	0.10	0.12	0.08	0.11	0.09	0.13	0.12
Total	100.01	100.01	99.99	100.01	100.00	100.00	100.00	99.99	100.00	100.01	100.00	100.00
LOI	0.65	0.60	0.33	0.25	1.04	0.37	0.07	0.13	0.44	0.43	0.56	0.83
Sc				25.4	23.0	27.9	26.8		22.2		39	28.4
Y				12.7	9.0	15.6	7.9		6.9		29.1	16.7
Co				26.5	22.1	25.9	25.9		20.8		37	26.7
Zn	62	59	82	60	62	71	66	72	65	70	73	69
Cu	53	54	55	59	55	51	23	107	102	57	72	59
Rb	99	87	87	101	100	81	76	47	94	94	46	81
Sr	393	356	354	381	369	392	397	426	358	374	432	388
Ba	772	683	567	817	740	604	620	523	732	730	322	578
Pb	18	10	31	14	18	23	17	32	45	24	14	24
Cs				3.18	4.29	7.6	2.28		4.03		4.08	7.2
La				23.1	22.7	16.5	15.4		22.3		11.7	14.6
Ce				39	38	26.7	25.1		41		28.1	25.7
Pr									4.18			2.89
Nd									15.6			11.6
Sm				4.04	3.95	2.75	2.43		3.22		2.28	2.51
Eu				1.01	1.08	0.84	0.75		1.08		0.84	0.83
Gd									4.09			2.97
Tb				0.87	0.60	0.59	0.45		0.52		0.44	0.42
Dy									3.57			2.94
Ho									0.77			0.64
Er									2.24			1.87
Tm									0.30			0.25
Yb				2.72	2.76	1.87	2.05		2.24		1.41	1.88
Lu									0.34			0.28
Y	31	27	32	33	36	20	20	29	24	40	16	20
Nb	7.1	4.11	4.95	5.7	4.87	4.60	3.46	3.32	5.1	6.7	2.86	3.87
Zr	148	132	128	127	132	96	96	73	113	139	63	96
Hf				3.86	3.78	2.38	2.60		3.00		1.63	2.69
Ta				0.44	0.40	<dl	0.29		0.35		<dl	<dl
Th				8.8	8.6	8.9	8.8		10.4		4.40	8.5
U				3.91	<dl	1.86	3.27		4.03		<dl	
	<dl											

Appendix 4. Major- and trace-element data of the Banda Arc volcanoes

No Island Sample	109 TE 1A	110 TE 1B1	111 TE 1B2	112 TE 1C	113 TE 2A	114 TE 2B1	115 TE 2B2	116 TE 3A	117 TE 3C	118 TE 3D	119 TE 4B	120 TE 5
SiO ₂	58.90	60.10	54.08	59.94	57.59	53.30	54.79	59.66	59.60	58.53	57.86	60.23
TiO ₂	0.55	0.52	0.79	0.54	0.64	0.91	0.73	0.51	0.53	0.63	0.62	0.52
Al ₂ O ₃	18.45	17.95	19.10	17.98	18.38	18.40	18.79	17.50	17.85	18.88	18.32	17.94
Fe ₂ O ₃ ^{tot}	7.14	6.34	8.20	6.45	7.03	8.45	7.23	6.51	6.41	6.49	7.17	6.31
MnO	0.18	0.17	0.18	0.18	0.17	0.18	0.16	0.14	0.13	0.16	0.17	0.14
MgO	2.81	2.68	4.22	2.63	3.23	5.52	5.14	2.63	2.64	2.62	3.23	2.55
CaO	6.85	6.66	8.98	6.60	7.50	8.98	8.90	6.67	6.74	6.88	7.49	6.57
Na ₂ O	3.17	3.34	2.93	3.43	3.19	2.71	2.58	4.15	3.86	3.34	3.11	3.59
K ₂ O	1.82	2.12	1.42	2.12	2.10	1.47	1.59	2.19	2.22	2.30	1.89	2.14
P ₂ O ₅	0.13	0.14	0.10	0.14	0.17	0.09	0.08	0.03	0.02	0.16	0.13	0.01
Total	100.00	100.02	100.00	100.01	100.00	100.01	99.99	99.99	100.00	99.99	99.99	100.00
LOI	1.26	0.42	0.30	0.49	0.07	1.16	0.43			0.98	0.09	
Sc			44	15.8	21.8	52		14.2	13.7			14.4
Cr			6.8	7.1	16.1	35		5.4	6.3			4.03
Co			26.7	17.5	19.7	28.7		20.6	46			20.1
Zn	75	66	69	67	68	72	62	67	69	70	67	68
Cu	20	42	89	41	39	95	47	37	37	52	47	33
Rb	61	78	48	76	73	47	54	80	74	81	65	78
Sr	531	542	596	542	531	497	485	521	516	508	528	534
Ba	697	777	529	763	705	530	579	846	815	711	655	842
Pb	21	27	17	27	24	25	18	28	27	34	17	27
Cs			3.32	5.2	3.26	3.99		5.7	5.7			5.4
La			27.6	32	35	22.2		33	32			34
Ce			52	56	52	40		64	59			59
Pr				6.0								
Nd				21.4								
Sm			6.5	4.06	4.19	3.98		4.18	3.85			4.21
Eu			1.52	1.19	1.12	0.99		1.12	1.06			1.09
Gd				4.07								
Tb			1.31	0.49	0.47	0.56		0.73	0.44			0.52
Dy				3.20								
Ho				0.70								
Er				2.05								
Tm				0.27								
Yb			3.49	2.04	1.61	2.19		1.78	1.86			1.64
Lu				0.30								
Y	27	21	36	22	24	22	22	20	20	24	22	21
Nb	6.8	10.5	9.4	9.7	7.5	3.85	5.8	10.3	9.8	10.4	7.3	9.5
Zr	113	135	102	137	116	97	103	123	120	141	120	127
Hf			3.22	3.75	3.32	2.56		3.72	3.48			3.68
Ta			0.48	0.55	0.49	0.49		0.54	0.53			0.66
Th			6.7	12.2	10.4	7.0		11.6	11.0			10.7
U			<dl	1.74	4.11	<dl		<dl	1.26			2.23

Appendix 4. Major- and trace-element data of the Banda Arc volcanoes

No Island Sample	121 TE 11	122 TE 12	123 TE 14A	124 TE 14B	125 TE 15	126 DA 1	127 DA 2	128 DA 3	129 DA 4	130 DA 5	131 DA 6	132 DA 7
SiO ₂	60.66	59.45	60.16	57.49	58.43	56.67	57.22	56.55	52.86	59.88	56.16	55.39
TiO ₂	0.50	0.54	0.51	0.64	0.54	0.69	0.63	0.60	0.60	0.69	0.66	0.66
Al ₂ O ₃	17.86	17.99	18.27	18.88	18.59	17.58	17.53	17.77	18.98	16.97	17.78	18.22
Fe ₂ O ₃	6.30	6.81	6.13	6.90	6.79	8.11	7.63	7.53	8.43	7.65	8.06	8.30
MnO	0.16	0.19	0.17	0.17	0.17	0.19	0.17	0.18	0.18	0.20	0.18	0.20
MgO	2.39	2.83	2.59	3.24	2.85	3.50	3.57	3.90	4.96	2.65	3.82	3.84
CaO	6.52	6.84	6.59	7.34	7.36	7.76	7.66	8.00	9.62	5.94	8.11	8.37
Na ₂ O	3.32	3.22	3.38	3.23	3.18	2.64	2.85	2.95	2.24	3.38	2.70	2.74
K ₂ O	2.14	1.98	2.09	1.97	1.93	2.70	2.60	2.41	2.04	2.51	2.37	2.16
P ₂ O ₅	0.15	0.15	0.12	0.13	0.15	0.14	0.14	0.12	0.09	0.13	0.15	0.14
Total	100.00	100.00	100.01	99.99	99.99	99.98	100.00	100.01	100.00	100.00	99.99	100.02
LOI	0.39	0.30	0.81	1.02	0.15	0.67	0.07	0.90	1.10	1.92	0.79	0.62
Sc	14.2			22.0	17.6		26.1	25.8	29.8	23.1	26.2	
Cr	5.5			10.6	5.3		11.1	11.3	15.7	4.98	10.6	
Co	15.7			17.0	16.9		24.4	26.8	33	19.7	26.4	
Zn	64	62	67	68	67	68	63	67	65	61	67	73
Cu	28	48	46	50	43	32	56	34	41	66	50	44
Rb	77	74	77	71	68	93	98	94	74	90	87	81
Sr	526	526	550	529	539	526	573	595	632	351	593	644
Ba	761	752	772	704	695	976	1040	981	978	840	972	937
Pb	21	14	31	27	23	30	26	29	25	21	30	28
Cs	2.90	2.51		4.81	3.01	6.1	6.2	6.6	4.50	3.04	6.4	
La	34	28.4		27.7	29.3	40	48	45	35	34	45	
Ce	57	51		50	50	70	75	71	59	60	68	
Pr		5.6		5.6	5.8	7.5			6.3			
Nd		19.9		20.6	20.9	25.6			22.7			
Sm	3.78	3.87		4.02	4.28	4.92	5.4	4.81	4.24	4.70	4.80	
Eu	1.04	1.09		1.26	1.18	1.39	1.23	1.29	1.20	1.16	1.23	
Gd		3.61		4.04	4.25	5.3			4.45			
Tb	0.49	0.48		0.54	0.57	0.67	0.64	0.79	0.52	0.67	0.77	
Dy		3.23		3.70	3.78	4.42			3.60			
Ho		0.68		0.79	0.78	0.88			0.72			
Er		1.90		2.24	2.16	2.60			1.96			
Tm		0.26		0.30	0.29	0.35			0.26			
Yb	1.95	1.88		2.20	2.09	2.54	2.05	2.31	1.89	2.89	2.09	
Lu		0.30		0.33	0.31	0.39			0.28			
Y	21	21	21	22	23	26	26	25	22	30	24	24
Nb	10.0	8.9	8.8	8.5	8.1	9.1	9.2	8.8	8.3	7.2	8.0	7.8
Zr	127	120	138	123	109	125	126	112	93	138	117	100
Hf	3.52			3.42	3.18		3.47	3.31	2.75	3.81	3.22	
Ta	0.75			0.46	0.43		0.72	0.49	0.29	0.55	0.58	
Th	11.0			10.4	9.8		21.9	18.8	16.4	13.2	18.2	
U	1.13			1.70	1.61		6.1	4.67	3.53	2.45	3.53	

Appendix 4. Major- and trace-element data of the Banda Arc volcanoes

No Island Sample	133 DA 8	134 DA 9A	135 DA 9B	136 RO 2	137 RO 7B	138 RO 7C2	139 RO 8B	140 RO 8C6	141 RO 8E	142 WE 1A1	143 WE 1H	144 TI TTVF
SiO ₂	57.45	56.19	56.63	58.93	57.61	57.47	59.95	71.61	72.16	71.15	72.90	53.25
TiO ₂	0.69	0.66	0.66	0.58	0.58	0.60	0.66	0.44	0.35	0.29	0.29	1.14
Al ₂ O ₃	17.67	18.08	17.69	16.34	18.52	19.14	18.00	15.20	14.25	14.74	14.32	16.25
Fe ₂ O ₃	8.22	7.94	8.16	6.89	6.80	6.15	5.58	2.28	2.52	2.51	2.85	10.56
MnO	0.20	0.18	0.18	0.15	0.15	0.12	0.13	0.03	0.08	0.06	0.05	0.18
MgO	3.73	3.82	3.75	4.63	3.76	3.71	3.23	0.31	0.41	1.09	0.75	5.74
CaO	7.25	7.94	7.83	7.74	8.33	8.38	7.31	2.15	1.83	0.66	1.99	9.65
Na ₂ O	2.62	2.67	2.56	2.64	2.54	2.68	2.95	4.07	4.04	3.06	3.66	2.54
K ₂ O	2.08	2.37	2.39	2.04	1.64	1.69	2.11	3.85	4.33	6.28	3.11	0.60
P ₂ O ₅	0.09	0.14	0.14	0.06	0.06	0.07	0.08	0.06	0.04	0.16	0.07	0.08
Total	100.00	99.99	99.99	100.00	99.99	100.01	100.00	100.00	100.01	100.00	99.99	99.99
LOI	1.79	1.11	1.15	1.15	0.83	0.44	1.59	0.62	3.90	1.94	1.32	5.53
Sc	27.1			26.8	32	31	24.0	9.5	9.1	7.5		36
Cr	18.1			61	23.3	20.0	31	2.78	2.49	12.9		115
Co	25.4			23.5	29.6	25.2	18.8	4.37	32	7.7		32
Zn	69	71	68	67	68	69	67	41	58	41	31	90
Cu	32	67	48	58	24	19	46	10	12	5	7	54
Rb	78	88	90	77	57	60	81	141	147	226	78	12
Sr	333	601	580	320	309	313	368	227	182	49	97	148
Ba	867	978	985	452	313	338	592	853	902	491	570	67
Pb	29	28	31	26	17	14	35	28	50	5	7	8
Cs	4.78			4.62	1.75	1.73	4.44	5.1	7.3	1.66		<dl
La	30.0			23.8	16.6	17.5	29.3	40	38	18.8		4.61
Ce	52			41	38	38	53	76	75	41		10.5
Pr	6.1			5.20				8.7				
Nd	24.3			19.7				32				
Sm	5.1			4.00	3.57		3.55	6.7	5.9	4.04		2.56
Eu	1.43			1.04	0.85		0.94	1.51	1.03	0.73		0.94
Gd	5.8			4.30				6.6				
Tb	0.84			0.59	0.70		0.52	0.88	0.66	0.43		0.53
Dy	5.6			4.09				5.7				
Ho	1.22			0.86				1.17				
Er	3.59			2.44				3.16				
Tm	0.48			0.33				0.42				
Yb	3.52			2.37	2.06	2.04	2.23	2.94	3.22	1.18		2.34
Lu	0.55			0.36				0.45				
Y	37	24	25	25	21	22	26	35	37	23	24	22
Nb	6.3	8.3	7.6	12.1	11.1	12.0	14.4	20.1	20.9	12.8	10.3	3.85
Zr	120	107	118	121	103	106	129	200	206	99	137	75
Hf	3.03			3.06	2.97		2.87	6.1	5.9	2.98		1.64
Ta	0.62			0.99	1.13		1.09	1.54	1.84	1.77		<dl
Th	11.4			7.9	6.5	6.6	10.4	17.8	17.7	10.9		0.72
U	3.57			2.58	2.18	2.61	2.86	5.3	5.0	2.20		<dl

APPENDIX 5

**TRACE-ELEMENT DATA OF EAST INDONESIAN
SEDIMENTS**

Trace-element, carbonate and organic-carbon data of East Indonesian Sediments. Track codes: Track I=G5-2, Track II=G5-4 and Track III=G5-6 (see Appendix 1.2 for sample locations). Types: T=Trip core, B=Box core, P=Piston core, D=DSDP Site 262 sample. The elements Zn, Cu, Rb, Sr, Ba, Pb, Y, Nb, Zr were determined by XRF; Sc, Cr, Co, Cs, La, Ce, Sm, Eu, Yb, Lu, Hf, Th and U were obtained by INAA. Complete REE sets are determined by ICP-MS, in that case the reported value for Cs was also determined by ICP-MS. Carbonate and organic carbon contents are reported in wt.%, all other values in ppm; <dl=below detection limit. See Appendix 3 for analytical techniques.

Appendix 5. Trace-element data of East-Indonesian sediments

No	1	2	3	4	5	6	7	8	9	10	11	12
Track	MB-1	MB-7	G5-1	G5-1	G5-2	G5-2	G5-2	G5-2	G5-2	G5-2	G5-2	G5-2
Sample	1	7	2	2	4	5	6	7	8	9	10	12
Type	B	B	T	P	B	B	B	B	B	B	B	B
Depth (cm)			40	0-350	4-10						1-5	1-9
CaCO ₃	9.7	36.1	1.7	13.0	30.3	33.7	20.5	16.5	11.7	22.7	19.8	47.8
Organic-C	1.44	1.09		1.02								
Sc			18.4	13.5	21.3	19.8	21.9		24.0		22.9	10.0
Cr			114	99	13.7	9.5	21.8		10.9		11.2	10.7
Co			28.6	22.9	7.6	8.8	8.5		8.6		8.8	5.3
Zn			137	104	79	83	80	95	89		88	49
Cu			68	64	14.1	18.9	18.1	18.4	16.8		14.8	18.4
K			23200	17600	3800	4200	3800	5600	6600		7200	5000
Rb			121	90	8.9	11.5	9.1	17.8	22.1		25.3	10.6
Sr			163	344	1466	1346	1383	655	503		520	1878
Ba			866	667	129	139	134	181	260		295	128
Pb			30	19	6.8	6.1	6.7	6.1	6.2		6.8	2.02
Cs	5.6	3.89	8.5	6.6	0.63	1.12	1.36		1.95		2.46	1.57
La	20.4	15.1	32	25.0	7.4	7.3	9.0		12.6		13.3	7.5
Ce	42	29.4	73	52	20.5	16.2	20.9		25.8		29.2	13.4
Pr	4.85	3.39		5.8								
Nd	18.6	13.1		20.2								
Sm	3.66	2.56	5.8	4.14	3.94	3.41	4.15		5.1		5.3	2.32
Eu	0.95	0.63	1.00	1.07	1.28	1.15	1.40		1.62		1.58	0.67
Gd	3.66	2.43		4.18								
Tb	0.50	0.35	1.35	0.58	1.04	0.79	1.24		1.15		1.22	0.54
Dy	3.47	2.39		3.81								
Ho	0.74	0.51		0.79								
Er	2.11	1.47		2.38								
Tm	0.29	0.20		0.32								
Yb	2.15	1.39	0.67	2.20	3.33	3.10	3.70		4.45		4.38	1.92
Lu	0.34	0.22	0.28	0.33	0.65	0.59	0.71		0.81		0.82	0.36
Y			27.3	21.3	32	27.4	31	37	38		39	15.1
Nb			9.7	8.1	<dl	<dl	<dl	<dl	<dl		2.32	<dl
Zr			126	91	68	64	73	109	118		117	14.1
Hf			3.26	2.66	2.64	2.43	3.00		3.47		3.81	1.53
Ta			0.72	0.57	<dl	<dl	0.17		<dl		0.17	<dl
Th			12.5	9.2	1.62	1.61	1.78		2.74		2.85	1.54
U			2.89	4.19	<dl	2.08	<dl		2.12		<dl	1.30

Appendix 5. Trace-element data of East-Indonesian sediments

No	13	14	15	16	17	18	19	20	21	22	23	24
Track	G5-2	G5-2	G5-2	G5-2	G5-2	G5-2	G5-2	G5-2	G5-2	G5-2	G5-2	G5-2
Sample	14	17	19	20	22	24	25	26	28	30	34	35
Type	B	B	B	B	B	B	B	B	B	B	B	B
Depth (cm)	1-3	1-5	1-4	1-3	2.5-5.5	1.0-2.5	13-15	1-7	2-5	1-5	2-4	1-5
CaCO ₃	22.4	0.0	0.1	0.3	6.6	0.0	0.0	0.5	1.7	0.0	32.2	61.7
Organic-C	0.75		1.02			0.72					0.51	
Sc	17.6	25.1	20.8	26.0		17.2	18.9	17.9	17.5	15.7	11.3	6.3
Cr	47	61	67	65		72	70	103	73	63	48	34
Co	13.7	24.0	28.3	32		18.0	16.7	17.8	19.7	20.5	8.6	6.2
Zn	88	114	120	117	105	101	120	119	115	111	84	52
Cu	41	47	60	58	22.8	34	49	53	48	43	32	20.1
K	15900	15900	21900	18800	24100	28800	27300	26400	24800	22700	20000	12400
Rb	68	60	111	83	117	155	137	135	127	108	84	40
Sr	535	140	147	168	390	108	125	139	209	364	778	1175
Ba	633	427	903	599	467	460	674	844	799	723	458	182
Pb	13.4	18.1	23.8	19.9	15.4	25.6	17.3	19.3	18.8	17.3	10.9	7.3
Cs	5.6	5.1	8.4	6.0		9.1	9.3	8.7	<dl	7.8	6.5	3.24
La	25.0	15.1	32	25.3		34	33	31	35	32	24.0	13.4
Ce	50	33	71	56		73	80	67	74	67	48	26.0
Pr						8.2						
Nd						31						
Sm	4.86	3.54	5.7	5.1		5.7	6.3	4.86	5.6	5.2	3.82	2.21
Eu	1.18	1.19	1.20	1.40		1.46	1.40	1.24	1.14	1.16	0.85	0.48
Gd						5.9						
Tb	0.68	0.80	0.87	0.92		0.81	0.78	0.69	0.86	0.93	0.60	0.34
Dy						5.5						
Ho						1.16						
Er						3.47						
Tm						0.45						
Yb	2.72	2.37	2.93	3.06		3.35	3.08	2.10	2.94	2.96	2.19	1.17
Lu	0.54	0.47	0.60	0.54		0.52	0.46	0.48	0.63	0.57	0.36	0.20
Y	23.8	23.7	29.5	29.3	25.3	34	29.7	29.8	29.6	26.8	21.5	12.1
Nb	4.02	3.87	7.5	5.1	8.7	11.6	8.3	8.7	8.7	6.9	4.73	2.44
Zr	90	92	128	113	138	194	149	147	141	122	90	42
Hf	2.82	2.25	3.54	3.03		5.5	4.19	3.92	3.89	3.58	2.91	1.60
Ta	0.49	<dl	0.56	0.41		0.91	0.82	0.72	0.56	0.60	0.43	0.32
Th	7.4	5.1	10.5	7.4		14.1	12.9	9.4	11.0	9.5	7.3	3.95
U	<dl	1.21	2.27	<dl		3.33	4.39	3.40	2.55	2.23	2.71	1.20

Appendix 5. Trace-element data of East-Indonesian sediments

No	25	26	27	28	29	30	31	32	33	34	35	36
Track	G5-2	G5-2	G5-2	G5-2	G5-2	G5-2	G5-2	G5-2	G5-2	G5-2	G5-2	G5-2
Sample	36	37	38	40	43	45	46	47	49	50	51	52
Type	B	B	B	B	B	B	B	B	B	B	P	B
Depth (cm)	2-3	1-8	7-9	5-11	1-3	1-2	8-15	5-10	8-13	10-11	0-347	6-11
CaCO ₃	67.0	51.2	41.6	51.1	45.7	62.9	34.4	25.0	33.2	13.8	16.4	10.7
Organic-C				1.28		0.85					1.41	
Sc	4.31		10.5	6.3	5.8	6.0					14.6	13.4
Cr	24.8		72	38	41	35					85	73
Co	4.90		11.4	8.8	7.9	6.6					14.9	14.0
Zn	43	41	96	55	52	65	104	121	110	125	130	122
Cu	16.6	11.4	38	13.9	17.1	19.4	33	37	34	39	35	41
K	9000	9300	17300	13000	11800	12200	20400	22200	22400	24700	22800	24700
Rb	28.3	34	74	45	42	41	87	103	96	116	118	117
Sr	1408	860	759	1103	1273	963	704	568	632	459	441	377
Ba	87	81	120	266	264	196	507	603	527	595	539	619
Pb	4.58	6.4	13.7	7.0	4.61	5.8	12.4	12.1	12.4	16.5	20.6	18.0
Cs	2.41		7.0	3.44	3.27	3.34					9.0	7.6
La	11.1		21.2	17.2	13.2	13.1					27.8	26.5
Ce	21.1		46	36	28.5	23.2					60	54
Pr											6.3	
Nd											24.0	
Sm	1.79		3.26	2.92	1.87	2.01					4.39	4.57
Eu	0.43		0.73	0.69	0.57	0.46					1.10	0.92
Gd											4.45	
Tb	0.27		0.51	0.44	0.32	0.33					0.64	0.53
Dy											3.94	
Ho											0.80	
Er											2.34	
Tm											0.31	
Yb	0.97		1.63	1.21	1.17	1.06					2.28	2.03
Lu	0.17		0.28	0.23	0.25	0.16					0.35	0.34
Y	11.0	12.3	20.1	14.9	13.4	10.4	21.6	22.2	22.2	26.1	24.2	25.2
Nb	<dl	<dl	5.4	3.29	2.98	<dl	5.5	6.6	6.1	8.8	7.4	7.7
Zr	20.5	39	76	62	57	39	85	99	94	113	111	120
Hf	1.24		2.17	2.03	1.87	1.32					2.99	2.90
Ta	0.18		0.40	0.29	0.27	0.22					0.63	0.53
Th	3.03		6.6	4.91	4.29	3.79					10.5	9.4
U	1.39		5.2	2.65	1.92	1.41					4.81	1.93

Appendix 5. Trace-element data of East-Indonesian sediments

No	37	38	39	40	41	42	43	44	45	46	47	48
Track	G5-2	G5-2	G5-2	G5-2	G5-2	G5-2	G5-2	G5-2	G5-2	G5-2	G5-4	G5-4
Sample	56	58	60	61	62	63	64	65	66	68	69	69
Type	P	B	B	B	B	B	B	B	B	B	B	P
Depth (cm)	0-804	2-7	4-8	3-6	2-7	4-9	1-5	1-4	1-6	13-14	9-15	0-722
CaCO ₃	8.6	13.5	18.6	21.8	30.9	41.1		35.4	85.2	45.0	9.9	8.8
Organic-C	1.32		2.24			1.67		2.12				1.19
Sc	13.4	13.9	14.1		10.7	11.8	10.8	10.5	1.44		11.6	9.9
Cr	125	2.60	91		74	88	83	86	20.9		73	70
Co	13.8	12.4	12.4		8.7	10.5	9.0	9.3	2.59		9.3	9.7
Zn	109	117	112	112	103	98	94	93	27.8	85	86	65
Cu	23.9	38	32	29.9	26.1	23.5	22.9	19.6	14.5	20.9	16.3	8.7
K	21800	24300	21500	21700	19900	19300	18200	16600	2320	15400	22200	16500
Rb	115	115	102	102	90	86	77	71	2.99	62	104	78
Sr	273	437	532	593	696	754	909	1036	2086	1289	295	233
Ba	448	539	481	436	357	320	246	194	13	147	310	253
Pb	21.9	14.4	16.0	18.0	13.8	13.0	13.3	13.0	1.23	10.9	16.5	13.9
Cs	9.2	9.8	7.9		6.9	8.7	6.6	8.0	0.71		8.1	5.2
La	31	28.6	25.9		22.9	25.6	22.8	23.6	3.63		29.0	25.6
Ce	64	58	51		49	57	48	53	5.7		64	58
Pr	7.3		5.9									
Nd	26.6		21.9									
Sm	5.4	5.4	4.15		3.96	3.91	4.04	3.48	0.71		5.1	4.73
Eu	1.20	1.12	1.01		0.85	0.98	0.93	0.92	0.18		1.12	1.07
Gd	5.1		4.15									
Tb	0.68	0.63	0.55		0.39	0.63	0.57	0.48	0.17		0.64	0.64
Dy	4.22		3.47									
Ho	0.92		0.75									
Er	2.58		2.25									
Tm	0.35		0.31									
Yb	2.58	2.45	2.26		1.71	2.11	1.87	1.69	0.35		2.35	2.09
Lu	0.38	0.37	0.36		0.25	0.37	0.27	0.28	<dl		0.38	0.36
Y	23.8	25.8	23.2	24.4	21.9	21.1	19.8	20.0	4.23	17.6	25.4	21.5
Nb	11.2	7.6	7.7	7.7	6.6	7.5	6.4	5.5	<dl	5.1	9.5	9.7
Zr	154	123	111	113	107	103	85	77	<dl	61	205	241
Hf	3.92	3.51	3.56		2.62	0.71	2.83	2.84	0.29		6.2	6.6
Ta	0.64	0.60	0.76		0.71	0.63	0.58	0.55	<dl		0.65	0.85
Th	10.3	10.3	10.4		8.3	9.3	8.5	8.0	0.97		11.2	11.7
U	2.95	3.25	5.5		4.25	3.59	4.30	4.11	1.29		3.01	3.32

Appendix 5. Trace-element data of East-Indonesian sediments

No	49	50	51	52	53	54	55	56	57	58	59	60
Track	G5-4	G5-4	G5-4	G5-4	G5-4	G5-4	G5-4	G5-4	G5-4	G5-4	G5-4	G5-4
Sample	70	71	72	74	75	75	76	77	78	79	80	81
Type	B	B	B	B	B	B	B	B	B	P	B	B
Depth (cm)	15-22	19-25	10-19	11-22	1-6	6-19	31-35	22-28	17-23	0-527	16-20	25-30
CaCO ₃	76.1	57.0	90.8	84.3	57.9	56.8	16.7	3.4	57.9	8.2	46.9	48.2
Organic-C		1.89				0.19				1.02		
Sc		3.25				4.10	15.8	16.7	6.5	17.1	8.6	8.3
Cr		33				57	99	90	44	98	54	53
Co		3.10				10.7	13.2	15.1	6.1	16.1	8.9	7.1
Zn	28.6	32	17.2	44	110	112	98	104	59	100	76	79
Cu	13.2	8.6	14.5	14.3	13.0	13.3	12.5	12.4	17.6	11.4	20.9	22.8
K	4000	5200	<dl	2660	14400	16500	25700	20400	13500	23600	16800	16300
Rb	9.1	12.8	<dl	4.70	34	36	120	134	48	126	65	61
Sr	2016	962	2536	2227	1351	1316	366	160	914	252	751	832
Ba	25	32	5	7	15	15	157	252	87	269	171	234
Pb	6.0	6.6	<dl	<dl	8.2	15.2	16.5	22.7	5.5	21.9	9.5	8.8
Cs		0.99				2.02	8.4	10.3	4.20	7.8	5.4	4.88
La		12.3				5.9	34	37	13.0	29.9	18.0	18.0
Ce		25.0				10.0	60	73	27.9	64	36	34
Pr										7.4		
Nd										27.3		
Sm		2.76				1.46	6.1	6.5	2.35	5.4	3.21	3.18
Eu		0.56				0.34	1.12	1.30	0.58	1.23	0.70	0.69
Gd										5.2		
Tb		0.34				0.12	0.55	0.67	0.35	0.68	0.39	0.40
Dy										4.07		
Ho										0.83		
Er										2.42		
Tm										0.33		
Yb		1.07				0.48	2.13	2.40	1.05	2.39	1.35	1.27
Lu		0.19				<dl	0.32	0.40	0.17	0.36	0.22	0.23
Y	8.3	11.6	3.45	5.9	8.6	9.0	25.4	27.9	11.9	24.5	16.2	15.6
Nb	<dl	<dl	<dl	<dl	<dl	<dl	8.6	11.3	3.23	11.4	4.79	4.20
Zr	31	115	<dl	<dl	<dl	6.8	130	165	55	143	77	79
Hf		3.72				0.54	3.35	4.57	1.85	3.99	2.37	2.34
Ta		0.15				<dl	0.60	0.63	0.32	0.96	0.40	0.43
Th		3.25				1.66	10.7	12.8	4.52	12.8	6.6	6.0
U		2.57				1.73	3.11	4.15	5.4	4.55	6.9	6.1

Appendix 5. Trace-element data of East-Indonesian sediments

No	61	62	63	64	65	66	67	68	69	70	71	72
Track	G5-4	G5-4	G5-4	G5-4	G5-4	G5-4	G5-4	G5-4	G5-4	G5-4	G5-4	G5-4
Sample	82	83	84	85	86	87	88	90	91	92	94	95
Type	B	B	B	P	B	B	B	B	B	B	B	B
Depth (cm)	16-21	21-30	11-20	0-422	24-29	24-29	28-31	20-21	21-29	12-17	12-14	29-34
CaCO ₃	45.0	27.7	25.7	15.0	47.5	62.0	40.0	71.2	55.3	39.7	68.8	70.6
Organic-C		1.61		1.40			0.99			1.15		
Sc	8.4	12.8	13.3	16.0	9.1	6.9	11.7		8.3	11.0		
Cr	54	81	82	91	53	41	67		63	66		
Co	7.6	12.5	13.4	15.4	8.7	6.4	11.2		7.3	11.4		
Zn	84	109	112	105	89	65	88	46	71	100	52	50
Cu	26.7	35	35	22.3	29.0	23.1	26.1	14.4	17.3	28.6	16.1	23.7
K	15900	22500	22400	22900	16700	13000	21300	9400	18700	22000	9500	9100
Rb	61	100	104	117	64	42	85	28.2	61	84	33	27.2
Sr	802	567	554	353	820	945	650	928	838	693	981	1667
Ba	281	360	366	322	296	204	234	206	220	160	154	139
Pb	10.8	15.2	14.4	17.6	8.9	6.3	10.1	7.0	4.28	10.1	<dl	3.93
Cs	4.67	7.4	8.3	7.9	5.0	3.96	7.1		4.72	6.0		
La	19.1	23.9	27.7	28.4	19.1	13.7	23.7		12.5	17.8		
Ce	34	47	50	58	35	24.8	41		23.1	40		
Pr		5.4		6.6								
Nd		20.6		25.3								
Sm	3.35	4.13	4.74	4.99	3.31	2.36	4.10		2.26	3.14		
Eu	0.71	0.97	1.00	1.14	0.71	0.55	0.78		0.48	0.81		
Gd		3.89		4.53								
Tb	0.43	0.49	0.68	0.60	0.32	0.30	0.46		0.23	0.45		
Dy		3.27		3.66								
Ho		0.67		0.77								
Er		1.97		2.16								
Tm		0.27		0.29								
Yb	1.32	1.95	1.98	2.09	1.38	1.09	1.66		1.01	1.47		
Lu	0.25	0.29	0.33	0.31	0.23	0.20	0.24		0.17	0.26		
Y	17.0	22.6	23.3	24.4	16.7	12.6	17.7	8.9	13.2	21.3	10.4	9.2
Nb	4.95	5.8	6.1	9.1	3.83	2.56	5.2	<dl	2.24	4.91	<dl	<dl
Zr	80	99	103	121	66	42	81	22.9	43	81	29.4	<dl
Hf	2.41	2.95	2.96	3.34	1.98	1.39	2.22		1.19	2.32		
Ta	0.33	0.58	0.45	0.63	0.34	0.17	0.34		0.20	0.41		
Th	6.1	8.3	8.8	10.7	6.1	4.39	7.1		4.05	6.3		
U	6.4	8.0	10.0	5.9	6.9	4.51	10.4		6.0	7.2		

Appendix 5. Trace-element data of East-Indonesian sediments

No	73	74	75	76	77	78	79	80	81	82	83	84
Track	G5-4	G5-4	G5-4	G5-4	G5-4	G5-4	G5-4	G5-4	G5-4	G5-4	G5-4	G5-4
Sample	97	99	102	104	106	110	111	114	115	115	116	117
Type	B	B	B	B	B	B	B	B	B	B	B	B
Depth (cm)	5-11	20-29	23-28	9-11	19-21	28-31	3-9	14-19	20-23	13-18	7-12	7-12
CaCO ₃	84.0	49.8	33.2	16.4	2.3	0.0	0.9	24.5	2.8	11.0	4.5	6.6
Organic-C		1.73		1.32	0.96	0.77						0.59
Sc		7.9	11.0	13.4	18.4	20.6	27.1	22.0	28.5	42	22.6	23.3
Cr		43	58	82	85	84	114	47	81	124	56	57
Co		7.6	11.5	16.5	16.9	16.9	22.2	14.8	21.9	34	17.1	17.6
Zn	26.4	79	101	115	155	113	110	74	80	92	80	77
Cu	23.3	41	50	71	97	79	64	49	54	44	67	66
K	2410	14200	20600	21300	28300	22900	18400	7800	10500	6400	11000	12000
Rb	3.80	51	84	98	159	105	73	30	40	27.6	45	50
Sr	3289	1528	751	330	106	170	199	485	387	280	293	340
Ba	20	450	487	675	481	563	628	389	235	467	467	585
Pb	6.1	6.1	12.8	16.7	24.1	21.5	15.1	9.7	10.3	10.2	13.9	14.6
Cs		4.33	6.3	7.1	10.0	8.5	5.5	2.26	3.41	1.95	3.62	3.97
La		14.8	20.8	24.7	28.5	22.9	17.2	7.6	11.4	8.2	12.3	13.2
Ce		29.2	46	58	63	58	42	19.8	23.7	20.5	30.0	31
Pr					6.5							
Nd					24.6							
Sr		2.70	3.72	4.42	4.73	4.52	3.65	2.13	2.85	2.44	3.32	3.16
Eu		0.58	0.86	0.97	1.12	1.11	0.99	0.61	0.86	0.70	0.97	0.86
Gd					4.56							
Tb		0.31	0.40	0.55	0.62	0.79	0.76	0.39	0.57	0.62	0.60	0.49
Dy					3.74							
Ho					0.71							
Er					2.37							
Tm					0.33							
Yb		1.33	1.74	2.06	2.31	2.46	2.14	1.49	1.96	2.09	2.36	2.14
Lu		0.20	0.28	0.38	0.37	0.42	0.36	0.29	0.36	0.36	0.43	0.36
Y	6.2	15.1	20.6	23.7	31	26.3	22.9	17.4	19.5	18.6	23.9	22.7
Nb	<dl	3.85	6.6	7.4	11.0	8.0	7.2	<dl	3.58	2.44	3.91	4.45
Zr	<dl	33	89	127	163	137	120	66	89	83	116	108
Hf		1.70	2.53	3.20	4.54	3.58	2.90	1.69	2.20	1.90	3.04	2.77
Ta		0.22	0.44	0.69	0.75	0.74	0.49	0.45	0.32	0.42	0.36	0.52
Th		5.1	7.7	9.1	12.9	10.4	6.4	3.03	6.4	3.01	5.1	5.2
U		5.9	5.1	5.7	4.98	5.6	2.09	1.79	2.09	0.92	1.14	1.01

Appendix 5. Trace-element data of East-Indonesian sediments

No	85	86	87	88	89	90	91	92	93	94	95	96
Track	G5-4	G5-6	G5-6	G5-6	G5-6	G5-6	G5-6	G5-6	G5-6	G5-6	G5-6	G5-6
Sample	118	121	122	123	124	125	126	127	128	129	130	132
Type	B	B	B	B	B	B	B	B	B	B	B	B
Depth (cm)	12-16	20-25	17-24	11-16	28-35	29-34	20-29	6-9	4.5-10	30-37	25-30	3-10
CaCO ₃	60.5	6.6	0.0	4.4	34.9	43.1	49.7	65.1	64.2	33.2	26.5	73.0
Organic-C				0.70						0.78		
Sc	8.8	17.7	18.2	23.5	12.6	11.7	9.7		8.5	12.7	12.7	
Cr	29.7	75	86	140	55	52	43		34	50	61	
Co	8.4	20.1	16.9	26.9	12.5	10.5	9.2		8.5	12.3	14.0	
Zn	45	137	124	116	93	85	79	43	48	96	98	38
Cu	31	80	81	77	59	50	48	33	26.1	43	52	26.1
K	5400	21600	22600	21400	18300	17100	15000	9700	7900	13500	18900	7800
Rb	18.7	96	100	95	70	62	50	27.8	22	69	87	23.6
Sr	806	274	306	574	672	727	779	852	926	661	741	1349
Ba	154	988	1076	1156	567	522	496	176	289	395	439	97
Pb	9.2	26.6	26.1	30.0	23.6	18.8	14.2	8.1	14.5	19.9	19.4	6.4
Cs	1.75	8.1	7.8	7.4	6.0	5.2	4.50		1.89	6.0	6.9	
La	7.1	27.8	33	53	23.0	21.0	15.9		16.7	20.8	23.8	
Ce	15.8	65	73	105	46	43	35		31	44	50	
Pr												
Nd												
Sm	1.59	5.00	5.3	7.8	4.19	4.00	3.37		2.75	4.11	4.66	
Eu	0.44	1.20	1.23	1.67	0.87	0.85	0.68		0.66	0.82	0.93	
Gd												
Tb	0.37	0.61	0.93	1.15	0.54	0.49	0.43		0.29	0.55	0.51	
Dy												
Ho												
Er												
Tm												
Yb	1.00	2.46	2.19	2.43	1.71	1.73	1.58		0.97	2.00	1.89	
Lu	0.17	0.40	0.39	0.41	0.33	0.29	0.24		0.18	0.30	0.37	
Y	11.1	26.0	25.7	26.6	19.9	17.9	15.9	10.2	11.5	19.7	22.0	7.8
Nb	<dl	8.1	9.4	11.6	5.9	5.3	4.02	<dl	3.53	6.3	9.3	3.23
Zr	41	124	130	130	86	73	60	32	43	87	96	22.5
Hf	1.08	3.31	3.42	3.65	2.59	2.24	1.85		1.30	2.51	2.65	
Ta	0.21	0.68	0.63	0.67	0.52	0.31	0.33		0.25	0.48	0.66	
Th	2.63	11.6	13.4	18.2	8.4	8.0	6.4		5.4	8.1	8.8	
U	0.43	2.20	2.75	3.52	5.9	7.7	7.4		1.21	4.71	3.29	

Appendix 5. Trace-element data of East-Indonesian sediments

No Track Sample Type Depth (cm)	97 G5-6 133 B 23-28	98 G5-6 134 B 8-11	99 G5-6 135 B 0-3	100 G5-6 136 B 15-20	101 G5-6 138 B 12-18	102 G5-6 139 B 32-33	103 G5-6 140 B 31-38	104 G5-6 141 B 31-38	105 G5-6 143 B 26-31	106 G5-6 144 B 33-39	107 G5-6 145 P 0-968	108 G5-6 146 B 21-30
CaCO ₃	27.9	1.6	84.5	23.7	55.9	59.6	28.0	25.4	14.2	13.4	21.5	24.0
Organic-C		0.38		0.46					0.70		1.26	
Sc	13.2	20.5		13.8	7.8	7.5	12.4	13.2	17.6	19.7	14.3	14.3
Cr	59	90		64	61	39	60	63	92	101	76	71
Co	13.3	13.0		13.5	10.0	6.5	14.4	16.9	19.3	21.9	18.0	18.2
Zn	108	109	44	94	62	65	101	104	101	107	108	109
Cu	47	35	14.8	25.6	22.6	26.5	42	45	49	59	43	51
K	20600	28500	3900	21500	13400	15400	21500	21400	21800	24600	20000	21900
Rb	86	199	12.5	111	49	51	94	93	97	111	98	97
Sr	536	114	960	326	844	889	610	586	334	332	507	552
B	472	322	116	486	376	218	503	545	343	372	433	516
Pb	16.4	33	6.1	19.8	8.7	6.5	14.3	14.2	13.9	12.8	13.8	14.2
Cs	6.8	9.6		7.4	3.43	4.38	7.3	7.5	7.1	9.1	6.5	7.9
La	24.4	48		35	14.5	16.0	24.2	24.7	25.2	28.3	26.0	27.0
Ce	51	90		74	30.0	33	51	55	58	62	53	58
Pr		10.8									6.0	
Nd		39									22.9	
Sm	4.92	7.5		6.8	3.08	3.03	4.54	4.81	5.7	5.9	4.76	5.3
Eu	0.97	1.58		1.25	0.64	0.60	0.86	1.00	1.22	1.28	1.11	0.99
Gd		7.3									4.56	
Tb	0.63	0.94		0.61	0.40	0.29	0.62	0.69	0.74	0.56	0.62	0.60
Dy		5.8									4.04	
Ho		1.13									0.78	
Er		2.97									2.16	
Tm		0.39									0.29	
Yb	2.07	2.80		2.49	1.27	1.21	1.84	1.94	2.36	2.62	2.15	2.04
Lu	0.36	0.43		0.37	0.21	0.23	0.34	0.35	0.46	0.42	0.32	0.35
Y	22.4	41	5.8	27.9	16.0	13.3	22.7	22.0	28.5	28.3	22.4	24.6
Nb	8.5	17.4	<dl	13.2	5.7	3.66	9.3	8.5	11.0	10.4	9.3	9.6
Zr	105	142	17.1	143	67	55	98	97	141	133	99	101
Hf	2.76	3.58		4.04	2.02	1.75	2.78	2.68	3.95	3.88	2.71	3.13
Ta	0.57	1.05		0.96	0.42	0.42	0.75	0.71	0.76	0.80	0.53	0.70
Th	9.1	20.3		14.2	5.3	5.7	9.2	9.4	9.8	11.0	9.0	10.1
U	1.84	3.04		9.1	2.00	2.87	2.83	2.91	2.67	2.75	4.02	2.59

Appendix 5. Trace-element data of East-Indonesian sediments

No	109	110	111	112	113	114	115	116	117	118	119	120
Track	G5-6	G5-6	G5-6	G5-6	G5-6	G5-6	G5-6	G5-6	G5-6	G5-6	G5-6	G5-6
Sample	147	148	149	149	150	151	152	153	154	155	156	157
Type	B	B	B	P	B	B	B	B	B	B	B	B
Depth (cm)	34-39	26-31	15-20	0-1520	24-32	29-34	23-28	23-28	31-38	21-30	32-36	31-36
CaCO ₃	26.3	35.7	83.0	32.5	41.1	53.5	50.5	43.9	54.3	57.2	56.3	37.7
Organic-C	0.86			1.00	1.25			1.31				0.98
Sc	12.8	11.3		12.4	10.9	8.3	9.1	9.7	7.6	8.0	7.9	12.5
Cr	65	59		69	61	48	53	57	43	44	48	65
Co	15.5	12.5		13.1	11.3	8.3	8.9	9.9	7.4	7.9	8.0	12.5
Zn	108	93	50	87	80	70	74	86	66	53	49	55
Cu	45	38	15.2	32	32	32	33	32	27.4	22.3	22.5	21.0
K	21400	20100	6500	19000	18800	16700	16700	16900	14300	14900	14300	17600
Rb	91	80	15.1	87	78	58	62	68	53	53	52	83
Sr	640	771	996	846	1215	1116	1159	1230	1570	1492	1717	1346
Ba	521	467	61	310	271	315	295	271	179	100	63	81
Pb	14.1	12.5	8.1	7.4	8.5	6.1	8.5	8.1	5.2	5.3	4.71	7.6
Cs	6.3	6.5		5.8	5.7	4.52	4.84	5.1	4.08	3.59	3.77	5.1
La	24.4	22.4		22.0	19.2	16.1	17.4	17.0	14.3	13.2	12.4	20.0
Ce	47	45		42	39	32	32	34	28.1	26.5	26.0	39
Pr	5.3			4.93								4.53
Nd	19.6			18.2								16.3
Sm	4.04	4.36		3.67	3.68	3.07	3.36	3.39	2.84	2.67	2.59	3.32
Eu	0.99	0.87		0.89	0.70	0.64	0.67	0.70	0.58	0.55	0.48	0.74
Gd	4.00			3.55								3.05
Tb	0.54	0.58		0.47	0.41	0.35	0.37	0.38	0.34	0.34	0.29	0.45
Dy	3.56			3.08								2.90
Ho	0.75			0.64								0.58
Er	2.16			1.89								1.61
Tm	0.29			0.24								0.22
Yb	2.14	1.83		1.68	1.70	1.29	1.60	1.32	1.19	1.00	1.04	1.57
Lu	0.33	0.32		0.26	0.26	0.21	0.21	0.22	0.20	0.14	0.20	0.24
Y	23.0	21.0	7.0	19.7	19.3	15.6	17.0	17.8	15.2	13.4	13.1	17.8
Nb	8.8	7.1	<dl	7.5	6.2	5.3	5.3	4.83	2.66	3.22	3.60	4.57
Zr	93	82	14.2	73	67	54	56	58	40	41	31	77
Hf	2.69	2.55		2.46	2.42	1.89	2.03	2.12	1.75	1.76	1.78	2.72
Ta	0.56	0.50		0.53	0.34	0.47	0.55	0.44	0.21	0.25	0.32	0.66
Th	9.1	8.0		7.6	7.2	5.9	6.2	6.3	5.1	5.1	4.88	7.8
U	3.27	3.11		5.6	6.2	5.5	4.76	5.7	5.9	6.6	9.5	6.7

Appendix 5. Trace-element data of East-Indonesian sediments

No	121	122	123	124	125	126	127	128	129	130	131	132
Track	G5-6	G5-6	G5-6	G5-6	G5-6	G5-6	G5-6	DSDP 262	DSDP 262	DSDP 262	DSDP 262	DSDP 262
Sample	158	159	160	161	162	163	164	Core 1-4	Core 14-5	Core 32-3	Core 40-2	Core 45-4
Type	B	B	B	B	B	B	P	D	D	D	D	D
Depth (cm)	22-26	22-26			11-14	6-12	0-885	50-52	69-71	60-62	60-62	61-63
CaCO ₃	68.6	57.0	90.8	92.3	89.6	92.2	53.5	50.6	24.6	60.5	49.9	96.6
Organic-C									0.53	0.82		
Sc	5.8						7.7	8.6	12.1	6.7	7.6	0.53
Cr	34						49	43	58	46	4.68	13.20
Co	6.0						7.3	8.8	13.7	6.9	6.4	0.25
Zn	39	38	22.3	23.6	23.7	16.9	58					
Cu	19.7	20.4	16.4	16.1	17.6	15.3	30					
K	11600	13600	996	1250	2490	1410	13500					
Rb	36	49	2.97	<dl	<dl	<dl	57					
Sr	1691	2118	2211	2757	2981	2368	1767					
Ba	40	48	6	7	9	<dl	131					
Pb	<dl	5.0	3.43	4.05	2.68	<dl	5.2					
Cs	2.49						3.46	3.70	5.6	2.93	3.37	0.22
La	9.2						13.1	18.5	31	13.3	13.9	1.53
Ce	19.7						25.4	42	63	24.6	33	2.90
Pr									7.1			
Nd									26.8			
Sm	1.97						2.42	3.31	5.4	2.34	2.63	<dl
Eu	0.41						0.57	0.76	1.36	0.51	0.58	<dl
Gd									5.5			
Tb	0.18						0.35	0.44	0.75	0.27	0.30	<dl
Dy									4.73			
Ho									0.97			
Er									2.79			
Tm									0.38			
Yb	0.73						1.13	1.47	2.69	1.16	1.16	<dl
Lu	0.14						0.13	0.24	0.42	0.20	0.19	<dl
Y	11.8	13.2	5.3	3.32	4.88	3.99	14.7					
Nb	1.96	3.15	<dl	<dl	<dl	<dl	4.66					
Zr	22.3	22.6	<dl	<dl	<dl	<dl	18.7					
Hf	1.48						1.49	2.11	3.40	1.61	2.26	<dl
Ta	0.22						0.29	0.60	0.87	0.38	0.24	<dl
Th	3.81						4.79	7.0	9.3	4.25	5.3	0.47
U	6.3						5.3	3.40	2.30	4.70	4.60	4.90

APPENDIX 6

Sr-, Nd- AND Pb-ISOTOPES AND PARENT DAUGHTER ELEMENTS OF THE BANDA ARC VOLCANICS

Sr, Nd and Pb isotope ratios and parent-daughter concentrations in Banda Arc volcanics. Abbreviations: WR=Whole Rock, (WR1, WR2 indicate duplicate determinations); Roman additions indicate different parts of a single sample. $^{87}\text{Sr}/^{86}\text{Sr}$ and $^{143}\text{Nd}/^{144}\text{Nd}$ are not corrected for NBS987 and La Jolla standards, respectively. Errors are 1 standard deviation of the mean. Pb isotope ratios are relative to values of $^{206}\text{Pb}/^{204}\text{Pb}=16.937$, $^{207}\text{Pb}/^{204}\text{Pb}=15.493$ and $^{208}\text{Pb}/^{204}\text{Pb}=36.705$ for the NBS981 standard. The estimated errors are: $^{206}\text{Pb}/^{204}\text{Pb}$, ± 0.010 , $^{207}\text{Pb}/^{204}\text{Pb}$, ± 0.012 and $^{208}\text{Pb}/^{204}\text{Pb}$, ± 0.035 . These are based on 18 measurements of NBS981. Concentration data are given in ppm. Rb and Sr were measured by XRF, Sm and Nd by ID-MS, and Th, U and Pb by ID-ICP-MS except one (*) which was determined by ID-MS. See Appendix 3 for analytical techniques.

Appendix 6. Sr-, Nd- and Pb-isotopes and parent-daughter elements of the Banda Arc volcanics

Sample	Type	$^{87}\text{Sr}/^{86}\text{Sr}$	$^{143}\text{Nd}/^{144}\text{Nd}$	$^{206}\text{Pb}/^{204}\text{Pb}$	$^{207}\text{Pb}/^{204}\text{Pb}$	$^{208}\text{Pb}/^{204}\text{Pb}$	Pb	Sr	Sm	Nd	U	Th	Pb
Banda Archipelago													
BA 3A	WR	0.704804 ±16	0.512866 ±03				26	180	5.79	19.2			
Banda 4	WR 1	0.704801 ±06	0.512870 ±14	18.680	15.627	38.854	18	184	4.48	14.6			
	WR 2			18.684	15.642	38.915							
BA 6A	WR	0.704832 ±10					25	184					
BA 11A2	WR 1	0.704812 ±13	0.512873 ±07	18.691	15.639	38.910	21	195	4.30	14.1	0.56	1.80	7.31
	WR 2			18.694	15.631	38.885							
BA 16	WR	0.704836 ±11					22	167					
BA 20A	WR	0.704821 ±17					27	177					
BA 27A	WR	0.704840 ±12					26	171					
BN 1A2	WR 1	0.704828 ±30					27	197					
	WR 2	0.704803 ±15											
BN 3A2	WR 1	0.704565 ±13	0.512838 ±09	18.667	15.630	38.853	12	270	2.86	9.51	0.31	1.21	4.42
	WR 2			18.650	15.620	38.843							
BN 7A	WR	0.704792 ±10					20	204					
BN 9A	WR 1	0.704813 ±08	0.512834 ±06	18.657	15.618	38.836	19	244	4.20	14.4	0.61	2.17	14.0
	WR 2			18.665	15.626	38.846							
BB 21A3	WR 1	0.704501 ±15	0.512911 ±08	18.682	15.636	38.906	11	209	3.65	11.2	0.33	1.04	4.65
	WR 2			18.670	15.621	38.840							
BB 28	WR	0.704614 ±23					11	233					
Manuk													
MA 1A	WR	0.705282 ±14	0.512730 ±07	18.754	15.647	38.973	44	227	3.83	15.0	1.16	4.56	10.4
MA 2A	WR	0.705192 ±08	0.512729 ±12				32	220	3.03	11.4			
MA 2B	WR	0.705516 ±15	0.512766 ±09				43	215	3.36	12.7			
MA 3C2	WR	0.705250 ±13					34	221					
MA 4B	WR	0.705282 ±13					39	217					
MA 5A	WR 1	0.705254 ±15	0.512743 ±15	18.744	15.636	38.921	36	219	3.22	12.2	0.87	3.54	9.60
	WR 2			18.755	15.646	38.951							

Appendix 6. Sr-, Nd- and Pb-isotopes and parent-daughter elements of the Banda Arc volcanics

Sample	Type	$^{87}\text{Sr}/^{86}\text{Sr}$	$^{143}\text{Nd}/^{144}\text{Nd}$	$^{206}\text{Pb}/^{204}\text{Pb}$	$^{207}\text{Pb}/^{204}\text{Pb}$	$^{208}\text{Pb}/^{204}\text{Pb}$	Rb	Sr	Sm	Nd	U	Th	Pb
Serua													
SE 2B	WR	0.707563 ±18	0.512593 ±13				53	263	2.69	10.4			
SE 9A3	WR 1	0.708352 ±18	0.512493 ±15	19.018	15.684	39.190	39	266	2.72	10.9	0.91	3.71	10.5
	WR 2			19.031	15.698	39.227							
SE 11Sc	WR (pumice)	0.708365 ±14					40	267					
SE 14A1	WR (pumice)	0.709156 ±12					42	253					
SE 17	WR	0.708413 ±14	0.512494 ±11				41	263	2.45	9.27			
SE 21A3	WR	0.709013 ±18	0.512437 ±05	19.038	15.695	39.231	56	268	2.81	11.9	1.33	5.15	11.4
SE 23A	WR	0.708946 ±22					52	280					
SE 25A	WR	0.709518 ±10	0.512403 ±04	19.019	15.694	39.226	44	266	3.11	12.8	1.09	4.44	11.4
SE 26A	WR	0.707792 ±20					45	279					
SE 27A	WR 1	0.707596 ±18	0.512599 ±33	19.084	15.696	39.270	47	279	2.66	10.5	1.30	4.33	11.2
	WR 2		0.512608 ±04						2.64	10.4			
SE 28A	WR	0.707548 ±15	0.512593 ±08				62	260	3.02	12.3			
Nila													
NI 1A1	WR	0.707728 ±16	0.512629 ±09	19.367	15.733	39.573	87	368	4.10	18.1	2.50	8.99	27.5
NI 5A	WR	0.707732 ±21					118	317					
NI 5B	Mafic inclusion 1	0.707092 ±19	0.512678 ±11	19.386	15.733	39.596	62	406	2.41	9.67			
	Mafic inclusion 2			19.373	15.720	39.553							
NI 6	Cumulate inclusion	0.707844 ±17	0.512634 ±05				41	422	3.08	13.1			
NI 10AI	Host	0.707791 ±12	0.512588 ±07	19.321	15.731	39.552	100	269	4.31	18.5			
NI 10AII	Cumulate-inclusion I	0.707751 ±09	0.512600 ±06						4.23	18.0			
	Residue	0.707717 ±06		19.313	15.720	39.514							
	Leach	0.707798 ±17		19.313	15.733	39.521							
NI 10AIII	Cumulate-inclusion II	0.707722 ±16	0.512601 ±07						2.64	10.5	1.05*	7.57*	13.2*
	Residue	0.707675 ±17		19.292	15.729	39.558							
	Leach	0.707770 ±06		19.300	15.723	39.485							
NI 12	WR	0.707705 ±11	0.512623 ±08				100	369	4.36	19.4			
NI 15I	Host	0.707711 ±10					76	397					
NI 15II	Mafic inclusion	0.707010 ±05					47	426					
NI 16	WR	0.707393 ±15	0.512644 ±09	19.398	15.736	39.601	94	358	3.21	15.2	3.33	10.00	45.4
NI 18AI	Mafic inclusion	0.706463 ±10	0.512689 ±07	19.382	15.729	39.579	46	432	2.27	9.26			
NI 18AII	Host 1	0.707002 ±15	0.512665 ±06	19.399	15.743	39.621	81	388	2.67	11.8	2.57	8.42	21.4
	Host 2								2.64	11.7			

Appendix 6. Sr-, Nd- and Pb-isotopes and parent-daughter elements of the Banda Arc volcanics

Sample	Type	$^{87}\text{Sr}/^{86}\text{Sr}$	$^{143}\text{Nd}/^{144}\text{Nd}$	$^{206}\text{Pb}/^{204}\text{Pb}$	$^{207}\text{Pb}/^{204}\text{Pb}$	$^{208}\text{Pb}/^{204}\text{Pb}$	Rb	Sr	Sm	Nd	U	Th	Pb
Teon													
TE 1B2	Mafic inclusion	0.707941 ±07	0.512526 ±09				48	596	6.43	27.1			
TE 1C	WR	0.707967 ±20	0.512515 ±07	19.416	15.726	39.626	76	542	3.92	21.0	2.96	11.5	31.1
TE 2B1	Mafic inclusion	0.709511 ±39	0.512577 ±04				47	497	3.74	16.3			
	Residue	0.709448 ±14											
TE 5	WR (pumice)	0.707971 ±17					78	534					
TE 11	WR	0.708255 ±10	0.512522 ±04				77	526	3.72	20.0			
TE 12	WR	0.708299 ±14	0.512527 ±07	19.429	15.734	39.659	74	526	3.67	19.5	2.21	9.60	11.0
TE 14B	WR	0.707544 ±23	0.512590 ±05	19.428	15.720	39.611	71	529	3.87	19.4	2.85	10.1	24.3
TE 15	WR	0.707344 ±13	0.512578 ±05	19.419	15.727	39.612	68	539	4.07	21.2	2.70	10.1	20.8
Damar													
DA 1	WR	0.706727 ±12	0.512573 ±05	19.360	15.729	39.703	93	526	4.88	25.4	4.92	18.9	26.7
DA 2	WR	0.706607 ±12					98	573					
DA 3	WR	0.706632 ±10					94	595					
DA 4	WR	0.706554 ±12	0.512587 ±06	19.348	15.716	39.639	74	632	4.34	22.7	4.16	16.3	21.7
DA 6	WR	0.706544 ±11	0.512589 ±08				87	593	4.83	25.3			
DA 8	WR	0.707018 ±15	0.512589 ±06	19.280	15.709	39.628	78	333	5.12	23.5	3.20	12.0	24.1
Romang (inactive)													
RO 2	WR	0.708520 ±11	0.512454 ±06	19.147	15.688	39.511	77	320	3.99	19.0	2.07	8.02	23.2
RO 7C2	WR	0.709144 ±15					60	313					
RO 8B	WR	0.708648 ±08	0.512460 ±04				81	368	4.41	21.6			
RO 8C6	WR	0.709195 ±11	0.512432 ±05	19.185	15.700	39.552	141	227	6.18	30.3	3.53	15.0	27.4
RO 8E	WR	0.709257 ±16					147	182					

APPENDIX 7

Sr-, Nd- AND Pb-ISOTOPES AND TRACE ELEMENTS OF EAST INDONESIAN SEDIMENTS

Sr, Nd and Pb isotope ratios and Sm, Nd, Th, U and Pb concentrations in East Indonesian Sediments. B=box-core, P=Piston core. $^{87}\text{Sr}/^{86}\text{Sr}$ and $^{143}\text{Nd}/^{144}\text{Nd}$ are not corrected for the NBS987 and La Jolla standards, respectively. Errors are 1 standard deviation of the mean. Pb isotope ratios are relative to values of $^{206}\text{Pb}/^{204}\text{Pb}=16.937$, $^{207}\text{Pb}/^{204}\text{Pb}=15.493$ and $^{208}\text{Pb}/^{204}\text{Pb}=36.705$ for the NBS981 standard. Two standard deviation errors for $^{206}\text{Pb}/^{204}\text{Pb}$, ± 0.010 , $^{207}\text{Pb}/^{204}\text{Pb}$, ± 0.012 and $^{208}\text{Pb}/^{204}\text{Pb}$, ± 0.035 are based on 18 measurements of NBS981. Concentration data are given in ppm. Sm and Nd were measured by ID-MS and Th, U and Pb by ID-ICP-MS. T_{DM} is the calculated Nd depleted mantle model age (DePaolo, 1981b). See Appendix 3 for analytical techniques.

Appendix 7. Sr,- Nd- and Pb-isotopes and trace elements of East Indonesian sediments

Sample	Type	Depth (cm)	$^{87}\text{Sr}/^{86}\text{Sr}$	$^{143}\text{Nd}/^{144}\text{Nd}$	$^{206}\text{Pb}/$ ^{204}Pb	$^{207}\text{Pb}/$ ^{204}Pb	$^{208}\text{Pb}/$ ^{204}Pb	Sm	Nd	$^{147}\text{Sm}/$ ^{144}Nd	T_{DM} (Ma)	U	Th	Pb
Seram Sea														
MB-1	B		0.710707 ±10		18.806	15.653	38.871							
MB-7	B		0.709784 ±14	0.512263 ±09	18.834	15.661	38.912	3.03	15.3	0.1195	1543	4.11	7.41	15.7
Central Banda Sea														
G5-1-2	P	0-350	0.710923 ±11	0.512257 ±08	18.784	15.654	38.961	4.06	20.4	0.1200	1560	0.26	9.25	22.9
Track I														
G5-2-14	B	1-3	0.709752 ±13	0.512365 ±04				4.08	18.6	0.1326	1600			
G5-2-19	B	1-4	0.713770 ±21	0.512292 ±08				5.10	24.4	0.1261	1607			
G5-2-24	B	1.0-2.5	0.722316 ±07	0.512172 ±05	18.645	15.655	38.700	6.10	31.0	0.1190	1677	2.64	12.3	29.1
G5-2-34	B	2-4	0.709994 ±10	0.512249 ±10	18.775	15.673	38.961	3.64	18.1	0.1214	1597	1.96	6.88	14.0
G5-2-40	B	5-11	0.709645 ±11	0.512155 ±07				2.95	14.3	0.1248	1809			
G5-2-45	B	1-2	0.709505 ±16	0.512236 ±07				1.74	8.78	0.1201	1594			
G5-2-51	P	0-347	0.711743 ±15	0.512207 ±08	18.728	15.649	38.826	4.57	24.0	0.1149	1558	3.95	10.5	23.3
G5-2-56	P	0-804	0.714311 ±13	0.512151 ±04	18.810	15.656	38.935	4.93	25.7	0.1160	1659	3.30	11.3	21.8
G5-2-60	B	4-8	0.711021 ±13	0.512195 ±08	18.765	15.646	38.846	4.39	23.0	0.1155	1585	3.66	9.92	19.2
G5-2-63	B	4-9	0.710352 ±13	0.512185 ±03				4.03	20.8	0.1172	1627			
G5-2-65	B	1-4	0.709892 ±10	0.512185 ±07	18.781	15.659	38.871	3.48	17.9	0.1179	1636	3.98	7.79	14.5
Aru Trough														
G5-4-69	P	0-722	0.713983 ±14	0.512058 ±08	18.903	15.679	38.968	4.25	32.1	0.1162	1802			
Track II														
G5-4-71	B	19-25	0.709358 ±17	0.512211 ±13	19.012	15.668	38.887	2.40	11.4	0.1273	1766	2.28	3.25	6.88
G5-4-75	B	6-19	0.709236 ±15	0.512270 ±09				1.39	6.15	0.1362	1849			
G5-4-79	P	0-527	0.715073 ±13	0.512138 ±06	18.884	15.671	38.955	5.45	28.0	0.1175	1703	4.03	10.9	16.8
G5-4-83	B	21-30	0.710590 ±12	0.512214 ±05	18.865	15.663	38.943	4.21	21.5	0.1185	1603	7.55	8.90	16.5
G5-4-85	P	0-422	0.712553 ±15	0.512158 ±04	18.896	15.670	38.959	4.92	25.2	0.1179	1679	5.15	10.4	16.9
G5-4-88	B	28-31	0.710239 ±15	0.512207 ±04	18.912	15.672	38.990	3.32	16.8	0.1195	1631	8.95	7.15	12.6
G5-4-92	B	12-17	0.709861 ±14	0.512291 ±08				3.13	16.0	0.1180	1477			
G5-4-99	B	20-29	0.709437 ±11	0.512225 ±05				2.52	12.7	0.1204	1617			
G5-4-104	B	9-11	0.711658 ±18	0.512187 ±07				4.37	22.2	0.1188	1650			
G5-4-106	B	19-21	0.721693 ±12	0.512167 ±05	18.881	15.689	39.063	5.74	29.5	0.1175	1659	4.58	9.59	20.2
G5-4-110	B	28-31	0.713108 ±10	0.512233 ±06				4.49	21.9	0.1237	1662			
G5-4-118	B	12-16	0.709248 ±11	0.512372 ±11				1.47	6.44	0.1375	1683			

Appendix 7. Sr,- Nd- and Pb-isotopes and trace elements of East Indonesian sediments

Sample	Type	Depth (cm)	$^{87}\text{Sr}/^{86}\text{Sr}$	$^{143}\text{Nd}/^{144}\text{Nd}$	$^{206}\text{Pb}/$ ^{204}Pb	$^{207}\text{Pb}/$ ^{204}Pb	$^{208}\text{Pb}/$ ^{204}Pb	Sm	Nd	$^{147}\text{Sm}/$ ^{144}Nd	T_{DM} (Ma)	U	Th	Pb
Track III														
G5-6-123	B	11-16	0.708071 ±18	0.512421 ±05				6.66	37.9	0.1076	1157			
G5-6-129	B	30-37	0.709793 ±08	0.512258 ±06				3.40	16.7	0.1228	1606			
G5-6-134	B 1	8-11	0.739404 ±12	0.511905 ±07	19.091	15.729	39.415	7.57	38.1	0.1199	2264	3.41	18.2	33.5
	2			0.511894 ±06	19.095	15.733	39.430							
G5-2-136	B	15-20	0.714746 ±17	0.512000 ±06	19.076	15.709	39.279	5.93	29.9	0.1200	1962	4.37	13.7	27.8
G5-2-143	B	26-31	0.710898 ±11	0.512299 ±08				5.21	24.6	0.1283	1635			
G5-2-145	P	0-968	0.710821 ±11	0.512192 ±06	18.932	15.680	39.099	4.39	21.7	0.1222	1701	3.50	8.95	15.3
G5-2-147	B	34-39	0.710481 ±15	0.512159 ±07	18.931	15.683	39.124	4.02	20.4	0.1190	1697	2.90	9.08	17.6
G5-2-149	P2	0-1520	0.710180 ±13	0.512128 ±04	18.948	15.684	39.072	3.61	18.4	0.1183	1732	4.98	7.73	12.9
G5-6-150	B	24-32	0.709881 ±11	0.512097 ±08	19.113	15.705	39.272	3.15	15.7	0.1210	1830	7.31	6.91	10.5
G5-2-153	B	23-28	0.709712 ±14	0.512129 ±05				2.91	14.5	0.1212	1782			
G5-2-157	B 1	31-36	0.710098 ±10	0.511959 ±07	19.573	15.786	39.763	3.23	16.3	0.1196	2018	6.16	8.07	9.00
	2			0.511942 ±02				3.27	16.4	0.1202	2056			
G5-6-164	P	0-885	0.709514 ±12	0.512107 ±05				1.95	9.88	0.1192	1780			
Leg 27 DSDP Site 262														
Core 1-4		5-52	0.709862 ±08	0.512108 ±05	18.990	15.709	39.094	3.19	15.9	0.1217	1825			
Core 16-5		69-71	0.711082 ±14	0.512182 ±08	18.950	15.712	39.105	5.26	26.0	0.1224	1720	4.43	5.23	10.1
Core 32-3		60-62	0.709419 ±15	0.512198 ±05	18.889	15.676	38.863	2.01	10.1	0.1198	1649			
Core 40-2		60-62	0.709706 ±14	0.512130 ±04	19.160	15.731	39.143	2.50	12.3	0.1232	1819	4.81	6.00	9.21
Core 45-4	1	61-63	0.709165 ±18	0.511993 ±17	19.237	15.727	38.659	0.326	1.57	0.1251	2082			
	2				19.229	15.722	38.645							

CURRICULUM VITAE

Pieter Zeger Vroon werd op 26 mei 1963 geboren te Culemborg. Na het behalen van de diploma's havo (1980) en Atheneum-B (1982) aan het Corderius College te Amersfoort, begon hij in 1982 met de studie geologie aan de Rijksuniversiteit van Utrecht. In 1983 werd het propaedeutisch examen afgelegd en een begin gemaakt met de hoofdrichting geochemie. Gedurende juli en augustus 1984 was hij voor het onderdeel "Vulkanisme van de Banda Boog" (GF5) betrokken bij de Snellius II Expeditie in Oost-Indonesië. De doctoraalfase van zijn studie bestond uit het hoofdvak endogene geochemie met het bijvak isotopen geologie. De afstudeeronderwerpen waren magmagenese in de Oostelijke Sunda Boog en eruptie mechanismen van het vulkanisme op Nisyros (Griekenland). In april 1987 werd het doctoraal examen (cum laude) behaald. Van mei 1987 tot mei 1991 was hij als assistent in opleiding verbonden aan de vakgroep geochemie. In die periode werd het onderzoek voor dit proefschrift gedaan. Momenteel is de auteur verbonden als "Postdoctoral Research Assistent" aan het Royal Holloway and Bedford New College, University of London.